EXPERIMENTAL STUDY OF FACTORS CONTROLLING THE EFFECTIVENESS OF HIGH-TEMPERATURE PROTECTIVE COATINGS FOR TUNGSTEN.

(9) Summary rept. 15 May 62 – 15 Jun 63,

Technical Documentary Report No. ASD-TDR-63-744

(11) July 15, 1963

AIR FORCE MATERIALS LABORATORY
RESEARCH AND TECHNOLOGY DIVISION
AIR FORCE SYSTEMS COMMAND, USAF
WRIGHT-PATTERSON AIR FORCE BASE, OHIO

(16) Project No. 7312, (12) Task No. 731201

(15) (Prepared under Contract No. AF 33(657)-8787 by the General Telephone & Electronics Laboratories, Inc., Bayside, New York, N.Y.
By C. D. Dickinson and L. L. Seigle, Authors.)

NOTICES

When Government drawings, specifications, or other data are used for any purpose other than in connection with a definitely related Government procurement operation, the United States Government thereby incurs no responsibility nor any obligation whatsoever; and the fact that the Government may have formulated, furnished, or in any way supplied the said drawings, specifications, or other data, is not to be regarded by implication or otherwise as in any manner licensing the holder or any other person or corporation, or conveying any rights or permission to manufacture, use, or sell any patented invention that may in any way be related thereto.

Qualified requesters may obtain copies of this report from the Armed Services Technical Information Agency, (ASTIA), Arlington Hall Station, Arlington 12, Virginia.

This report has been released to the Office of Technical Services, U.S. Department of Commerce, Washington 25, D.C., for sale to the general public.

Copies of this report should not be returned to the Aeronautical Systems Division unless return is required by security considerations, contractual obligations, or notice on a specific document.

FOREWORD

This is the summary report prepared by General Telephone & Electronics Laboratories Inc., Bayside, New York, on Air Force Contract AF 33(657)-8787, Task No. 731201, Project No. 7312. The work was administered by the Directorate of Materials and Processes, Air Force Materials Laboratory, Research and Technology Division. Mr. Norman M. Geyer was project engineer.

This report covers work done from May 15, 1962 to June 15, 1963.

X-ray and microprobe analysis of the structures and compositions of specimens tested at the GT&E Laboratories was carried out by Battelle Memorial Institute. Contributing to the work at Battelle Memorial Institute were Messrs. David I. Phalen, Dale A. Vaughan, Neil A. Richard, Alfred E. Austin and Dr. Charles M. Schwartz.

The authors wish to acknowledge the contributions of Dr. Michael G. Nicholas who was associated with the program until October 30, 1962. In addition Dr. John V. Cathcart of Oak Ridge National Laboratory, Prof. Rustum Roy of Pennsylvania State University, Prof. Bruce Wagner of Northwestern University, and Prof. Harold Margolin of New York University made substantial contributions to the work in their capacity as consultants. Dr. Louis S. Castleman and Mr. Paul Lublin of the General Telephone & Electronics Laboratories also contributed valuable discussions. The authors also wish to acknowledge the work of Mr. Frank Bucherati in the preparation of alloys and oxidation testing, and the metallographic studies by Mr. Harry Woods.

The Contractor's number is TR 63-461.12.

ABSTRACT

The oxidation at elevated temperatures of Zr-Th, Zr-Y, Hf-Y, Hf-W, Hf-W-Re, Al-Cr-Sn, and Al-La-Sn alloys, as well as ZrN, HfN and ZrN-ThN combinations has been studied in order to clarify specific aspects of the problem of protecting tungsten against oxidation at high temperatures. Experimental results showed that there was much less tendency for ZrO_2, ThO_2 and HfO_2 scales to crack during growth at high than at low temperatures. Furthermore, multiphased scales were more resistant to spalling than single-phased scales, and protective oxides could be grown on many alloys. However, even in sound and coherent scales composed of these oxides, oxygen diffused so rapidly that it is doubtful that these oxides could form the basis of a protective system at 2000°C.

The sequence of layers at the metal-air interface of the Zr-Th and Zr-Y alloys formed by diffusion controlled oxidation was governed by a simple rule; namely, that the diffusion path in the appropriate isothermal section of the ternary equilibrium diagram is a straight line connecting the alloy composition with the oxygen corner. This rule is expected to apply to all ternary systems in which the oxidation process is dominated by the rapid diffusion of oxygen atoms in all layers. If significant migration of cations occurs, however, the rule is not applicable.

Observations have been made of the rate of formation, nature and morphology of scales formed on the brittle refractory compounds W_2Hf, ZrNi, HfN and ZrN-ThN, and those formed on liquid Zr-Y, Al-Cr-Sn and Al-La-Sn alloys. These obervations are discussed in terms of their implications for the development of oxidation protection systems for tungsten at high temperatures.

This technical documentary report has been reviewed and is approved.

I. Perlmutter

I. Perlmutter, Chief,
Physical Metallurgy Branch,
Metals and Ceramics Division,
Air Force Materials Laboratory

TABLE OF CONTENTS

TABLE OF CONTENTS (cont'd.)

TABLE OF CONTENTS (cont'd.)

LIST OF ILLUSTRATIONS

LIST OF ILLUSTRATIONS (cont'd.)

LIST OF ILLUSTRATIONS (cont'd.)

LIST OF TABLES

1. INTRODUCTION

The object of this program is to improve our knowledge and understanding of the factors controlling the efficacy of oxidation-resistant coatings for tungsten at temperatures of 2000°C and above. An analysis of the behavior of existing high-temperature coatings, conducted by these Laboratories under Contract AF 33(616)-8175, [1,2] led to the selection of five processes as being of major importance in determining the protectiveness of a coating system:

1. Breakaway, or the change from "parabolic" to "linear" oxide film growth. This phenomenon is accompanied by destruction of the protective character of the oxide film.

2. Multicomponent diffusion-controlled reactions leading to a specific sequence and morphology of oxide and other phases at the air-coating interface. In many practical systems two metal components as well as oxygen are involved, and this process is referred to, for convenience, as "ternary diffusion."

3. Loss of material by evaporation of the coating or substrate or by the formation of volatile oxidation products.

4. Interactions between the coating and the protected substrate.

5. Diffusion through the oxide film. When the film is protective, the rates of cation and/or anion diffusion control the progress of the oxidation reaction.

The first of these five processes, breakaway, is believed to be the most important, since no coating is really protective unless it forms a coherent outer oxide film. Previous work in these Laboratories under Contract AF 33(616)-8175 showed that the mechanical properties of the substrate influence breakaway and, in particular, that the use of a liquid substrate delays its onset during the growth of HfO_2, ZrO_2 and ThO_2 films. One objective of the present program is to extend this preliminary study by evaluating (1) the influence of liquid substrates on the growth of complex refractory oxides, and (2) the effect of solid substrate mechanical properties on the growth of simple refractory oxides.

A second objective of the program is to increase our understanding of the rules governing the sequence and morphology of phases formed at the air-coating interface by reaction of the coating with oxygen, i.e., of the "ternary diffusion" process. The success of a coating depends primarily

upon its ability to form a particular surface oxide of the several that might be produced. As explained in the previous reports [1,2] the sequence of oxide and other layers at the surface depends upon complex diffusional, as well as thermodynamic, factors, the details of which are not yet completely understood. Some progress has been made in rationalizing the influence of multicomponent diffusion on the sequence and morphology of phases in ternary metal systems by Clark and Rhines [3] and by Kirkaldy. [4] It is our objective to apply and extend this knowledge to representative ternary metal-oxygen systems of potential significance for ultra-high temperature coatings.

From a fundamental research standpoint, the ideal system for study is one in which (1) the metal(s)-oxygen phase diagrams are completely known, (2) the structures and properties of all of the oxides occurring in the system are known, and (3) the oxidation behavior of the component metals is understood. For this program, however, it was also necessary to choose systems of potential value as high-temperature coatings for tungsten; consequently the primary criterion for selection was that the oxides produced should be refractory. In addition, it was considered desirable, although not essential, that the component metals also have a high melting temperature. Within this limitation, systems were chosen which were classified sufficiently to suggest that the fundamental objectives might be attained to some degree, but which, at the least, would permit the collection of considerable information about the behavior of potential coating materials for tungsten at high temperatures. The following systems were selected for study:

1. Zr-Th-O
2. Zr-Y-O and Hf-Y-O
3. W-Hf-O and modifications containing rhenium
4. ZrN-O, HfN-O, and ZrN-ThN-O
5. Sn-Al-Cr-O and Sn-Al-La-O

The experimental approach consisted of preparing samples of the metal alloys, oxidizing these at several temperatures, primarily in air, measuring weight changes upon oxidation, and studying the structures by microscopic, chemical, X-ray diffraction, X-ray fluorescence and microprobe analyses. In the following sections, details of experimental procedure and results for each system will be presented in the order indicated. In Section 7 the information obtained on all five systems is analyzed and interpreted in terms of the factors governing protective behavior at high temperatures.

2. THE Zr-Th-O SYSTEM

The Zr-Th-O system was selected for a study of the applicability of Clark and Rhines rules[3] governing the sequence of phases formed by diffusion in a ternary system to oxidation of a binary alloy. The Th-Zr-O system appeared to be one of the best systems for satisfying both the practical and the fundamental criteria for this study. Both ThO_2 and ZrO_2 are among the most refractory oxides known, and all mixtures of these two oxides are refractory. Although the melting points of Th-Zr alloys are below 1800°C, and mostly below 1600°C, this is not necessarily a drawback with respect to their coating potential since the use of liquid substrates has been shown to delay the onset of breakaway.[2] The Zr-Th,[5] ZrO_2-ThO_2[6] and Zr-O[7] binary equilibrium diagrams are fairly well known, and therefore some attempt at estimating the Th-Zr-O diagram can be made. The Zr-O and ThO_2-ZrO_2 phase diagrams are given in Figs. II-1 and II-2 in Appendix II, and the Th-Zr phase diagram is given in Fig. 1. Finally, information is available about the oxidation behavior of elemental Zr and Th.[2]

2.1 EXPERIMENTAL PROCEDURE

Alloys containing 30, 55, 70 and 85%Th* (14, 31, 48 and 69 a/o, respectively) were arc melted in the form of buttons and forged and rolled at room temperature to strip 0.075-in. thick, with intermediate and final vacuum anneals of 5 hours at 1200°C. The compositions and test temperatures are indicated by the circles in Fig. 1. Strips were cut into 1/2 in. x 1/4 in. coupons and 1/16-in.-diameter holes were drilled near one end. Coupons so produced were oxidized in a platinum-rhodium wound furnace by suspending the sample on a platinum-rhodium wire. Specimens were oxidized in flowing air at 750°, 1200°, and 1600°C for several times to define the kinetics of oxidation by weight-gain measurements. Both sequential-oxidation tests on a single specimen and noncyclic tests for a single time interval were used. Melted buttons in a ZrO_2 crucible were used for oxidation studies at 1600°C, since the alloys at that temperature are liquid. A number of samples were oxidized in a mixture of argon-20% oxygen and pure oxygen using procedures essentially the same as for oxidation in air.

Metallographic specimens were prepared, and the thicknesses of the layers formed during oxidation were measured. Specific samples were selected on the basis of metallographic examinations for microprobe and X-ray diffraction analysis of the structure and composition of the layers

* Both weight and atomic percent are used and are designated by % and a/o, respectively, throughout the report.

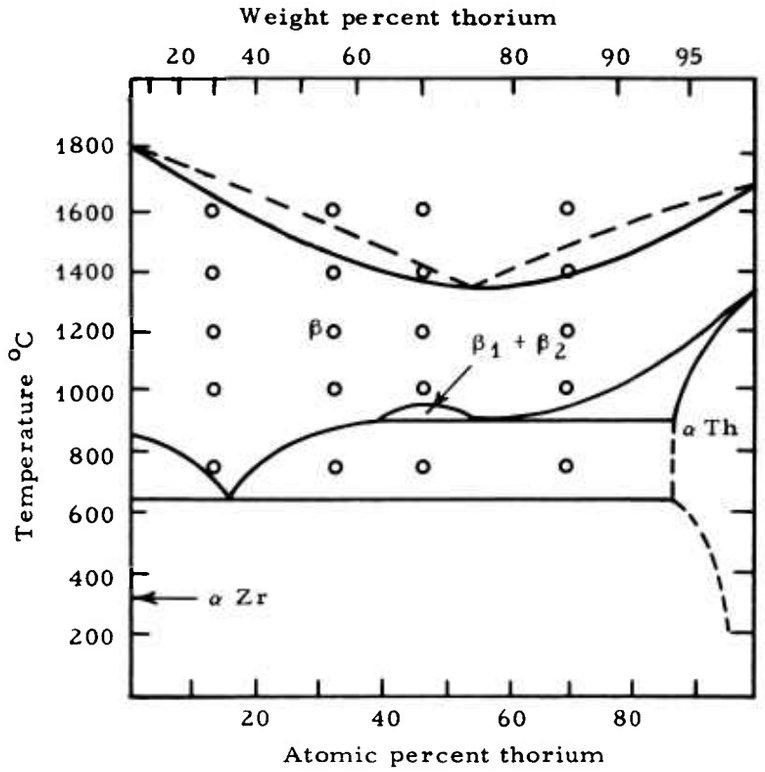

Fig. 1. The thorium-zirconium phase diagram.[5] (Circles indicate alloys tested and temperatures of oxidation.)

formed. These analyses were performed at the Battelle Memorial Institute. The experimental procedure is given in Appendix I. Samples of Zr-30%, Zr-55% and Zr-85% alloys oxidized at 1200°C, and one sample of the Zr-30%Th alloy oxidized at 1400°C, were examined in sufficient detail to characterize the composition and structure of the layers formed for interpretation in terms of ternary diffusion processes.

2.2 RESULTS

2.2.1 Rate of Oxidation

The rate of oxidation was determined by measuring the weight gain of the specimens after exposure at 750, 1000, 1200, 1400 and 1600°C. The results for each alloy are shown in Figs. 2 through 5, and the type of test used is indicated. In these figures, the log of the specific weight gain is plotted as a function of the log of time; the slope of the resulting curve is the reciprocal of the index of reaction, n, in the following equation:

$$\left(\frac{\Delta W}{A}\right)^n = Kt. \qquad (1)$$

In almost all cases, the data for both noncyclic and cyclic tests for a given temperature and composition are well described by a straight line with a slope of 1 or 1/2, indicating nonprotective (linear) or protective (parabolic) film growth, respectively. The rate constants presented in Table I were determined from the straight lines of log ($\Delta W/A$) vs log t plots by assuming that either linear (n=1) or parabolic (n=2) growth best describes the kinetics of the oxidation reaction.

At 750 and 1000°C linear oxidation was observed on all compositions tested, and the oxide formed was externally cracked. The tests were sequential cyclic runs on one sample, but cracking apparently occurred even on the first run; this was indicated by the fact that for the alloys containing 70-85%Th, the weight gained at 1000°C in the initial run is greater than that gained at 1200°C in the same time.

At 1200°C individual specimens were used for each test, and the plotted data followed a line with a slope of 1/2, indicating parabolic growth. The scales were sound and dense, and the edges and corners were intact in most cases; a sharp corner was retained on the oxide.

At 1400°C both cyclic and individual tests were run. In the Zr-30Th and Zr-55Th alloy, a line with a slope of 1/2 describes the results of both types of tests. In the Zr-70%Th alloy at 1400°C, the weight gains for individual specimen tests indicate a slope of 1/2 (Fig. 3), but in

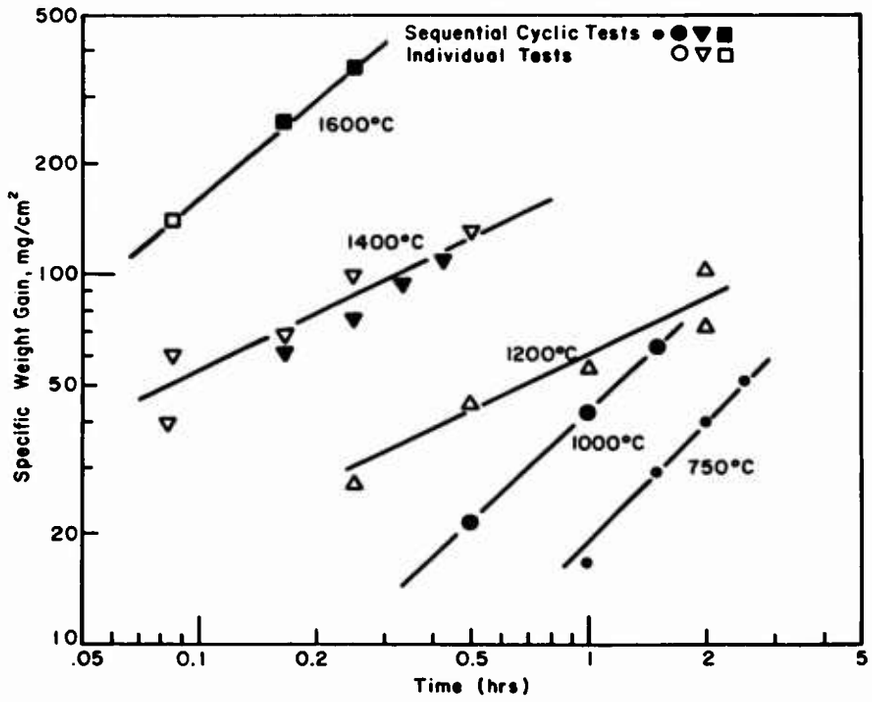

Fig. 2. Weight gained in oxidation of Zr-30%Th sheet in dry air.

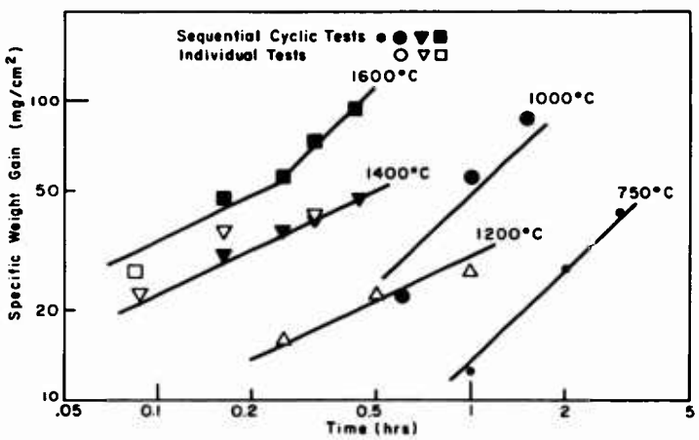

Fig. 3. Weight gained in oxidation of Zr-55%Th sheet in dry air.

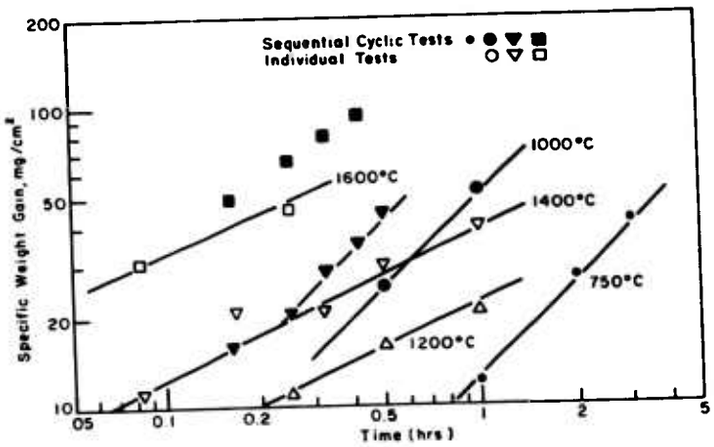

Fig. 4. Weight gained in oxidation of Zr-70%Th sheet in dry air.

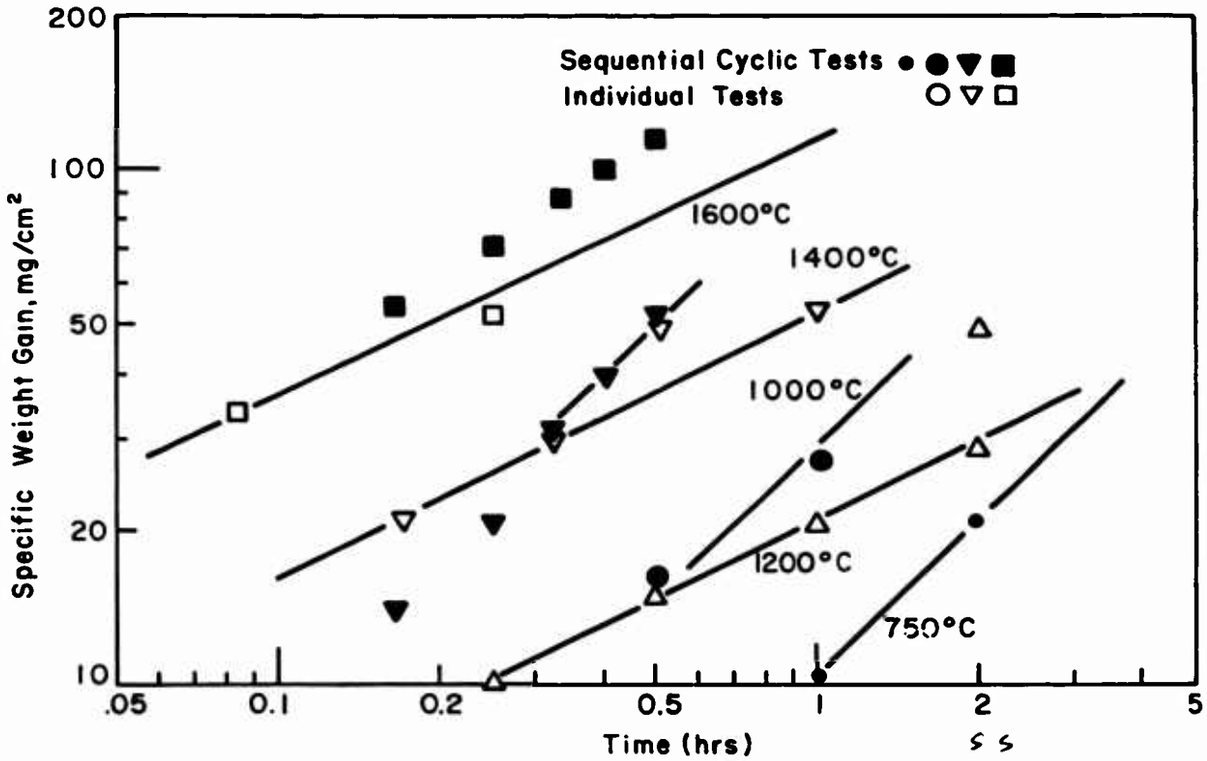

Fig. 5. Weight gained in oxidation of Zr-85%Th sheet in dry air.

TABLE I

The effect of Temperature and Composition on ghe Growth Rate in Oxidation of Zr-Th Alloys at 750°C to 1600°C

	Zr - 30 % Th		Zr - 55 % Th		Zr - 70 % Th		Zr - 85 % Th	
TEMP (°C)	K_l* gm/cm² hr	K_p** gm²/cm⁴ hr	K_l* gm/cm² hr	K_p** gm²/cm⁴ hr	K_l* gm/cm² hr	K_p** gm²/cm⁴ hr	K_l* gm/cm² hr	K_p** gm²/cm⁴ hr
750	2.4×10^{-2}	---	1.5×10^{-2}	---	2.3×10^{-2}	---	2.2×10^{-2}	---
1000	4.2×10^{-2}	---	5.7×10^{-2}	---	5.2×10^{-2}	---	2.9×10^{-2}	---
1200	---	3.14×10^{-3}	---	9.6×10^{-4}	---	4.3×10^{-4}	---	4.3×10^{-4}
1400	---	3.2×10^{-2}	---	6.7×10^{-3}	---	1.6×10^{-3}	---	2.92×10^{-3}
1600	1.7	---	2.2×10^{-1}	1.02×10^{-2}	---	6.10×10^{-3}	---	1.3×10^{-2}

*K_l = LINEAR GROWTH RATE CONSTANT, i.e., $n \cong 1$ in $n \log \frac{\Delta W}{A} = \log Kt$

**K_n = PARABOLIC GROWTH RATE CONSTANT, i.e., $n \cong 2$ in $n \log \frac{\Delta W}{A} = \log Kt$

sequential tests beyond 0.25 hours the slope changes toward a linear rate, indicating breakaway. In the Zr-85%Th alloy only the individual tests fit a line with a slope of 1/2; the cyclic results indicate breakaway oxidation.

At 1600°C only the Zr-30%Th alloy is solid at temperature. In the noncyclic tests, the rate of weight gain on the liquid Zr-(70-85%)Th alloys is parabolic, but slopes of 0.68 were obtained for cyclic tests. In the solid Zr-30%Th alloy only cyclic tests were run, and a slope of one was observed (Fig. 2). The results of oxidation of the Zr-55%Th alloy can be described by a curve with an initial slope of 1/2 (Fig. 3), and a slope of 1 for times greater than 0.25 hr. The oxides formed at 1600°C appeared to be dense and sound, but on standing at room temperature, the oxides formed on the liquid alloys disintegrated in the atmosphere to form a very fine powder.

2.2.2 Structure of the Surface Zone

2.2.2.1 Metallographic Studies

Metallographic examination revealed that at 750 and 1000°C, oxidation of all alloys proceeded by linear nonprotective growth, and the oxide formed contained many cracks parallel to the surface of the specimen, as indicated in Fig. 6. Examination of the metallic substrate of specimens oxidized at 750°C indicated no change in substrate structure, and microhardness tests showed no increase in hardness of the metal adjacent to the metal-oxide interface. Thus the amount of oxygen which penetrates or dissolves in the substrate must be relatively small. At 750 and 1000°C, breakaway due to fracture of the oxide is evidently the controlling process in the rate of oxidation. Oxygen permeates through the cracks to the metal-oxide interface, forming new oxide which, in turn, spalls and does not protect the substrate. Under these conditions, the substrate is oxidized essentially in situ and solid-state diffusion processes do not control the composition of the oxide layer.

Cross sections through the surface layers of samples that exhibited parabolic growth at 1200 and 1400°C were studied. The thicknesses of the layers formed are given in Table II. The microstructures of the samples oxidized in air at 1200°C, and 1400°C are given in Fig. 7.

In general, the structures in Fig. 7 indicate that the layers formed during oxidation were quite dependent on thorium content at 1200 and 1400°C. At these temperatures the rate of growth is apparently diffusion-controlled in all compositions, and compact adherent oxides are formed;

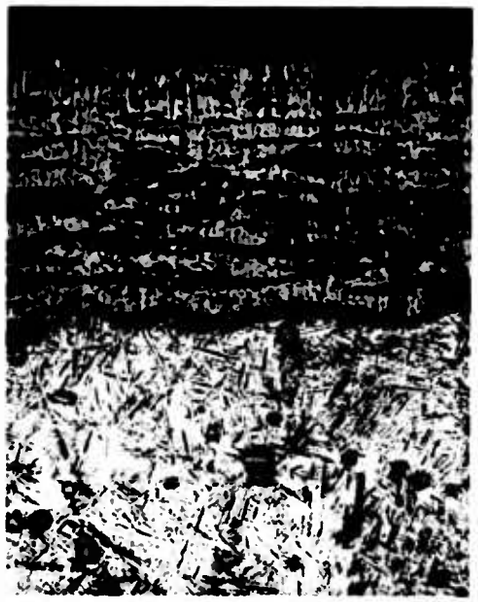

Fig. 6. Surface of a 70 w/o Th-Zr alloy exposed to air for 3 hours at 750°C. (250X)

TABLE II

A Comparison of Weight Gain, Thickness of Oxides and Other Layers Measured by Microscopic and Microhardness Measurements

Alloy	Time (min)	Wt. gain/area (mg/cm^2)	Thickness of			% change in thickness of sample
			$ThO_2 + ZrO_2$ cm x 10^{-2}	$THO_2 + Zr(\alpha+\beta)$ cm x 10^{-2}	$ThO_2 + \alpha Zr$ cm x 10^{-2}	
Zr-30 Th	1200°C 15	27	1.32	1.32	.41	8.6
	30	45	2.12	1.35	--	--
	60	55	2.61	3.59	.61	19.3
	120	72	4.24	5.56	1.12	29.2
	1400°C 5	60.5	3.10	2.54	.75	--
	10	67.3	3.56	2.96	.89	14.5
	10	38	3.44	1.67	.86	--
	15	99	5.80	3.12	.71	25.0
	25	110	4.05	2.30	.8	--
	30	128	6.8	>5.15	1.79	52.0
Zr-55 Th	1200°C 15	16	1.4	--	--	6.3
	30	23	1.65	1.4	--	--
	60	27.6	2.05	1.25	.53	5.4
	1400°C 10	37	2.75	1.41	.58	3.2
	20	43.1	3.68	1.70	.53	17.3
	25	48	3.18	1.4	.52	--
Zr-70 Th	1200°C 60	20.3	1.4	--	--	--
Zr-85 Th	1200°C 30	15.5	1.27	--	1.14(a)	--
	60	20.3	1.57	--	.30(a)	3.4
	120	29.2	2.7	--	1.65(a)	8.3

(a) Depleted zone not internally oxidized.

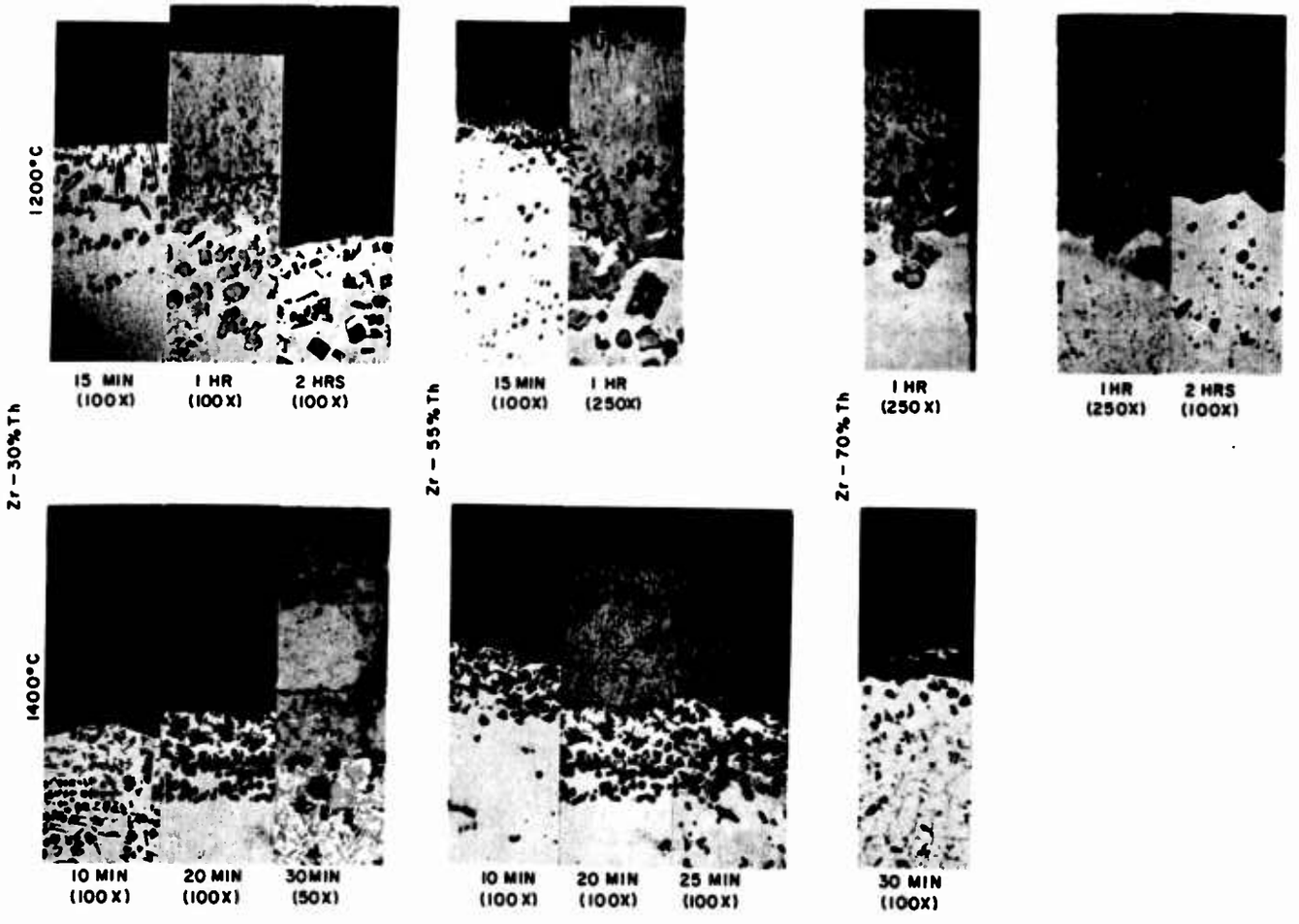

Fig. 7. Microstructures of layers formed in the oxidation of Zr-Th alloys. (Magnification reduced 30% in reproduction.)

however, the layers and structures observed in the Zr-30%Th and Zr-55%Th alloys (thorium lean) differ from those in the Zr-70Th and Zr-85%Th (thorium rich) alloys. In the thorium lean alloys several layers which thicken with time are observed as follows:

1. An external two-phased oxide;
2. An internally oxidized layer consisting of a single-phase metal matrix containing oxide particles;
3. A two-phased metal matrix containing oxides formed by internal oxidation. The two-phased structure appears to have formed on cooling and was apparently single-phased 1200°C.

Hardness traverses of the single-phase metallic layer beneath the oxide were made on alloys oxidized at 1200 and 1400°C. The results given for the Zr-30%Th alloy in Fig. 8 are typical of the hardness traverses for both the Zr-30%Th and Zr-55%Th alloys. This layer has a hardness above 1000 VHN near the oxide-metal interface, and in its entirety, is harder than the substrate from which it is formed. The hardness of the metal in layer 3 is also greater than that of the substrate.

All of the layers thicken with time, and in the Zr-30%Th alloy, which was oxidized 30 minutes at 1400°C, the internally oxidized zone (layer 3) penetrated almost to the centerline of the specimen. In this sample large fissures in layer 2 and in the corners of the outer oxide layer were observed. The oxide was grossly distorted by growth, but cracks were observed only at corners and in the regions of the support hole in the specimen. In specimens oxidized at shorter times at 1400°C or equivalently shorter time at 1200°C, the corners were essentially intact and the corner angle of 90° was sharply outlined.

In the Zr-70%Th and Zr-85%Th alloys, the external oxide is the only layer that grows appreciably with time, and the rate of growth is considerably less than the rate in the thorium-lean alloys. Some indication of a small amount of internal oxidation at 1200°C may be present in the Zr-70%Th alloy structure shown in Fig. 7; however, internal oxidation and the solution of oxygen in the metallic matrix do not occur to any large degree in the thorium-rich alloys. Although no growing two-phased region at the metal-oxide interface was observed by GT&E Laboratories, and hardness immediately adjacent to the metal-oxide interface indicated no hardening from oxygen solution, the Battelle investigators report the presence of a thin layer containing a high proportion of α-Zr (see Third Quarterly Progress Report).

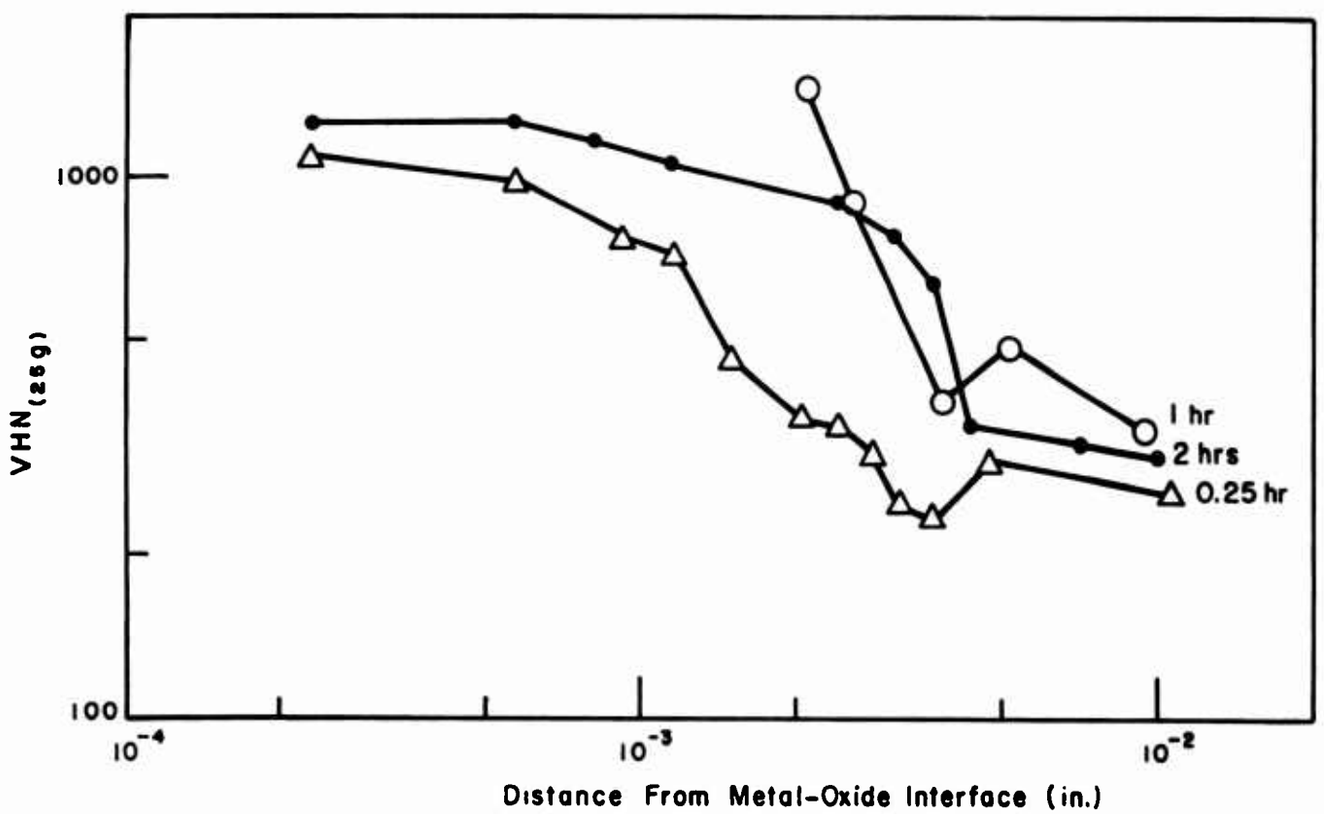

Fig. 8 The effect of oxidation time at 1200°C on the hardness of the metallic phase adjacent to the external oxide in Zr-30%Th specimens.

At 1600°C observations were complicated by the fact that only the Zr-30%Th alloy was solid at temperature. In addition, the scales that formed on the liquid alloys were initially sound and nonporous but rapidly disintegrated at room temperature; as a result, microstructure observations could not be made. However, the disintegrated scales were analyzed by X-ray diffraction techniques with the following results:

Alloy	Scale Composition
Zr-55%Th	ThO_2 + 10%ZrO_2 + (ZrN detected - 5%)
Zr-70%Th	ThO_2 + -5% (ZrN, possibly ZrO_2 detected <5%)
Zr-85%Th	ThO_2 + < 5% (ZrN + several unidentified lines - trace ZrO_2?)

The scale is identified as primarily ThO_2, but the odd behavior at room temperature suggests the possibility that the scale formed at 1600°C on the liquid alloys contained ThN which later reacted to form ThO_2, producing the observed disintegration at room temperature. The ZrO_2 observed in the Zr-55%Th alloy may have formed after the composition being oxidized was partially solid. These results indicate that thermodynamic considerations rather than diffusion processes are overriding in the oxidation of the liquid Zr-Th alloys. Chemical analysis of the residual metal of Zr-55%Th samples oxidized for 15 and 30 minutes at 1600°C indicated thorium contents of 45 and 46.7%, respectively. An alloy containing 45% thorium would be partly solid at 1600°C. Microscopic examination revealed localized areas where an oxygen-saturated zone had formed and internal oxidation had occurred similar to that observed in the oxidation of the solid alloy.

2.2.2.2 Microprobe and X-ray Diffraction Studies

The results of microprobe, X-ray diffraction and X-ray fluorescence analysis of the Zr-30, Zr-55 and Zr-85Th alloys oxidized at 1200°C for 1/2 and 2 hours and the Zr-30%Th alloy oxidized at 1400°C for 20 minutes are given in Section 4.1 of Appendix I. These results may be summarized as follows:

1. The major constituents of the oxide layers on all samples oxidized in air were ThO_2 and monoclinic ZrO_2. Appreciable quantities of cubic ZrO_2 were observed in the scale of the Zr-30Th alloys oxidized at 1200°C, and small amounts were formed in other specimens. In addition, small quantities of ZrN were detected in most samples, usually near the oxide-metal interface. Monoclinic ZrO_2 is the stable phase at

room temperature (Fig. II-2), while cubic ZrO_2 may have existed as a metastable phase at the oxidation temperature in conjunction with, or instead of, the stable tetragonal phase.

2. Although a precise determination could not be carried out (owing to the existence of preferred orientation in the oxide layer), the relative intensities of X-ray diffraction lines indicated that the proportion of ZrO_2 and ThO_2 in the scale on all alloys was approximately that corresponding to the base metal composition. X-ray fluorescence analysis confirmed this result for the Zr-30Th alloy, but indicated a slight excess of Th in the scale of the Zr-85Th alloy.

3. Microprobe analysis showed a relatively low solubility of Zr in ThO_2 and Th in ZrO_2. However the solubility limits could not be precisely defined because of the small size of the particles in the structure. Indications of as much as 15w/o Zr in ThO_2 were considered to be untrustworthy. X-ray lattice parameter measurements indicated a solubility of less than 5% Zr in ThO_2 and vice-versa. These solubility limits were verified by equilibrating a powder mixture of 75 mole percent ThO_2, 20 mole percent ZrO_2 and 5 mole percent Zr at 1600°C for 16 hours in the GT&E Laboratories and determining the lattice parameters of the phases after cooling to room temperature.

4. ThO_2 was identified but ZrO_2 was not detected in the zones of internal oxidation, below the metal-oxide interface. The single-phase metal matrix in the Th-lean alloys just below the scale (white zone) was identified by X-ray diffraction analysis as α-Zr with an expanded lattice parameter, presumably stabilized at temperature by the presence of O and N in solution. Microprobe data indicated that $<0.6\%$ Th was soluble in this phase. The layer below this consisted of β + ThO_2 at temperature, but upon cooling, the matrix separated into α-Zr + α-Th. Microprobe analysis showed a variation of the Th content of this layer from <0.6% at the α - β interface to a value typical of the unaffected substrate at the base metal -β + ThO_2 interface.

5. No significant metal-concentration gradients existed in the substrates of the 30 and 55% Th alloys below the zone of internal oxidation, but a concentration gradient in the substrate of the Zr-85Th alloy was detected beneath the oxide layer. These data indicate, again, that virtually no diffusion of the metallic constituents between layers took place in the low-Th alloys, while a slight migration of Th to the oxide layer occurred in the Zr-85Th alloy.

Additional GT&E Laboratories' analyses of the oxide layers made by wet chemical and X-ray fluorescence techniques are presented in Table III. These data confirm that only slight diffusion of metal atoms occurs between layers in the high-Th alloys, since the Zr/Th ratio was almost the same in the alloys oxidized at 1000°C, where breakaway occurred, and those oxidized at 1200°C where diffusion-controlled growth occurred. On the other hand, the oxide on the Zr-85Th alloy oxidized at 1400°C was almost pure ThO_2 since the alloy was apparently liquid at this temperature. Finally, the nitrogen content of the scale in the 85Th alloy was low, except at the metal-oxide interface.

TABLE III

Chemical Analyses of Sections of Oxided Zr-Th Alloys

Alloy	Description of Sample	Weight Ratio Zr/Th	Nitrogen Content
Zr-70%Th	Zr/Th ratio of oxide formed at 1000°C in 2 hours	0.42	
Zr-70%Th	Zr/Th ratio of oxide formed at 1200°C in 3 hours	0.45	
Zr-85%Th	Zr/Th ratio of oxide formed at 1000°C in 1 hour	0.19	
Zr-85%Th	Zr/Th ratio of oxide formed at 1200°C in 1-1/2 hours	0.20	
Zr-85%Th	Zr/Th ratio of oxide formed at 1400°C in 1/4 hour (substrate is liquid)	Zr/Th = 0.01	
Zr-85%Th	Nitrogen content in sample oxidized at 800°C		
	External oxide		0.28%
	Metal-oxide interface		4.13%
	Metal		0.004%

By combining the microprobe, X-ray, chemical, metallographic, and microhardness results, it is possible to describe the phases present in each layer with greater precision, to assign Zr/Th ratios to the phases observed, and to estimate the oxygen gradient in the various layers. For example, in the Zr-30%Th alloy and the Zr-55%Th alloys (14 a/o and 31 a/o Th respectively), the sequence of layers that existed at 1200°C is as follows:

1. ZrO_2 (less than 4 a/o Th) and ThO_2 (less than 5 a/o Zr). Only tetragonal ZrO_2 should have existed at 1200°C, according to the equilibrium diagram (Fig. II-2) transforming to monoclinic ZrO_2 upon cooling, but cubic ZrO_2 may have also been present as a metastable phase. ZrN was present as a discrete phase near the metal-oxide interface. The bulk concentration of Th in the oxide was uniform throughout and not significantly greater than that of the substrate.

2. ThO_2 (less than 5 a/o Zr) + α-Zr (less than 0.6 a/o Th). The oxygen content of the α-Zr is high, probably between 30 and 10 a/o.

3. ThO_2 (less than 5 a/o Zr) + β-Zr (from 0.6 a/o Th to 30 a/o Th). The oxygen content of the metal matrix varies from the saturation concentration (~3 a/o) to that of the original alloy. The ratio of Th to Zr in the metal increases from 5 a/o and 14 a/o to the original alloy compositions of 14 and 31 a/o Th, respectively. Although the Th/Zr ratio in the metal matrix varies with distance, when ThO_2 is included, the overall ratio of Th/Zr is constant and does not vary with distance. The gradient in the matrix therefor does not represent mass transport of Th from the substrate to the oxide.

In the Zr-85%Th (69 a/o Th) alloy, the sequence of layers or phases, and the approximate compositions at 1200°C, were as follows:

1. An external two-phased oxide (ZrO_2 + ThO_2) similar in composition to that formed on the Th-lean alloys, but with a considerably higher ratio of ThO_2 to ZrO_2. The bulk concentration of Th in the oxide is slightly greater than that of the original alloy.

2. An extremely thin layer which contains particles of α-Zr + β-Zr at temperature (see Fig. 3(a) and (d) of Appendix I) and presumably some absorbed oxygen at the metal-oxide interface.

3. A Th-depleted zone in which the Th content increases from approximately 24 a/o Th at the metal-oxide interface to the matrix composition of 60 a/o Th. This layer does not contain oxygen in amounts greater than that of the original substrate. The Th gradient beneath the oxide-containing zones shows mass transport of Th to the oxide.

2.2.3 Oxidation of Th-Zr Alloys in Nitrogen-Free Atmospheres

The occurrence of nitrogen and nitrides in the scale complicates the interpretation of the oxidation of Zr-Th alloys in air due to the addition of a fourth component. It appeared that only small amounts of nitrogen were present, suggesting that this element did not strongly influence the oxidation process. However, a study of the oxidation process in a nitrogen-free atmosphere was necessary to determine the validity of this assumption. Accordingly, samples of the Zr-55, Zr-70 and Zr-85%Th alloys were oxidized in a flowing atmosphere of argon-20% oxygen for times of 1/2 to 8 hours.

In addition, samples of the alloys were oxidized in pure flowing oxygen at 4 hours. Finally, a group of samples which were preoxidized in argon-20% oxygen to produce a weight gain of about 5 mg/cm^2 on the Zr-70 and Zr-85%Th alloy were further oxidized in flowing air from 1 and 4 hours at 1200°C. The resulting weight gains for the three experiments are compared with the results for oxidation of the same alloys in air in Figs. 9, 10 and 11.

The rate of oxidation of all three alloys is decreased if argon is substituted for nitrogen in the oxidizing atmosphere. The ratio of weight gain for a given time in air to that in argon-oxygen is greater for the Zr-85%Th alloy and less for the Zr-55%Th alloy, but the difference in rate is consistent and significant for all alloys. The weight gains after 4 hours in pure oxygen are slightly but consistently greater than that in a mixture of argon and oxygen for all three alloys, indicating that a change in oxygen partial pressure from 0.2 atmosphere to 1 atmosphere results in a slight increase in the rate of oxidation. However, the weight gains in pure oxygen are less than those in air for all three compositions. The oxide formed during preoxidation on the Zr-70 and 85%Th alloys apparently does not serve as a barrier to nitrogen diffusion since the subsequent weight gains of preoxidized samples after 1 hour and 4 hours in air were greater than those observed when the samples were oxidized in air during the entire test. In these tests, the atmosphere was changed without intermittent cooling so that the change in rate results only from a change in the nitrogen content during the test.

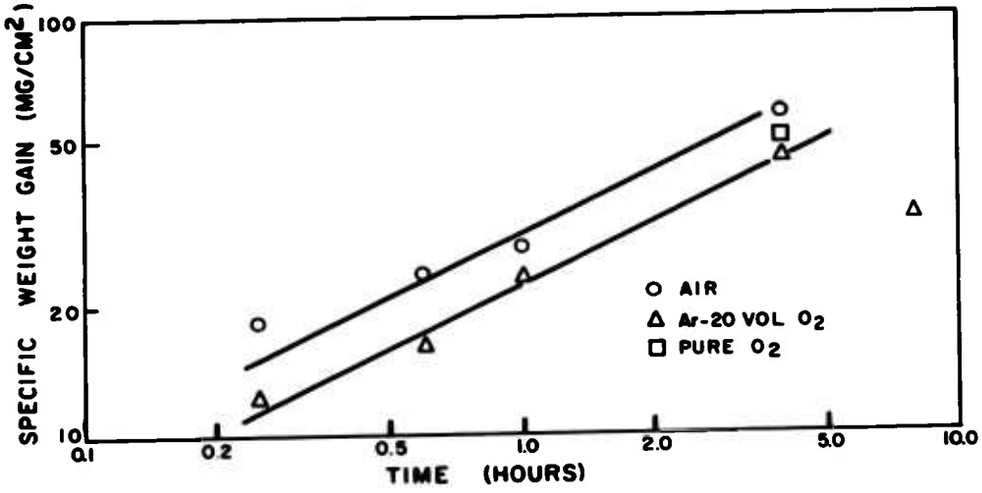

Fig. 9. Comparison of the weight gain during oxidation of Zr-55%Th sheet in oxygen, oxygen-argon and air at 1200°C.

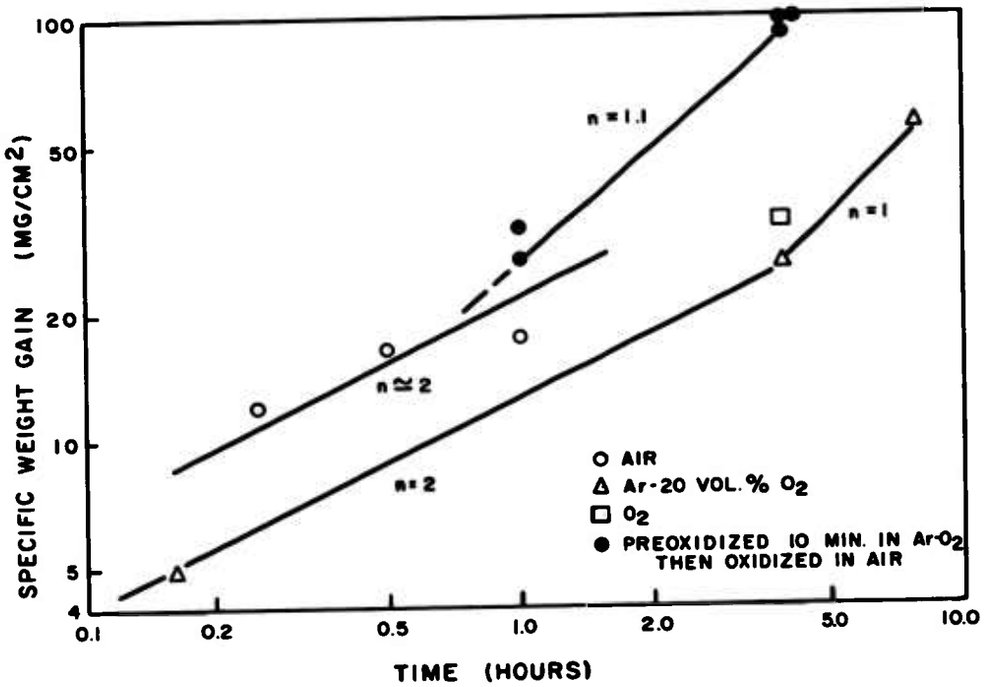

Fig. 10. Comparison of the weight gain during oxidation of Zr-70%Th sheet in oxygen, oxygen-argon and air at 1200°C.

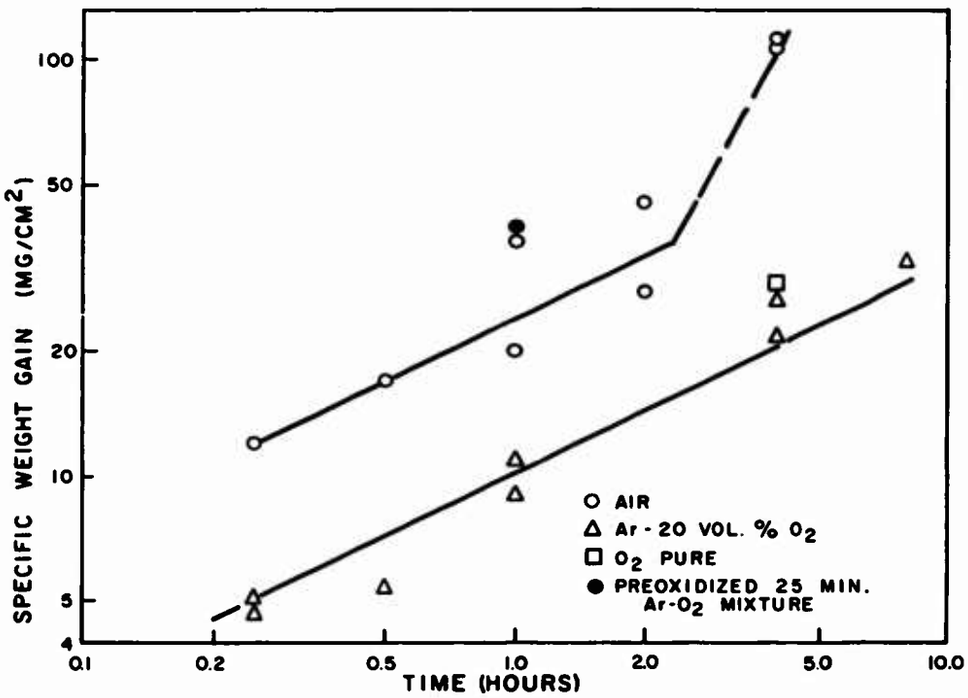

Fig. 11. Comparison of the weight gain during oxidation of Zr-85%Th sheet in oxygen, oxygen-argon and air at 1200°C.

The microstructures of samples which were metallographically examined are given in Fig. 12, and the layers are thinner than those formed in air as expected. In the Zr-55% Th alloy both oxide and internally oxidized layers are formed, and the thickness of each layer for a given weight gain is essentially the same as that observed on samples oxidized in air. In the Zr-70%Th alloy, however, a definite layer of alpha Zr and a layer which contains ThO_2 particles in contact with both the alpha and the beta Zr layer is observed. The external oxide appears to be two-phased ZrO_2 + ThO_2. In the Zr-85%Th alloy the oxide appears to be single phased and some of the ThO_2 particles in beta-Zr near the metal-oxide interface may have formed during oxidation.

A sample of the Zr-85%Th alloy which was oxidized 8 hours at 1200°C in argon-20% oxygen was submitted for microprobe and X-ray diffraction analyses; the results are shown in Fig. I-3 of Appendix I. Microprobe analysis of the external oxide indicated only 82% ThO_2, but X-ray diffraction analysis did not detect ZrO_2 in the outer oxide. Microprobe indications of Zr equivalent to about 18% ZrO_2 in the scale were obtained, which is much more than the 4% ZrO_2 in solution at temperature indicated by the equilibrium diagram. Metallographic examination at the GT&E Laboratories revealed two phases in the microstructure; the reason for the discrepancy remains unexplained. The Th content of the matrix at the metal-oxide interface is 30%, compared with 40% for the same alloy oxidized 2 hours at 1200°C in air. The results suggest that the decrease in the rate of diffusion of oxygen in the absence of nitrogen only slightly altered the diffusion path in this alloy.

2.3 DISCUSSION OF RESULTS

2.3.1 Rate of Oxidation

The rates of oxidation at 1200, 1400 and 1600°C of the Zr-Th alloys are compared with previously determined rates of formation of ZrO_2 on liquid Zr-Sn alloys and ThO_2 on Th-Sn alloys in Fig. 13. At 1600°C the parabolic rate constant for the alloys is located directly between the rate constants for the oxidation of Zr and Th in Sn alloys. At 1200° and 1400°C the rates observed for the Zr-30Th and Zr-55Th alloys are considerably higher than a straight-line average of the rates for Th and Zr in Sn. This suggests that the occurrence of internal oxidation is important in determining the overall rate constant for these alloys. The rate constants for the Zr-70%Th alloy at 1200 and 1400°C, and for the Zr-85%Th alloy at 1200°C in which little or no internal oxidation occurred are between the rate constants for the oxidation of pure Th and Zr.

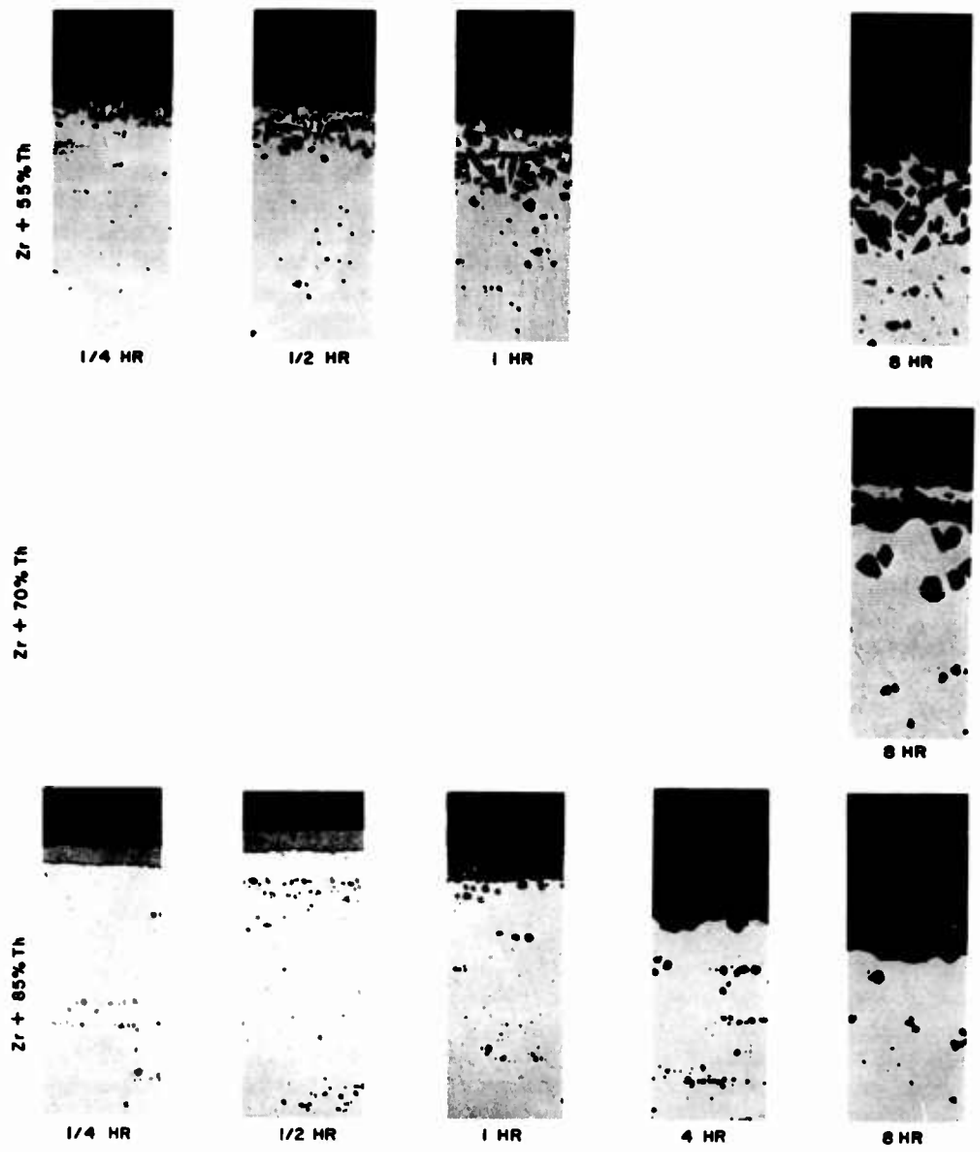

Fig. 12. Layers formed in oxidation of zirconium-thorium alloys in a mixture of 80% argon - 20% oxygen - at 1200°C (magnification reduced ~30% in reproduction).

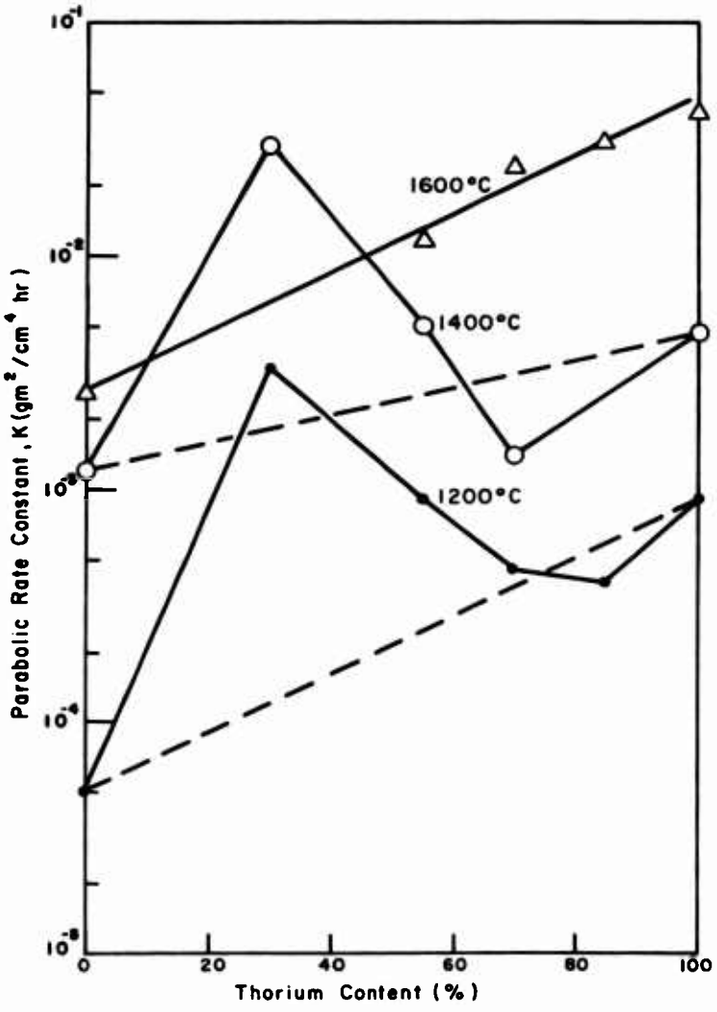

Fig. 13. The effect of thorium content on the parabolic rate constant in oxidation of Zr-Th alloys at 1200 to 1600°C. (Parabolic rates for Zr and Th obtained by interpolation or extrapolation for oxidation rates of Th-Sn and Zr-Sn alloys in Ref. 2.)

In terms of the formation of a protective barrier against oxidation of tungsten above 2000°C, the formation of refractory oxides of Th and Zr alloys (and as well, the pure oxides) has little to offer in a practical coating system, even though the growth process is diffusion-controlled at high temperatures and the oxides are solid. The rate of growth of all oxides formed from this system is too great at 1200 to 1600°C to be considered practicable, and the growth rates above 2000°C should be even more rapid unless some totally unexpected and unpredictable rate-controlling process is involved. Thus, even though a high melting point and the prevention of breakaway in the growth of refractory oxides is required for protection, these two requirements are not sufficient to ensure protection.

Internal oxidation eventually does lead to failure by breakaway in the Zr-30Th and Zr-55%Th alloys. In the Zr-30%Th alloy, oxidized for 30 minutes at 1400°C, considerable spalling of the oxygen-saturated Zr had caused cracks in the oxide at the corners of the specimens; these cracks were apparently responsible for the increase in the rate of growth at longer times at 1400°C, and for shorter times at 1600°C. The most surprising fact is that the oxide does not spall in most of the alloys, even though the oxidation process causes a 10% or more increase in the thickness of the specimen. Even the corners after 10% increase in thickness retained a sharp 90° angle and are essentially sound, with no indication of cracking in spite of the fact that the oxide is apparently being formed by anion diffusion to the metal-oxide interface.

The fact that the oxide can undergo such distortion without cracking indicates that the two-phased structure of thoria surrounded by a mixutre of zirconia or zirconia plus thoria has considerable ductility at temperatures of 1200°C and above. Breakaway oxidation does occur by spalling and cracking at temperatures of 1000°C and below where the oxide is apparently less plastic.

However, growth stresses are not the only stresses that cause spalling in the oxide. There are indications, in the Zr-Th-O system, that the two-phased oxides that grow protectively at 1200°C and above differ in their resistance to thermal shock stresses with composition. For example, the oxides form protective layers on the Zr-14 and Zr-31 a/o Th alloys at 1200°C, and the rate of growth is parabolic for both cyclic and individual oxidation tests. The ZrO_2 matrix two-phased oxide formed at 1200 to 1400°C on these alloys is evidently resistant to thermal shock. However, for the Zr-48 and 69 a/o Th alloys, linear growth was observed at 1200 to 1400°C in cyclic tests, while parabolic growth was observed when individual specimens were used for each test. The ThO_2 matrix in the oxides formed on these alloys is less resistant to thermal shock.

If the growth of each layer observed after oxidation at 1200 to 1400°C is truly diffusion-controlled, then all layers should thicken with time, according to Eq. (1) where n = 2 and k is a different constant for each layer. The weight gain should be directly related to the rate of thickening of each zone and to the total thickness. In Fig. 14, the weight gain versus the thickness of the oxide layer, and the thickness of the oxide layer plus internally oxidized zone, are plotted for the Zr-30%Th alloy tested at 1200 and 1400°C. A linear relationship is obtained for both cases. Two conclusions are possible from these curves. First the thickness of the oxide layer for a given weight gain is independent of temperature, indicating that the oxide density (and probably composition) does not change with temperature. Second, the thickness of the internally oxidized zone does change with temperature, the layer being thicker for a given weight gain at 1200°C than at 1400°C. In the thorium-rich alloys, only the oxide layer grows with time, and the thickness of the oxide for a given weight gain is greater than that shown for the oxide layer in Fig. 14. This is not unexpected, since hardness and microstructure results indicate that almost all of the oxygen is in the oxide layer in the thorium-rich alloys.

The results of testing in argon-20% oxygen atmosphere suggest that oxygen diffuses more slowly through a nitrogen-free zirconium or thorium oxide than through one containing nitrogen. These results are consistent with the previously reported influence of both nitrogen diffusion[8] and oxygen[9] content on the oxidation rate of pure or slightly alloyed zirconium. The mechanism by which nitrogen influences the rate of oxidation is not known, since exacting experiments needed to define such a factor have not been made. However, the influence of nitrogen on the rate of oxygen diffusion alone could be an important consideration since a change in the rate of diffusion of one component could alter the composition path.

The influence of nitrogen on the oxidation rate of an alloy with a previously formed nitrogen-free scale is of particular interest since the oxide formed should serve as a barrier against nitridization unless the nitrogen dissolves and diffuses through the oxide. The increase in oxidation rate and change in kinetics that resulted from the introduction of nitrogen after preoxidation confirm the fact that nitrogen does diffuse through the oxide and is therefore soluble in the oxides.

2.3.2 Structure of Surface Zone

In order to discuss the sequence of phases at the air-coating interface in terms of the "ternary-diffusion" concept, it is first necessary to construct a tentative phase diagram for the Th-Zr-O ternary system. The Zr-Th and Zr-O binary diagrams are known and the quasibinary

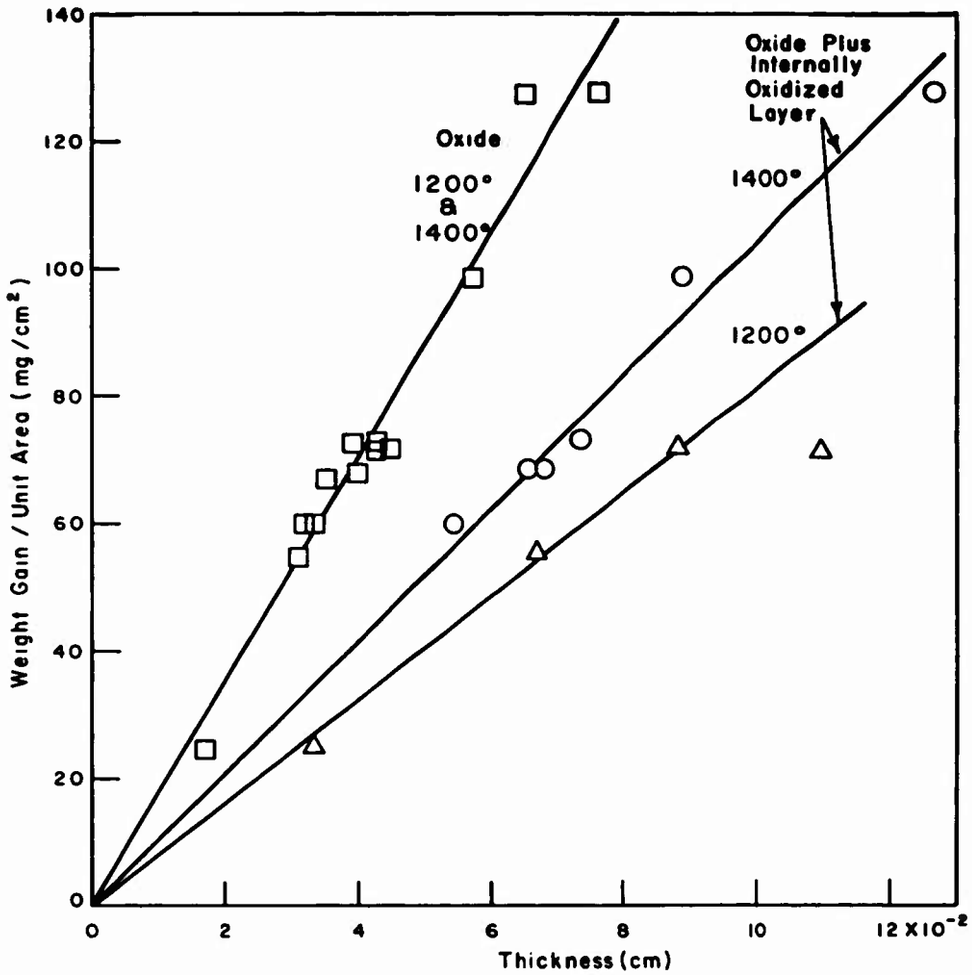

Fig. 14. Comparison of weight gain with oxide thickness and total oxide + internal oxidized layer for a Zr-30%Th alloy oxidized at 1200 and 1400°C.

ZrO_2-ThO_2 diagram is also known. The Th-O diagram is not known, but the existence of oxide particles in a melted button containing 1500 ppm O_2 suggests that the solubility of oxygen in thorium is low.

The metallographic, hardness, X-ray diffraction and microprobe results of alloys oxidized at 1200°C define the zirconium-thorium ratio of the phases observed, the structure at temperature or structures which result from transformation on cooling, and permit an estimate of the oxygen gradient in the substrate. These results have been used to construct the tentative 1200°C isotherm shown in Fig. 15. The cubic zirconia found in the oxide of the Zr-30%Th alloy has not been included in this diagram since Roy and Mumpton have shown that cubic zirconia observed in ThO_2-ZrO_2 mixtures is a metastable rather than stable phase.[6] It is not known whether the metastable phase is formed at temperature or on cooling, but a three-phased region should not be observed in the diffusion zone if the structure is at equilibrium. The low solubility of Th (0.60 a/o) in the oxygen-rich internally oxidized zone of the Zr-14 a/o Th and Zr-31 a/o Th alloys indicates that the oxygen content of the Zr-O phases at the limit of solubility of Th in these phases should not differ greatly from that in the Zr-O binary diagram.

The identification of the internal oxide as ThO_2 in these zones suggests that the two-phase regions containing ThO_2 exist at very low Th and O contents. Finally, the Zr contents of the ThO_2 in the oxide and $\alpha + ThO_2$ layers in the Th-lean alloys was defined as about 5 w/o; thus the ThO_2 single-phase region is defined with the additional assumption that this region is only slightly oxygen-lean. Three-phase regions were evident in the couples as boundaries between layers consisting of $\alpha + ThO_2 + ZrO_2$, and $\alpha + \beta + ThO_2$. Using these facts and assumptions in conjunction with the known binary diagrams, the 1200°C isotherm presented in Fig. 15 was constructed.

The diffusion paths of the Zr-14 a/o Th, Zr-31 a/o Th and Zr-60 a/o Th alloys at 1200°C, as derived from the experimental data, are also indicated in Fig. 15. For the Zr-14 a/o Th and Zr-31 a/o Th alloys the composition path through the ternary phase diagram is represented by a straight line connecting the composition of the base alloy with the oxygen corner, based on the numerous indications that the Zr to Th ratio throughout the various layers is essentially constant. The composition path crosses tie lines in the $\beta + ThO_2$ field, $\alpha + ThO_2$ field, and $ThO_2 + ZrO_2$ fields, which is consistent with the observed growth of three two-phased layers during oxidation. The linear path is also consistent with the Th concentration gradients observed in the $\alpha + ThO_2$ and $\beta + ThO_2$ layers in the specimens. The composition path of the Zr-48 a/o Th alloy is not shown since no microprobe and X-ray diffraction analyses were made.

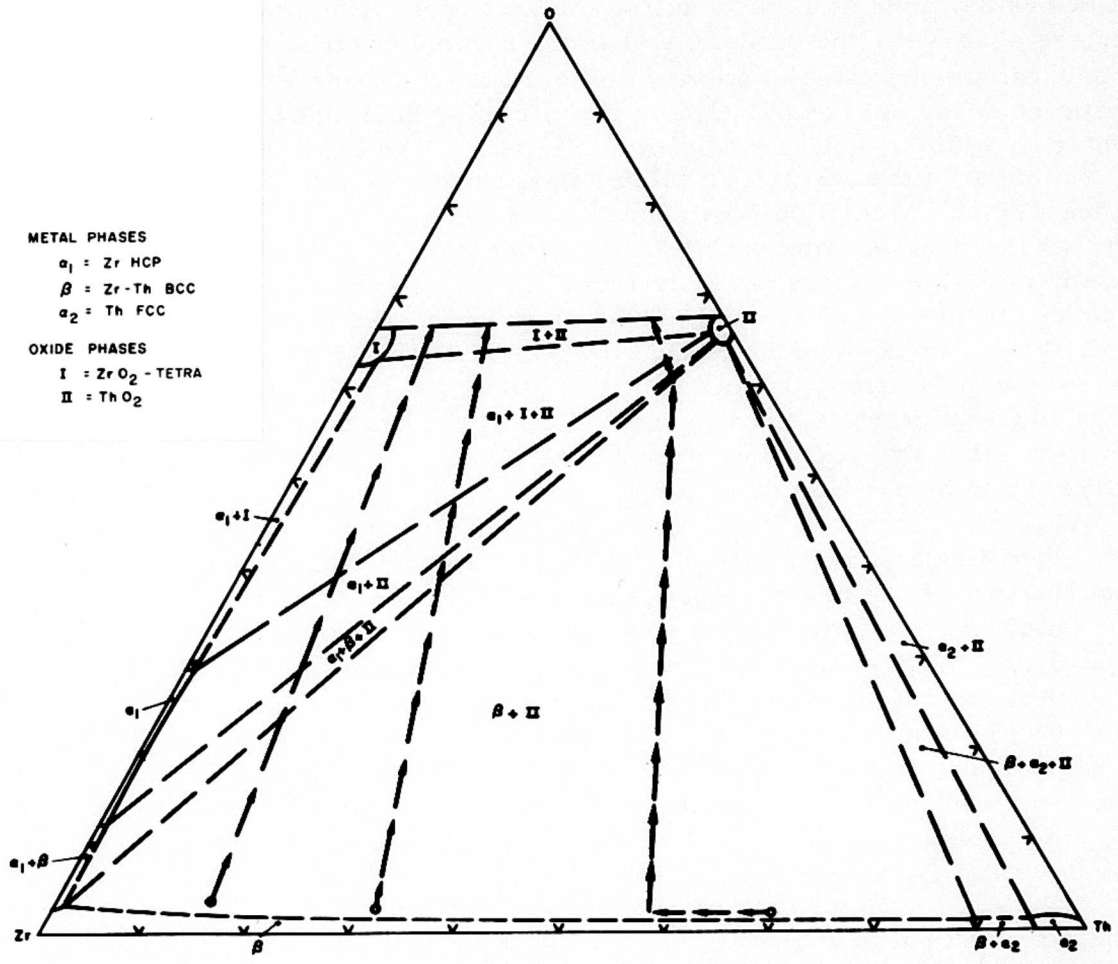

Fig. 15. Tentative phase diagram at 1200°C of Th-Zr-O system based on microprobe, X-ray and microstructure observations in oxidation of three Zr-Th alloys. Composition paths for oxidation of three Zr-Th alloys are indicated by arrowed lines.

In the 69 a/o Th alloy the situation is somewhat different because of the slight but noticeable concentration of Th to the oxide layer and the existence of a diffusion gradient in the metal substrate below the zone of oxidation. Therefore, the diffusion path through the $ZrO_2 + ThO_2$ region in the ternary section must lie slightly to the right of the straight line connecting the oxygen corner with the alloy composition. On the other hand, a diminution in Th content with no change in the concentration of oxygen in the substrate diffusion zone indicates that the diffusion path at the alloy terminus must initially proceed to the left, parallel to the base of the triangle, in the $\beta + ThO_2$ zone, and therefore lie to the left of a straight line connecting the alloy composition with the oxygen corner. Furthermore, since there was no appreciable zone of internal oxidation in the 69 a/o alloy oxidized in air, the diffusion path must be nearly, but not exactly, parallel to the tie lines in the $\beta + ThO_2$ zone. The fact that the metal-oxide interface was irregular indicates that it should not be drawn exactly parallel. These data have been used in drawing the compositional path for the Zr-69 Th alloy shown in Fig. 15.

The diffusion paths in Fig. 15 suggest a mechanism for the diffusion processes in these alloys during oxidation. In the Zr-14 to 31 a/o Th alloys, the flux of oxygen through both the oxide and the metal is so rapid that the solubility limits for oxygen are reached in the substrate before any noticeable diffusion of metal has occurred. Thorium oxide then nucleates and grows as an internal oxide until the matrix is locally depleted in Th, and the oxygen diffuses further into the substrate to nucleate additional ThO_2-rich particles at a point further removed from the surface of the specimen.

Since the thickness of the internally oxidized layers in relation to the thickness of the external oxide decreases with increasing temperature, the rate of diffusion of Th in the metal relative to that of oxygen in the oxide must increase with increasing temperature if this picture is correct.

A report by Speiser and Gordon[10] on the oxidation of Cb-Zr alloys also indicates that oxidation of alloys containing approximately 50 a/o Zr occurs by a process involving internal oxidation. However, in contrast to the internal oxide observed in the Th-Zr system, the internal oxide formed in the Zr-Cb system is a continuous Zr-rich oxide which forms from α-Zr platelets. Solution of oxygen in the Zr-Cb matrix causes the formation of α-Zr platelets which then oxidize at a more rapid rate and in preference to Cb-rich β; as a result a continuous network of internal oxide is formed.

The slower rate of oxygen diffusion in the Zr-69 a/o Th alloy permits the migration of a small excess of Th into the scale, and the development of a concentration gradient of Th in the metal substrate. The slower rate of oxygen diffusion may be related to the fact that the scale formed on this alloy was a continuous ThO_2 phase with dispersed ZrO_2, whereas the continuous phase in the scales on the 14 and 31 a/o Th alloys was ZrO_2.

Nitrogen has been ignored in the analysis of the diffusion paths even though ZrN was detected in the scales, and the oxidation rates were lower in the absence of nitrogen. The sequence and morphology of layers formed in the specimens oxidized in oxygen and argon-oxygen did not differ substantially from those formed in air, and it appears that the influence of nitrogen on the diffusion path was slight. For example, the layers formed on the 31 a/o Th alloy were identical in air and Ar-O, and the thickness of the layers for a given weight gain the same. Therefore the essentially straight line diffusion paths are typical for layer growth in air or Ar-O.

2.4 CONCLUSIONS

The results of our studies on the oxidation of Zr-Th alloys have led to the following conclusions:

1. Oxidation at temperatures from 750 to 1000°C is linear due to the spalling of the oxide formed, which results from the generation of mechanical stresses during the growth of the oxide.

2. Oxidation at 1200 to 1400°C is diffusion controlled and the oxides formed are compact and adherent for individual test specimens. However, thermal cycling in sequential testing produced breakaway in the Zr-70 and Zr-85% Th alloys but not in the thorium lean Zr-30 and 55%Th alloy.

3. The two-phased oxides formed at 1200°C and above accomodate increases in thickness of 10% or more without cracking or breakaway oxidation.

4. The rates of diffusion-controlled oxidation are considerably higher for alloys that form internally oxidized zones than for alloys that do not.

5. Insofar as the limited data on diffusion paths and the phase diagram in the Zr-Th-O system are valid:

(a) In those alloys in which oxidation rates are extremely rapid because of the overridingly rapid rate of oxygen diffusion, the composition path in the ternary phase diagram can be described by a straight line between the alloy composition and oxygen.

(b) Therefore, in systems in which oxygen diffusion dominates the oxidation process, a knowledge of the phase diagram of the ternary system is sufficient to predict the layers formed, and the diffusivities of all components in all phases need not be known.

(c) A decrease in the relative rate of diffusion of oxygen to that of the two metals permits transport of thorium by diffusion to the metal-oxide interface in the Zr-69% Th alloy. Thus, layers with metal diffusion gradients are possible even in alloys in which oxygen is the dominant diffusing component, and the composition path during oxidation must be determined for several compositions in each unexplored system.

6. The diffusion rates in ThO_2 - ZrO_2 two-phased oxides depend primarily on which oxide is the matrix oxide. In this system, oxygen diffuses more rapidly through a ZrO_2 matrix than one with a ThO_2 matrix.

7. Nitrogen in air increases the rate of oxygen diffusion and the rate of oxidation in all alloys studied.

3. THE Zr-Y-O AND THE Hf-Y-O SYSTEMS

There were several motives for studying the Zr-Y-O and the Hf-Y-O systems. Zirconium, hafnium, and yttrium oxides are not only refractory themselves, but a refractory compound oxide with a fluorite structure exists from 10-50% Y. It was desired to ascertain the conditions under which this oxide could be formed from solid or liquid Zr-Y and Hf-Y alloys. In the course of so doing, it was hoped to further define the rules governing the sequence and morphology of layers formed during oxidation of complex systems. Finally, if the compound oxide could be grown as an adherent layer, it was hoped to compare its behavior with that of the elementary oxides and gain insight into its desirability as a protective layer.

The Hf-Y phase diagram[11] is known and the yttrium-rich end of the Zr-Y phase diagram has also been defined.[12] Both are simple eutectic systems with limited solubility in the terminal phases (Figs. 16 and 17). The eutectic in the Zr-Y system is at 1310°C and the Hf-Y system is about 1430°C. An additional point of interest is that both Hf and Zr form refractory compounds with rhenium which could conceivably be used as a reservoir material in a protective coating system.

The ZrO_2-Y_2O_3 quasi-binary phase diagram is known and given in Appendix II, Fig. II-3.[13] A cubic oxide exists from about 10 to 50 mole % yttria, stable to room temperature. Presumably the HfO_2-Y_2O_3 diagram is similar. All three oxides are refractory and the eutectic in the ZrO_2-Y_2O_3 system is above 2000°C. The Hf-O phase diagram in Fig. II-4 of Appendix II is similar to the Zr-O diagram except that monoclinic HfO_2 is stable to about 1700°C instead of 900°C.[14]

3.1 PROCEDURE

Alloys of Hf-Y containing from 5 to 50% Y and alloys of Zr-Y containing 5 to 100% Y were arc melted to form buttons. The buttons were forged and rolled at approximately 800°C to 0.100-in.-thick sheet. The sheet was sectioned into coupons, surface ground, and a hole was drilled in one end for support during oxidation. Alloys containing yttrium in amounts less than or equal to 50% were vacuum-annealed 6 hours at 1200°C and yttrium-rich alloys were annealed at 900°C. All alloys were oxidized in a platinum-rhodium wound furnace in flowing dry air at temperatures from 800 to 1600°C. Alloys of Zr plus 35, 42.5 and 50 a/o Y were oxidized at 1700 and 1800°C with an induction heating system. Compositions and oxidation temperatures are indicated by the circles in Figs. 16 and 17. Samples of the Zr-5, 10, 25, 35 and 50 a/o Y oxidized 1/2 hour at 1200°C and samples of the Zr-15, 25, 35 and 50 a/o Y alloys oxidized 1/4 hour at

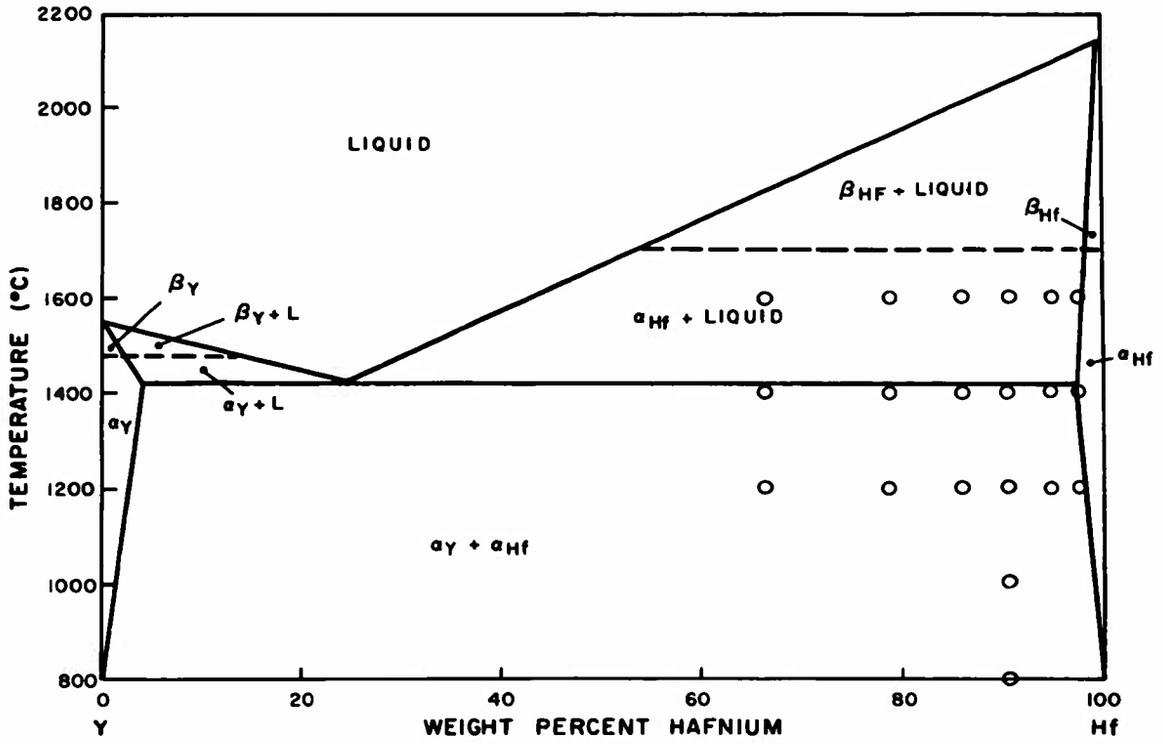

Fig. 16. Yttrium-hafnium constitution diagram according to Lundine and Klodt.[11] Points indicate composition and temperature of oxidation tests.

1600°C were submitted for X-ray and microprobe examination. Metallographic and weight-gain data were used to evaluate the kinetics of oxidation in both systems at temperatures up to 1600°C.

Even at temperatures above the melting point of the alloys, samples could be suspended from a platinum wire supported on a zirconia crucible during oxidation, the strength of the oxide being sufficient to hold the sample intact during test. In the induction furnace test the samples were supported on a zirconia crucible standing on end, and the external oxide formed during heating provided sufficient strength to prevent collapse of samples of the three compositions tested.

In the course of the investigations, the similarities in behavior suggested that a comprehensive study be conducted on only one system, the Zr-Y-O system. A brief discussion of the oxidation of the Hf-Y alloys will precede the presentation and discussion of results for the Zr-Y-O system.

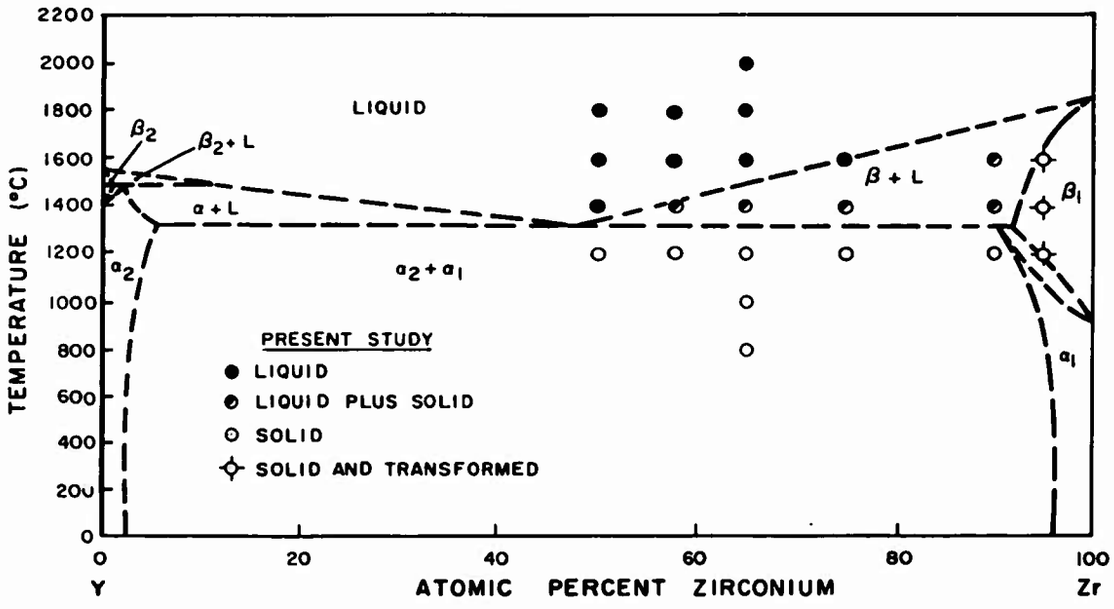

Fig. 17. A tentative Zr-Y phase diagram indicated by Reference 12 and results of the present study. Circled points indicate compositions and temperatures of oxidation tests.

3.2 Hf-Y-O SYSTEM - RESULTS AND DISCUSSION

The weight gains for various temperatures and times during the oxidation of Hf-Y alloys are given in Table IV. Plots of the log weight gain vs log time for all compositions indicated parabolic or approximately parabolic growth at temperatures of 1200 to 1600°C. Only one alloy, Hf-18 a/o Y, was oxidized at a lower temperature, 1000°C. Growth was linear rather than parabolic, and porous nonprotective oxides were formed. At 1200 to 1600°C oxides formed on the hafnium-yttrium alloys are generally protective at temperature but show considerable spalling and edge cracking after cooling to room temperature, as indicated in Fig. 18. The oxide formed on the hafnium-yttrium alloys is two phased and the morphology in the oxide resembles that of the substrate from which it is formed, as shown in Fig. 19 for the Hf-5, 10 and 25 a/o Y alloys. The micrographs also indicate the tendency to spall at the metal (or α-Hf)-oxide interface. Some evidence of internal cracking is apparent in the oxide formed on the Hf-5 a/o Y alloy at 1200 and 1400°C.

Two samples of the Hf-18 a/o Y alloys, one oxidized at 1400°C for 1/2 hour and the other at 1600°C for 1/4 hour, were submitted for X-ray diffraction, microprobe, X-ray fluorescent analysis; the results are given in Appendix I, Section 4.4. In brief, the results of X-ray fluorescent analysis show little change in the hafnium-to-yttrium ratio throughout the oxygen-affected zones. Monoclinic and cubic HfO_2 are present, as well as a small amount of Y_2O_3.

The effect of yttrium content on the weight gain from oxidation for one hour at 1200, 1400 and 1600°C is given in Fig. 20. The weight gain in one hour increases to a maximum at about 10 a/o Y, and the weight gains of all compositions are higher than the previously determined[2] parabolic growth rate of HfO_2 on Hf-Sn alloys.

Cracking and spalling of the oxide made microprobe analysis difficult. Since the behavior of the Hf-Y and Zr-Y alloys under oxidizing conditions was observed to be quite similar, it was decided to concentrate on the Zr-Y system, particularly since the zirconia-yttria phase diagram is known, while the hafnia-yttria is not.

3.3 Zr-Y-O SYSTEM - RESULTS

3.3.1 Kinetics of Oxidation

The weight gains during oxidation of the Zr-Y alloys containing 5, 10, 25 a/o Y are compared with those for pure zirconium in Table V at temperatures of 1200 to 1600°C. The oxidation of pure zirconium is

TABLE IV

Weight Gain and Thickness Observations in the Oxidation of Hf-Y Alloys at 1000° to 1600°C in Dry Flowing Air

Alloy composition	Temp °C	Specific weight gain						Thickness		Remarks*
		Time (hrs)	Δw/a mg/cm²	Time (hrs)	Δw/a mg/cm²	Time (hrs)	Δw/a mg/cm²	Time (hrs)	Oxide + Int. oxide (mils)	
Hf-5 a/o Y	1200	0.25	44.3	0.5	57.4	1	75.0	0.5	21.3	
	1400	0.25	68.3	0.5	86.4	1	120.0	0.5	27.8	
	1600	0.084	24.8	0.25	48.1	0.5	62.4	0.5	41.2	
Hf-10 a/o Y	1200	0.25	60.1	0.5	76.5	1.0	114.4	0.25	15.7	
	1400	0.25	84.7	0.5	115.6	1.0	98.2	0.25	27.9	
	1600	0.084	60.2	0.25	107.4	-	--	0.084	13.9	
Hf-18 a/o Y	1000	0.25	21.1	1.67	76.9	2.0	117.1	1.0	18.6	1/n = 1
				1.0	65.3					
	1200	0.25	41.4	0.5	81.8	1.0	85.6	1.0	18.0	
		0.25	55.0							
	1400	0.084	36.4	0.5	92.7	1.0	80.4	0.17	15.5	
		0.17	53.4	0.5	80.1			0.5	34.3	
	1600	0.084	61.8	0.25	111.7	0.25	73.6	0.087	20.5	
Hf-25 Y	1200	0.5	75.9	1.0	120.2	2.0	148.6	0.5	19.8	
	1400	0.25	69.5	0.5	99.7	1.0	91.0	0.5	24.9	
	1600	0.084	49.5	0.25	73.0			0.084	13.6	
Hf-35 Y	1200	0.50	45.8	1.0	64.4	2.0	152.5	0.5	10.9	1/n = 1
	1400	0.25	67.1	0.5	42.1	1.0	99.7	0.5	11.9	at > 1 hour
				0.5	53.6					
	1600	0.084		0.25	72.1			0.084	12.2	1/n ≅ 0.3
Hf-50 Y	1200	0.5	30.5	1.0	42.7	2.0	72.3	0.5	8.4	
	1400	0.25	54.0	0.5	65.8	1.0	83.1	0.5	18.6	1/n ≅ 0.3
	1600	0.084	45.8	0.25	70.0			0.084	11.1	

* Log-log slope is approximately 0.5 unless indicated.

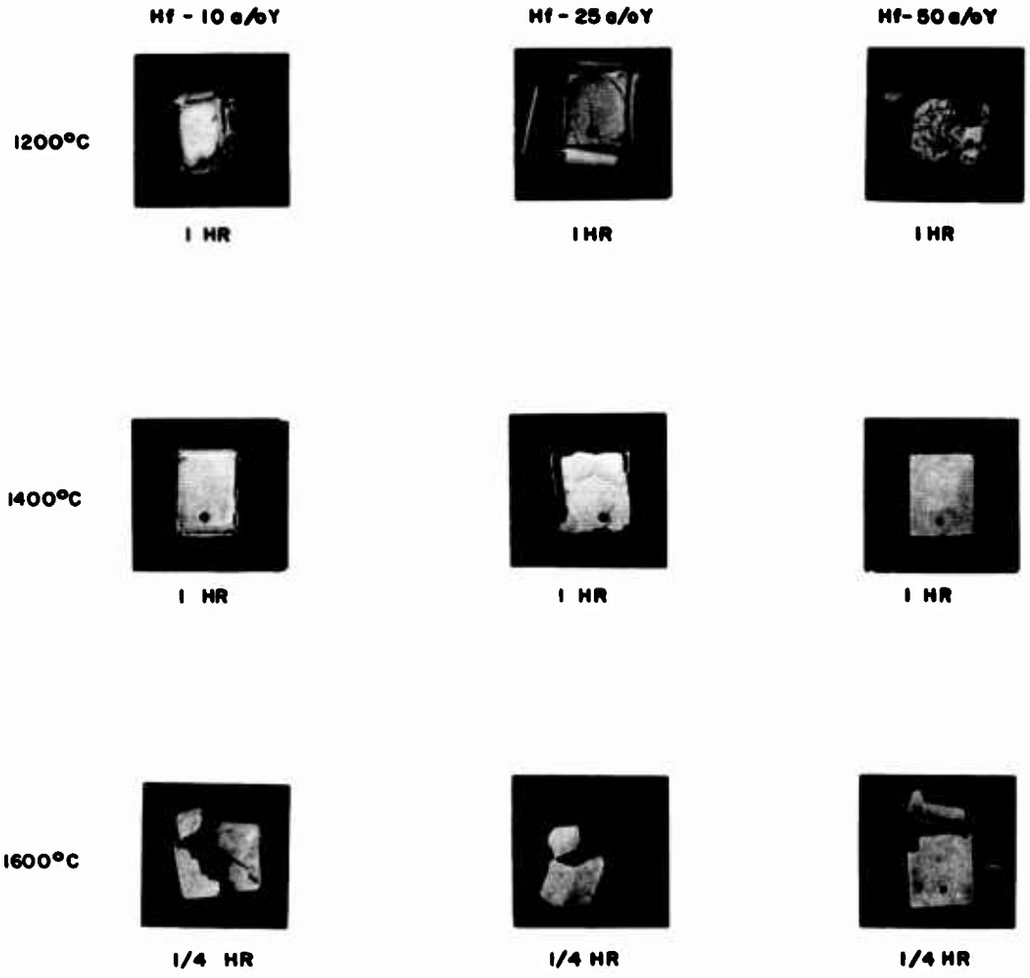

Fig. 18. External appearance of oxidized Hf-Y alloy.

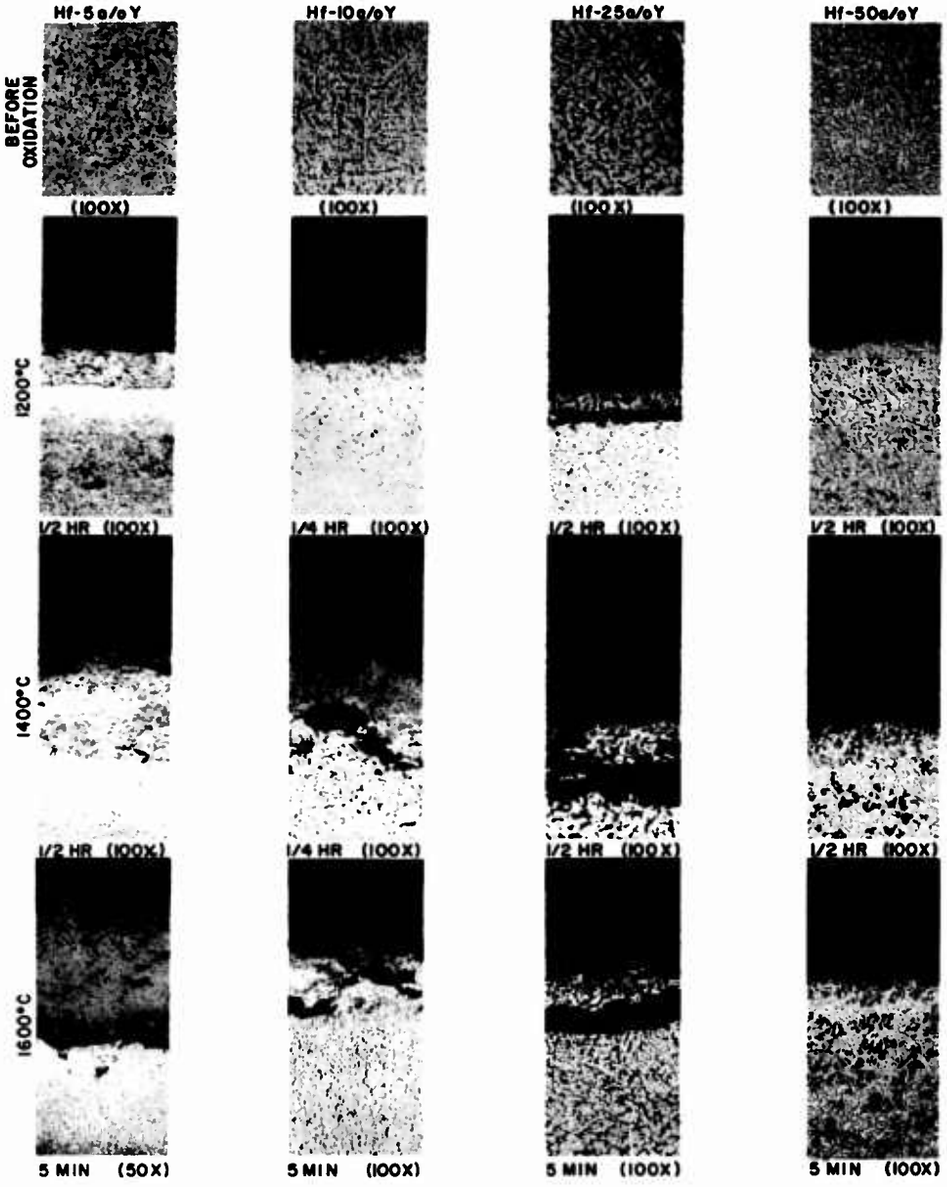

Fig. 19. Layers formed in the oxidation of Hf-Y alloys in air at 1200 to 1600°C (magnification reduced by 45% in reproduction).

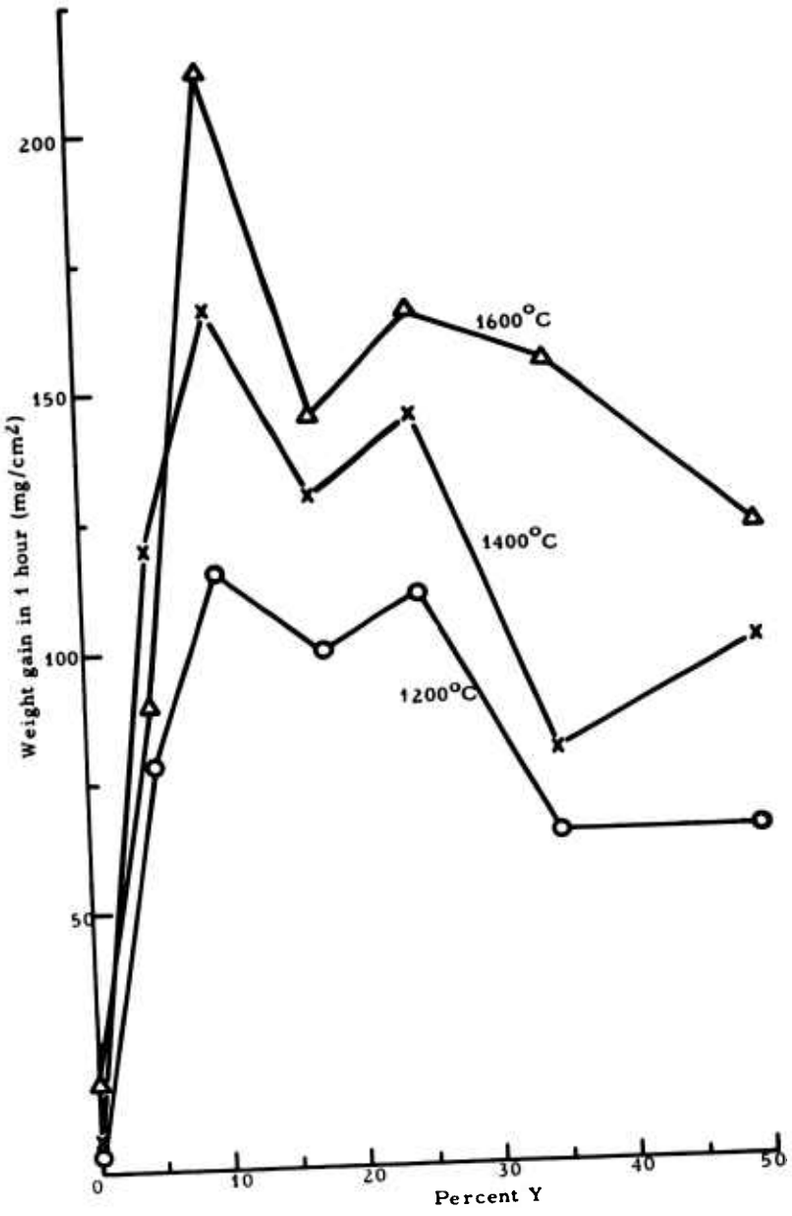

Fig. 20. The effect of Y content on the weight gained in 1 hour oxidation of Hf-Y alloys. The weight gains for 0% Hf were obtained on liquid Hf-Sn alloys in Reference 2.

TABLE V

Weight Gains During the Oxidation of Zr-Y Alloys

	Pure Zr		Zr 5 a/o Y		Zr 10 a/o Y		Zr 25 a/o Y	
Temp °C	Time (hr)	Δw/a mg/cm²	Time (hr)	Δw/a mg/cm²	Time (hr)	Δw/a mg/cm²	Time (hr)	Δw/a mg/cm²
1200	0.084	25.8	0.084	21.8	0.084	43.1	0.084	29.7
	0.25	74.7	0.25	45.2				
	0.5	110.9	0.5	43.5	0.5	85.4	0.5	70.6
			0.5	73.7			0.5	59.1
			0.5	81.5			0.5	75.0
	1.0	165.8(a)	1.0	126.4	1.0	128.8	1.0	78.3
			2.0	141.1	2.0	135.4	2.0	103.3
1400	0.084	64.2	0.084	77.1	0.084	42.6	0.084	68.9
			0.084	89.5	0.25	78.8	0.084	39.1
	0.25	103.8	0.25	71.5	0.25	82.1	0.25	97.1
	0.5	141.4	0.5	104.7	0.5	79.5	0.25	60.1
	1.0	166.9(a)	1.0	140.3	1.0	143.5	0.5	120.8
							0.5	79.5
							1.0	100.8
1600	0.084	104.	0.084	100.0	0.084	89.1	0.084	34.6
			0.084	90.3			0.25	79.1
	0.25	154.	0.25	142.0	0.25	130.6	0.25	91.9
	0.5	173(a)	0.25	145.3			0.5	60.4
	1.0	179(a)					1.0	141.0

(a) Sample has oxygen affected zone throughout.

quite rapid and linear rates are observed until appreciable portions of the cross-section of the sample are consumed. The growth rates at 1200 to 1600°C for the 5, 10 and 25 a/o Y alloys are parabolic or approximately parabolic with one anomaly. In the Zr-25 a/o Y alloy oxidized at 1600°C, considerable scatter was observed.

The weights gained during the oxidation of alloys containing 35, 42.5 and and 50 a/o Y at temperatures from 1000 to 2000°C are given in Figs. 21 to 23. The rate of growth of the Zr-35 a/o Y alloy at 1000°C is linear, indicating breakaway. At temperatures of 1200 and 1400°C the growth rate is parabolic or approximately parabolic for all three compositions. At 1600°C again considerable scatter is observed in the data for all three alloys. Two lines with a slope of 1/2 have been used to represent these points because, as will be described in detail later, two different oxidation processes were observed, proceeding at different rates, but both apparently diffusion controlled. At 1800°C the rate of growth is parabolic and unexpectedly low in the Zr-35 and 42.5 a/o Y alloys; the weight gain after 1/4 hour was 58 and 50 gm/cm^2 respectively. In the Zr-50 a/o Y alloy at 1800°C weight gains of about 45 gm/cm^2 were indicated for alloys oxidized 5, 10 and 15 minutes; the weight gain for the three times is essentially constant.

The results of oxidation of the Zr-95 a/o Y alloy and pure yttrium at 1200, 1400 and 1500°C are given in Fig. 24. Tests at 1600°C on these two alloys were not possible because the samples were extremely fluid at temperature. The data for pure yttrium could not easily be fitted by a straight line and it appears that more than one oxidation process was operative. Rates of weight gain for times up to 1/2 hour on the Zr-95 a/o Y alloy are parabolic and low. Breakaway is observed in the Zr-95 a/o Y alloy at 1200°C for times greater than 1/2 hour and at 1400°C for times greater than 1 hour.

Samples of the Zr-35 and Zr-5 a/o Y alloys were oxidized in argon-20%-oxygen mixture to determine if nitrogen influenced the rate of oxidation of these alloys. At 1400°C for the Zr-5 a/o and 1200°C and 1400°C for the Zr-35 a/o Y alloys, nitrogen in the air had no influence on the rate of oxidation. In the Zr-5 a/o Y alloy at 1200°C, the rate of weight gain in the absence of nitrogen was approximately half that in dry flowing air. The reasons for the rather isolated composition and temperature at which nitrogen influences the oxidation rate in the Zr-Y system is not obvious.

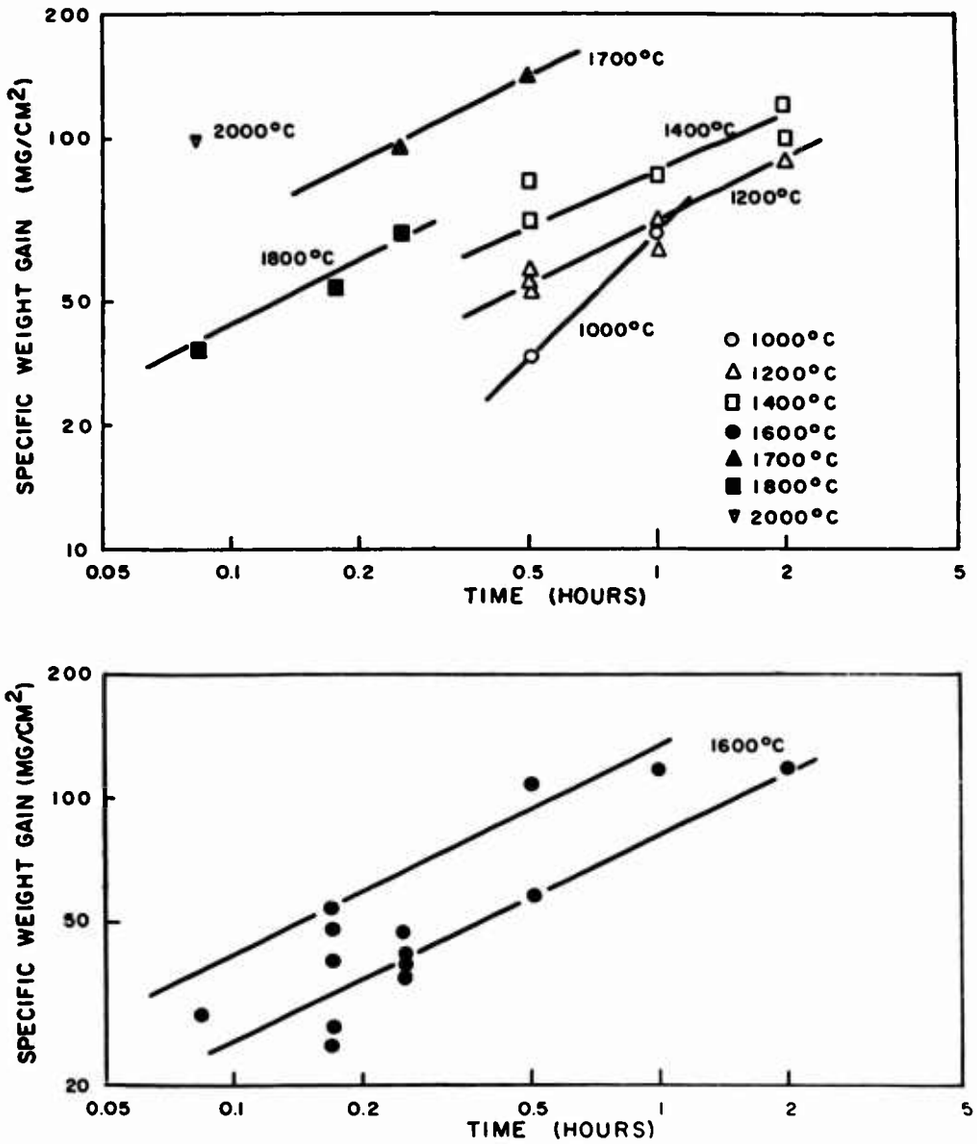

Fig. 21. Weight gains in oxidation of Zr-35 a/o Y alloy in air at 1000 to 2000°C.

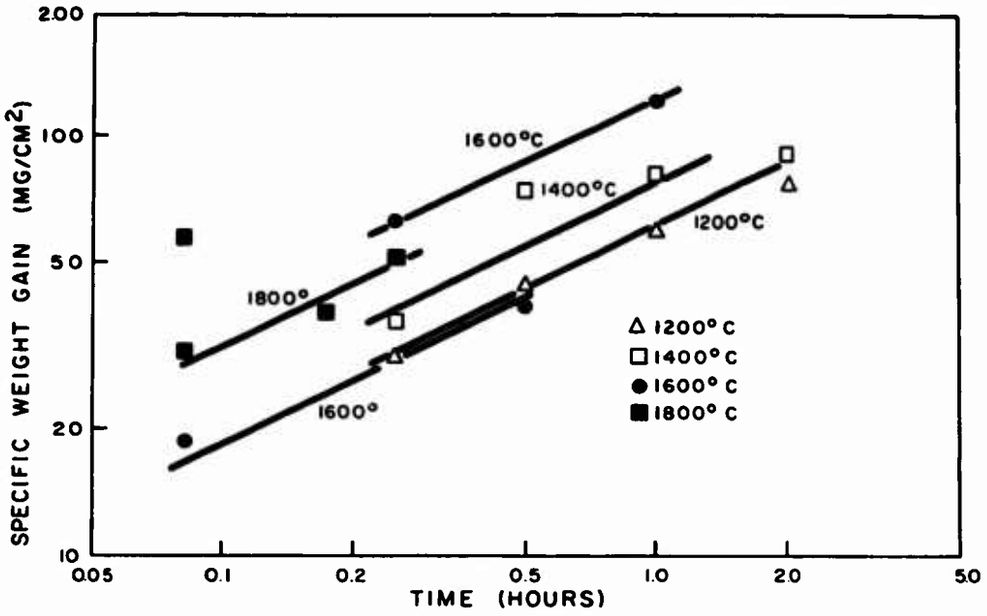

Fig. 22. Weight gains in oxidation of Zr-42.5 a/o Y alloy in air at 1200 to 1800°C.

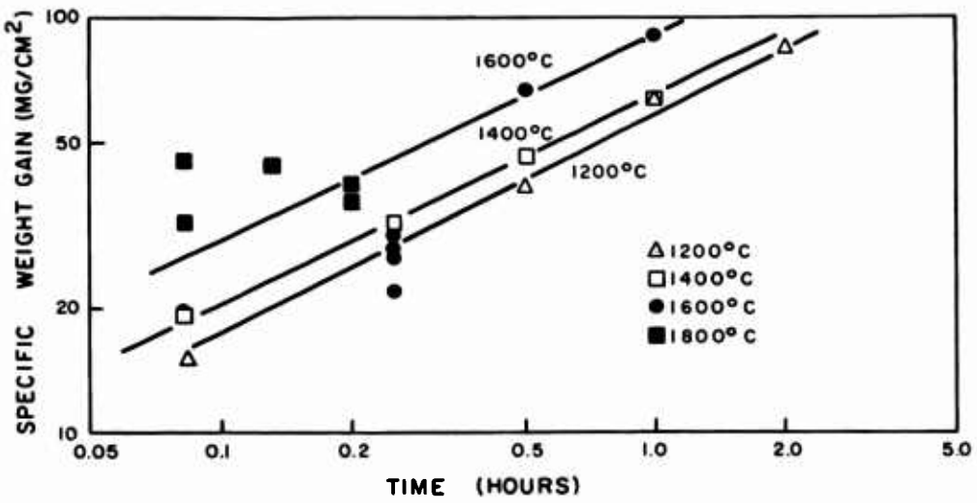

Fig. 23. Weight gains in oxidation of Zr-50 a/o Y alloy in air at 1200 to 1800°C.

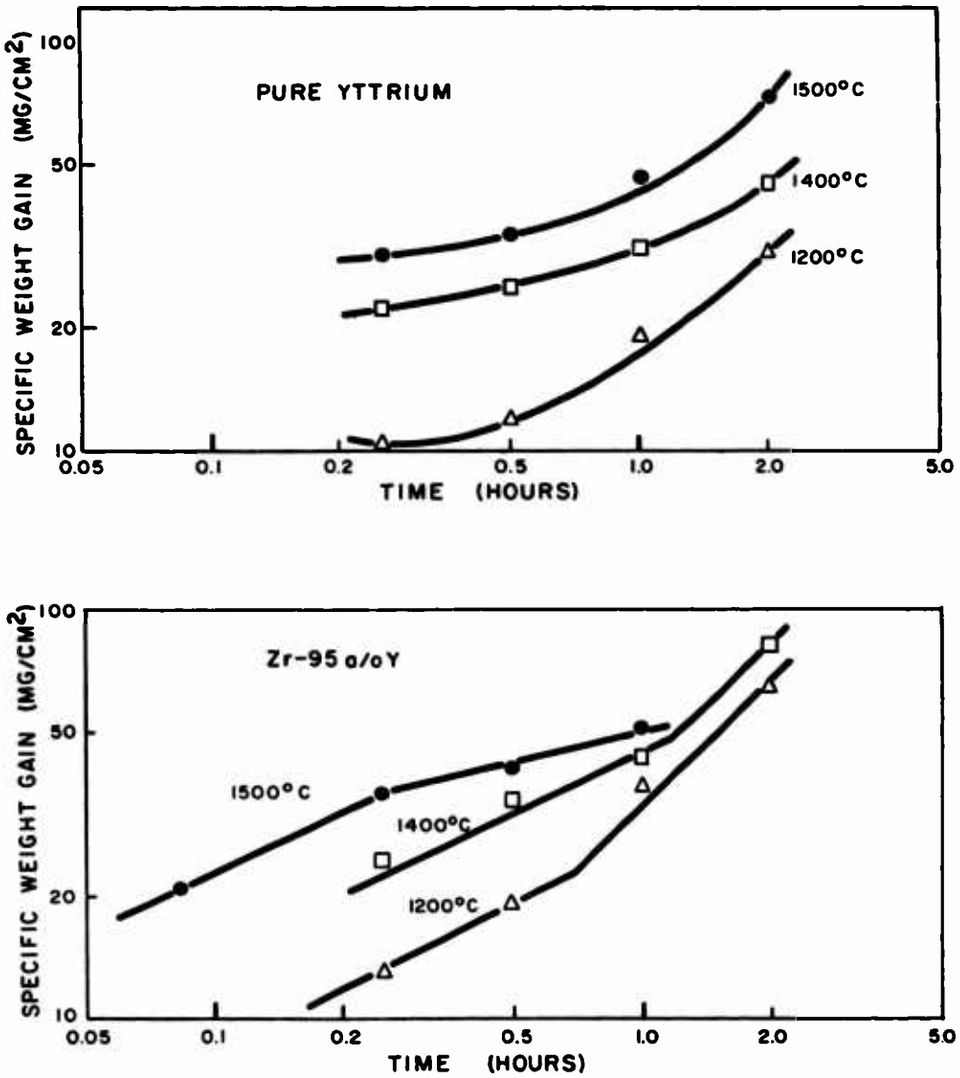

Fig. 24. Weight gains in oxidation of Zr-95 a/o Y and pure yttrium at 1200 to 1500°C.

3.3.2 External Appearance and Microstructures of Oxidized Samples

The external appearance of the oxide formed on the Zr-Y alloys in the range of 5 to 50 a/o Y is quite different from that of the oxide formed on the Hf-Y alloy, as shown in Fig. 25; the oxides formed are in general adherent and crack-free even at the edges after cooling to room temperature. One exception is the Zr-50 a/o Y alloy oxidized at 1200°C; this sample showed numerous surface cracks and edge cracks similar to those observed in the Hf-Y-O system. Most compositions tested at 1600°C are liquid at temperature, and the fact that the oxide remains intact, even though the samples are liquid and suspended from a platinum-rhodium rod, is of particular interest. This suggests that the oxide and oxygen-saturated internal layers formed on heating have sufficient strength to support the remaining liquid at 1400 to 2000°C.

The microstructures of pure Zr, and the Zr-5, 10 and 25 a/o Y alloys after oxidation are shown in Fig. 26. The oxide formed on pure zirconium at 1200 and 1400°C is quite badly spalled, suggesting that the linear oxidation rate (breakaway) is the result of fracture in the oxide or at the metal-oxide interface, caused by mechanical stresses. At 1600°C, although the oxide is porous, it does appear to be free of cracks and grows parabolically. The oxide formed in the Zr-5 a/o and Zr-10 a/o Y alloys seems to be sound, dense and adherent. A trace amount of second phase is visible in the oxide formed on Zr-5 a/o Y alloy, and the amount of this phase increases with yttrium content.

Two different morphologies are exhibited by the Zr-25 a/o Y alloy oxidized at 1600°C. The oxide on the sample oxidized for 1/4 hour is thicker, consistent with the higher weight gain, than that on the sample oxidized for 1/2 hour. The continuous layer of Y_2O_3 observed in the sample oxidized for 1/2 hour did not form on the sample oxidized for 1/4 hour. Apparently the morphology of the scale is somewhat dependent upon the heating rate or other unknown factors. The rate of weight gain seems to depend on whether or not a continuous layer of single-phased oxide, presumably Y_2O_3, is initially formed, and it is for this reason that so much scatter in the points for the alloys oxidized at 1600°C was observed.

Internal oxidation is observed in all alloys containing yttrium. A single-phased metal + oxide region is present beneath the scale in many of the alloys, evidently α-Zr + Y_2O_3 at temperature. This is followed by a zone consisting of α-Zr + α-Y + Y_2O_3 at room temperature and the morphology of the oxide suggests that the solid or liquid yttrium-rich phase was oxidized in situ or that considerable oxide precipitated from it on cooling. Peculiar metal + oxide layers are visible in a number of the photomicrographs, e.g., pure Zr at 1200°C, and in addition porosity is

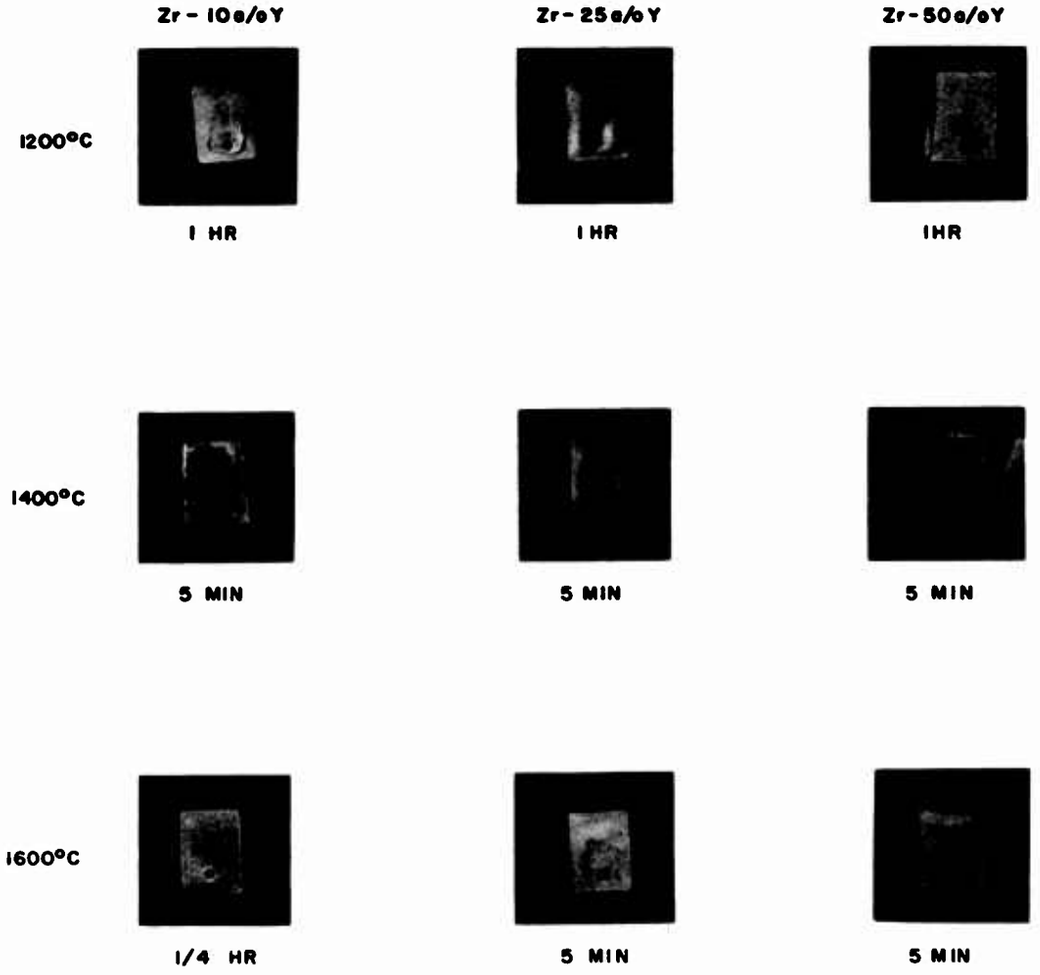

Fig. 25. External appearance of oxidized Zr-Y alloy.

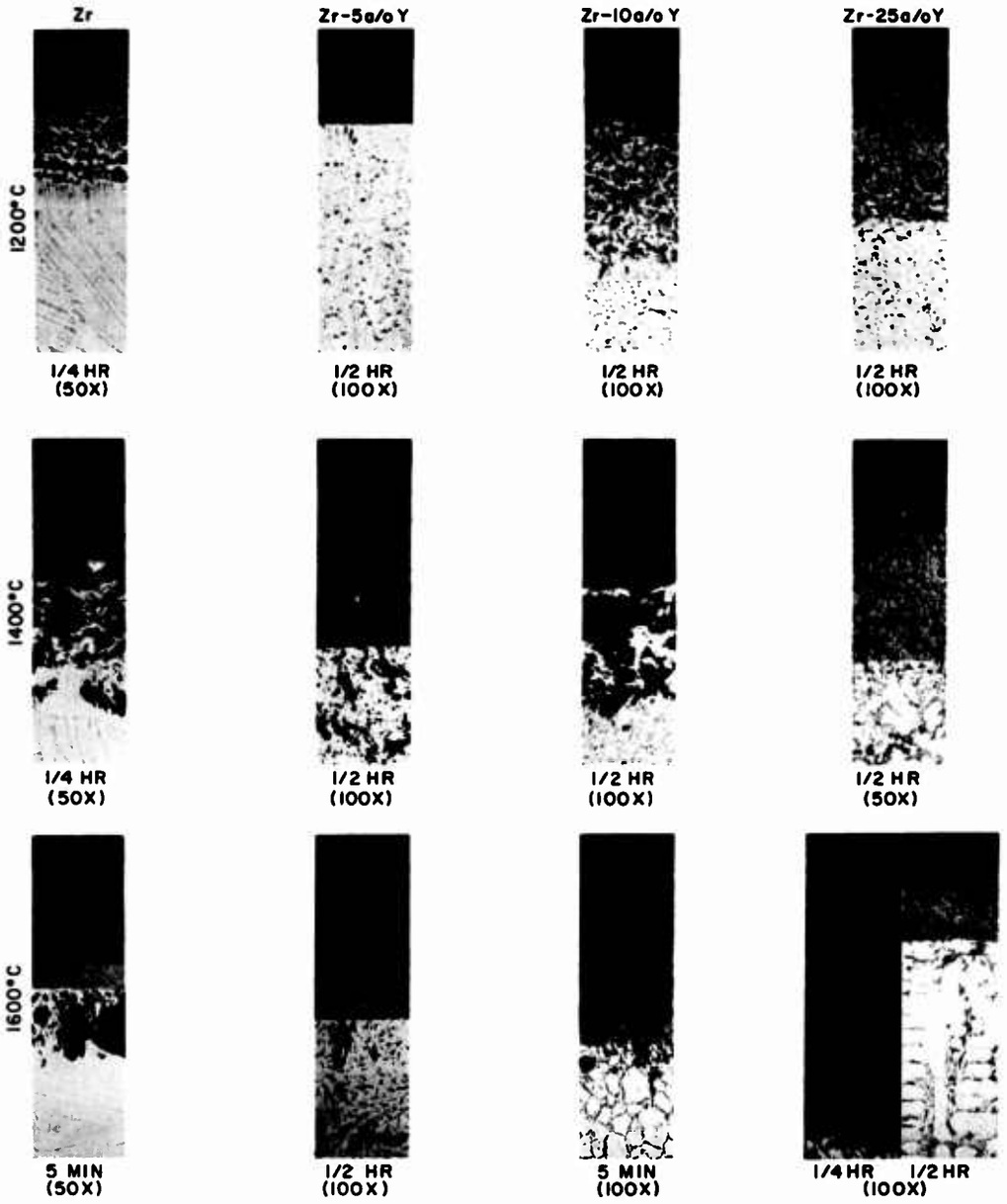

Fig. 26. Microstructures of layers formed in the oxidation of Zr-Y alloys (magnification reduced by 35% in reproduction).

observed in the substrate of a number of the alloys oxidized at 1400 and 1600°C. The structures of the unaffected metal regions suggest that the 5 a/o Y alloy was solid at 1600°C, while the 10 and 25 a/o Y alloys were partially or completely liquid at 1400 to 1600°C.

Samples of the Zr-30 to 50 a/o Y are shown in Fig. 27. Those samples oxidized at 1200°C were all solid at temperature, while the alloys oxidized at 1400°C were partially or completely liquid at temperature. The oxides formed are similar in that they contain light ZrO_2 phases and a dark Y_2O_3 phase. The Y_2O_3 phase tends to occur in the form of a network around the ZrO_2 phase. A zone of internal oxidation exists in all alloys at 1200 and 1400°C in which the yttrium-rich metallic phase appears to have oxidized in situ to form essentially Y_2O_3. At 1400°C this metallic phase was apparently liquid.

At 1600°C, oxidation is characterized by the formation of a two-phased oxide on the external surface of the sample; next, a single-phased Y_2O_3 layer; then an internally oxidized zone. In the Zr-50 a/o Y alloy there was a suggestion of a metallic layer free of oxide just beneath the scale in the 1/4-hour sample. The external two-phased oxide formed on the Zr-35 a/o Y alloy after 5, 15 and 30 minutes is essentially the same thickness for all three times. Only the single-phased Y_2O_3 layer grows with time, suggesting that the external oxide was formed on heating.

The layers formed at 1600°C, associated with low and high weight gains in these alloys, may be compared by referring to the 1/4- and 1/2-hour samples of the Zr 50 a/o Y alloy oxidized at 1600°C (Fig. 27). The 1/4-hour sample exhibits a sound coherent layer of dark oxide (Y_2O_3) at the metal-oxide interface which is absent from the 1/2-hour sample. Here, as in the 25 a/o Y sample (Fig. 26) the low rate of weight gain is associated with the presence of this single-phased oxide layer.

The layers formed on all three alloys at 1800°C are similar except for the thickness of the external two-phased oxide which presumably formed during heating. These samples were heated by standing on end on a zirconia crucible in an induction furnace. The sample was held intact by the external oxide even though the metal inside was liquid at 1800°C. In all three samples a single-phased layer that is similar in appearance to the Y_2O_3 that was identified at lower temperatures, forms a dense diffusion barrier. Beneath this, in all three alloys a metal + oxide layer forms in a morphology which suggests precipitation of the oxide from a saturated solution on cooling. It is possible that an oxygen-saturated zirconium-rich phase could exist as a solid layer at 1800°C, according to the phase diagrams, which would decompose to α-Zr + Y_2O_3 on cooling.

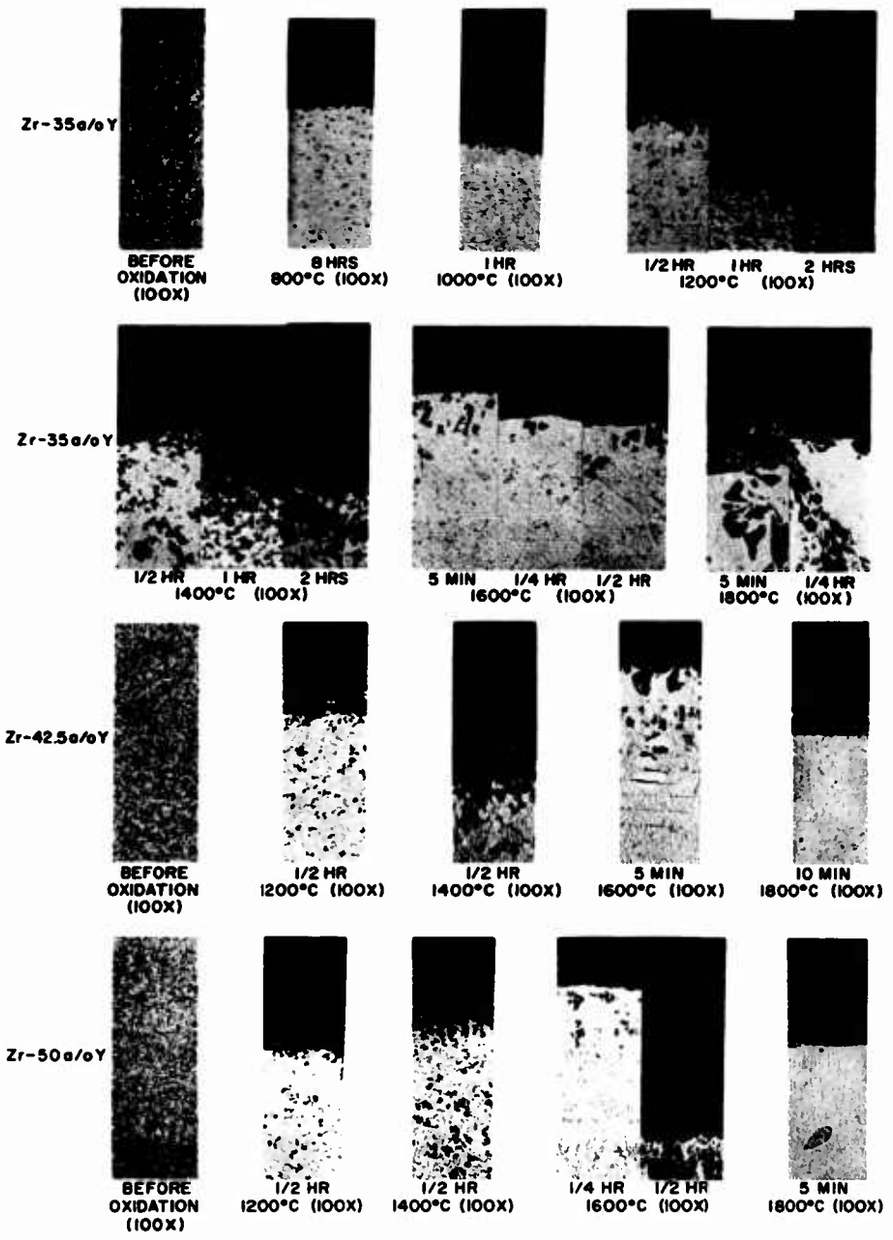

Fig. 27. Microstructures of layers formed in the oxidation of Zr-Y alloys (magnification reduced by ~50% in reproduction).

The microstructures of the Zr-95 a/o Y alloy and pure yttrium in Fig. 28 are peculiar in that angular and lamellar oxides are present throughout the metal after oxidation. At 1200°C the internal oxide is predominantly angular in shape. In pure yttrium, although very little oxide appears on the surface after 1/2 hour at 1200°C, the sample is full of internal oxide, suggesting that solution and diffusion of oxygen in the metal is a major process in the initial stage of oxidation of these alloys. Eventually, oxide layers form on all alloys, but the metallic portion of the sample is uniformly a two-phased metal + oxide on cooling.

The shapes of the particles suggested that the oxide had formed from a supersaturated solid solution; therefore a sample of each alloy was quenched in molten Woods metal after oxidation at 1500°C. The array of oxide lamelli is much finer and the thickness of the platelets is reduced by the increased cooling rate (Fig. 28), indicating that the oxygen was in solid solution at the temperature of test. Reference 12 gives a maximum solubility of 0.1% oxygen in yttrium at the liquidus; however, the amount of oxide precipitated suggests a larger oxygen solubility.

The oxide on the yttrium-rich alloys is separated from the substrate and apparently contains flaws. The kinetic data in Fig. 24 indicate that breakaway eventually occurred in the Zr-95 a/o Y alloy at 1200 and 1400°C. However, the overall rate of oxidation was considerably lower in these alloys than in the higher Zr compositions, and the oxide was evidently initially adherent.

3.3.3 Structure and Composition Identification

Electron microprobe, X-ray diffraction and fluorescent analysis of the zirconium-rich Zr-Y alloys oxidized at 1200 and 1600°C are discussed in Appendix I, Section 4.3. The formation of a single-phased layer of cubic ZrO_2 is not observed, although cubic ZrO_2 is present in the oxides. On the contrary, layers which contain three phases, cubic and monoclinic ZrO_2 + Y_2O_3, are observed on the alloys oxidized at 1200°C and on the external surface of the alloys oxidized at 1600°C. The black single-phased layer which grows on the liquid alloys has been identified as 98 mole % Y_2O_3 by microprobe analysis. In addition to the microprobe analysis, the metallic portions of the oxygen-saturated pure yttrium samples oxidized at 1200, 1400 and 1500°C were submitted for oxygen and nitrogen analysis. The results are as follows:

Temperature (°C)	Oxygen (a/o)	Nitrogen (%)
1200 - 1 hr	15.3	0.129
1400 - 1 hr	25.9	0.183
1500 - 1/2 hr	30.6	0.230

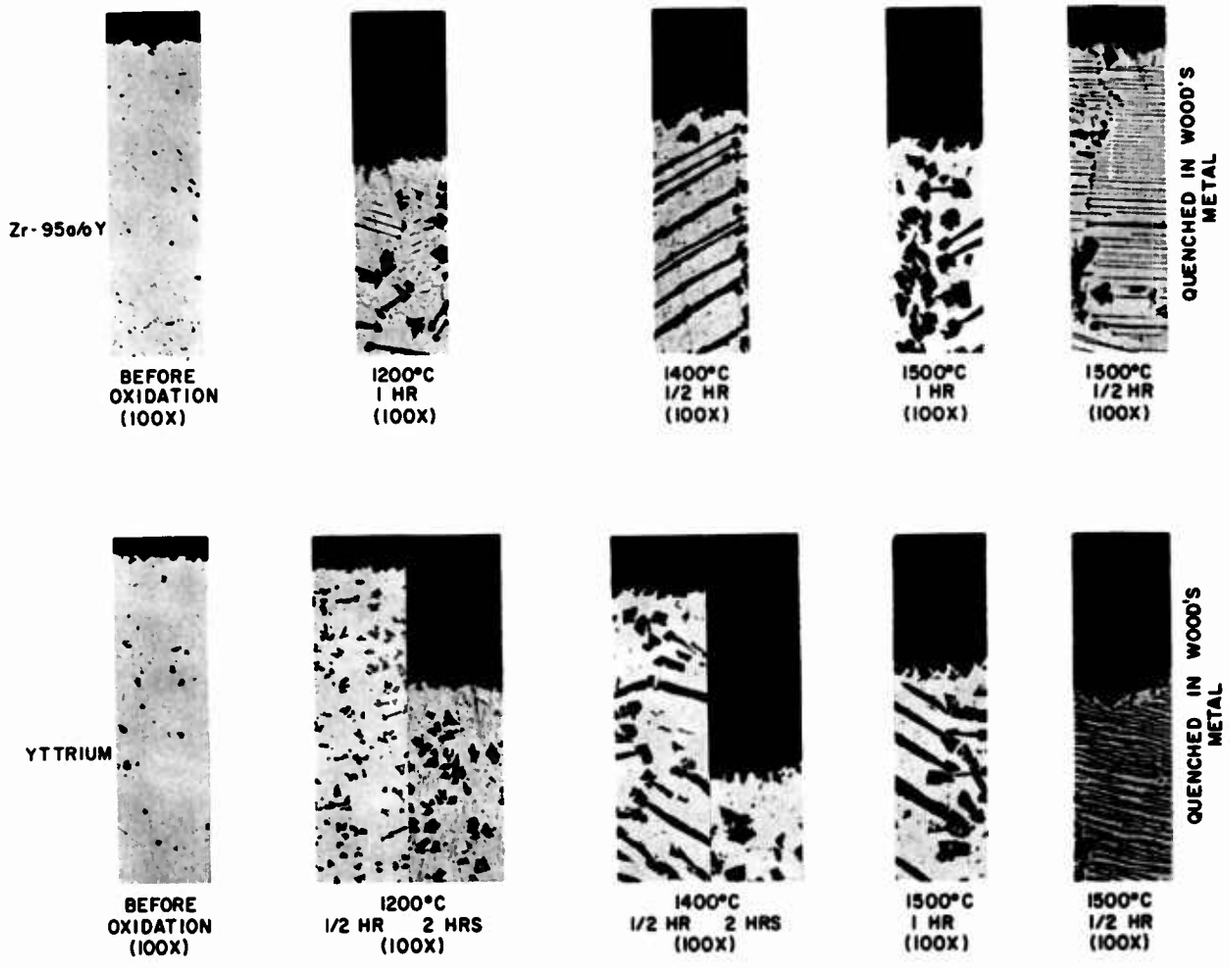

Fig. 28. Microstructures of layers formed in the oxidation of Zr-Y alloys (magnification reduced by ~40% in reproduction).

If it is assumed that the oxygen was in solid solution at temperature, the oxygen values shown in the preceding table should represent a reasonable approximation to the oxygen solubility at the three temperatures.

By combining the results of X-ray, microprobe, metallographic, and microhardness analyses it is possible to describe the sequence of layers formed in the Zr-Y alloys at 1200°C and also to gain insight into the sequence of events that occur and the layers that form upon oxidation at 1600°C.

X-ray fluorescence analysis of the layers formed indicated that the zirconium-to-yttrium ratio did not change from layer to layer. Therefore, transport of the metal ions evidently did not occur and oxygen diffusion dominated the oxidation process. The metallic phases originally present were oxidized more or less in situ and oxides as well may have precipitated on cooling, to produce complex layers containing more than two phases. The sequences of layers formed are described below:

1. In the Zr-5 a/o Y alloy the layers are as follows:

    a. The external oxide is largely monoclinic ZrO_2 which has formed on cooling from tetragonal ZrO_2. Y_2O_3 and yttrium-stabilized cubic ZrO_2 occur as isolated particles in the oxide.

    b. The layer beneath the oxide is essentially α-Zr at temperature but contains Y_2O_3, probably formed by oxidation of α-Y in situ.

    c. Beneath the α layer is an oxygen-affected zone and unaffected substrate which was β-Zr at temperature but contains small Y_2O_3 particles which were evidently precipitated from particles of α-Y on cooling.

2. In the Zr-10 a/o Y alloy, the layers consist of:

    a. An external oxide containing cubic and tetragonal ZrO_2 at temperature. The ratio of cubic to tetragonal ZrO_2 increases with distance from the air-oxide interface. Small Y_2O_3 particles are also observed.

    b. An internal layer of α-ZrO_2 saturated with oxygen (microstructure also indicates Y_2O_3 particles which probably formed at temperature).

    c. A core in which α_1 (Zr-rich), α_2 (Y-rich), and Y_2O_3 coexist. The Y_2O_3 presumably forms from α_2 on cooling.

3. In the Zr-25 a/o Y alloy to Zr-50 a/o Y alloy, the sequence of layers is:

   a. An external oxide which contains Y_2O_3 precipitated from the oxygen-rich α-Zr phase. The bulk composition of the ZrO_2 phases is approximately 10% Y and the Y_2O_3 contains about 2% Zr.

   b. An internal layer which contains oxygen-saturated α-Zr (approximately 10% Y) and particles of Y_2O_3.

   c. An internal core consisting of Zr and Y solid solutions and Y_2O_3. (The Y_2O_3 apparently precipitated on cooling.)

4. In the pure Y sample and the sample containing 5 a/o Zr, the layers formed are essentially as follows:

   a. An external oxide of Y_2O_3.

   b. An oxygen-saturated metallic layer which extends throughout the sample and which precipitates Y_2O_3 on cooling to room temperature.

The precipitation of Y_2O_3 in the oxygen-saturated yttrium-rich alloys suggests that the Y_2O_3 observed in the substrate of the other Zr-Y alloys precipitated from the yttrium-rich phase during cooling. The yttrium content of 10 a/o in the α-Zr observed in the Zr-35 a/o Y suggests that the yttrium content of α-Zr in equilibrium with Y_2O_3 and α-Y at 1200°C is 10 a/o Y.

Layer growth at 1600°C is complicated by several factors. Many of the alloys being oxidized were liquid at temperature. An external oxide formed on heating which is not characteristic of the isothermal 1600°C oxidation process. Finally, two different sequences of layers were observed for samples of the same composition in the Zr-25 to Zr-50 a/o Y alloys oxidized at 1600°C, suggesting that alternative rate-controlling processes occur.

The samples in which a continuous barrier of Y_2O_3 formed at 1600°C, and which oxidized more slowly, are represented by the Zr-35 and Zr-50 a/o Y alloy in Fig. 6, Appendix I. The external oxide, presumably formed on heating, contains three phases, Y_2O_3, monoclinic ZrO_2, and cubic ZrO_2, in a morphology similar to that observed on samples of the same composition oxidized at 1200°C. Below this external multiphase layer are:

1. A layer of single-phased Y_2O_3 which contains approximately 2% Zr in solid solution.

2. An oxygen-saturated metallic layer consisting of solid zirconium containing approximately 10% Y and a liquid phase (at temperature) rich in yttrium (approximately 78 a/o Y). This layer is not observed in all samples.

3. A layer which contains oxygen-saturated α-Zr and yttrium-rich particles as well as Y_2O_3. The Y_2O_3 may have formed at temperature or on cooling from the yttrium-rich phase, depending upon the oxygen activity.

The morphology of the yttrium-rich phases suggests that they were liquid at temperature. However, the composition (10 to 12% Y) and morphology of the oxygen-saturated Zr-rich phase indicate that this phase was solid at temperature. A Zr-rich layer completely free of internal oxide particles is apparent in the samples used for microprobe analysis and is evident in some of the samples oxidized at 1600°C in Fig. 27.

The sequence of layers on those samples on which a continuous Y_2O_3 zone did not form, and which oxidized at more rapid rates at 1600°C was similar to that of the Zr-25 a/o Y alloy in Fig. 6, Appendix I. The structures observed are characterized by:

1. The absence of a continuous layer of Y_2O_3.

2. The formation of a three-phased layer containing Y_2O_3, cubic ZrO_2, and monoclinic ZrO_2 (which formed from tetragonal ZrO_2).

3. Beneath the oxide a two-phased layer which has the characteristic appearance of oxygen-saturated α-Zr surrounded by an yttrium-rich liquid phase, and an yttrium-rich oxide which may have formed in situ from a liquid phase at temperature or may have precipitated on cooling. The morphology of the internally oxidized zone and the Y_2O_3 in the oxide suggests that the liquid and solid phases oxidize independently in situ in a manner similar to that observed at 1200°C.

3.4 Zr-Y-O SYSTEM - DISCUSSION OF RESULTS

3.4.1 Construction of the 1200 and 1600°C Isotherms in the Zr-Y-O System

For analysis of the oxidation behavior of the Zr-Y alloys, some knowledge of the Zr-Y-O phase diagram is necessary. In order to derive composition paths for the alloys oxidized at 1200°C, a knowledge of the 1200°C isotherm is essential. Furthermore, even though analysis in terms of ternary diffusion cannot be applied to liquid alloys, the rather peculiar and variable 1600°C oxidation results can be rationalized on the basis of the 1600°C isotherm. Therefore, prior to discussing the layers formed during oxidation, or the kinetics of oxidation, existing information and that obtained from structural analysis during the present investigation will be used to construct the necessary sections through the ternary equilibrium diagram.

The ZrO_2-Y_2O_3 diagram of Duwez, et al,[13] was accepted for the quasi-binary oxide diagram. The Zr-O phase diagram is well established.[7] The Y-O phase diagram shown in Fig. 29 has been derived from the following information. Known oxide phase diagrams of rare earth metals with oxygen show a peritectic between M_2O_3 and the metal. Some authors suggest that M-O phases exist; however, this is still in doubt, and Y_2O_3 was the only yttrium-rich oxide observed in our studies. It was observed that samples of pure yttrium heated to 1500°C are solid, while those heated to 1600°C are liquid, even though appreciable amounts of oxygen are dissolved during heating. This information has been used to establish the solidus boundary between 1500 and 1600°C. The assumption that the solubility of oxygen in yttrium is at least the amount indicated by the chemical analysis tabulated in Section 3.3.3 has been used to construct the boundaries between the α_2 or β_2 regions and the two-phased region with Y_2O_3. From the difference in appearance of the oxide transformation structures in pure yttrium oxidized at 1200 and 1400°C it has been deduced that a eutectoid exists between these two temperatures at an undefined composition, assumed to lie between 15 and 25 a/o Y.

The Zr-Y phase diagram has been defined for alloys containing up to 50% Zr[12] and is also expected to be similar to the Hf-Y diagram which is known. The eutectic horizontal apparently extends at 1310°C up to about 90 a/o Zr since alloys oxidized at 1200°C were observed to be solid at temperature, while samples containing 10 to 50% Y were liquid or partially liquid at 1400°C. The position of the boundary between β_1 and α_1 in the zirconium-rich region is suggested by the transformation structures in the annealed Zr-5 a/o Y specimen (Fig. 30), and in the samples of the 5 a/o Y alloy oxidized at 1200 to 1600°C, and by the absence of this

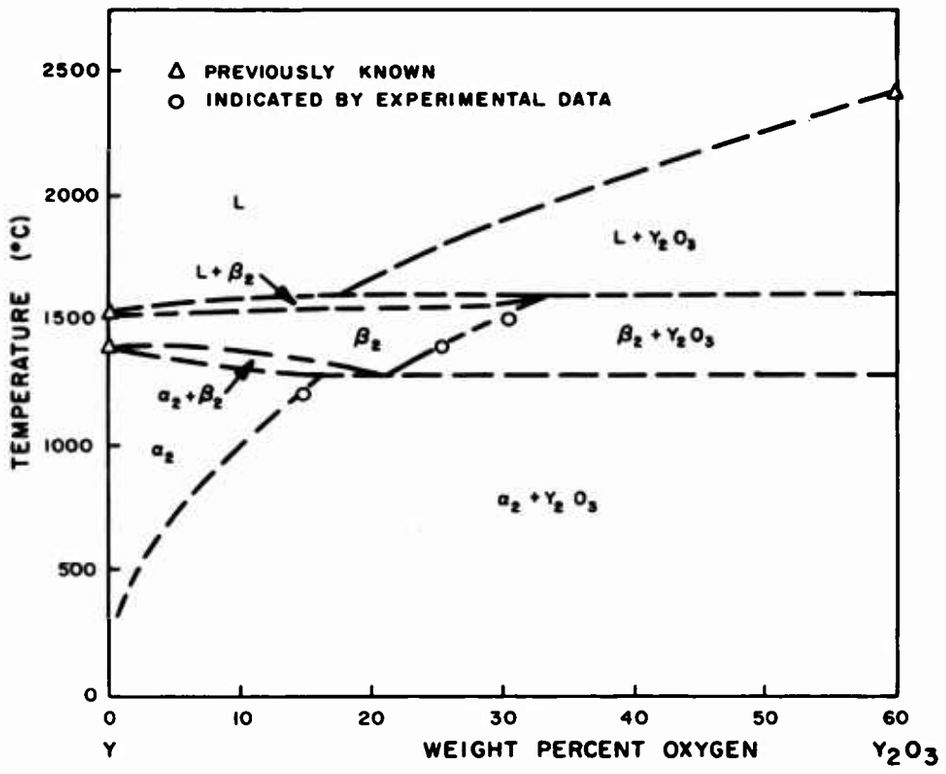

Fig. 29. Suggested phase diagram for the Y-O system based on experimental observations of oxidation of yttrium and other rare earth oxygen diagrams.

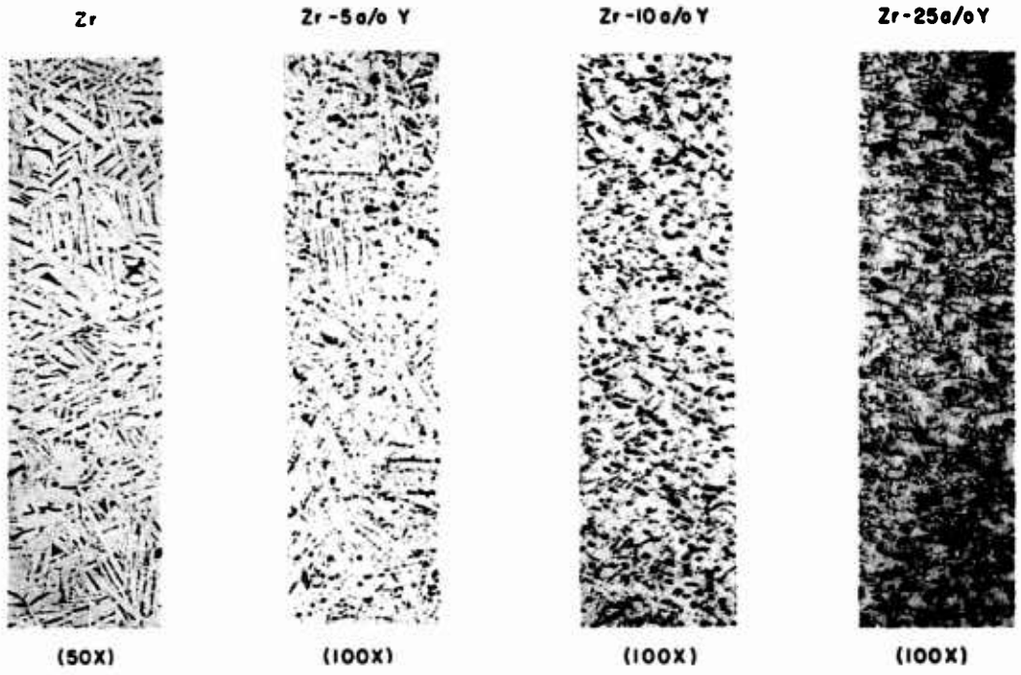

Fig. 30. Microstructure of Zr-Y alloys before oxidation (annealed at 1200°C).

structure in the Zr-10 a/o Y alloy. The boundary between β and the β + liquid is between 5 and 10 a/o Zr; this is indicated by the suggestion of melting at 1400 to 1600°C in the Zr-10 a/o Y alloy whereas there is no indication of a liquid at these temperatures in the 5 a/o Y alloy. It is particularly significant to note that the Zr-25 a/o Y alloy at 1600°C is on the liquidus boundary and that the Zr-5 a/o Y alloy at this temperature is on the solidus boundary.

By combining the microprobe, metallographic, and X-ray results, it is also possible to define compositions and phases present in sections of the ternary phase diagram. In constructing the 1200°C isotherm, the following observations from specimens oxidized at 1200°C have been used:

1. The only oxides observed in the layers formed during oxidation were cubic ZrO_2, Y_2O_3, and monoclinic ZrO_2 formed from tetragonal ZrO_2 on cooling.

2. An α-Zr + Y_2O_3 layer is observed in all samples containing 10% yttrium or more and the composition of the yttrium-rich α-Zr is between 10 and 12% yttrium.

3. The presence of small amounts of Y_2O_3 and cubic ZrO_2 in the oxide of the Zr-5%Y sample suggests that the solubility of Y in α-Zr is < 5% in the presence of ZrO_2.

4. It is assumed that Y_2O_3 that coexisted in the substrate with transformed α-Zr plus α-Y was formed by precipitation of Y_2O_3 from α-Y on cooling and was not present at 1200°C; therefore a β-Zr + Y_2O_3 field does not exist.

If the above results are combined with the phases required by the binary and quasi-binary phase diagrams at 1200°C, the two-phased fields which exist at 1200°C are defined. An estimate of the zirconium to yttrium ratios in the three-phased fields connected to alpha zirconium are given by the microprobe analyses of α-Zr in the α + Y_2O_3 layer and observation of cubic zirconia in the oxide formed on the Zr-5 a/o Y alloy. The resulting estimate of the 1200°C isotherm is given in Fig. 31.

In the construction of the 1600°C isotherm the following facts were used:

1. Metal + oxide layers were observed in samples containing from 25 to 35 a/o Y, and the oxygen-rich solid zirconium phase contained between 8 and 12 a/o Y in the α-Zr + Y_2O_3 layer.

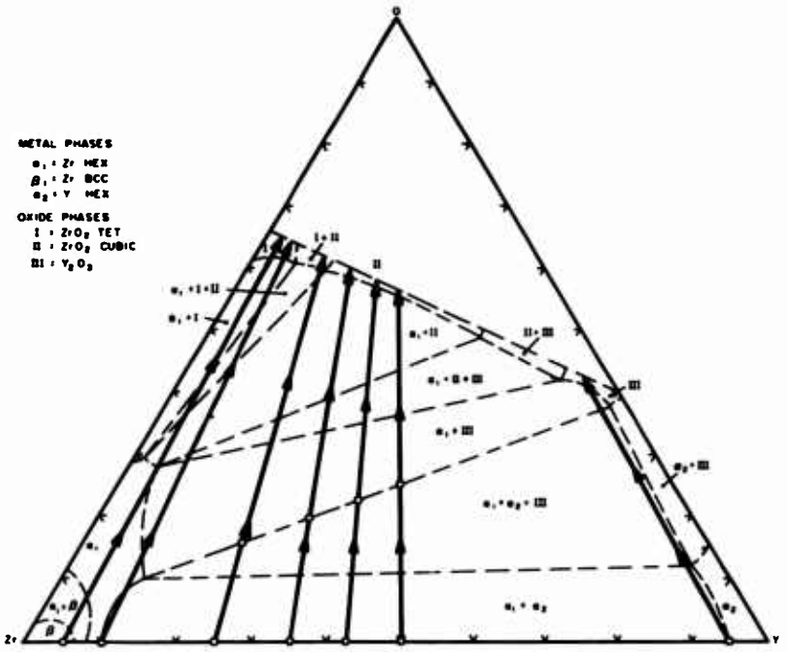

Fig. 31. Tentative Zr-Y-O diagram and composition paths suggested by structures and compositions of phases observed in oxidation of Zr-Y alloys at 1200°C.

2. Layers containing solid metallic alpha zirconium and a liquid yttrium-rich phase indicate an yttrium content in the solid of 10 a/o Y and a zirconium content of 22% in the liquid yttrium-rich phase in an oxygen-rich zone. These results require an α + liquid and an $\alpha + Y_2O_3$ two-phased region and help estimate the zirconium and yttrium contents of the phases in these two-phased regions.

3. The Y_2O_3 observed in layers in which yttrium-rich and zirconium-rich metal phases are present is assumed to have formed by precipitation on cooling from the oxygen-containing yttrium-rich phase.

By combining the above information with the phases and compositions of boundaries indicated in the binary and quasi-binary diagrams, it is possible to construct reasonable approximation of the 1600°C isotherm in the Zr-Y-O system, although the exact location of the corners of the three-phased fields are not known. The resulting estimate of the 1600°C isotherm is given in Fig. 32.

3.4.2 Multicomponent Diffusion in Oxidation at 1200°C

With a tentative equilibrium diagram, it is now possible to construct diffusion paths for the alloys oxidized at 1200°C. The analyses performed at Battelle Memorial Institute (Appendix I) indicate that oxygen diffusion is the major transport mechanism in the Zr-Y, as in the Zr-Th alloys, and comparatively little interdiffusion of the metal ions takes place. Therefore, the diffusion paths should be, to a close approximation, those given by the straight lines connecting the alloy compositions with the oxygen corner of the diagram as shown in Fig. 31.

It may be seen from these diffusion paths that the scale formed on the Zr-5 a/o Y alloy at 1200°C should consist of tetragonal ZrO_2 which on cooling transforms to the monoclinic form. Below the oxide, the predicted layers are

1. α-Zr + tetragonal ZrO_2
2. α-Zr + cubic ZrO_2
3. α-Zr + Y_2O_3 (borderline)
4. α-Zr
5. β-Zr (which would transform on cooling to α-Zr + α-Y).

The structures observed on the oxidized specimen differ from the above sequence in a number of respects. Particularly, small amounts of a virtually pure Y_2O_3 phase are observed in all layers. The oxide scale

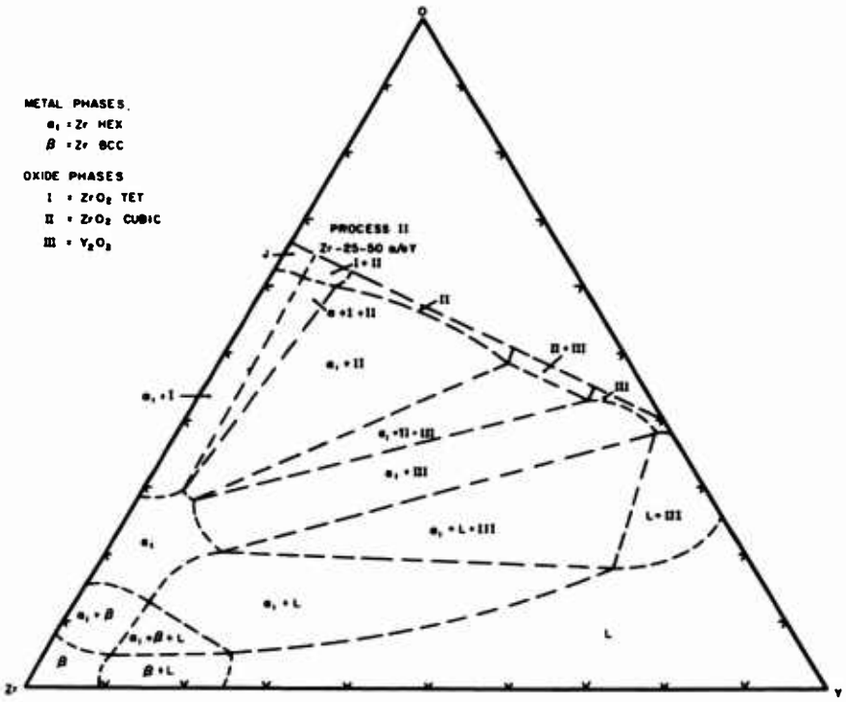

Fig. 32. Tentative 1600°C isotherm of the Zr-Y-O system and composition paths indicated by structure and compositions of phases observed in oxidation of Zr-Y alloys at 1600°C. Alternate paths are indicated for Zr-25 to Zr-50 alloys by shaded arrows.

contains cubic ZrO_2 throughout and apparently also a small quantity of Y_2O_3.

The sequence of layers predicted for the Zr-10 a/o Y alloy by the diffusion path of Fig. 31 is as follows:

1. Tetragonal ZrO_2
2. α-Zr + tetragonal ZrO_2
3. α-Zr + cubic ZrO_2
4. α-Zr + Y_2O_3
5. α-Zr.

Appreciable quantities of cubic ZrO_2 are observed in the actual oxide layer, the proportion increasing with depth below the surface (Appendix I, Fig. 5. Furthermore, small particles of Y_2O_3 are observed throughout all of the layers. The expected α-Zr + ZrO_2 layer is clearly present in this specimen.

Figure 31 predicts the same sequence of layers for all of the 25 - 50 a/o Y alloys at 1200°C:

1. Cubic ZrO_2
2. α-Zr + cubic ZrO_2
3. α-Zr + Y_2O_3
4. α-Zr + α-Y.

The observed structures differ from those predicted by the presence of large amounts of tetragonal (monoclinic) ZrO_2 and Y_2O_3 in the oxide layers as well as in the regions immediately beneath these.

Finally, the predicted and observed layers in the 95 a/o Y alloy at 1200°C are as follows:

1. Y_2O_3
2. α-Y + Y_2O_3
3. α-Y + α-Zr.

In this sample the only evidence of an α + Y_2O_3 layer is the irregular metal oxide interface.

It is clear that the sequence of phases actually observed in many of the oxidation specimens differs from that predicted by the diffusion paths of Fig. 31 by the presence of excess Y_2O_3 or tetragonal (monoclinic) ZrO_2 in some of the layers. Furthermore the number of phases in some layers is in excess of the maximum of two required by the rules for ternary diffusion. Therefore these layers cannot represent strictly equilibrium structures. However, the observed structures can be reconciled with the

diffusion paths of Fig. 31 by a consideration of the fact that the alloys undergoing oxidation were composed of two phases at temperature, one containing about 95 a/o Y and the other close to 90 a/o Zr. The presence of tetragonal ZrO_2 in the alloys containing higher amounts of yttrium and the presence and morphology of the Y_2O_3 observed throughout all layers, suggest that each of these phases oxidized more or less independently, and that interdiffusion of cations between the phases during oxidation was incomplete, if not entirely negligible. Therefore, the layers observed actually correspond to two separate diffusion paths, represented by the lines for the 10 and 95 a/o Y alloys in Fig. 31.

It is clear that this situation is brought about by the overriding rapid rate of diffusion of oxygen in both the oxide and metal phases in this system, which results in virtually complete oxidation of the alloy before equilibration of the phases produced from the initial constituents can occur by lateral diffusion of the cations. It is conceivable that some interactions between the resultant oxide phases continue to occur, but these must be relatively slow processes. The Y_2O_3 observed in the unaltered substrate of the samples probably formed during cooling since yttrium and the yttrium-rich phase in all two-phased alloys dissolve considerable oxygen at 1200°C but precipitate this oxygen even with rapid cooling. The rapidity of this precipitation and the small amount of oxygen retained in solution in α-Y are indicated by the fact that Y_2O_3 was observed in yttrium containing 0.1% O_2 in Reference 12.

3.4.3 Relation of Structures Observed During Oxidation at 1600°C to the Phase Diagram

The relation of the phase diagram to the processes governing oxidation at 1600°C is particularly interesting since oxygen and yttrium could be transported through both liquid and solid metal regions in the same sample. The Zr-5 a/o Y alloy is solid at temperature, and the paths and layers formed are quite similar to those observed at 1200°C with one exception -- the matrix phase at temperature is β-Zr and a layer which may be α-Zr and perhaps a layer containing α + cubic ZrO_2 is observed. The Zr-10 a/o Y alloy is largely solid but a liquid phase does exist in the unoxidized alloy. However, the structures suggest that solid-state reactions predominate. Also, the formation of a second phase which is either Y_2O_3 or cubic ZrO_2 indicates an oxygen transport path across tie-lines in the α + Y_2O_3 and α + cubic ZrO_2 two-phased fields leading to three-phased oxides similar to those observed at 1200°C. In these two alloys oxidation of phases in situ due to the rapid diffusion of oxygen occurs.

In the absence of oxygen, alloys containing more than 25 a/o Y are liquid at 1600°C. In these alloys oxidation occurring during heating leads to the formation of an external multiphased oxide and, probably to an oxygen-affected region as observed in solid samples oxidized at lower temperatures. Both the phase diagram and the microstructures suggest the formation of an internal layer (α-Zr + liquid) in all samples. Since Y_2O_3 can exist at temperature only with a moderately low concentration of zirconium, the formation and growth of a continuous Y_2O_3 layer will occur only if the transport of yttrium to the metal-oxide interface is rapid enough. The formation of a solid layer of alpha zirconium below the external oxide, either during heating or at longer times at temperature, could significantly reduce the transport rate of yttrium from the liquid and change the sequence of events during oxidation. An alternative process could result if no continuous Y_2O_3 layer formed. Oxidation of the yttrium-rich liquid and zirconium-rich solid in situ could then occur and the morphology of the oxide formed would be similar to that observed in the Zr-10 a/o Y alloy at 1600°C. The layers formed on samples that exhibited high weight gains suggest that such a process did occur during the initial stages of oxidation since no continuous Y_2O_3 layer was formed.

Even in those samples in which a continuous layer of Y_2O_3 is formed there is no guarantee that growth of a solid + liquid layer or depletion of the liquid substrate will not eventually prevent the continued growth of the Y_2O_3 layer.

Thus the formation of solid metallic layers in addition to the oxides seriously perturbs the oxidation process. Accidents or subtle variations during the initial stages can have a drastic influence on the course of reaction under such circumstances.

3.4.4 Kinetics of Oxidation

A better definition of the layers formed and the composition path for various compositions and temperatures is quite helpful in an analysis of the kinetics of oxidation. Diffusion, however, is not involved at 1000°C. Breakaway oxidation is observed at temperatures of 800 to 1000°C in the Zr-Y alloys and 1000°C in the Hf-Y alloys. The two-phased oxides formed at 1200°C and above apparently can relax the stresses developed during oxidation, probably by grain-boundary glide processes such as those studied in Reference 15. The fact that single-phased ZrO_2 cannot accommodate these stresses is not explained on the basis of the data obtained. It is possible that alloying either promotes plastic deformation in oxides or that a finer grain-size with more surfaces for grain boundary glide are maintained as a result of the introduction of a second phase.

The difference in the behavior of the Zr-base and Hf-base alloys in terms of spalling and edge effects suggests that the two oxides differ in resistance to thermal shock. However, there is a possibility that the edge cracks in the Hf-Y-O system may have existed at temperature. Since HfO_2 and the Hf-base alloys have higher melting temperatures than ZrO_2 and the equivalent Zr-base alloys, the greater tendency toward cracking in the Hf-Y-O system may be explained on the basis of higher hardness at temperature. However, the parabolic growth rates observed suggest that the oxides formed in both systems are ductile at 1200°C.

The influence of composition on the oxidation rate in the Zr-Y system is shown in Figs. 33 and 34 for the three temperatures of test. A maximum rate of oxidation exists for alloys containing 5 to 10 a/o Y at all three temperatures if the parabolic growth rates of ZrO_2 from liquid Zr-Sn alloys are considered. This coincides approximately with the minimum in resistivity reported at 10% Y in the ZrO_2-Y_2O_3 oxide system.[16] The oxidation rate of pure, solid ZrO_2 at 1200°C is linear and higher than that of the Zr-Y alloys. The oxidation rates of the alloys are approximately proportional to the amount of ZrO_2, both cubic and monoclinic, observed in the scales, which suggests that the diffusion of oxygen through ZrO_2 containing Y is more rapid than through Y_2O_3. However, the oxidation rate of Zr-Sn alloys, which formed virtually pure ZrO_2 scales, is lower than that of pure Y. Another point is that the Zr-rich oxide phases are the matrix phases of the Zr-25 a/o Y alloy, but the oxides on alloys which contain greater than 35 a/o Y have a network of Y_2O_3.

In the Zr-25 to 50 a/o alloys, the observations of two different parabolic growth rates at 1600°C are also explained on the basis of the alternative paths. Depletion of yttrium in the liquid substrate, and the formation of internal layers which are solid but of a different composition than the forming oxide, could cause a significant change in the rate at which the more reactive yttrium is supplied to the interface between α-Zr + Y_2O_3 and Y_2O_3 layer. Under these conditions, a change in the kinetics of oxidation would be expected.

A low, overall rate of oxidation is observed for pure yttrium, in spite of the fact that rapid diffusion of oxygen occurs initially to form a saturated solution. The formation of an yttrium oxide from a refractory reservoir could form the basis for a protective system which would be quite refractory; however, the overall rate of growth of the oxide at 1500°C is still considerably higher than that of Al_2O_3 on Al. The same may be siad of the Zr-Y alloys.

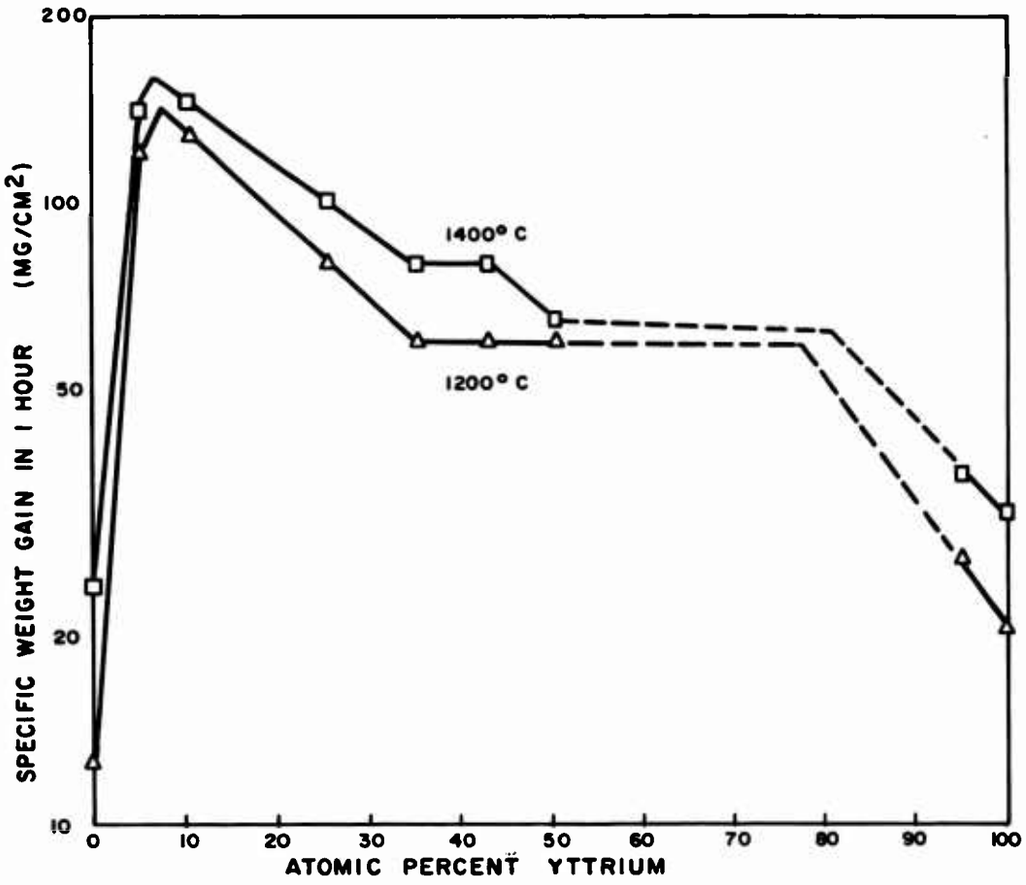

Fig. 33. The effect of Y content on the weight gains in one hour during oxidation of Zr-Y alloys at 1200 and 1400°C in air. Values for pure Zr are from oxidation of liquid Sn-Zr alloy in Reference 2.

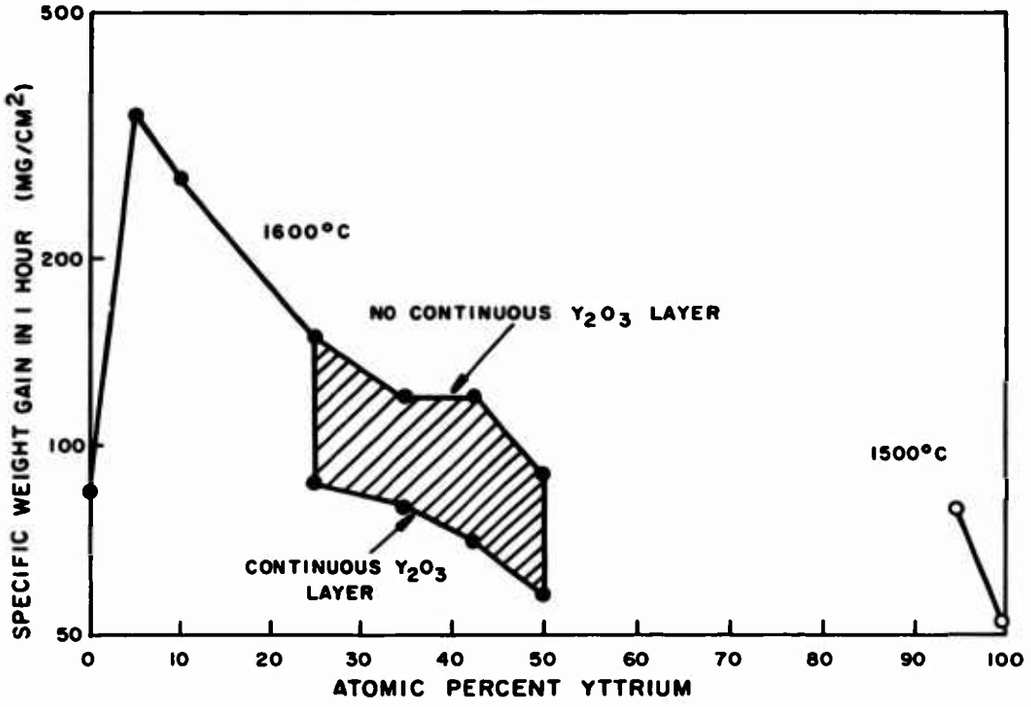

Fig. 34. The effect of Y content on the oxidation weight gain in one hour at 1600°C (1500°C for Y rich alloys). Values for pure Zr are from oxidation results on Zr-Sn alloys in Reference 2.

3.5 Zr-Y-O SYSTEM - SUMMARY AND CONCLUSIONS

1. In the Zr-Y-O system, oxidation processes are dominated by oxygen diffusion at 1200°C and no appreciable migration of either yttrium or zirconium is observed.

2. The alloys undergoing oxidation at 1200°C consist of two phases widely separated in composition and each of these phases oxidizes more or less independently of the other. The layer sequences observed on the alloy surfaces can be described by two separate diffusion paths in the ternary equilibrium diagram, one for each of the initial phases.

3. Two modes of oxidation of liquid Zr-Y alloys at 1600°C occur, dependent upon the sequence of formation of several solid layers which may form during the oxidation process. The particular sequence occurring is determined by the initial conditions of layer growth.

4. The following factors have an important bearing in the kinetics of oxidation of Zr-Y and Zr-Hf alloys.

   a. The oxides formed protectively at temperatures of 1200°C and above in both systems and the two-phased oxides did not break away, possibly because they were sufficiently plastic above 1200°C. However, at 1000°C and below the oxides formed were subject to breakaway. Differences in the resistance to thermal shock are observed which suggest that Zr-based two-phased oxides are more able to relax stresses than the Hf-based oxides.

   b. In diffusion-controlled oxidation, the rates of growth are determined primarily by the composition of the oxide layer. The rates of oxidation of alloys on which Y_2O_3 forms as the matrix phase in the oxide are lower than those of alloys on which ZrO_2 forms as the matrix phase.

   c. The bulk composition of the oxide which formed at the maximum rate is essentially the same as that which produced minimum electrical resistance in the ZrO_2-Y_2O_3 system at high temperatures in Reference 16.

4. THE W-Hf-O SYSTEM AND THE W_2Hf-Re_2Hf-O SYSTEM

The W-Hf-O system is one of special interest in the oxidation protection of tungsten at very high temperatures because of the refractory nature of HfO_2 and the existence of a refractory intermetallic compound, W_2Hf, which could form the basis of a protective coating system. The prime objective in studying the oxidation of W-Hf alloys was to obtain information on (1) the kinetics of oxide growth and (2) the role of ternary diffusion in the overall oxidation process. Secondary objectives were to determine if a hard, brittle substrate or vaporization of tungsten oxides had a significant influence on the tendency toward breakaway and linear oxidation in such a system.

The W-Hf phase diagram is known[17] and is indicated in Fig. 35 along with compositions of the alloys and temperatures of the oxidation tests performed in this system. The Hf-O phase diagram is also known,[18] and is given in Fig. II-4 of Appendix II. The oxide compounds in the W-O system have been identified,[19] and a portion of the tentative binary W-O phase diagram is given in Fig. II-5 of Appendix II. The quasi-binary phase diagrams between the oxides of tungsten and hafnium oxide are not known, but compound oxides in the analogous W-Zr-O system have been reported.[20]

Publication of the Mo-Re-Hf ternary phase diagram[21] during the course of this investigation provided evidence that an extended single-phased region might exist in the quasi-binary W_2Hf-Re_2Hf system similar to that reported for Mo-Re-Hf alloys. Therefore, W-Re-Hf alloys were investigated to determine the effect of variations in rhenium and hafnium content on the composition of the oxide formed over the intermetallic compound. The further influence of a vaporizing species such as Re_2O_7 on the tendency toward breakaway was also of interest. A W-Re-Hf intermetallic compound with a high melting point is of obvious potential as a coating for tungsten. The W-Hf-O and the W-Re-Hf-O systems will be discussed separately.

4.1 THE W-Hf-O SYSTEM

4.1.1 Experimental Procedure

Alloys containing 2, 20, 33, 35, 70 and 95 a/o Hf were prepared by mixing appropriate blends of tungsten and hafnium hydride powder, pressing these blends, sintering in vacua, and arc melting to form small buttons. Those samples which could be machined were cut to produce flat and parallel surfaces and annealed at 1300°C for 16 hours. A hole was then drilled in one end to support the specimen during oxidation. The W-33, 35 and 70 a/o Hf alloys could not be cut without cracking, so that individual arc-melted buttons or sections of arc-melted buttons of these alloys were used for oxidation tests.

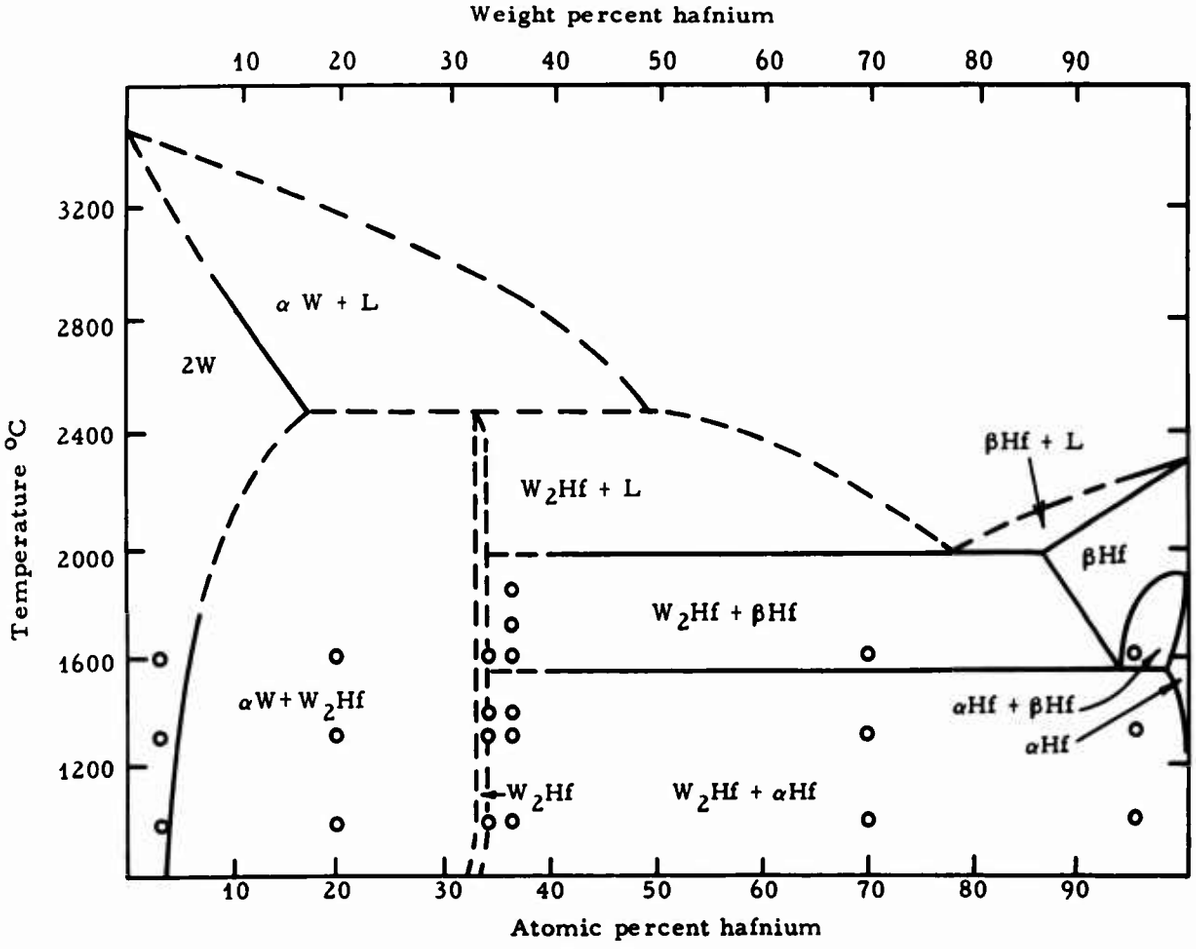

Fig. 35. The tungsten-hafnium phase diagram.[17] Compositions and temperatures of oxidation test are indicated by circles.

During the course of investigation it was found that nonequilibrium structures existed in the W-20 to 35 a/o Hf alloys. Additional samples of W-35 a/o Hf were produced in the form of arc-melted buttons, and annealed for 16 hours at 2130°C prior to oxidation.

During the oxidation tests, the sample was supported on a section of a zirconia crucible. Samples of the six compositions were oxidized at 1000 to 1600°C for various times as shown in Fig. 33, and measurements of weight gain during oxidation and oxide thickness were made. Cyclic oxidation tests were used for many samples, but duplicate individual runs were made at 1000, 1300 and 1400°C for the W-33 and W-35 a/o Hf alloys, since cracks in the oxide due to cycling were observed after cyclic tests.

Specimens of the W-20 a/o Hf and W-70 a/o Hf alloys oxidized at 1300°C were submitted for microprobe and X-ray identification of the layers formed. Additional samples of specific layers from oxidized W-33 to W-35 a/o Hf alloys were submitted for chemical and X-ray diffraction analysis. A microprobe analysis was also obtained on the black layers formed on the W-35 a/o Hf alloy oxidized at 1700°C.

Weight-gain measurements were made, and specific weight gains were calculated for samples with measurable surface areas. In most alloys the rate of recession of the metal interface and the oxide thickness were measured on the cross section of the specimens prepared for microscopic examination. On samples that were irregular in shape, metallographic measurements of metal recession were inaccurate. Selected samples were sandblasted to remove the oxides and weighed to estimate metal recession rate.

4.1.2 Results

4.1.2.1 Kinetics

Measurement of the kinetics of oxidation in the W-Hf-O system at various temperatures was difficult for several reasons. First, many samples were irregular in shape and an accurate determination of the area was difficult. Second, the possibility of evaporation of tungsten oxides during test at higher temperatures made the interpretation of the weight gains, as well as oxide thicknesses, somewhat doubtful. Third, the thickness of the oxide formed was difficult to measure, particularly at 1300°C, because of a separation of the external oxide from the sample. Finally, the thickness of remaining metal was difficult to measure because of the irregular shapes, and metal recession rates could therefore not easily be determined.

A compilation of the results is given in Table VI for the six alloys annealed at 1300°C and the W-35 a/o Hf alloy annealed at 2130°C. Results of cyclic tests are given for most samples at 1000, 1300 and 1600°C, and continuous tests at 1000, 1300 and 1400°C for the 33 and 35 a/o Hf alloys. The results at 1000 to 1800°C for the W-35 a/o Hf annealed at 2130°C are also based on individual test specimens held continuously at temperature.

At 1000°C the W-2 a/o and the W-95 a/o Hf alloys had parabolic oxidation rates and low weight gains during oxidation. The W-33 and W-35 a/o Hf alloys exhibited linear growth rates in both cyclic and individual tests at 1000°C, indicating breakaway. The metal recession rates also indicate rapid oxidation. The W-70 a/o Hf samples oxidized at 1000°C at a rate corresponding to a slope of 0.6 for the log time vs log weight-gain curve. The weight gain at 1000°C in one hour is significantly greater than that at 1300°C. The edges of the W-70 a/o Hf samples oxidized at 1000°C were badly cracked, resulting in a cruciform oxide pattern, usually indicative of rapid linear growth.

At 1300°C most alloys exhibited approximately parabolic growth rates but vaporization occurred during oxidation of some samples. The W-35 a/o Hf (1300° anneal) and the W-95 a/o Hf samples oxidized linearly. In cyclic tests the W-33 Hf sample also oxidized by a linear rate process, probably as a result of cracking which occurred in the oxide on cooling between cycles.

At 1600°C, slight fuming was observed for all compositions tested, and vaporization of tungsten oxide evidently occurred. Weight gains or metal recession rates for several alloys seem to be between parabolic and linear (slopes of 0.75). The slopes of the curves of weight gain vs time on a log-log graph for the W-33, W-35 a/o Hf (2130° anneal) and W-70 a/o Hf alloys suggest parabolic or protective growth. The fact that weight gains rather than weight losses, were observed for all samples suggests that oxide layers grow even though evaporation does occur.

A sample of the W-35 a/o Hf alloy was heated to 1800°C in an induction coil. The evolution of fumes at 1800°C was slightly less than at 1300 to 1400°C. After 30 minutes, a small sample gained weight due to the formation of a layer of WO_3 and a thick black internal oxide. Even after 1/2 hour at 1800°C, the sample was not completely oxidized.

The colors of the external oxide formed on the W-Hf alloys after testing are also indicated in Table VI. The external oxides are predominantly yellow or white at 1000 to 1300°C and black-to-yellow or black at 1600°C. A black or blue-black internal suboxide formed on almost all compositions at 1300 to 1600°C.

TABLE VI

A Comparison of Weight Gains with Metal Recession of W-Hf Alloys Oxidized in Air at Various Temperatures

Alloy	Temp. (°C)	Wt. Gain in 1 Hr. (mg/cm²)	Estimate of Rate Process Based on ΔW/A(a)	Oxide Thickness or Metal Recession			Color
				Time (hr.)	Thickness (cm x 10^{-3})	Metal Rec. (cm x 10^{-3})	
W-2 a/o Hf	1000	12.5	parabolic	3.	1.5	2.3	green-black
	1300	82.0	parabolic	2.	40.5	37.4	black
	1600	370.	slope = 0.75 (e)	(0.17	0.1	25.8	black
				(0.5	-	66.	
W-20 a/o Hf	1000	15.0	slope = 0.75	2.66	-	9.3	yellow
	1300	30.0	parabolic	2.25	g	54.7	white-green
	1600	100.0	linear	0.25	-	87.9	blue-yellow
W-33 a/o Hf	1000	--	linear	2.25	50.8	30.2	yellow-white
	1000(b)	--	linear	2.	g	20.5	" "
	1300	--	linear	1.25	g	12.7	" "
	1300(b)	--	parabolic, slope = 0.75(d)	1.	g	10.2	" "
	1400(b)	--	parabolic	1.	g	--	" "
	1600	--	parabolic(e)	0.25	g	20.5	" "
	1600(b)	--	slope = 0.72(e)				
W-35 a/o Hf	1000	20-48	linear	2.25	23.5	29.	yellow-white
	1300	58.	slope = 0.75(d)	1.75	g	25.9	white
	1300(b)	--	1(h) slope = 0.75(d)	1.	g	10.2	yellow-white
	1400(b)	--	parabolic(d)	0.5	-	31.6	" "
W-70 a/o Hf	1000	130.	~parabolic, slope = 0.6(f)	0.75	71.	28.3	yellow
	1300	86.	parabolic	0.75	g	23.5	white
	1600	--	slope = 0.42(h)	1.1	61.	45.7	black
W-95 a/o Hf	1000	8.	parabolic	3.5	76.2	3.8	white
	1300	46.	linear	2.	g	38.2	"
	1600	--	linear	0.25	1.27	40.6	black
W-35 a/o Hf(c)	1000(b)	78.	slope = 0.74	0.25	4.8(e)	28.0	
	1300(b)	24.5	-- (e)	1.	22.2(i)	16.5	
	1600(b)	80.	parabolic (e)	0.25	19.0(i)	12.5	black+yellow ctg
	1700(b)	70.	< parabolic (e)	0.33	50.8(i)	--	" "
	1800(b)	170.	linear(e)	0.5	80.	35.0	" "

(a) Slopes are from log-log plots.
(b) Individual tests; all others cyclic.
(c) Annealed 2130°C; all other annealed at 1300°C.
(d) Rate types or slope determined by recession indications.
(e) Vaporization indicated by recession or erratic weight gains.
(f) Cruciform scale formation.
(g) External oxide spalled on cooling.
(h) Slopes of log weight gain vs log t curves used; areas not calculated.
(i) Irregular thickness make estimate necessary.

4.1.2.2 Structural Observations

The microstructures of the oxides formed on the W-Hf alloys are given in Fig. 36 for the alloys containing 2 to 95 a/o Hf and in Fig. 37 for the W-35 a/o Hf alloy annealed at 2130°C prior to test. At all test temperatures, the alloys annealed 16 hours at 1300°C prior to oxidation are multiphased, with the exception of the W-2 a/o Hf alloy. Two-phased structures are expected in the W-20 and W-70 a/o Hf alloy, and possibly in the W-95 a/o Hf alloy. However, the W-33 Hf alloys should be single-phased, or nearly so, according to the equilibrium diagram (Fig. 35).

The compound W_2Hf forms by a peritectic reaction, and apparently 16 hours at 1300°C did not equilibrate the three-phased cast structure of the tungsten-rich alloys.

The oxides formed at 1000°C contained cracks which in general were related to the number of thermal cycles during test, indicating that the cracks formed on heating or cooling, rather than at temperature. Only the oxide layers formed on the W-70 a/o Hf and W-95 a/o Hf alloys appeared to have spalled at temperature as indicated by the thick porous oxide formation and the clearly defined edge effect. However, according to weight measurements, the oxidation rate of the W-95 a/o Hf alloys was parabolic at 1000°C.

At 1300°C dark adherent oxide layers are observed at the metal-oxide interface of all compositions, although the external oxide on some samples had separated prior to mounting. With the exception of the W-2 a/o Hf alloy, alterations in the metallic substrate are observed after oxidation at 1300°C. The adherent inner oxides and the strength of the outer oxides which cracked-off on cooling indicate that dense protective layers form by diffusion at 1300°C.

Several alloys exhibited peculiarities in behavior at 1600°C. For example, the oxide formed on the W-2 a/o Hf alloy after five minutes is thicker than that which remains after 1/4 hour, and internal oxide particles are observed throughout the sample. In the W-20 a/o Hf alloy, a layer suggesting internal oxidation is also observed. However, the structure of the W-33 a/o Hf alloy oxidized at 1600°C is similar to that at 1300°C and does not indicate internal oxidation. The oxide formed on the W-70 a/o Hf alloy is two-phased and extremely porous. A dense, two-phased oxide appears on the W-95 a/o Hf alloy oxidized at 1600°C.

In almost all alloys oxidized at 1300°C and the W_2Hf alloys oxidized at 1600°C, a black single-phased oxide formed at the metal-oxide interface even though the alloys were multiphased.

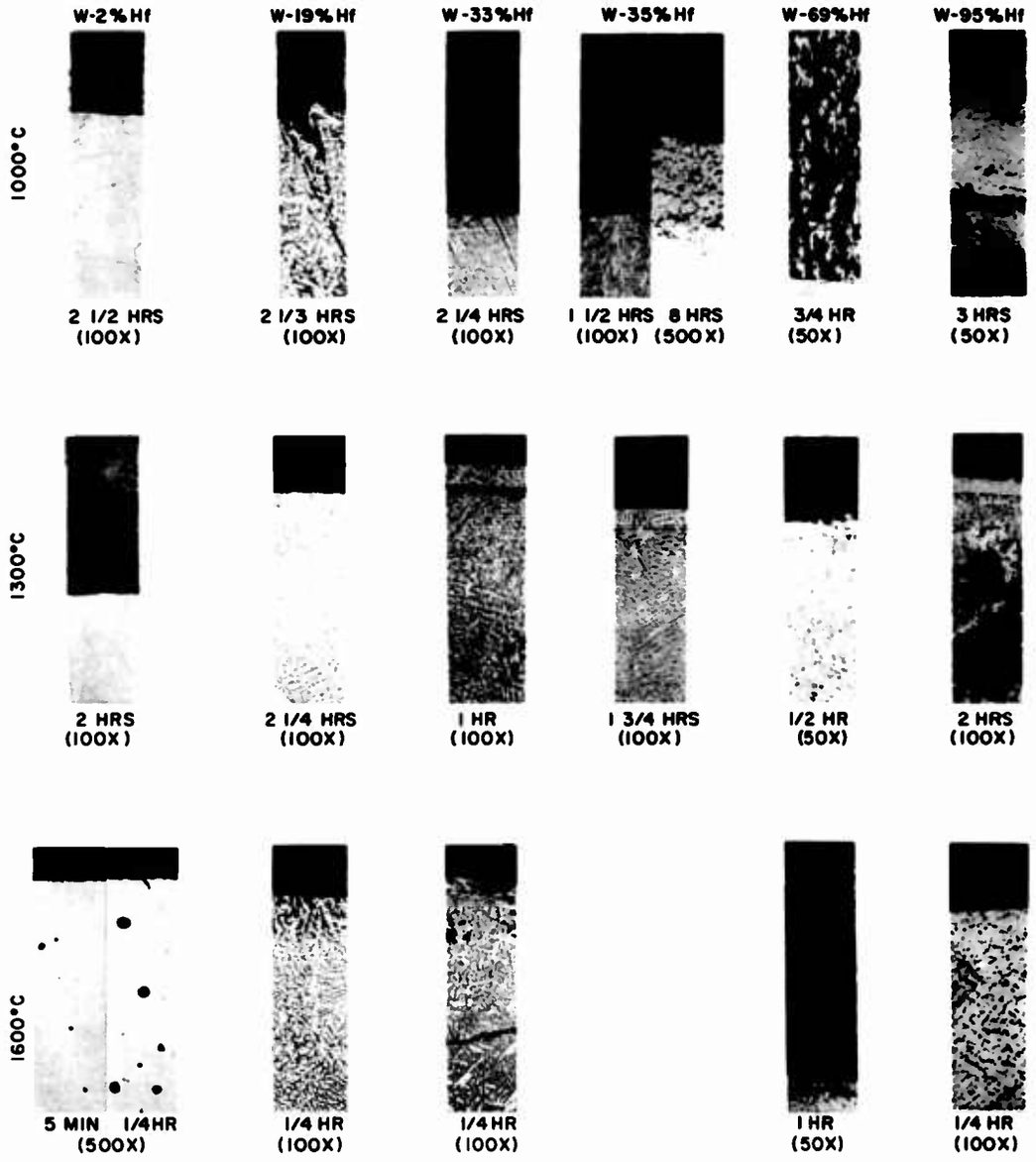

Fig. 36. Microstructures of layers formed in the oxidation of W-Hf alloys (magnification reduced by ~40% in reproduction).

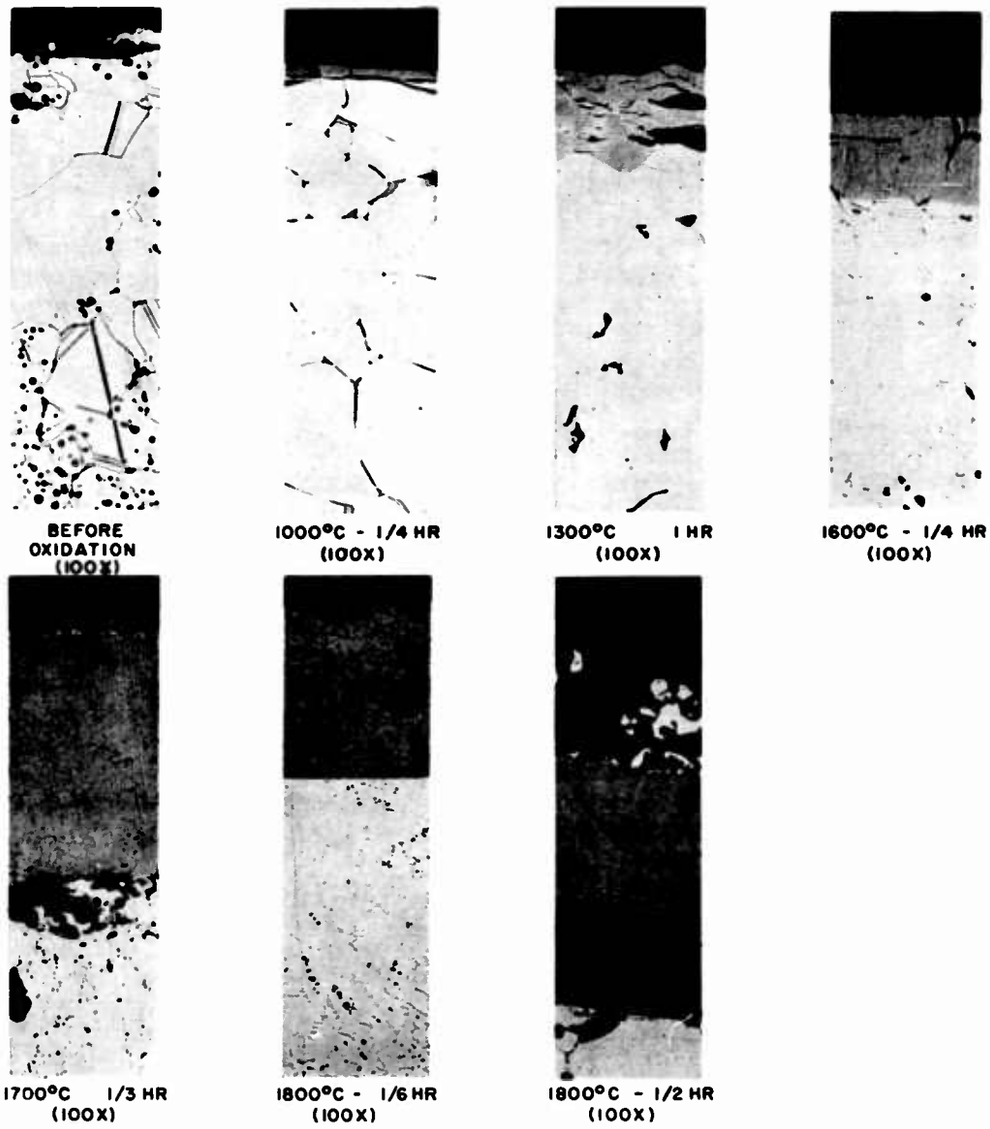

Fig. 37. Microstructures of layers formed in the oxidation of W + 35% Hf (magnification reduced by ~10% in reproduction).

The microstructure of the W-35 a/o Hf alloy annealed at 2130°C for 16 hours is single-phased. Cracks were present in the matrix due to brittleness of the intermetallic compound. At 1000 and 1300°C a single-phased black oxide and a gray oxygen-affected zone is observed. Both zones seem to be dense and adherent, particularly at 1300°C. In fact, the black oxide could be removed only with great difficulty. The gray oxygen-affected zone is also observed at 1600°C, but a two-phased oxide exists as the outer layer. In the sample oxidized at 1700°C, a thick, essentially single-phased zone grows at the metal-oxide interface, and an external two-phased oxide is also observed. The single-phased oxygen-affected zone is also seen at 1800°C, but the two-phased layer is apparent only in the sample oxidized for 1/2 hour at 1800°C. Vaporization of the two-phased layer does not occur, and consequently, oxidation of the substrate is not too rapid.

4.1.2.3 Chemical, Microprobe and Diffraction Analyses

Samples of the W-20 a/o and W-70 Hf alloys oxidized at 1300°C were submitted for microprobe and X-ray analyses to Battelle Memorial Institute. The results are given in Appendix I, Section 4.5. Additional samples of specific layers of W-33 to W-35 a/o Hf alloys were submitted for chemical analysis by X-ray spectrographic or wet chemical methods, and for X-ray identification of the phases present. A microprobe trace of the black oxides formed on the W-35 a/o Hf alloy (annealed at 2130°C) at 1700°C was also obtained. The results given in Table VII compile the information obtained from all tests.

The original metallic portion of the W-20, W-33, and W-35 a/o Hf alloys (annealed at 1300°C for 16 hours) contained three phases: tungsten solid solution, the compound W_2Hf, and the hafnium solid solution. This is in agreement with the microstructural observations. The W-35 a/o Hf alloy annealed at 2130°C for 16 hours consisted of single-phased W_2Hf, and the W-70 a/o Hf alloy annealed at 1300°C contained only W_2Hf and the hafnium solid solution, as indicated by the phase diagram.

A single-phased oxide layer at the metal-oxide interface was observed on the W-20 a/o Hf alloy which had a cubic structure with a lattice parameter of 3.76 A. Microprobe analysis indicates that the tungsten-to-hafnium ratio in this phase is approximately 5 to 1. A similar layer formed on the W-35 a/o Hf alloy at 1700°C indicated the same phase at a W/Hf ratio of 2.85 to 1. The bulk of the black adherent oxide which formed at 1300°C on the samples of W-33 to W-35 a/o Hf alloys also was the same cubic phase. A series of diffraction lines which were related neither to this cubic phase nor to any known tungsten or hafnium oxides was also observed in the patterns of several layers richer in oxygen.

TABLE VII

Structure and Chemical Analyses of Layers Formed in the Oxidation of W-Hf Alloys

	W - 19 Hf	W - 32.5 Hf	W - 35 Hf	W - 70 a/o Hf	W - 35 Hf[a]
Temp. of Oxidation (°C)	1300	1300	1300	1300	1700
Outer Oxide I					
Micro or color	Multiphase	Yellow-white two-phase	White-Yellow		
Chemical			49.9% Hf (18 a/o W 11 a/o Hf)[b]		W/Hf = .75
X-ray Diffraction	$W_{18}O_{49}$+HfO_2 + I[e]			$W_{18}O_{43}$+HfO_2 + cubic+unk. I[e]	
Microprobe	89 w/o W 11 w/o Hf				
Chemical		1400°C 1 hr. 28.9 Hf (13 a/o W 9 a/o Hf)[b]	1400°C 1 hr. 21.8 Hf (19.5 a/o W 7.1 a/o Hf)[b]		Blue oxide = I_W/I_{Hf} = 10/1 Other oxide = I_W/I_{Hf} = ≤ 6/1
Oxide II					
Micro or color	Single-phase		Black Oxide 1300 - 2 hrs.	Multi-phased	Grey single-phase
Chemical					W/Hf = 2.85
X-ray Diffraction	Cubic $_o$ = 3.75	Cubic (+unk. I)[e]	Cubic(+unk. I) +HfO_2[e]	HfO_2+cubic+I[e]	Cu(+I+HfO_2)[e] Cu(+I)[e][g]
Microprobe	83.7 W				W/Hf = 2.6/1
Affected Zone					
Micro or color	1-2 phases	1-2 phases (black oxide + base metal)			
Chemical		W/Hf = 2.11			
X-ray Diffraction	W_2Hf+(2) W_{ss}II[d]			W_{ss}II+HfO_2[d]	
Microprobe	66.2 W in W_2Hf				W/Hf = 1.75/1 Matrix I_W/I_{Hf} = 1.55[f] Second phase I_W/I_{Hf} = .2[f]
Base Metal					
Micro	2-3 phases				
Chemical		67.5 W 32.5 Hf	W-34.9 Hf		
X-ray Diffraction	W_{ss}+Hf_{ss}+W_2Hf	$W_{ss}$$Hf_{ss}$+$W_2Hf$	W_{ss}+Hf_{ss}+W_2Hf	W_2Hf+Hf_{ss} W_2Hf·Hf_{ss}	W_2Hf
Microprobe	85.5 W			67 w/o W 21-33 w/o W	I_W/I_{Hf} = 1.67[f] Calculated W = 66% H_f = 34%

(a) Annealed 2130°C for 16 hours; all other samples annealed at 1300°C.
(b) Calculated assuming WO_3 and HfO_2.
(c) From microstructure.
(d) W_{ss}II expanded b.c.c. with a lattice parameter greater than W.
(e) I represents unidentified phase indicated by 6 diffraction lines.
(f) Values indicated are from a second independent microprobe trace.
(g) Analysis on outer oxide is from 1300°C test.

It was not possible to define a composition or a crystal structure on the basis of the data available.

The phases identified in the grey, oxygen-affected layer in the W_2Hf oxidized alloy at 1300°C are W_2Hf plus a body-centered cubic solid solution with a lattice parameter slightly expanded from that of tungsten. In the W-70 a/o Hf alloy a similar phase is observed in the oxygen-affected layer in equilibrium with HfO_2. This layer in turn is in equilibrium with W_2Hf plus hafnium solid solution at the interface between the oxygen-affected layer and the unaffected substrate. One microprobe analysis of the W_2Hf alloy annealed at 2130°C and oxidized at 1700°C indicates a layer in which the atomic ratio of oxygen to metal is 1:1 and in which the tungsten-to-hafnium atomic ratio is approximately 1:75:1. The tungsten-to-hafnium ratio of the oxide at the external surface was identified as approximately 2.8:1 by one X-ray fluoresence analysis. The outer oxide was identified as the cubic phase but the crystal structure of the oxide of the affected zone was not obtained. A second analysis of the same sample indicated that the layers were two-phased and intensity ratios in the inner layer suggest that the dispersed phase is HfO_2. A phase with a W/Hf ratio of 10: 1 is observed in the outer layer.

4.1.3 Discussion of the Results

4.1.3.1 Kinetics of Oxidation

The kinetics of oxidation of the W-Hf alloys is complex owing to the occurrence of evaporation as well as spalling of the scale.

Metal recession values give the best indication of oxidation rates, and plots of the metal recession rates vs Hf content are given in Figs. 38 and 39. The points for 100% Hf on these figures represent the thickness of HfO_2 formed parabolically on liquid Hf-Sn alloys, taken from Reference 2.

The oxidation rates of all of the W-Hf alloys are greater than that of the liquid Hf-Sn alloy. The variation of oxidation rate with composition is irregular.

At 1000°C the maximum in the oxidation rate at 70 a/o Hf seems to be associated with the formation of a particularly voluminous and porous scale. Preferential oxidation of the Hf-rich phase was observed in this alloy. The alloy also contained a considerable quantity of the compound W_2Hf which separated from the melt on solidification, and it is seen that at 1000°C the W-35 a/o HP alloy annealed at 2130°C, which is almost pure W_2Hf, oxidized very rapidly. On the other hand, the 95 a/o Hf alloy oxidized slowly.

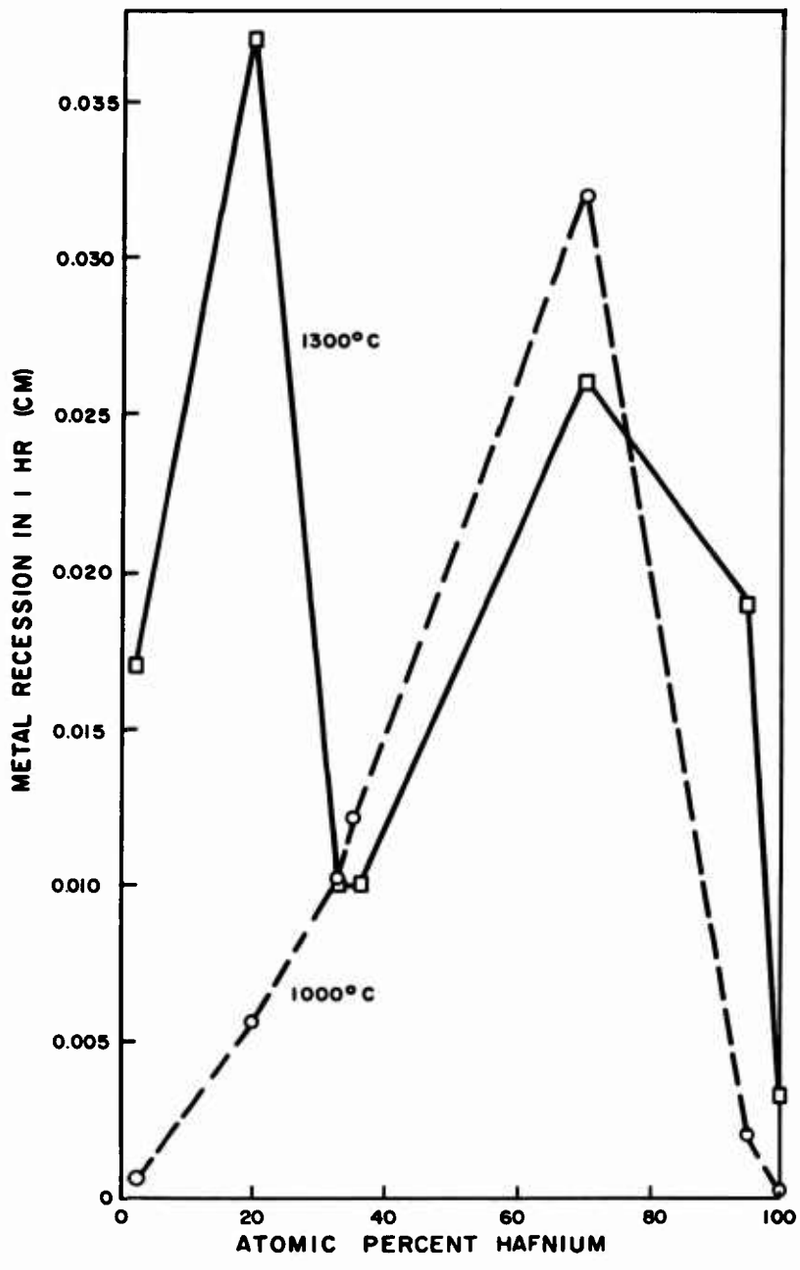

Fig. 38. The effect of Hf content on the metal recession in one hour at 1000°C and 1300°C. Values for 100% Hf are oxide thicknesses formed on Hf-Sn liquid.

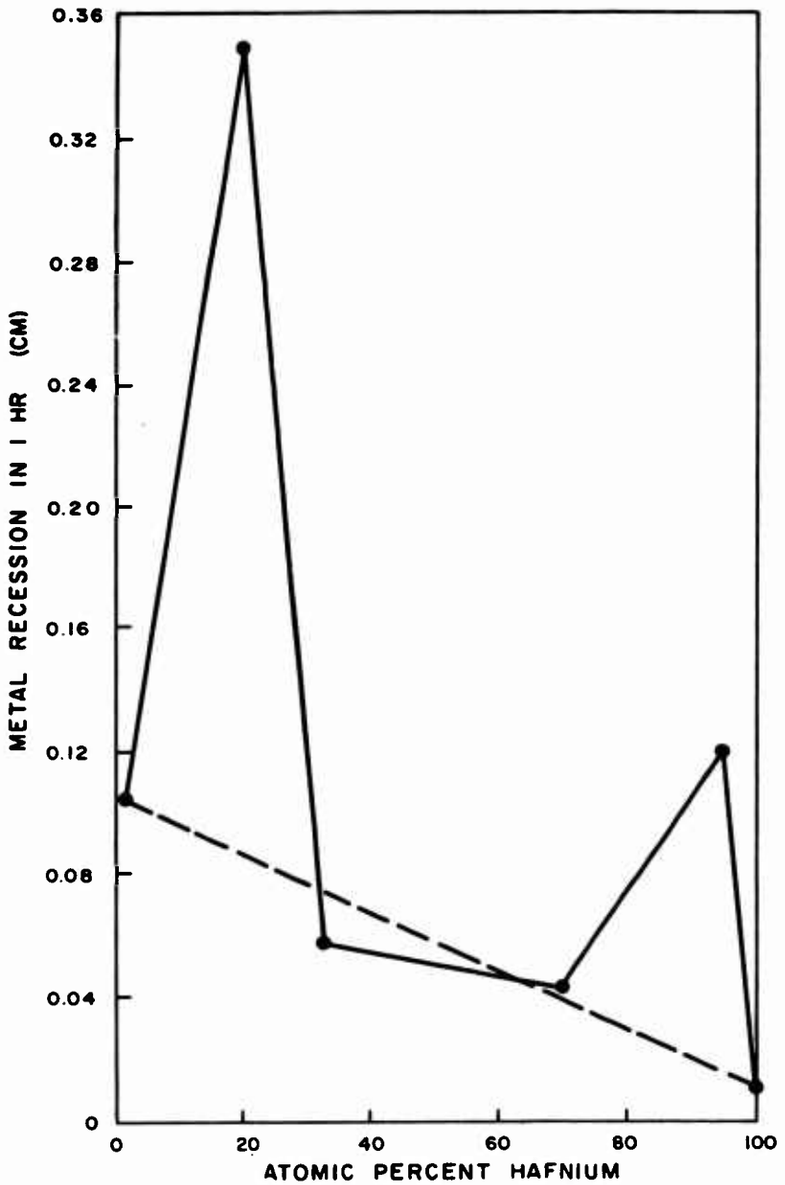

Fig. 39. The effect of Hf content on the metal recession in one hour at 1600°C in W-Hf alloys.

At 1300°C a minimum in oxidation rate at 33-35 a/o Hf is observed and the rates are lower than those observed at 1000°C. A dark, adherent subscale formed on all compositions at 1300°C, which afforded a degree of protection.

An even greater differential in the oxidation rates of the 20 and 33 a/o Hf alloys has developed at 1600°C, while the 70 a/o HP alloy is now better behaved, even though a quite porous scale has formed. In spite of the occurrence of vaporization, the alloys gained weight during oxidation.

The W-35 a/o Hf alloy annealed at 2130°C, which was almost pure W_2Hf, oxidized considerably more rapidly than the corresponding two-phased alloys at 1000 and 1300°C, but less rapidly at 1600°C. The oxides which formed on these alloys were alike, suggesting that the properties of the substrate enhanced the tendency toward breakaway of the intermetallic compound.

4.1.3.2 Multicomponent Diffusion at 1300°C

A complete interpretation of the diffusional processes of importance in the oxidation of W-Hf alloys is impossible due to the complexity of the system and lack of knowledge of the pertinent equilibrium diagrams. Nevertheless, some discussion of the results in terms of the interplay of diffusional and phase equilibrium factors is worthwhile.

First, it is quite clear from the structures identified in the oxidation specimens that complex oxides exist in the W-Hf-O system.

A cubic phase with a lattice parameter of 3.76 A was observed as an internal oxide layer in almost all samples oxidized at 1300°C. The single-phased layer formed on the W-20 a/o Hf alloy at 1300°C indicates a tungsten-to-hafnium ratio of 5:1, and fluorescent analysis of the cubic oxide formed on the intermetallic compound W_2Hf at 1700°C indicates a tungsten-to-hafnium ratio of about 2.8:1. The fact that this phase is found either with or adjacent to W_2Hf suggests an oxygen-to-metal ratio of 2:1 or less.

A second ternary phase observed in the oxidized specimens is the grey, BCC phase observed on the W_2Hf compound. That this is more than a solution of oxygen in tungsten is suggested by the fact that this phase coexists with W_2Hf, HfO_2, and α-Hf in the oxidized W-70 a/o Hf alloy. A third ternary phase with a W-Hf ratio of 1.75:1 and an oxygen-to-metal ratio of 1:1 is indicated by microprobe analysis of the oxide formed at 1700°C on the W-35 a/o Hf alloy (annealed at 2150°C), and a fourth oxide with W-Hf ratio of 10:1 was also observed on this specimen. Finally,

a number of unidentified lines were observed on the X-ray pattern of some of the oxides in conjunction with $W_{18}O_{49}$, HfO_2 and the ternary cubic oxide, suggesting the existence of a fifth ternary oxide with a metal-to-oxygen ratio greater than 2:1.

Certain observations may be made about the diffusion processes occurring during oxidation. In the W-20 a/o Hf alloy the layer identified as the single-phased cubic oxide has a hafnium content greater than that of the substrate from which it is formed. The layer observed above this contains a mixture of $W_{18}O_{49}$ and HfO_2 at a hafnium concentration less than that of the metallic substrate. Thus, there is a net transport by diffusion of tungsten to the outer layer and a depletion of tungsten in the cubic oxide during oxidation at 1300°C.

In the W-33 a/o Hf alloy, a single-phased cubic oxide layer also appears, and this layer contains a higher ratio of tungsten-to-hafnium than the base alloy from which it forms. Chemical analysis of the outer two-phased oxide formed on the sample oxidized at 1400°C yielded 28.9% Hf, which indicates that this layer is enriched in hafnium.

The tungsten-to-hafnium ratio in the outer oxide on the 35 a/o Hf alloy is also greater than that of the base metal, while the single-phased black oxide contains less hafnium than the intermetallic compound.

It is clear that at temperatures of 1300°C and above, transport of tungsten and hafnium occurs during oxidation, and an important factor in the oxidation process is the formation of the simple cubic oxide mentioned above. Neither WO_2 nor HfO_2 are observed as layers in the alloys from W-20 to W-70 a/o Hf. Mass transport of tungsten and hafnium is determined by the interoxide compounds rather than by the simple oxides.

The observation of at least two ternary oxides which do not appear to vaporize rapidly at temperatures as high as 1800°C on the W-35 a/o Hf alloy is also significant (see Table VI). The amount of oxide which vaporized does not increase significantly with temperature and is not great. The interoxide compound appears to be refractory and thermodynamically very stable, perhaps as stable as HfO_2. The process of layer formation at temperatures up to 1300°C apparently is similar to that at 1300°C as observed microstructurally, except that the rate of thickening of the internal single-phased layers increases rapidly with temperature. This suggests that even though the cubic oxide is stable at high temperatures, it is not a satisfactory barrier for oxygen or metal diffusion in an oxidizing environment.

4.1.4 Conclusions

1. Neither HfO_2 nor WO_2 forms as a coherent layer upon the oxidation of W-Hf alloys containing 20-70 a/o Hf.

2. A simple cubic phase with an apparent oxygen-to-metal ratio of 2:1 and a ratio of tungsten-to-hafnium of 5:1 to 3:1 exists in the W-Hf-O system at 1300°C. The growth of this layer is apparently an important rate-controlling process.

3. The cubic oxide formed at temperature of 1300°C and above is not highly volatile and reduces the rate of evaporation during oxidation. However, oxidation rates of the alloys were more rapid than that of liquid Hf-Sn, and it does not appear that any of the compositions studied would be useful as a protective coating for W.

4. In the hafnium-rich alloys, poor ductility at 1000°C is the most probable cause of breakaway. The tungsten-rich oxide formed on the hafnium-lean alloys is apparently not prone to breakaway.

5. At temperatures as high as 1800°C, weight gains rather than losses are obtained, indicating that diffusion in the growth of oxide layers is a more important process than vaporization.

6. Adherent, protective oxides may form on the intermetallic compound, even though the compound itself is brittle. However, the oxidation rate of the compound was quite rapid.

4.2. THE W_2Hf-Re_2Hf SYSTEM

4.2.1 Experimental Procedure

The procedure used in preparing alloys for this study was to blend, press, and arc melt buttons of the appropriate compositions and then to anneal each button for 16 hours at 2000°C prior to testing. The annealed samples were oxidized at temperatures of 1000, 1300, 1600 and 1700°C for three times, and weight changes and oxide thicknesses were determined. The samples were irregular in shape so that accurate measurement of the surface area of the samples was difficult. The compositions of the alloys produced are as follows:

W (%)	Re (%)	Hf (%)
63.0	--	36.0
37.0	25.0	38.0
33.5	34.9	32.6
16.7	50.7	32.6
--	66.6	33.4
--	67.5	32.5

Specimens of the W-25Re-38Hf alloy and the W-50Re-32.6Hf alloy oxidized at 1000°C and 1600°C were prepared for microprobe and X-ray identification of the layers formed. In addition, a microprobe analysis of the Hf-67.5Re alloy (Re_2Hf) was made. Sections of specific layers formed on samples during oxidation were separated for chemical or X-ray diffraction analysis, and the fume generated in the oxidation of the rhenium-rich alloys was collected and identified by X-ray fluorescence analysis.

4.2.2 Results

The weight gains or losses observed for the various samples are given in Table VIII together with the thickness of the oxide formed on samples that were prepared metallographically. The rhenium-rich alloys lost rather than gained weight, and the amount of fuming observed was considerably greater than that produced by the oxidation of tungsten-hafnium alloys. Both the weight losses and the amount of fuming increased with rhenium content.

Figure 40 shows the micrographs of the W-25Re-38Hf, W-34Re-32.6Hf, and W-50Re-32.6Hf alloys. Prior to oxidation the alloys consist of a single-phased matrix in which small amounts of one or two dispersed phases and porosity are evident. Cracks in the unoxidized substrates of some alloys suggest that the intermetallic compound is brittle -- an observation verified by the difficulties encountered in preparing specimens. Two or three distinct oxide layers are observed at almost all temperatures. The internal and external oxides appear to be dense and adherent, although some porosity is observed in the middle layer of some samples. The three layers have different optical properties under polarized light. The oxide thickens with increased temperature, in spite of the occurrence of vaporization.

The structures of three alloys close to Re_2Hf are shown in Fig. 41. Appreciable amounts of a second and perhaps third phase are observed in all samples except the Re-35Hf alloy. The matrix phase is Re_2Hf in all samples. Only a few specimens of the Re_2Hf alloys other than the Re-35Hf alloy were oxidized, and the kinetics of oxidation was evaluated only for

TABLE VIII

The Effect of Re Content on the Weight Changes and Oxide Thickness Formed in Oxidation of W_2Hf-Re_2Hf Alloys

Test Temp. (°C)	W-35 a/o Hf			W-25% Re-38% Hf			W-34% Re-33% Hf			W-50% Re-33% Hf			Re-35% Hf		
	Time (hrs)	ΔW/A (mg/cm^2)	Oxide Thickness ($cm \times 10^{-3}$)	Time (hrs)	ΔW/A (mg/cm^2)	Oxide Thickness ($cm \times 10^{-3}$)	Time (hrs)	ΔW/A (mg/cm^2)	Oxide Thickness ($cm \times 10^{-3}$)	Time (hrs)	ΔW/A (mg/cm^2)	Oxide Thickness ($cm \times 10^{-3}$)	Time (hrs)	ΔW/A (mg/cm^2)	Oxide Thickness ($cm \times 10^{-3}$)
1000	0.25	32.3	4.8	0.25	2.8	4.6	0.25	-1.73	7.1	0.25	-28.9	20.3	0.25	-135.7	20.8
	0.5	50.7	-	1	-45.3	-	0.5	-4.68	-	0.5	-53.6	-	0.5	-230.7	-
	-	-	-	1	-	95.0	1	-	19.3	1	-	36.3	-	-	-
1300	0.5	27.9	-	0.5	41.1	-	0.5	40.6	-	0.5	-47.7	-	0.5	-290.0	-
	1	24.5	22.2	1	-28.1	26.4	1	93.8	-	1	-162.3	31.8	1	-484.6	64.0
1600	-	-	-	.083	15.8	24.4	.083	56.9	-	.083	.31	-	-	-	-
	.083	44.9	-	.083	20.6	-	.083	-	21.8	.083	-	38.1	.083	-115.5	-
	0.25	37.7	19.0	0.25	20.6	42.1	0.25	27.0	33.	0.25	-3.5	15.2	0.25	-229.3	52.0
	0.5	54.2	-	0.25	39.2	32.3	0.5	34.6	-	0.5	4.6	-	0.5	-411.0	-
	-	-	-	1	48.3	-	-	-	-	-	-	-	-	-	-
1700	0.083	40.5	-	.083	33.3	-	.083	25.9	-	.083	- .3	-	.083	-113.5	-
	0.33	53.8	50.8	0.25	55.1	56.4	0.25	25.6	57.9	0.25	-4.9	38.4	0.25	-307.1	111.8
1800	0.16	36.6	31	-	-	-	-	-	-	-	-	-	-	-	-
	0.5	88.8	80	-	-	-	-	-	-	-	-	-	-	-	-

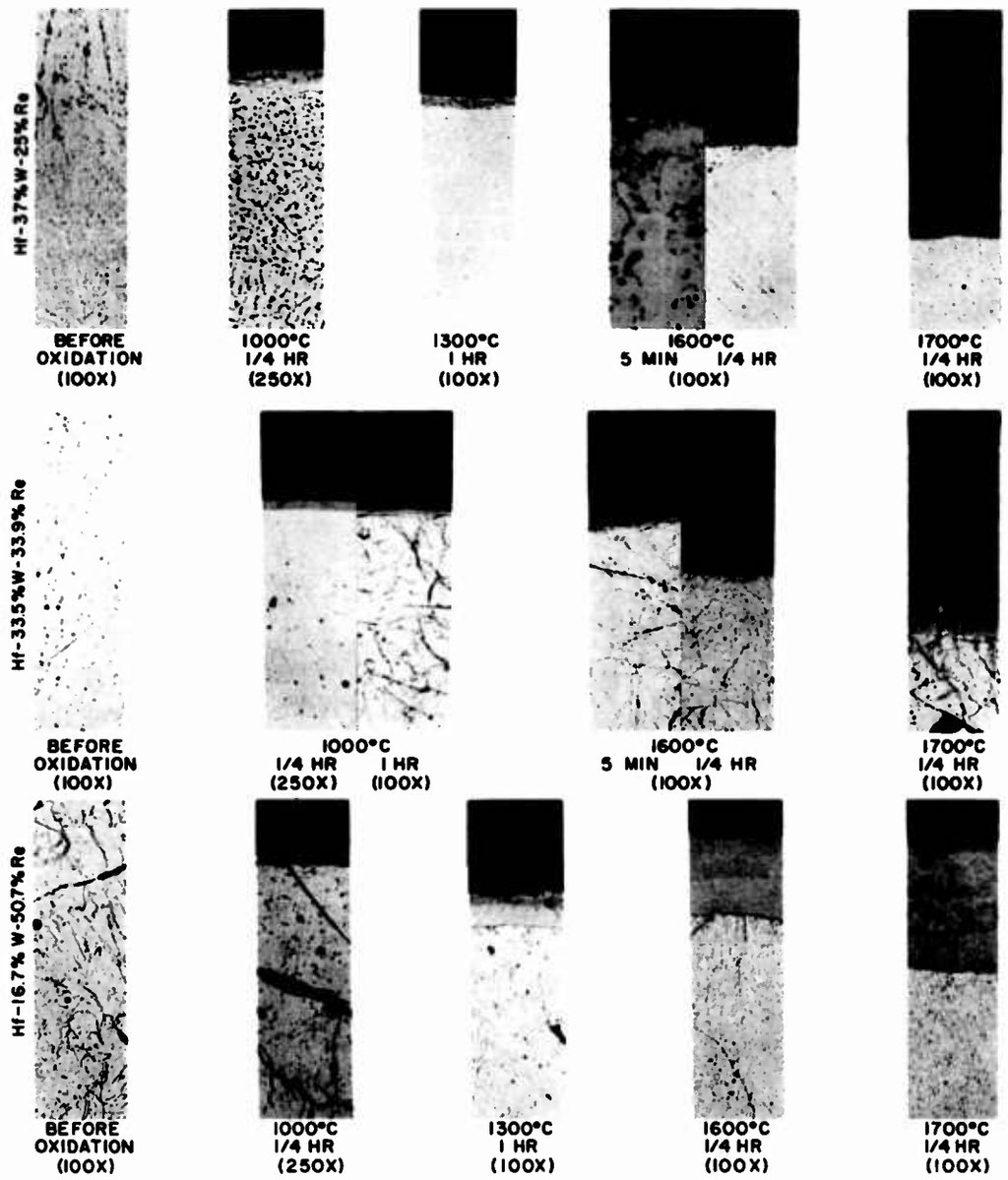

Fig. 40. Microstructures of layers formed in the oxidation of Hf-W-Re alloys (magnification reduced by ~ 40% in reproduction).

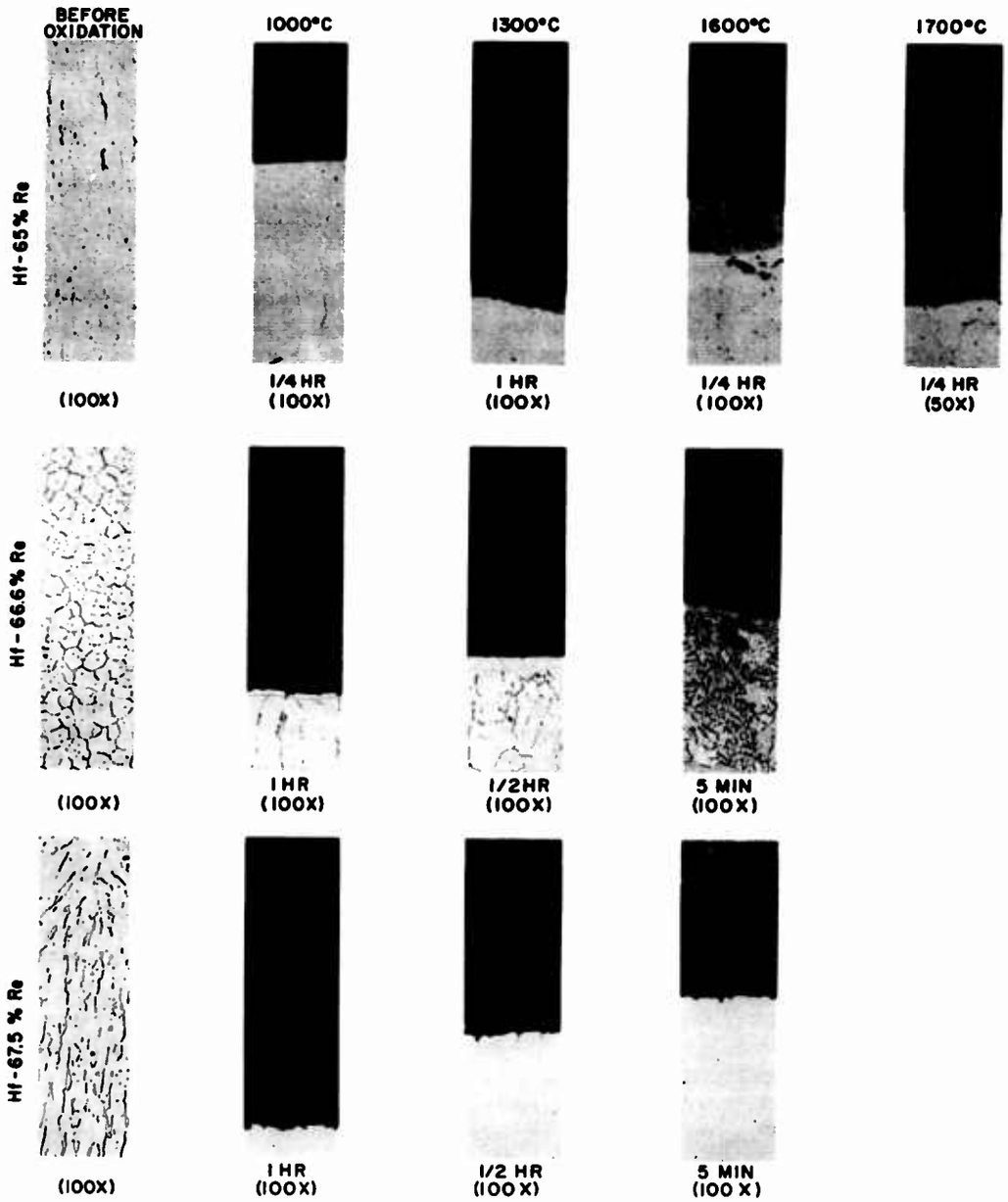

Fig. 41. Microstructures of layers formed in the oxidation of Hf-Re alloys (magnification reduced by ~ 40% in reproduction).

the latter. The oxides formed on all three alloys contain channels that apparently result from vaporization of Re_2O_7; this phenomenon suggests breakaway by vaporization at all temperatures. The oxides were extremely powdery on all three alloys, and the results suggest that no diffusion barrier to oxidation is formed. These results are consistent with the rapid weight loss of these alloys.

The results of microprobe and X-ray diffraction and fluorescence analyses of the oxides formed on the W-Re-Hf alloys are given in Appendix I. Additional X-ray diffraction and X-ray fluorescence analyses were also made of various oxides that were separated from oxidized samples. A compilation of the results of the chemical, microprobe and X-ray analyses is given in Table IX for the alloys oxidized at 1000°C, and in Table X for the alloys oxidized at 1600 to 1700°C. As indicated in Appendix I, the diffraction patterns of the oxides formed in the various layers are extremely complex. There are four possible tungsten oxides, at least three oxides of rhenium, hafnium oxide, ternary W-Hf oxides and perhaps others which might occur. HfO_2 was identified in almost all layers as well as tungsten oxides in some layers. Lines characteristic of Re metal are also evident in the first two layers of the oxides formed at 1600°C.

X-ray examination of the W-Hf-Re alloys before oxidation in all cases indicated Re_2Hf as the matrix phase. Faint, unidentified lines were observed in addition. The lattice parameter of Re_2Hf is slightly increased by the addition of tungsten, but it is apparent that a single-phased region with the crystal structure of Re_2Hf does exist to at least 25% Re.

The external oxide on the W-25Re-38Hf alloy contains no rhenium, as evidenced by both the X-ray fluorescence ratio, Hf (Hf+Re) = 1, and an independent X-ray fluorescence analysis which indicated a tungsten-to-hafnium weight ratio of 0.93, with no rhenium detected. Results for the W-51Re-32.6Hf alloy also suggest that rhenium oxide is vaporized during oxidation. Microprobe analysis of the oxide formed at 1000°C on the Re-32.5 Hf alloy show rhenium only in the vicinity of the metal-oxide interface, and only 6% Re in this region. The tungsten-to-hafnium ratio in the oxide is essentially the same as that in the substrate. Vaporized oxide collected on alundum and analyzed contained no tungsten or hafnium but did show a strong indication of rhenium.

At 1600-1700°C the formation of the oxygen-affected zone, labeled Oxide III in Table X, apparently only involves the diffusion of oxygen, since the microprobe analysis on two samples indicates that the rhenium, tungsten and hafnium contents are the same in this layer as in the substrate from which it has formed.

TABLE IX

Summary of Phases and Compositions of Layers Formed in Oxidation

	of W_2Hf - Re_2Hf Alloys at 1000°C		
Outer Surface of Oxide	**W-25Re-38Hf**	**W-51Re-32.6Hf**	**Re-32.5Hf**
X-ray Diffraction	$A^{(a)}$ (WO_3+HfO_2)	$H^{(a)}$ (WO_3+HfO_2)	
Chem	W/Hf = .93, NO Re		
X-ray Fluoresc.	I_{Hf}/I_{Hf} + Re = 1	I_{Hf}/I_{Hf}+Re = 1	
Microprobe		.5% Re - 32%W - 62.5%Hf-	100% Hf
Inner Oxide Area			
X-ray Diffraction	$B^{(a)}$	$I^{(a)}$	
Chem.			
X-ray Fluoresc.			
Microprobe			6% Re- 94%Hf
Base Metal			
X-ray Diffract.	$G^{(a)}$ Re_2Hf (expanded)	Re_2Hf (expanded)	Re_2Hf
Chem			
X-ray Fluoresc.	I_{Hf}/I_{Hf}+Re = .485	I_{Hf}/I_{Hf} + Re = 33.8	
Microprobe		51%Re-19%W-30%Hf	71%Re-.3%W-29%Hf

(a) Refers to diffraction patterns in Fig. 11 and 12 - Appendix I.

TABLE X

Summary of Phase and Compositions of Layers Formed in the Oxidation of W_2HfRe_2Hf Alloys at 1600 - 1700°C

Nodules	W-35a/o Hf	W-25% Re -38% Hf	W-35% Re-33% Hf	W-50% Re - 33% Hf
X-ray Dif. Chemical X-ray Fluor. Microprobe		C(a) HfO_2 + Unk.	WO_3 + HfO_2 + Unk	K(a) HfO_2+Unk W/Hf = 1.49 No Re
Oxide I X-ray Difrac. Chemical X-ray Fluor. Microprobe	W-Hf = .75/1	C & D(a) $I_{Hf}/I_{(Hf+Re)}$ = .814 -428 outside 16.5% Re-1.5% W 82% Hf inside 30%Re-28%W-41%Hf		L(a) $I_{Hf}/I_{(Hf+Re)}$= 1.0to .634 58.5%Re-2.5%W-39%Hf
Oxide II X-ray Diffrac. Chemical X-ray Fluor. Microprobe	Sc. a_o = 3.76 + (HfO_2+Unk) W/Hf = 2.85 W/Hf = 2.61/1	E(a) $I_{Hf/I_{(Hf+Re)}}$= .350 30% Re = 44% W = 26% Hf		M(a) $I_{Hf/I_{Hf+Re}}$ = .368 59% Re = 18% W = 23% Hf
Oxide III X-ray Diffrac. Chemical X-ray Fluor Microprobe	W/Hf = 1.75/1	F(a) $I_{Hf/I_{(Hf+Re)}}$%.06 27% Re = 36% W - 37% Hf		N(a) $I_{Hf/I_{Hf+Re}}$ = .189 50% Re - 19% W - 31% Hf
Substrate X-ray Diffrac. Chemical X-ray Fluor. Microprobe	W_2Hf	G(a) expanded Re_2Hf $I_{Hf/I_{(Hf+Re)}}$ = .432 27% Re - 36% W - 37% Hf	expanded Re_2Hf	O expanded Re_2Hf $I_{Hf/I_{(Hf+Re)}}$= 0.252 50% Re - 19% W - 31% Hf

(a) Refers to X-ray Patterns in Figs. 11 and 12 - Appendix I - Mostly HfO_2 +.

The formation of the intermediate and outer layers of oxide observed in Fig. 40 do involve mass transport by diffusion of cations in the oxide. A depletion of hafnium in the intermediate layer is observed in both the W-25Re-38Hf alloy and in the W-50Re-33Hf alloy. A corresponding increase in the hafnium-to-rhenium ratio and in the hafnium content of the outer oxide is also indicated. An increase in hafnium content in the external layer could result from vaporization of both rhenium and tungsten oxide. However, the decrease in hafnium content in the intermediate layer suggests transport of hafnium to the external oxide.

A characteristic of the oxide formed on the W_2Hf-Re_2Hf alloys at 1600 to 1700°C was the formation of yellow nodules which grew on the surface of the sample during oxidation. A tungsten-to-hafnium weight ratio of 1.49:1 was indicated by chemical analysis. No rhenium was present in the nodule. X-ray diffraction analysis of the nodules indicated HfO_2+WO_3+ unidentified lines. The only change in tungsten content in the internal oxide layers is that which would be expected, based on depletion of hafnium. A tungsten gradient exists in the external oxide in which the tungsten content decreases toward the external interface.

4.2.3 Discussion of Results

It is apparent that an intermetallic compound exists over a wide range of compositions in the W-Hf-Re system, similar to that observed in the molybdenum counterpart. The intermetallic compound has a melting point above 2000°C since no melting was observed in the samples annealed at that temperature.

Because of the complexity of the processes involved in oxidation and the structures formed, it is difficult to interpret the results completely. Possibly the most outstanding fact is that a coherent protective layer of refractory HfO_2 does not form on the intermetallic compound, so that oxidation is quite rapid under all conditions investigated. At 1000°C the results suggest that the high Re alloys, in particular, oxidize virtually in situ with evaporation of rhenium oxide from the scale. The scale on the tungsten-free compound Re_2Hf is disrupted by this vaporization process and evidently affords no protection whatsoever. More coherent scales form on the W-containing alloys which minimize but do not prevent evaporation at 1000°C, and the high volatilility of rhenium oxides is a major factor in the oxidation of all alloys at this temperature.

In the W-free, Re_2Hf samples breakaway oxidation (including channeling through which rhenium oxide is vented) is observed at temperatures as high as 1700°C. However, in the W-Re-Hf alloys, diffusion of tungsten, hafnium and rhenium in the two external layers occurs to a noticeable

extent at 1600 and 1700°C. The transport of the three elements in the oxide zones can be described as follows. Hafnium transport from the intermediate layer to the external oxide occurs by diffusion, but the increase in hafnium content toward the external surface of the outer oxide is also caused by vaporization of Re_2O_7 and perhaps a tungsten oxide, or by diffusion of tungsten. In the W-Re-Hf alloys, vaporization of rhenium occurs at the external interface, as evidenced by the fact that the rhenium content of the intermediate layer changes only as a result of hafnium depletion, and a gradient in rhenium exists in the external oxide, indicating that diffusion of rhenium to the external surface precedes vaporization at 1600°C and above. The tungsten content also remains essentially unchanged in the intermediate oxide layer but decreases rapidly in the external oxide to a low value at the oxygen air interface. The nodules that form at the external surface contain only hafnium and tungsten as oxides and are rich in tungsten. The formation of these nodules, as well as the possible vaporization of W_3O_9 at very high temperatures, causes depletion of tungsten at the external surface. In contrast to the behavior at 1000°C and perhaps at 1300°C, diffusion at high temperatures is an important process within the oxide layers and vaporization does not occur internally.

4.2.4 Conclusions

1. An intermetallic compound with the crystal structure of Re_2Hf exists over an extended range of compositions in the W-Re-Hf system.

2. Under all conditions, this compound oxidizes quite rapidly and a truly protective oxide does not form upon it.

3. Oxidation of W-free Re_2Hf proceeds by breakaway due to vaporization at all temperatures from 1000 to 1700°C, and weight losses are observed at all temperatures due to evaporation of rhenium oxide.

4. At 1000°C and above in the W_2Hf-Re_2Hf alloys, diffusion of hafnium to the external oxide from an intermediate layer, and diffusion of tungsten and rhenium to the external surface in the outer oxide, are important processes during oxidation.

5. At 1600 and 1700°C oxidation of Re_2Hf-W_2Hf alloys causes weight gains, indicating that less volatile oxides form at these temperatures, although vaporization does occur at the external surface.

5. THE Sn-Al-Cr-O AND Sn-Al-La-O SYSTEMS

In previous experimental work on the growth of refractory oxides from liquid substrates,[2] it was demonstrated that liquid substrates could be used effectively to prevent breakaway in those oxides in which breakaway was caused by stresses at the oxide metal interface. However, the parabolic growth rates of hafnia, zirconia and thoria from liquid substrates also demonstrate that the rate of oxygen diffusion in the relatively pure oxides formed was greater than could be tolerated at temperatures above 1600°C in a protective system. Although methods of decreasing diffusion rates in oxides at very high temperatures are relatively unexplored, approaches that have been proposed involve either the addition of small amounts of a second element to change the defect structure of the oxide or the addition of larger amounts of a second element to form an oxide of a different crystal structure. Both approaches involve alloying and require knowledge of the factors governing the oxide compositions formed on a liquid alloy substrate. Therefore, experimental studies of the growth of oxides on Sn-Al-Cr and Sn-Al-La alloys were conducted with the primary objective of determining the influence of liquid alloy composition on the nature of the oxide phases produced during oxidation and the secondary objective of determining the influence of composition and temperature on the diffusion-controlled oxidation rate. The two systems will be discussed separately in the following sections.

5.1 THE Sn-Al-Cr-O SYSTEM

5.1.1 Procedure

The Sn-Al-Cr-O system is of particular interest since chromium oxide and aluminum oxide both have higher free energies of formation than tin oxide. In the temperature range of 1000 to 1900°K, the standard free energy of formation of aluminum oxide (-216 to 160 kcal/gm mole O_2)[22] is greater than that of chromium oxide (-139 to 102 kcal/gm mole O_2). The phase diagram for the Cr_2O_3-Al_2O_3 quasi-binary is known, and consists of a simple solid solution between the two oxides with a liquidus curve deviating slightly from a straight line between the melting points of the two oxides. Information on the diffusion rate of O_{18} in pure and impure alumina[23] at temperatures up to 1775°C indicates that impurities have a marked effect on the diffusion rate at lower temperatures, but that at temperatures of 1600°C and above, the diffusion rate is more dependent on the intrinsic defect concentration than impurity content.

Henzler and Henry[24] have demonstrated that the addition of 1% Cr_2O_3 to Al_2O_3 causes a substantial increase in the resistivity at 1000 to 1400°C, and a similar peak in resistivity at 95% Cr_2O_3 is observed. Since both Cr and Al have a valence of three in their oxides, it is difficult to explain these results on the basis of a change in defect concentration. A secondary objective was to determine if the increase in resistivity of the oxide is associated with a decrease in the rate of oxidation of Al-Cr alloys.

Alloys containing 5%Al and approximately 95%Sn with additions of 0.05, 0.1, 0.25, 0.5 and 1% chromium were melted in alumina crucibles in inert atmosphere at 1350°C.

The top surface of the alloy button was machined flat and the alloys placed in a crucible similar to that used for melting. Samples were oxidized in the liquid state at temperatures of 1300, 1600 and 1700°C and the weight gained during oxidation was measured. In addition, metallographic specimens were prepared of selected samples, and the thickness of the oxides was measured. Chemical analyses of the initial alloys and of the oxide formed on the Sn-5Al-.05%Cr alloy were obtained.

5.1.2 Results

Contraction of the liquid melts during solidification caused the oxide to distort and wrinkle. Therefore, in calculating specific weight gains, the area of the exposed surface in the crucible was calculated from the diameter of the initial button, and the alloy weights and size of the crucible were maintained constant. This procedure provided a reasonably accurate measurement of the areas. The effect of chromium additions on rate of oxidation, based on the specific weight gains at 1300, 1600 and 1700°C, is given in Table XI. Also included in this table are values obtained when the alloys were oxidized in zirconia crucibles at 1600°C. The specific weight gains of several samples tested at 1600°C in zirconia crucibles are significantly higher than the weight gains observed when identical samples were tested in alumina crucibles. Also, there seem to be irregularities in the weight gains of a few samples oxidized in alumina crucibles. A comparison of the weight gains and oxide thicknesses of samples that were examined metallographically in the Sn-Al-Cr-O system are given in Table XII. The thicknesses of the oxides should be related to the weight gains and the specific weight gains are reasonable except for those samples which were oxidized at 1600°C in zirconia crucibles. In those samples, specific weight gains are significantly higher than would be expected from the thickness of the oxide formed on the top surface.

The effect of Cr on the oxidation rates is seen to be quite small. At 1300°C there may be a minimum at 0.05 Cr. At 1600°C and 1700°C Cr may have slightly increased the rate of oxidation, but the effect is small.

TABLE XI

The Effect of Cr Additions on the Oxidation of Sn-5 Al Alloys at 1300 to 1700°C

Alloy	Specific weight gain in mg/cm² at								
	1300°C			1600°C				1700°C	
	8 hr	16 hr	32 hr	2 hr	4 hr	8 hr	16 hr	0.087 hr	2 hr
Sn-5 Al	3.4	3.5	5.0	6.0	3.1	6.2[b]	--	4.0[b]	16.3
Sn-5 Al (c)	1.9	2.8	4.1	-	-	5.6[b]	--	-	--
Sn-5 Al - 05 Cr	6.0	-	3.3	7.4[a]		10.7 11.8	--	4.5	14.9
Sn-5 Al - 05Cr[c]	2.3	-	-	-		11.1	31.2	-	--
Sn-5 Al - .1 Cr	3.0	2.8	6.2	3.0	4.4	11.0	--	4.5	14.9
Sn-5 Al - .1Cr[c]	2.0	-	-	-	-	20.4	33.8	-	--
Sn-5 Al - .25 Cr	3.9	-	-	-	-	30.0	54.8	-	--
Sn-5 Al - .5 Cr	3.7	3.8	5.6	4.2	6.8	10.2	--	4.6	16.1
Sn-5 Al [c]	3.7	-	-	-	-	60.6	62.8	-	--
Sn-5 Al - 1 Cr	-	4.9	6.1	4.5[d]	7.1	18.2	--	5.6	22.4

(a) Weight gain high based on thickness

(b) Weight gain low based on thickness or weight gains at shorter times

(c) Weight gains high at 1600°C from reaction with ZrO_2 crucible

(d) This test was 2.83 hours at 1600°0

TABLE XII

A Comparison of Thickness of Oxide with Specific Weight Gain in the Oxidation of Sn-Al-Cr Alloys

Alloy	Temp. (°C)	Time (hr)	W/A (mg/cm^2)	Thickness (mils)
Sn-5 Al	1300	32	5.03	.3
	1600	2	6.01	.2
		8	6.25	.6
	1700	2	16.34	.8
Sn-5 Al-.05 Cr	1300	32	3.28	.2
	1600	2	7.41	.25
		8	10.7	.6
		8	11.1	.7
		16	31.2	.9 (a)
	1700	2	4.89	.8
Sn-5 Al-.1 Cr	1600	2	3.01	.25
	1600	8	20.4	1.6 (a)
	1600	16	33.8	1.0 (a)
Sn-5 Al-.25 Cr	1600	8	30	1.1 (a)
	1600	16	55	1.5 (a)
Sn-5 Al- .5 Cr	1300	32	5.63	.5
	1600	8	10.22	.6
	1600	8	60.6	9.5 (a)
	1600	16	62.8	1.5 (a)
	1700	2	16.10	.85

(a) Reaction with ZrO_2 crucible may have caused high weight gain and also may affect thicknesses.

The microstructures of the oxides formed on the Sn-Al and Sn-Al-Cr alloys at 1600°C are shown in Fig. 42. The oxides formed appear to be dense and adherent although some evidence of cracking due to the gross distortion which occurs on cooling and solidification is observed. The oxides formed separate from the substrate in some places, but are adherent overall and difficult to remove. The addition of chromium to the Sn-Al alloy seems to cause the formation of an intermetallic compound (that may have been solid at temperature) in addition to the Sn-Al compound that forms on cooling. Neither the structures nor the composition of the compounds in the substrate were identified.

Chemical analyses of specific samples or layers produced during oxidation of Sn-Al-Cr alloys are given in Table XIII. Since both aluminum and and chromium have relatively high vapor pressures below their melting points, it was necessary to verify that chromium and aluminum were being retained in the liquid alloys after melting. The aluminum contents for all alloys except the Sn-5%Al-1%Cr indicate approximately 5% aluminum. The reason for the low aluminum content in the one alloy is not known. Chromium also appears to be retained after melting since chemical analysis of the final melts gave approximately the intended composition.

Spectrographic analysis was used to determine if Zr contamination occurred in those specimens oxidized in zirconia crucibles at 1600°C. The fact that zirconium was detected in the metal suggests that a reaction does occur and that the unusually high weight gains and oxide thicknesses of those alloys which were oxidized in zirconia crucibles at high temperatures are spurious results.

In order to determine the Cr content of the oxide, a sample was prepared by oxidizing the Sn-5%Al-.05%Cr alloy under cyclic conditions for 17 cycles and a total of 32 hours at 1300°C. The repeated stresses that resulted from the gross distortions encountered in melting and freezing produced an oxide that could be removed from the surface for analysis. The oxide contained 0.125% chromium, which is approximately 1/10 the ratio of chromium to aluminum in the base metal.

5.1.3 Discussion of Results

Chemical analysis of the oxide formed at 1300°C on the 5%Al-.05%Cr alloy indicate that the ratio of aluminum to chromium in the oxide is approximately 1000 to 1, while in the alloy it is 100 to 1. This partition is expected from the values of the free energies of formation of aluminum oxide and chromium oxide, and indicates how purely thermodynamic factors control the composition of the oxides formed on liquid alloys.

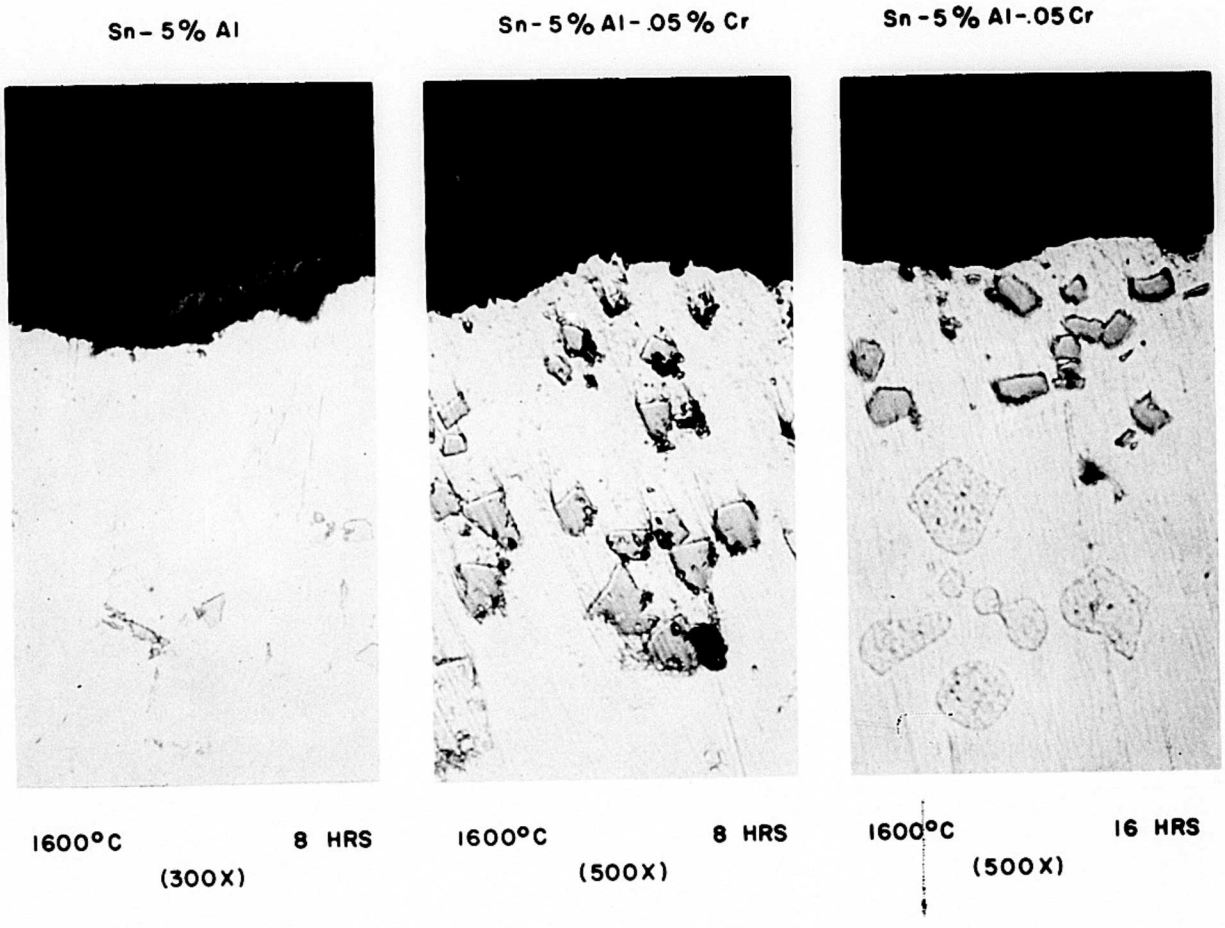

Fig. 42. Microstructures of layers formed in the oxidation of Sn-Al and Sn-Al-Cr alloys.

TABLE XIII

Chemical Analyses of Specific Samples in the Sn-Al-O System

Sample	% Al	% Cr	Other
Sn-5% Al, as melted	5.58		
Sn-5% Al-.1 Cr, as melted	5.49	.14	
Sn-5% Al-.5 Cr, as melted	5.15	.42	
Sn-5% Al-1% Cr, as melted	2.64	1.5	
Oxide from Sn-5%Al-.05 Cr oxidized (cyclic) 32 hr. at 1300°C		.125	
Sn-5 Al-.1 Cr, metal from sample oxidized 1600°C 5 min. in a ZrO_2 crucible			Zr detected

The effects of chromium content and temperature on the thickness of the oxides formed at 1300, 1600 and 1700°C are given in Fig. 43. The thickness of the oxides rather than the weight gains have been used since the thickness measurements are believed to be more reliable. At 1300°C there may be a minimum at 0.05%Cr. At 1600 and 1700°C there was no change, or a slight change, due to Cr, in agreement with Reference 23 on the effect of impurities on the diffusion rate of oxygen in Al_2O_3. Small additions of chromium seem to initially decrease the rate of oxidation at 1300°C; however, this result cannot be correlated with the data of Henry and Henzler[24] which indicate an increase in resistivity at low Cr_2O_3 contents, because the composition for minimum rate of oxidation and the composition at which maximum resistivity was obtained are not the same.

The fact that the thin films of oxide formed on the liquid alloys oxide can withstand considerable distortion without disintegration is in agreement with mechanical properties obtained on sapphire and ruby crystals at temperatures up to 1000°C.[25] Since the films are thin, the stresses involved are primarily bending stresses. In tests of pure sapphire, the modulus of rupture increases in a temperature range of 800 to 1000°C. In Reference 25 the author proposes that plastic deformation, at least micro-plastic deformation, occurs in both pure Al_2O_3 and ruby (Al_2O_3+Cr) at temperatures above 1000°C.

5.1.4 Conclusions

1. Chromium as well as aluminum is present in the oxide formed over liquid Sn-Al-Cr alloys. The ratio of chromium to aluminum in the oxide is less than that in the base metal in accord with the relative magnitudes of the free energies of formation of Al_2O_3 and Cr_2O_3.

2. The addition of 0.05 to 0.1% Cr to a Sn-5% Al alloy seems to decrease the thickness of the oxide formed in 32 hours at 1300°C; but chromium content has no effect on the rate of thickening of the oxide at temperatures of 1600°C and above.

3. The thin oxide films formed on the Sn-Al and Sn-Al-Cr alloys are adherent and withstand considerable distortion without cracking.

5.2 THE Sn-Al-La-O SYSTEM

5.2.1 Procedure

Experimental studies of the Sn-Al-La-O system were conducted to provide further information on the factors governing the formation of a complex oxide from a liquid substrate. The Al_2O_3-La_2O_3 quasi-binary

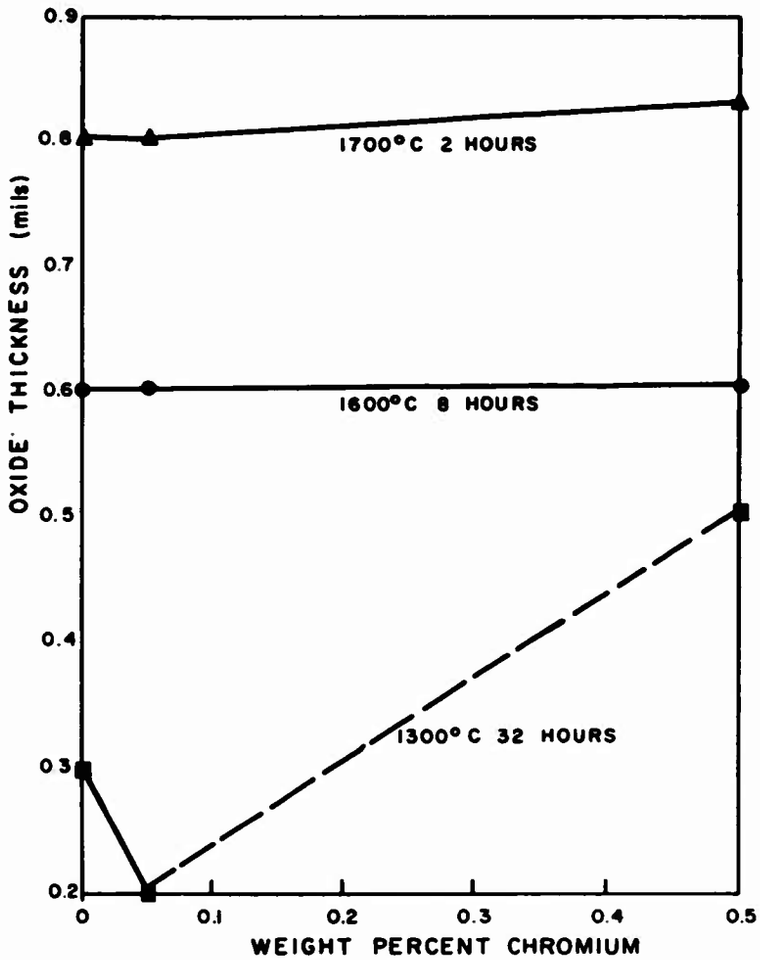

Fig. 43, The effect of Cr content and temperature on the thickness of oxide formed in oxidation on Sn-Al-Cr alloys.

phase diagram is not completely known; however, the liquidus indicates[26] a minimum melting point of about 1850°C at approximately 20a/oLa_2O_3.

An interoxide compound, $La_2O_3 \cdot Al_2O_3$, is known to exist and is identified as a perovskite in Reference 27 and a hexagonal structure in Reference 28. In the temperature range of 1000 to 1800°K the free energy of formation of La_2O_3 (-252 to -196 kcal/gm mol O_2) is greater than that of aluminum oxide (-216 to -160 kcal/gm mol O_2). The free energy of formation of the compound oxide is not known. The alloy should be liquid at almost all temperatures although an intermetallic compound, $LaAl_2$, which melts at 1400°C, has been reported.[5]

The procedure used in studying the oxidation of Sn-Al-La alloys was essentially the same as that finally developed for study of the Sn-Al-Cr alloys. Samples were melted in Al_2O_3 crucibles at 1500°C, the top surfaces of the ingots so formed were machined and the ingots were placed in similar Al_2O_3 crucibles for oxidation in the platinum rhodium wound furnace or in an induction coil. Alloys of the following compositions were prepared: Sn-15%Al, Sn-15%Al-1%La, Sn-14%Al-5.4%La, Sn-13.5%Al-9%La, and Sn-13%Al-13%La (% ≡ w/o).

The alloys were oxidized at 1300, 1600 and 1700°C for two or three times at each temperature, and the specific weight gained during each test was calculated on the basis of the area of the top surface of the ingot. Selected specimens were prepared for microscopic examination, and the thicknesses of the oxides formed on these samples were determined. A sample of the Sn-13.5%Al-9%La alloy was analyzed by the microprobe. In addition, an approximate measure of the ratio of lanthanum in the oxide to that in the base metal was obtained by sparking the oxide surface and a machined surface of the base alloy under identical conditions, and determining the relative amounts of lanthanum, aluminum and tin evolved using a mass spectrograph. Samples of the oxides were scraped from the surfaces of the specimens, and X-ray diffraction analysis of the structures carried out.

5.2.2 Results

The weight gains and thicknesses of oxides formed at 1300, 1600 and 1700°C are given in Table XIV. The results obtained for a Sn-16.6%Al alloy in Reference 2 are also included for comparison. The specific weight gains at 1300 and 1700°C indicate that the extent of oxidation increases at these two temperatures with increase in lanthanum content of the base alloy, while at 1600°C additions of 1 and 5.4%La seem to decrease the rate of weight gain. At 1700°C the weight gains suggest approximately parabolic growth for all alloys, while at 1600°C signs of linear oxidation appear in the eight-hour tests for several alloys. Indications of a more rapid reaction at the crucible wall were noted.

TABLE XIV

The Effect of La Additions on the Oxidation of Sn-Al-La Alloys at 1300 and 1600°C

	1300°C		1600°C						1700°C	
	16 hours		2 hours		4 hours		8 hours		1/2 hour	2 hours
Alloy	ΔW/A mg/cm²	Thick. mils	ΔW/A mg/cm²	Thick. mils	ΔW/A mg/cm²	Thick. mils	ΔW/A mg/cm²	Thick. mils	ΔW/A mg/cm²	ΔW/A mg/cm²
Sn-15 Al	2.35	--	7.4	0.75	11.5	0.75	22.1	--	6.6	13.3
Sn-15 Al - 1 La	3.36	0.1	6.23	0.23	10.35	0.4	17.3	0.6	17.7	36.6
Sn-14 Al - 5.4 La	5.61	1.2	10.81	--	10.0	0.66	14.0	1.5	26.9	38.0
Sn-13.5 Al-9 La	11.56	1.5	31.04	--	15.6	1.0	28.4	0.5	39.0	77.0
Sn-13 Al - 13 La	74.7	--	43.9	0.8	47.0	2.5	2.1	3.0	51.0	90.0

	1300°C				1600°C			
	8 hours		16 hours		2 hours		8 hours	
Alloy	ΔW/A mg/cm²	Thick. mils	ΔW/A mg/cm²	Thick. mils	ΔW/A mg/cm²	Thick. mils	ΔW/A mg/cm²	Thick. mils
Sn-16.6 Al	2.5		11.7		15.3		27.0	0.94
	7.7		8.8				21.1	
							25.2	0.73
							31.0	

The external appearance of the alloys after oxidation was significantly influenced by lanthanum content of the alloy. The alloys containing 1 and 5.4% lanthanum formed oxides very similar to those formed on the Sn-15%Al alloys. A grayish-white oxide, distorted by the volume change during solidification, was formed on all three alloys. The oxides formed on the alloys containing 9 and 13% lanthanum had a characteristic black-gray appearance and a texture which suggested that the external oxide was powdery. The oxide film could not be removed by use of scotch tape or other adhesive, however, showing that the film was adherent to the surface. Another characteristic of the oxidized lanthanum-rich samples was the occurrence of pellets approximately 3/16 in. in diameter on which an oxide film had formed that was quite different from that on the surface of the specimen.

Microstructures of the oxides formed on the alloys are given in Fig. 44. The oxide formed on the Sn-15%Al-1%La alloy is very similar in appearance to that formed on the Sn-15%Al sample in that it is dense and adherent over most of the surface. The oxide formed on the sample containing 5.4%La at 1600°C is similarly dense and adherent and also appears to be single phased. However, the oxide formed on this alloy at 1700°C appears to be two-phased. The fractures in the oxide formed on the Sn-13.5%AL-9%La alloy are apparently the major cause for the difference in the external appearance of the oxide formed on this alloy and the alloy containing 13%La.

The oxide formed on the samples of all five alloys oxidized two hours at 1700°C were scraped from the surface after cooling. X-ray diffraction results indicated that the material removed from each surface, including the zero La alloy, contained alpha Al_2O_3 + Sn + several unidentified lines. No complex oxides were detected above the alloy samples.

Microprobe analysis of the Sn-13.5-9%La sample oxidized for two hours at 1600°C indicates that lanthanum is present in the oxide, but the amount of lanthanum in the oxide is less than that in the base metal. Unfortunately, a quantitative determination of the lanthanum to aluminum ratio was not obtained. Mass spectrographic analysis of a sample of the same alloy oxidized at 1700°C for two hours also indicated that the lanthanum content of the oxide is less than that of the base metal. The spark apparently penetrated the oxide, since indications of large amounts of tin were obtained from the oxide surface. The intensity ratios of lanthanum to aluminum were 0.2 for the metal surface, in contrast with 0.1 for the oxidized surface.

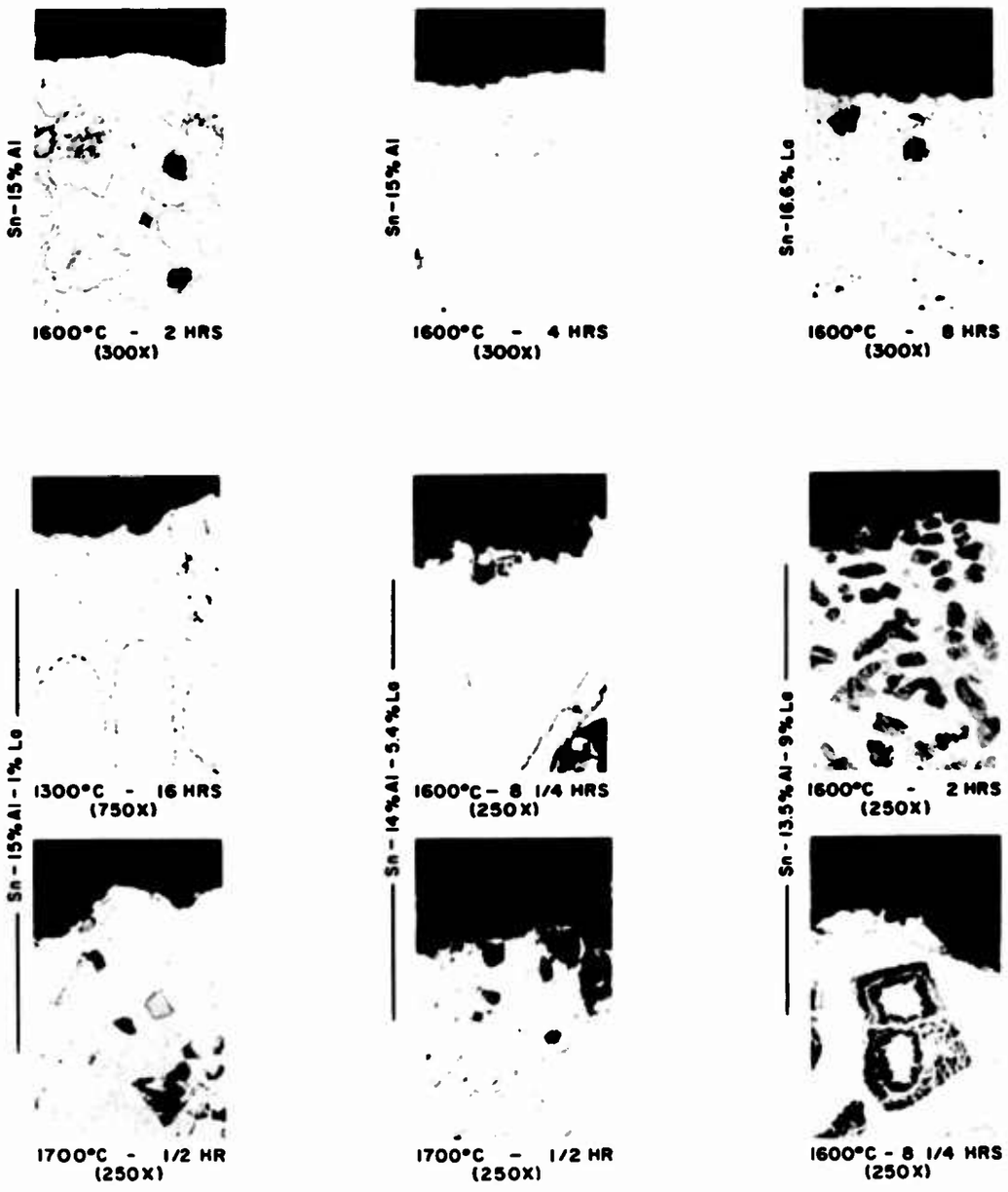

Fig. 44. Microstructures of layers formed in the oxidation of Sn-Al and Sn-Al-La alloys (magnification reduced ~ 20% in reproduction).

5.2.3 Discussion of Results and Conclusions

The outstanding fact which emerges from this study is that La additions significantly increase the rate of oxidation of Sn-Al alloys, and La apparently does not produce a desirable modification in the characteristics of Al_2O_3 layers. It is peculiar that not only was there no evidence of the formation of a complex oxide, but the concentration of La in the scale appeared to be less than that in the base metal. The free energy of formation of La_2O_3 is only slightly greater than that of Al_2O_3, however, and deviations from ideality in the solid solutions might explain the latter behavior. The reason for the increased growth rate of La-containing oxides is not revealed by these studies. Such an increase could be attributed to an increase in the mobilities of diffusing ions in the Al_2O_3 + La scale, an increase in concentration gradients across the oxide, or breakaway. The La-containing scales were more prone to cracking than the La-free, but it appeared that the cracks formed upon cooking rather than at temperature. Therefore, it is felt that either of the first two causes is a more likely possibility.

To summarize the results of this study, the following conclusions may be drawn:

1. The addition of lanthanum, in general, increases the rate of oxidation of liquid Sn-Al alloys, although 1 and 5.4% La alloys oxidized somewhat more slowly at 1600°C than their La-free counterpart.

2. The crystal structure of the scale formed on Sn-15%Al-La alloys oxidized at 1700°C indicated that the oxide formed is predominantly Al_2O_3 even on alloys containing up to 13% lanthanum. No complex oxide was observed in the scale.

3. The oxide formed contains lanthanum evidently in solid solution but the amount of lanthanum present in the oxide is less than that in the base metal.

6. THE ZrN, HfN, AND ThN-ZrN-O SYSTEMS

Study of the oxidation of the nitrides is of interest from both the applied and fundamental viewpoints in the design of protective coating systems for tungsten. The nitrides of many of the elements that form reactive oxides are themselves refractory and do not react with tungsten except at very high temperature. This combination of properties makes nitrides ideal as barrier or reservoir layers in the protective coating of tungsten. From a basic research standpoint, however, the study of oxidation of nitrides is important in that nitrides represent a type of refractory compound (nitrides, carbides, and borides) in which either the rigidity of the substrate or the evolution of the gas during oxidation could cause breakaway. Therefore, the study of nitrides was undertaken (1) to determine if, during the oxidation of nitrides, nitrogen was released internally to cause breakaway, and (2) to determine the effect of the mechanical properties of the substrates (i.e., high strength but low elevated-temperature ductility) on the tendency toward breakaway.

The alloys selected for study were ZrN and HfN, produced by nitridization of pure zirconium and hafnium rods, and nitrided Zr-Th alloys. In the following sections the experiments with ZrN and HfN are discussed together, and the experiments with nitrided Zr-Th alloys are presented separately.

6.1 The ZrN-O and HfN-O SYSTEMS

6.1.1 Procedure

In both the Zr-N and Hf-N systems, the mononitrides are the only compounds that exist, and both possess a NaCl structure. The lattice parameter of ZrN is 4.57 and the melting point 2980°C, while the lattice parameter of HfN is 4.52 and the melting point 3300°C. The general shape of the Zr-N diagram is similar to that of the Zr-O system in that the addition of nitrogen increases the alpha to beta transformation temperature.[5] For example, at 1300°C with increasing nitrogen content, β-Zr is stable to 2 a/o nitrogen; the alpha + beta field exists between 2 and 12 a/o nitrogen and alpha exists between 12 and 22 a/o nitrogen. The phase diagram for the Hf-N system is probably similar, although the composition limits of the one- and two-phased fields are not known.

The production of reasonably thick layers of zirconium or hafnium nitride for oxidation tests was difficult because of the low rate of growth of the nitrides. The procedure finally devised consisted of resistance heating hafnium or zirconium rods in nitrogen at 1600 to 1700°C, for times of 17 to 48 hours. The diameter of the Zr rods used was approximately 1/8 in., while the Hf rods were approximately 0.2 in. in diameter.

Samples of the nitrided specimens were oxidized at 1200 and 1600°C by induction heating in air for various times. The thickness of oxide formed was measured under the microscope, but many samples were oxidized throughout as the result of permeation of oxygen through cracks in the nitrided layers. Consequently, weight-gain measurements or thickness measurements of the oxide formed on such samples were meaningless.

6.1.2 Results and Discussion

The rates of nitride layer formation on zirconium and hafnium are extremely slow even at temperatures as high as 1800°C. It appears that zirconium is more rapidly nitrided than hafnium at 1200 and 1350°C, but the reverse is true at 1640°C, as shown in Fig. 45. Since the weight gains/unit area are proportioned to $t^{\frac{1}{2}}$, the nitriding rates appear to be diffusion controlled. The activation energies are 52.3 kcal/gm mole for nitriding of hafnium and 49.4 kcal/gm mole for the nitriding of zirconium. The activation energy for zirconium nitriding is in good agreement with published values.

Cross sections of the nitride layers formed on zirconium after 21 hours at 1700°C and on hafnium after 18 hours at 1500°C followed by 32 hours at 1600°C are given in Fig. 46. The microstructures indicate that neither Zr nor Hf is completely nitrided even after extended times at temperatures above 1600°C. Microhardness readings after short-time nitriding treatments at 1200°C indicate that the cores of the samples are significantly harder than the pure metals. Therefore, nitrogen diffusion to saturate the substrate in nitrogen must occur at a relatively rapid rate. However, the subsequent formation of ZrN occurs very slowly. Cracks and porosity in the internal nitrogen-affected layers are observed in both the zirconium and hafnium samples in the as-nitrided condition. The external layer formed on both samples has the characteristic golden color of the nitrides, and is apparently ZrN or HfN. The dark two-phased region in the ZrN sample apparently is the result of transformation during cooling.

The external appearance after oxidation of the nitrided rod specimens is also shown in Fig. 46. Permeation of nitrogen through the cracks in the core of the rod permitted oxidation throughout, and after 5 minutes at 1200°C the ZrN sample had spalled. At 1600°C the external oxide that formed appeared to be generally dense and protective, but growth stresses due to internal oxygen permeation caused flaws or fracture in the oxide.

The microstructures shown in Fig. 46 indicate that a relatively thick layer of ZrN is formed by nitriding at 1700°C for 48 hours. Oxidation of this sample at 1200°C for 5, 10 and 15 minutes produces a uniform

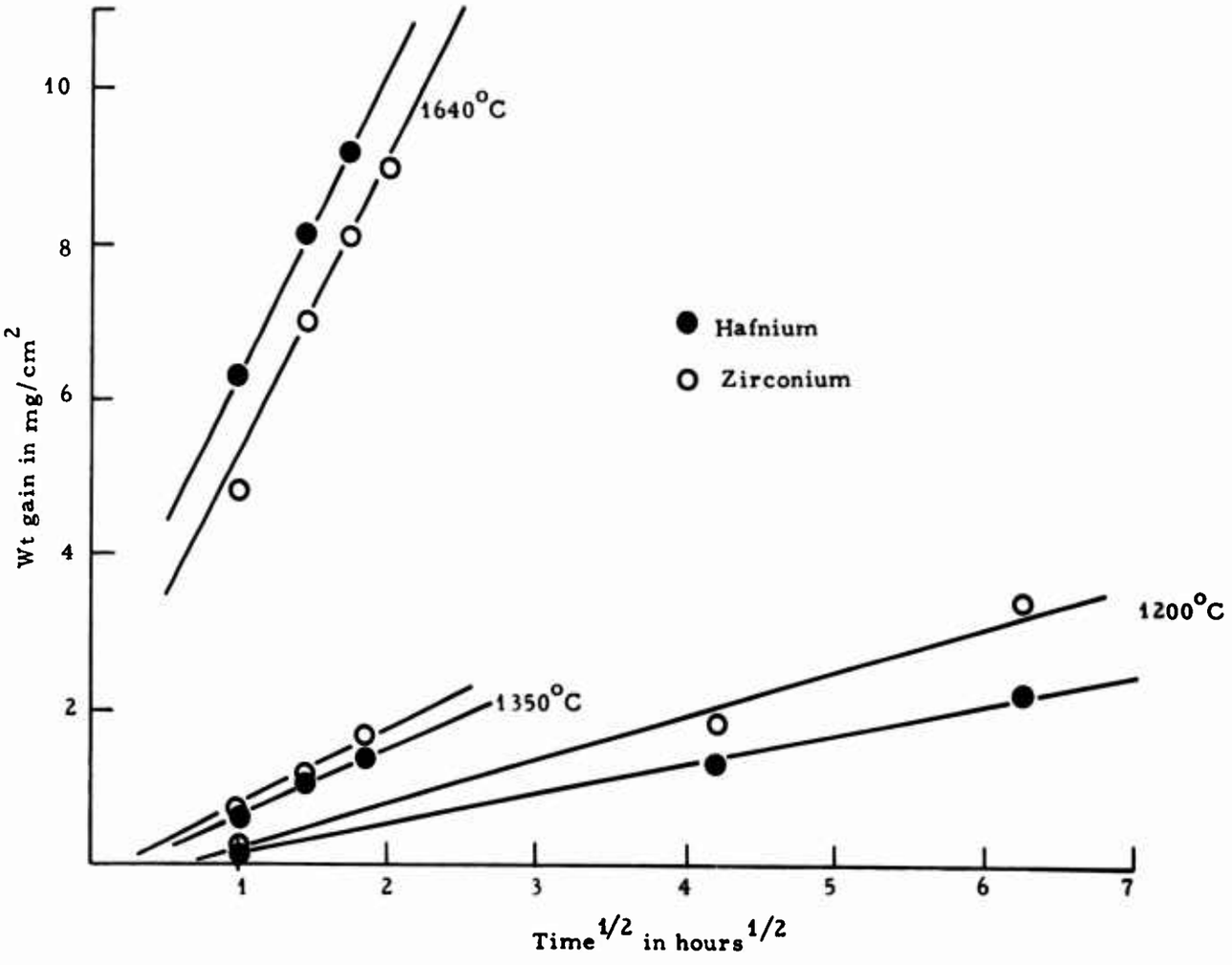

Fig. 45. Nitriding of hafnium and zirconium as a function of time at 1640, 1350 and 1200° C.

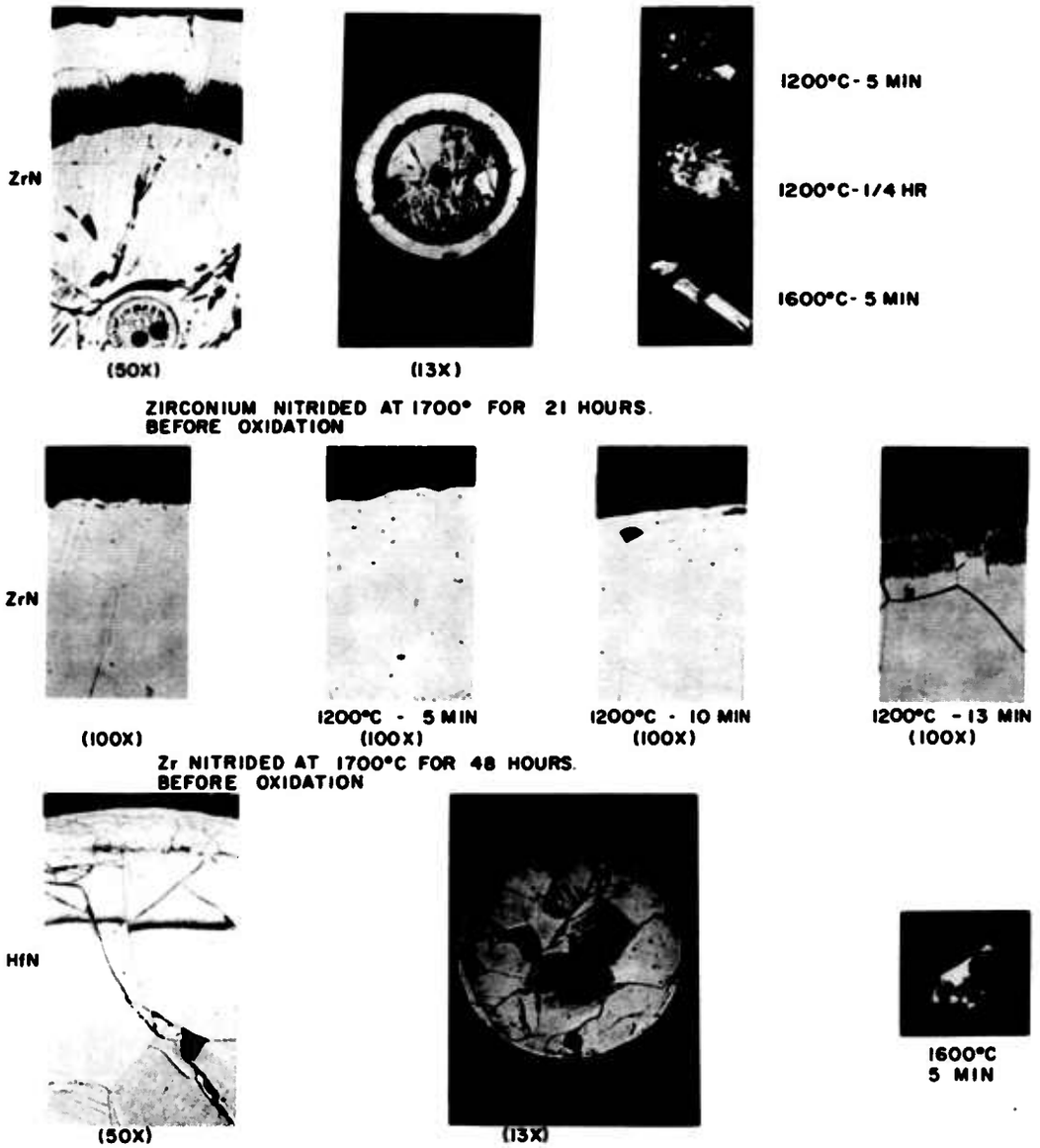

Fig. 46. Oxidation of nitrided zirconium and hafnium (magnification reduced ~40% in reproduction).

oxide layer, and portions of the layer, particularly that portion near the metal oxide interface, are dense and adherent. Porosity or fracture is observed, however, and is particularly evident in the outer portion of the oxide formed in 5 and 15 minutes. The rate of thickening of the oxide is linear at 1200°C, and oxide thicknesses of 0.0033, 0.0065, and 0.010 cm were observed after test times of 5, 10 and 13 minutes, respectively. These results indicate that at 1200°C the oxidation of zirconium nitride involves breakaway due to mechanical factors or the vaporization of nitrogen.

6.2 ZrN-ThN-O SYSTEM

6.2.1 Procedure and Results

The study of the ZrN-ThN-O system was initiated (1) to obtain additional information on the effect of a brittle substrate or evolution of gas on the tendency toward breakaway, and (2) to compare the oxidation behavior of nitrided with unnitrided Th-Zr alloys, particularly at high temperatures where a single-phased scale should be observed.

ZrN and ThN are isotropic and the lattice parameters of the face centered cubic structures are 4.57 A and 5.21 A, respectively. Although the 14% difference in lattice parameters is higher than might be desired for complete miscibility between the two nitrides, there is a reasonable possibility of solid solution formation. Th_2N_3 also exists in the Th-N system.

Samples of the Zr-30, Zr-55, Zr-70 and Zr-85%Th alloys produced as indicated in Section 2 were cut into coupons and nitrided at various temperatures from 500 to 1900°C by furnace heating in a nitrogen atmosphere. Samples nitrided for 6 hours at 1300°C were oxidized at temperatures of 1150, 1200 and 1600°C, and the weight gains during nitridization and during subsequent oxidation were measured. Microscopic examination and thickness measurements of the oxide formed were obtained and a sample of the nitrided Zr-30%Th alloy oxidized at 1200°C for 10 minutes was submitted to Battelle Memorial Institute for microprobe and X-ray analysis of the layers formed during oxidation.

The weight gains during nitriding of the Zr-30, 55, 70 and 85%Th alloys, together with thickness measurements of the nitride formed on the Zr-30%Th and Zr-55%Th alloys, are given in Table XV. The rate of nitrogen pick-up is very dependent on composition. For example, the amount picked up in 6 hours at 1300°C was only 1.08 mg/cm^2 for the Zr-30%Th alloy, but was 21 to 50 mg/cm^2 for the Zr-85%Th alloy. Structures typical of nitrided specimens are shown in Fig. 47 for three alloys. In the Zr-30%Th alloy an external single-phased layer, probably ZrN, is formed at the surface.

TABLE XV

Oxidation of Partially Nitrided Zr-Th Coupons at Several Temperatures

Composition	Nitrided 1300°C, 6 hrs		Oxidation						Remarks
	Wt. gain (mg/cm^2)	Thickness nitride (cm)	Temp. (°C)	Time (hr)	Wt. gain (mg/cm^2)	Oxide (cm)	Internal layer (cm)	Saturated layer (cm)	
Zr-30 Th	1.48	0.0004							
	1.77	--	1150	0.25	29	--	--	--	White
				0.5	35				
				0.75	39				
	1.08	--	1200	0.09	33				
				0.17	56				
	1.80	--	1200	0.17	--	0.020	0.014	0.003	Micro-probe
	1.78	--	1600	0.17	87	0.044	0.044	--	
Zr-55 Th	5.57	0.0007 & 0.00164(2)	1150	0.25	51.4				
	5.1								
	5.15		1200	0.09	35				
				0.17	59				
	3.7		1200	0.17	--	0.036			
	3.7		1600	0.17	46	0.038	0.030	--	Spalled
Zr-70 Th	26.1		1150	0.25	21.5				
Zr-85 Th	21.4(1)		--						
	54.1(1)		1150	0.25	11				
	47.9(1)		1200	0.09	8.9				
				0.17	14.0				
	22.1(1)		1200	0.17		0.026	0.008		Oxide decomposes
	51.1(1)		1600	0.17	21.2	0.015	0.046		

(1) Samples blistered.
(2) Two zones in microstructure.

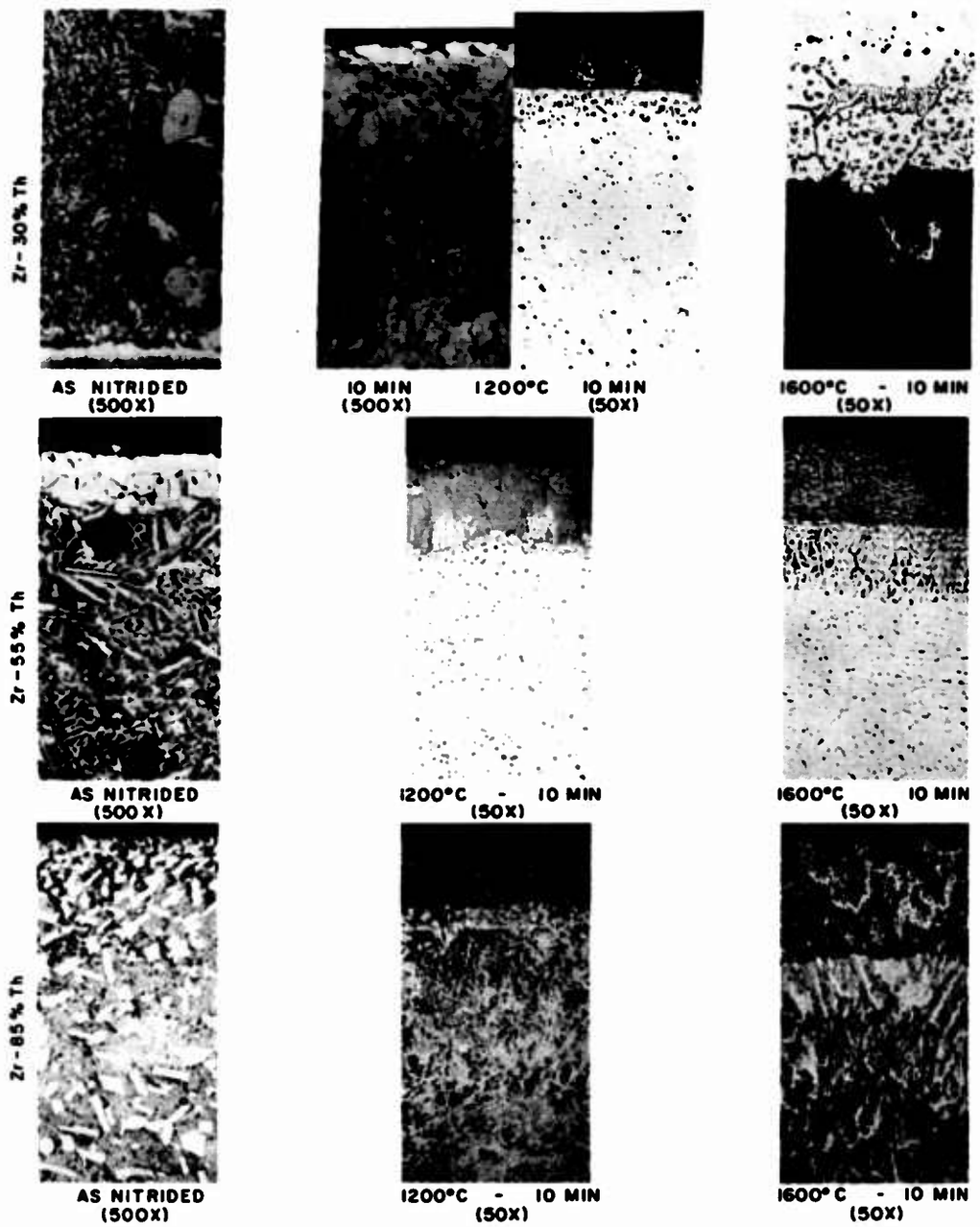

Fig. 47. Layers formed in the oxidation of Zr-Th alloys that have been nitrided at 1300°C for six hours (magnification reduced ~20% in reproduction).

A similar layer is observed in the Zr-55%Th alloy; however, in this sample, a subscale layer which may be α-Zr saturated with nitrogen is also observed. In the Zr-85%Th alloy, the nitride is two phased, consisting of a grey matrix, probably a thorium-rich nitride and angular Widemanstatten particles which have the typical gold-to-orange color of ZrN. Thus, the increased nitriding rate in the 70 and 85%Th alloys is associated with the formation of a matrix of thorium-rich nitride. Samples of nitrided Zr-70%Th and Zr-85%Th decompose rapidly in air, and the structure observed in the microscope changes drastically within 5 minutes.

Oxidation of the partially nitrided specimens at 1150 and 1200°C occurs quite rapidly, as shown in Table XV, and the structures observed in the Zr-30%Th and Zr-55%Th alloys are quite similar to those observed in the oxidation at 1200°C of the unnitrided alloys of the same composition. Hardness traverses indicate an oxygen or nitrogen-saturated α-Zr layer immediately adjacent to the external oxide, and particles which may be nitrides are also observed in the oxide layer.

In the Zr-85%Th alloy the structure is quite different from that produced by oxidation of the unnitrided alloy, as shown in Fig. 47. In the nitrided specimen a porous layer of mixed oxides is formed at 1200°C which is apparently nonprotective, and a subscale layer, apparently ThO_2 and ZrN, is also observed.

Oxidation proceeds rapidly at 1600°C, and the oxides formed after 10 minutes are 0.06 to 0.09 cm thick. The structures of layers observed after oxidation at 1600°C (Fig. 47) are quite different from those observed after oxidation at 1200°C. In the nitrided Zr-85%Th alloy the outer layer of mixed oxides is not badly spalled, and this layer seems to be coherent with the layer that contains ThO_2 plus residual ZrN. Oxidation proceeds quite readily in the thorium-rich nitride matrix, but apparently ZrN reacts more slowly with oxygen. The oxide formed on the Zr-70%Th and Zr-85%Th alloy also decomposed or disintegrated to a fine powder on standing, even in a desiccator. The scale formed at 1600°C on the nitrided Zr-55%Th alloy is also two phased, and the continuous phase is the darker ThO_2.

The results of the microprobe analysis of the Zr-30%Th alloy submitted to Battelle are discussed in Section 4.2 of Appendix I. It is possible not only to characterize the layers formed during oxidation but, as well, to gain some insight into the structure and composition of the layers previously formed during nitridization. The structure of the oxidized sample of partially nitrided Zr-30%Th alloy is given in Fig. 4 of Appendix I. The original structures of the samples are shown in Fig. 47. Two oxide layers are observed: a thin external oxide identified by X-ray diffraction analysis

as ZrO_2 and a thicker two- or three-phased oxide. Beneath the oxides an $\alpha+ThO_2$ layer, and a $\beta+ThO_2$ layer are present, and in these layers the ThO_2 particles contain some zirconium, while the finely dispersed phase appears to be pure ThO_2.

If the morphology of the layers and particles in the oxidized specimens are compared with the morphology in the nitrided alloy prior to oxidation, it appears that the thin external layer was originally pure ZrN which has been converted to ZrO_2.

It is also apparent that the two-phased, as-nitrided structure shown in Fig. 47 is stable at 1200°C since the phases were apparently oxidized in situ and the morphology of the oxidized structure is similar to that of the nitrided structure.

6.2.2 Discussion of Results

The effect of composition on the rate of nitriding can be rationalized in terms of the structures observed. The nitride formed on the Zr-30%Th and the Zr-55%Th alloys has the characteristic gold color of ZrN, and apparently diffusion of nitrogen through ZrN occurs at a very slow rate. The formation of a two-phased nitride on the Zr-70%Th and Zr-85%Th alloys suggests that there is a two-phased region in the ZrN-ThN quasi-binary phase diagram. The matrix phase in the latter alloys is apparently a thorium-rich nitride, either ThN or Th_2N_3, and the fact that the nitriding rate is more rapid indicates a more rapid diffusion rate of nitrogen in thorium nitride. The tendency for the nitrides of these alloys to decompose in air is also characteristic of thorium nitrides.

A complete analysis of the oxidation of the Th and Zr nitrides is impossible because of the complexity of the systems and the paucity of the data; however, a few conclusions may be drawn. The two nitride phases present in the nitrided thorium-rich alloys (70 and 85% thorium) apparently oxidized in situ. Initially, oxidation caused the formation of a continuous thorium-rich oxide matrix, leaving the zirconium-rich nitride phase unoxidized. Later, the ZrN phase was oxidized, eventually producing a two-phased oxide with essentially the same morphology as the initial nitrided structure.

In the Zr-33%Th and Zr-55%Th alloys, nitriding produced an external layer of ZrN and an internal two-phased layer, consisting of Th-rich particles in a Zr-rich matrix. Upon oxidation, the outer layer of ZrN and the Th-rich particles in the internal two-phased layer oxidize in situ so that their morphology is preserved. The Zr-rich matrix is altered during oxidation by the formation of several layers somewhat like those occurring upon oxidation of the Zr-30%Th alloy previously described.

A consideration of the tendency toward breakaway during oxidation of the nitrided specimens is of special interest for two reasons. First, the nitride substrate is somewhat stronger than the unnitrided metal but is relatively brittle, and probably unable to relay interface stresses. Second, as evidenced by the fact that only small weight changes were experienced in the thorium-rich samples during oxidation at times and temperatures that produced relatively thick oxide layers, nitrogen is released by the reaction with oxygen. Unless this nitrogen escapes by diffusion, the internal pressures could cause spalling of the oxide and breakaway.

Microstructural evidence, as well as the rate of thickening of the oxide formed on the ZrN sample at 1200°C, suggests that breakaway does occur at 1200°C on all completely nitrided samples. Breakaway is even suggested by the structure of the Zr-55%Th alloy nitrided for 6 hours at 1300°C and oxidized for 10 minutes at 1200°C. The oxide formed at 1200°C on the Zr-30%Th alloy has the appearance of a dense and adherent protective layer, but this sample was incompletely nitrided.

At 1600°C the results, particularly those for the ZrN-ThN-O system, indicate that oxidation occurs without breakaway and that dense adherent oxides are formed. Unfortunately even this observation does not differentiate between the influence of the mechanical properties of the substrate and the influence of the evolution of the gas; both the substrate and oxide might be expected to deform plastically at 1600°C, but diffusion of nitrogen would also be more rapid at 1600°C, so that evolution of nitrogen at the air-oxide interface could result.

6.3 CONCLUSIONS

1. The rate of nitridization of zirconium, hafnium and zirconium-rich Zr-Th alloys is diffusion-controlled and extremely slow. The rate of nitridization of Th-rich Zr-Th alloys is more rapid. Diffusion seems to occur more rapidly in ThN than in ZrN.

2. ZrN-ThN mixtures with a thorium-rich nitride matrix decompose rapidly in air at room temperature. The oxide formed on the Zr-85%Th alloy also crumbles to a fine powder on standing in air.

3. The oxidation of ZrN at 1200°C is linear, and breakaway is evident in structures formed during oxidation at 1200°C of nitrided samples of Zr-Th alloys containing 55 and 85%Th. Protective diffusion-controlled growth is suggested by the structures formed at 1600°C on the latter two alloys.

4. It is impossible to determine whether breakaway at 1200°C is caused by the formation of gaseous nitrogen in the oxide or by a change in the mechanical properties in the substrate. The results at 1600°C for the oxidation of nitrided Th-Zr alloys, however, require that evolution of nitrogen occurs by diffusion to the external surface, and suggest that stresses that could otherwise cause breakaway are relaxed due to plastic deformation in the oxide and/or in the matrix.

7. IMPLICATIONS OF THE RESULTS FOR THE DESIGN OF HIGH-TEMPERATURE PROTECTIVE COATINGS FOR TUNGSTEN

The foregoing work represents a study of certain metal-oxygen systems which are felt to be typical or representative of those which come into consideration for the protection of tungsten at temperatures above 2000°C. Each of these systems was chosen in the hope that its behavior would help to clarify specific aspects of the problem of protection against oxidation at high temperatures. In this phase of the program the aspects particularly under consideration were (1) the phenomenon of "breakaway" and (2) the reactions at the metal-air interface which determine the sequence of layers formed at this interface, or "ternary diffusion." However, the results also permit comments to be made about other processes of importance in this problem. Having discussed each system individually in the previous sections of the report, it is now appropriate to consider the results in terms of the various processes which underlie the behavior of protective systems at high temperature and the implications for the protection of tungsten above 2000°C.

7.1 BREAKAWAY

Many potentially useful oxides such as ThO_2, HfO_2, and ZrO_2 undergo breakaway when grown on their parent metals at low temperatures (see Reference 2). It was demonstrated in previous work[2] that breakaway can be prevented, or substantially inhibited by the use of a liquid substrate. However, the use of liquid substrates may not always be practical in coatings systems. One of the significant facts which has clearly emerged from this series of investigations is that the tendency for ThO_2, HfO_2, and ZrO_2 to crack during growth is much less at high than at low temperatures. No instances of cracking of these oxides was observed when the oxidation temperature was above 1400°C, even for the growth of ZrO_2 on unalloyed Zr. This may be due to the fact that refractory oxides exhibit a degree of plasticity at high temperatures[15, 28] which permits the relaxation of stresses that would otherwise cause fracture and spalling. It appears likely, therefore, that breakaway due to spalling at temperature will not be a problem in coatings used at 2000°C and above.

The above comments refer to the behavior at temperature. The problem of cracking is clearly not avoided when thermal cycling between high and low temperatures occurs, since oxides which grow adherently at high temperatures frequently crack when cooled to room temperature. It is important to note, therefore, that the multiphased oxides formed on many of the alloys investigated were less prone to cracking than the oxide formed

on pure Zr. For example, the scales formed on all of the Zr-Th alloys at 1200°C were adherent while ZrO_2 spalled from unalloyed Zr at 1400°C. Protective scales formed on Hf-Y and Zr-Y alloys at 1200°C and on most W-Hf alloys at 1300°C. Moreover, the multiphase scales formed on many of the Zr-Th alloys were resistant to spalling upon thermal cycling. A difference in the behavior of the ThO_2-rich and ZrO_2-rich oxides was noted here; the scales with ThO_2 matrix tended to crack upon cooling, while those with ZrO_2 matrix did not. It was again observed that the scales formed on the Zr-Y alloys resisted cracking upon cooling, while those formed on the Hf-Y alloys cracked badly upon cooling. These results suggest that multiphased oxides are more resistant to cracking than single-phased oxides, and that ZrO_2-base scales are less prone to cracking than those based upon ThO_2 or HfO_2, in spite of the phase transformation in solid ZrO_2.

Since breakaway and cracking upon thermal cycling are complex processes influenced by many parameters, the underlying reasons for the behavior described above are not clear. An increase in plasticity brought about by the presence of many grain boundaries and phase interfaces in the multi-component scale may be imagined. It might also be postulated that the fracture strength of the multicomponent scale is higher, due to a finer grained structure and the presence of dispersed phases.

A question of particular interest in these studies was whether or not breakaway would be accentuated by the use of a hard, rigid substrate in contrast to a plastic or fluid one, and it was for this reason primarily that the W-Hf alloys were selected for investigation. Unfortunately, the scales which formed on the W-Hf alloys were extremely complex and quite different from those which formed on unalloyed Hf or liquid Hf-Sn alloys, namely HfO_2. Therefore, a direct comparison of the spalling characteristics during oxidation of the W-Hf alloys with those other materials cannot be made. It may be significant, however, that the tendency toward breakaway of the W-35Hf alloy annealed at 2130°C, which was entirely W_2Hf, was no worse than that of the same alloy annealed at 1300°C, which was only partially W_2Hf, suggesting that the presence of the intermetallic compound was not seriously detrimental. It is well known that many practical coating systems are based upon intermetallic compounds.

7.2 LAYER GROWTH AT THE AIR-METAL INTERFACE (Ternary Diffusion)

The success of a protective coating depends upon its ability to form a particular surface oxide of the several that might be produced. Design of protective systems calls for a knowledge of the factors that

determine the sequence of oxide and other layers which are formed during the oxidation process. However, the necessary thermodynamic and kinetic data for systems of interest are very meagre.

The difficulties that are encountered in attempting to predict oxide compositions and structures in the absence of sufficient basic data are well exemplified by the results for a number of the systems investigated in this program. On the basis of the free energy of formation of hafnium and tungsten oxides, it was anticipated that HfO_2 would form on tungsten-hafnium alloys, such as W_2Hf, for example. In reality HfO_2 did not form as a continuous layer, but several unidentified W-Hf oxides, and these phases rather than HfO_2 appeared to control the oxidation process. Even more complex structures were developed on the W_2Hf-Re_2Hf alloys, and here again the properties of oxides other than HfO_2 played an important role in determining the oxidation behavior. Under such circumstances it is not only out of the question to anticipate the layers which will form upon oxidation, but it is also very difficult to explain the results in terms of the "diffusion path" concept which requires a fairly complete knowledge of the ternary equilibrium diagram.

If the metals-oxygen phase diagram is known or may be approximated from a knowledge of the binary systems and the structures formed during oxidation, some progress can be made in rationalizing or predicting layer sequences. As a matter of fact, for a number of the alloys studied, the layer sequence is governed by a simple rule; namely, that the diffusion path in the ternary isothermal section is an approximately straight line connecting the alloy composition with the oxygen corner. This is true for the Zr-Th alloys and, with modification, for the Zr-Y alloys.

The particularly simple diffusion path which characterizes the layer sequence at the metal-air interface of these alloys is determined by the fact that transport of oxygen through the layers occurs much more rapidly than transport of metal ions, so that the alloy is oxidized virtually in situ. It seems logical that the predominance of anion diffusion in the oxide layer should be a necessary condition for oxidation in situ, but several other conditions must also be fulfilled. One of these is sufficient solubility and mobility of oxygen in the metallic layers. If this is absent, oxidation in situ might still be possible if oxides of the same metal-metal ratio as the alloy can form. It seems possible that a wide enough range of alloys satisfy these criteria to make the rule of some practical value, although it cannot be applied indiscriminately.

7.3 RATE OF DIFFUSION-CONTROLLED OXIDATION

Although diffusion in oxides was not a central topic in this phase of the program, but is to be considered in detail in the next, nevertheless some remarks about the rates of diffusion-controlled oxidation seem worthwhile at this time. If the scale formed upon a coating is refractory, nonvolatile, coherent, and protective oxidation still proceeds by diffusion through the oxide layers, and the minimum rate of oxidation which can be visualized is this diffusion-controlled rate. The parabolic rate constant derived from the kinetics data in these studies help to indicate the suitability of various oxides for use in protective systems, from the viewpoint of their diffusion characteristics. It has been shown that at 1600°C the k values for the formation of coherent oxide layers on Zr-Th alloys lie between 6×10^{-3} and 10^{-2} $gm^2\ cm^{-4}\ hr^{-1}$, and are between those for the formation of ZrO_2 and ThO_2 scales on liquid Zr-Sn and Th-Sn alloys, $k = 3 \times 10^{-3}$ and 5×10^{-2} $gm^2\ cm^{-4}\ hr^{-1}$, respectively. The value $k = 10^{-2}$ $gm^2\ cm^{-4}\ hr^{-1}$ corresponds to an oxide growth of 0.1 gm per cm^2, or approximately 0.025 cm (0.010 in.) in the first hour. This is an appreciable fraction of the sheet thicknesses which come into question for aerospace applications (10-40 mils) and it does not appear likely that ZrO_2-ThO_2 scales would furnish adequate protection against oxidation at 2000°C for many applications, due to the rapidity of diffusion in these oxide mixtures.

At 1600°C the k value for the growth of Al_2O_3 on liquid Al-Sn alloys is 10^{-5} $gm^2\ cm^{-4}\ hr^{-1}$. Therefore, diffusion occurs much more rapidly in ZrO_2 and ThO_2 even though these oxides are more refractory than Al_2O_3. A high melting point is clearly not a guarantee that an oxide will possess low diffusion rates. The factors controlling diffusion rates in oxides are complex and will be dealt with in the continuation of this program.

The parabolic rate constants for the diffusion-controlled growth of oxide layers on Zr-Y and Hf-Y alloys at 1600°C vary from about 1 to 100 times those for the growth of ZrO_2 and HfO_2 on liquid Zr-Sn and Hf-Sn alloys, 3×10^{-3} and 1×10^{-3} $gm^2\ cm^{-4}\ hr^{-1}$, respectively, and the data strongly suggest that Y increases the rate of diffusion of oxygen in ZrO_2 and HfO_2.

Weight gain data for the oxidation of pure Y suggest a value of k for the growth of Y_2O_3 of approximately 3×10^{-3} $gm^2\ cm^{-4}\ hr^{-1}$ at 1500°C, which is of the same order of magnitude as the k values for growth of ZrO_2 and HfO_2 on liquid Zr-Sn and Hf-Sn alloys, and far higher than that for growth of Al_2O_3. Hence, none of the very refractory oxides dealt with so far in this program look promising for protection at 2000°C and above.

REFERENCES

1. M. Nicholas, A.L. Pranatis, C.D. Dickinson, "The Analysis of the Basic Factors Involved in the Protection of Tungsten Against Oxidation," Part I, ASD-TDR-62-205.

2. M.G. Nicholas and C.D. Dickinson, "An Analysis of the Basic Factors Involved in the Protection of Tungsten Against Oxidation," ASD-TDR-62-205, Part II, September 1962.

3. J.B. Clark, F.N. Rhines, Trans. A.S.M., 51, p.199 (1959).

4. J.S. Kirkaldy and L.C. Brown, "Diffusion Behavior in Ternary Multiphased Systems," paper based on research for National Research Council of Canada and the American Iron & Steel Institute, submitted to Transactions of the Metals Division of C.I.M. (1962).

5. M. Hansen, "Constitution of Binary Alloys," McGraw-Hill Book Co., New York.

6. F.A. Mumpton and R. Roy, "Low Temperature Equilibria Among ZrO_2, ThO_2 and UO_2," J. of the American Ceramic Soc., 43, 234 (1960).

7. B. Lustman and F. Kerze, "The Metallurgy of Zirconium," McGraw-Hill Book Co. Inc. (1955).

8. H.A. Porte, J.G. Schnizlein, R.C. Vogel and D.F. Fischer, "Oxidation of Zirconium and Zirconium Alloys," Journal of the Electrochemical Society, p.506 (June 1960).

9. K. Osthagen and P. Kofstad, "Oxidation of Zirconium and Zirconium Oxygen Alloys at 800°C," J. of the Electrochemical Society, 109, No. 3, 205 (March 1962).

10. G.M. Gordon and R. Speiser, "Protection of Niobium Against Oxidation at Elevated Temperatures," Final Report on N60nr-222(28), Oct. 14, 1961.

11. C.E. Lundine and D.T. Klodt, from "The Technology of Scandium Yttrium and the Rare Earths," literature survey by B. Love, WADD TR-60-864, pp. 194-226 (April 1961).

12. C.E. Lundine and D.T. Klodt from Binary Equilibrium Phase Diagrams in Rare Earth Metals, p. 215, "The Rare Earths" by F.N. Spedding and A.H. Daane, John Wiley & Sons Inc., New York and London (1961).

REFERENCES (Cont'd.)

13. P. Duwez, F. Brown, Jr. and F. Odell, "The Zirconia Yttria System," J. of the Electrochemical Society, 98, No. 9, 356 (Sept. 1951).

14. E. Rudy and P. Stecher, "Zum Aufbau Des Systems Hafnium Sauerstoff," J. of the Less Common Metals, Vol. 5, p. 78 (1963).

15. G.T. Murray, J. Silgailis and A.J. Mountvale, "The Role of Grain Boundary in the Deformation of Ceramic Materials," Summary report on ASD-TDR-62-225 (Dec. 1962).

16. J.M. Dixon, L.D. Lagrange, V. Merten, C.F. Miller and J.T. Porter II, "Electrical Resistance of Stabilized Zirconia at Elevated Temperatures," J. of the Electrochemical Society, 110, No. 4, 276 (April 1963).

17. Von Horst Braun and Erwin Rudy, "Zum Aufbau des Systems Hafnium-Wolfram," Z. Metallk, 51, 360-363 (1960).

18. E. Rudy and P. Stecher, "Zum Aufbau des Systems Hafnium-Sauerstoff," J. of the Less Common Metals, Vol. 5, 78-89 (1963).

19. R. Speiser and G.R. St. Pierre, "Research on the Oxidation Behavior of Tungsten," AF33(616)-5721, Report 10, Dec. 10, 1960.

20. J. Graham, A.D. Wadsley, J.H. Weymouth and L.S. Williams, "A New Ternary Oxide, ZrW_2O_8," J. of the American Ceramic Society, p.570 (1959).

21. E.J. Rapperport et al, "Refractory Metal Constitution Diagrams," WADD TR-60-132, Part II (Sept. 1962).

22. J.P. Coughlin, Contributions to the Data on Theoretical Metallurgy, Part VII, "Heats and Free Energies of Formation of Inorganic Oxides," U.S. Government Printing Office, Washington D.C. (1954).

23. Y. Oishi and W.D. Kingery, J. Chem. Phys., Vol. 33, p. 480 (1960).

24. J.R. Henzler and E.C. Henry, J. Amer. Ceramic Soc., 36, p. 76 (1953).

25. J.B. Wachtman, Jr. and L.H. Maxwell, "Strength of Synthetic Single Crystal Sapphire and Ruby as a Function of Temperature and Orientation," J. Amer. Ceramic Soc., 42, 432 (1959).

REFERENCES (Cont'd.)

26. E.M. Levine, "Phase Diagrams for Ceramists," Part II, J. Amer. Ceramic Soc., Columbus, Ohio (1959).

27. M.L. Keith and R. Roy, "Structural Relations Among Double Oxides of Trivalent Elements," American Minerologist, 39, 1-23 (1954).

28. S. Geller and V.B. Bala, "Crystallographic Studies of Perovskite-Like Compounds, II, Rare Earth Aluminates," Acta Cryst., 9, 1019-1025 (1956).

APPENDIX I

STRUCTURAL STUDIES ON OXIDATION OF REFRACTORY COMPOUNDS AT HIGH TEMPERATURE

David I. Phalen, Dale A. Vaughan, Neil A. Richard,
Alfred E. Austin, and Charles M. Schwartz

BATTELLE MEMORIAL INSTITUTE
505 King Avenue
Columbus 1, Ohio

TABLE OF CONTENTS

LIST OF ILLUSTRATIONS

1. INTRODUCTION

The potential effectiveness of a refractory compound or multicomponent layer for the protection of structural members in very high temperature applications has been under investigation by General Telephone & Electronics Laboratories, Inc. Although this layer would be expected to oxidize in service, it would be expected to provide the sources of reactions necessary for development of a stable oxide. There are a number of factors which determine the behavior of systems involving reactions between complex alloys or compounds and oxygen. Structural and compositional variations which occur during high-temperature oxidation treatment are of major concern due to their effect upon the properties of the resulting oxide phases and of the remaining material. Through the development of an understanding of the mechanism of the reactions involved in a selected number of ternary and quatenary systems, general principles would be established which would guide in selection of materials and would advance barrier-coating technology.

It was the objective of the Battelle investigations to identify compositions and structures of oxide layers and residual substrata of oxidized material systems supplied by General Telephone & Electronics Laboratories, Inc. The purpose of these studies was to aid in understanding the mechanism of oxidation for multicomponent systems, the nature of the paths leading to the formation of the desired oxides and the diffusion gradients, by detailed characterization of phases formed during oxidation.

2. SUMMARY

Specimens supplied by General Telephone & Electronics Laboratories, Inc., have been employed to study the high temperature air oxidation behavior of several refractory alloys under the following conditions.

Composition	Oxidation Treatment
Zr-30Th	1/2 hour at 1200 C
Zr-30Th	2 hours at 1200 C
Zr-30Th	20 minutes at 1400 C
Zr-55Th	1/2 hour at 1200 C
Zr-85Th	1/2 hour at 1200 C
Zr-85Th	2 hours at 1200 C
Zr-85Th	8 hours at 1200 C in 80% Argon + 20% oxygen
Zr-30Th Nitrided 6 hours at 1300 C	10 minutes at 1200 C
Zr-5Y	1/2 hour at 1200 C
Zr-10Y	1/2 hour at 1200 C
Zr-25Y	1/2 hour at 1200 C
Zr-35Y	1/2 hour at 1200 C
Zr-50Y	1/2 hour at 1200 C
Zr-5Y	1/4 hour at 1600 C
Zr-10Y	1/4 hour at 1600 C
Zr-25Y	1/4 hour at 1600 C
Zr-35Y	1/4 hour at 1600 C
Zr-50Y	1/4 hour at 1600 C
Hf-18Y	1/2 hour at 1400 C
Hf-18Y	1/4 hour at 1600 C
W-79Hf	2-1/4 hours at 1300 C
W-69Hf	1/2 hour at 1300 C
Hf-37W-25Re	1 hour at 1000 C
Hf-16.7W-50.7Re	1 hour at 1000 C
Hf-37W-25Re	5 minutes at 1600 C
Hf-16.7W-50.7Re	5 minutes at 1000 C

The structural characteristics throughout the oxide coating and base metal were studied by X-ray diffraction. The average metal composition in the oxide and substrate were studied by X-ray fluorescence, while the metal composition in specific areas and the gradient within the substrate were determined by electron microprobe techniques.

3. EXPERIMENTAL PROCEDURE

The structural and compositional characteristics of the oxidation products formed on refractory compounds at high temperature have been studied by X-ray diffraction, X-ray fluorescence and electron microprobe techniques to aid in understanding the mechanism of oxidation in several binary and ternary systems.

3.1 Phase Analysis

The phase distribution analysis through the oxide layers on Zr-Th, Zr-Th-N, and Hf-W systems was performed by X-ray diffractometer techniques. Diffractometer recordings were taken at desired intervals, usually 0.001 in., through the coating, with successive layers being removed by abrasion on silicon carbide paper. Specific particles were mechanically extracted for analysis by X-ray diffraction, powder employing photographic recording. The relative intensities of several diffraction lines for each phase obtained by the diffractometer method differed from those of the powder method due to preferred orientation of the oxide crystals during growth of oxide. This preferred orientation, unfortunately, prohibited quantitative analyses of the various oxide phases, in these systems. However, a qualitative analysis of phase composition was made on the basis of the diffracted intensity for one characteristic line of each phase.

The experimental procedure was improved for the study of the oxidation products on the Hf-Y, Zr-Y, and Hf-W-Re alloys. In these systems, the oxide was removed in steps by turning off layers on a lathe. The powder from each layer was collected and analyzed by X-ray powder diffraction. This technique eliminates any problem of preferred orientation and allows quantitative analysis by comparison with diffraction patterns obtained from mixtures of known composition.

Although it was not intended to determine quantitatively the lattice parameters of the observed phases, whenever possible the qualitative change in lattice parameter are indicated in the results. From the change, or lack of it, information was gained as to the solubilities between the observed phases.

.2 X-ray Fluorescence

Simultaneously, the average metal composition was measured by X-ray fluorescence analysis, whenever possible. The changes in the metal composition were determined by measuring the intensity of a characteristic line of the spectra emitted by each element and calculating $I_1/\Sigma I_1 + I_2 + \cdots I_i$ where I_1 is the diffracted intensity for a characteristic line of the element being measured and $\Sigma I_1 + I + \cdots I_i$ is the sum of the diffracted intensities of one characteristic line from each element present in the alloy. Oxygen and nitrogen content cannot be determined by this method and were neglected in the present study. For the Zr-Y system, the adsorption of the characteristic X-rays is very nearly the same for the two elements and the quantity $I_y/\Sigma I_{Zr} + I_Y$ yields the percentage of yttrium directly. In other systems where large differences in atomic number occur, a linear relationship was assumed between $I_1/\Sigma I_1 + I_2$ for the base metal composition and 0 or 100 per cent of the elements for which the compositions were to be determined. Because of the large difference in attenuation of the characteristic X-rays of one element by the other, this method does not provide absolute quantitative analyses, but relative changes in composition are readily determined. Since the available X-ray fluorescence unit employs tungsten radiation for the excitation energy, this element could not be measured without resorting to standard samples which were unavailable. Therefore, only hafnium and rhenium were measured for the Hf-W-Re alloys and the data are presented as $\frac{I_{Hf}}{I_{Hf} + I_{Re}}$. This type of data provides only relative changes in the hafnium and rhenium content, but the variation in tungsten was obtained by electron microprobe analysis.

Since the characteristic X-rays generated within the surface irradiated have a limited range (0.001") due to adsorption by the elements present, only the surface layers are analyzed. Thus, by removal of successive layers from the surface a distribution of the elements can be determined as a function of depth below the original air-oxide interface.

It should be noted that the oxide scale on some specimens, both at the surface and at the metal-oxide interface, was irregular. As a result of these surface irregularities, it was not possible to analyze the phase and

average metal content as a function of depth, by the method of layer removal. Also, since the layers of oxide were removed parallel to the surface, the depth at which the metal–oxide interface was observed may differ from that measured from a photomicrograph which represents only a localized area.

3.3 Electron-Probe Analysis

Compositional variations on a point-by-point basis through the oxide coating and into the base metal of selected alloys were obtained by electron microprobe analyses on polished cross sections. Because of the strong interaction of the X-rays, generated by the electron beam of the analyzer, with the elements present in the specimen, the methods of interpreting the raw data are described in some detail.

The characteristic X-ray intensity, produced by an element (a) of atomic number Z in a sample irradiated with an electron beam, is given by the equation

$$I_a = C_a \int_a^{\infty} \Phi\,(\rho_s Z)\, \exp - [(\mu/\rho)\ \rho_s Z \operatorname{cosec} \psi]\, d(\rho_s Z)$$

where I_a is the X-ray intensity and C_a the mass concentration of a; Φ is an excitation efficiency function; μ/ρ is the X-ray mass absorption coefficient characteristic of both the composition of the sample and the energy of the emitted X-rays; ψ is the emergence angle of the X-rays from the specimen and the term ρ_s corresponds to the mass per unit volume in the excited region ($\simeq$ 5 microns) of the sample. It can be seen from this equation that the X-ray generation efficiency as well as the self-absorption characteristics of the sample are sensitive to the bulk density, ρ_s. If the specimen is of uniform low bulk density, the intensities may be adjusted by normalization. Adjustment of the experimental intensities to compensate for large local variations in bulk density, as in some of the oxide layers described below, cannot be carried out with quantitative reliability. However, the data do indicate qualitatively the relative changes in composition through the oxide scales. For dense oxide scales and below the metal–oxide interface, the bulk density is not a problem and the data can be treated quantitatively.

Throughout the base metal the above equation was employed to convert observed intensities, relative to those of pure metals, to weight fractions of the elements. In the case of the oxide scale, however, the characteristic X-ray intensities were measured and then divided by the intensity obtained for the pure metallic elements. These intensity ratios were then converted to weight per cent of the oxide based upon the theoretical intensity ratio for dense bodies of the mixed oxides, but this method can only be employed qualitatively for porous or low density oxide particles.

Two additional problems are encountered in electron microprobe analysis. The first is the electrostatic charging of the oxide surface by the impinging electron beam, resulting in beam movement which effectively defocuses the electron beam. This problem was corrected, on most specimens, by evaporating a 500 Å film of aluminum on the surface prior to examination. The second problem is the small size of certain structural components in both the metal and the oxide, compared to the width of the electron beam, which prevented complete resolution of the compositions of these local regions. Those cases where resolution was a problem are indicated below as the data are presented.

Complete traces of the elemental variation through the oxide and base metal were made only on the Zr-Th alloys. Since the thorium and zirconium contents varied inversely, only the variation in ThO_2 or thorium content will be presented.

Although in the Battelle program it was not intended to carry out a complete metallographic study of the specimens under investigation, photomicrographs of certain specimens are presented in order to correlate the structural and elemental analyses with specific areas under discussion.

4. EXPERIMENTAL RESULTS AND DISCUSSION

Because of the number of systems, the presentation of the results and discussion is divided into sections based upon the components of the base material. Variations in alloying content are included in the section for a given system. The data are presented graphically for each system and discussed in the respective section.

4.1 The Zr-Th System

The structural and compositional characteristics of the reaction products that form on Zr-30, 55, and 85 weight per cent Th alloys when oxidized for 1/2 hour at 1200 C, on Zr-30 and 85 weight per cent Th alloys when oxidized for 2 hours at 1200 C, and on the Zr-30 weight per cent Th alloy oxidized 20 minutes at 1400 C, in dry air, plus those formed on the Zr-85 weight per cent Th alloy after oxidation for 8 hours at 1200 C in 80 per cent argon - 20 per cent oxygen have been studied. The phase distribution, microstructures and compositional analyses for these oxidized alloys are shown in Figures 1, 2, and 3.

Monoclinic ZrO_2, Cubic ZrO_2, ZrN, and ThO_2 are the oxidation products observed on the various specimens. For these studies comprising the initial system investigated, diffractometer methods were employed to investigate the phase distribution through the oxide layer. While this method provides direct measurement of diffraction line intensities, from which relative concentration of phases can be obtained, the conversion of line intensities to the amounts of the various phases present is not possible when preferred orientation exists for one or more of the phases. Differences in the degree of preferred orientation, particularly in the ThO_2 phase, were observed for the various specimens examined, which indicate variations in growth behavior of the oxide scale.

At the air-oxide interface, the degree of preferred orientation decreases with increasing thorium content, becoming randomly oriented in the 85 Th alloys. The preferred orientation was limited to the outer layers of scale on the Zr-30Th alloys but persisted to a greater depth in the scale on the Zr-55Th specimen. The two Zr-85Th alloys had different oxide growth characteristics. After oxidation for 1/2 hour at 1200 C, the oxide phases were randomly oriented throughout the scale; however, after two hours at 1200 C the oxide crystallites on the surface were randomly oriented but the subsurface oxide indicated preferred orientation. Due to the superposition of several of the diffraction lines of ZrO_2, ZrN, and ThO_2, it was difficult to estimate the amount of preferred orientation or to convert the diffraction-line intensities to amounts of the phases present. However, by selecting diffraction lines which could be unequivocally identified for each phase, their intensities could be evaluated in terms of depth below the air-oxide interface, as shown in Figures 1, 2, and 3.

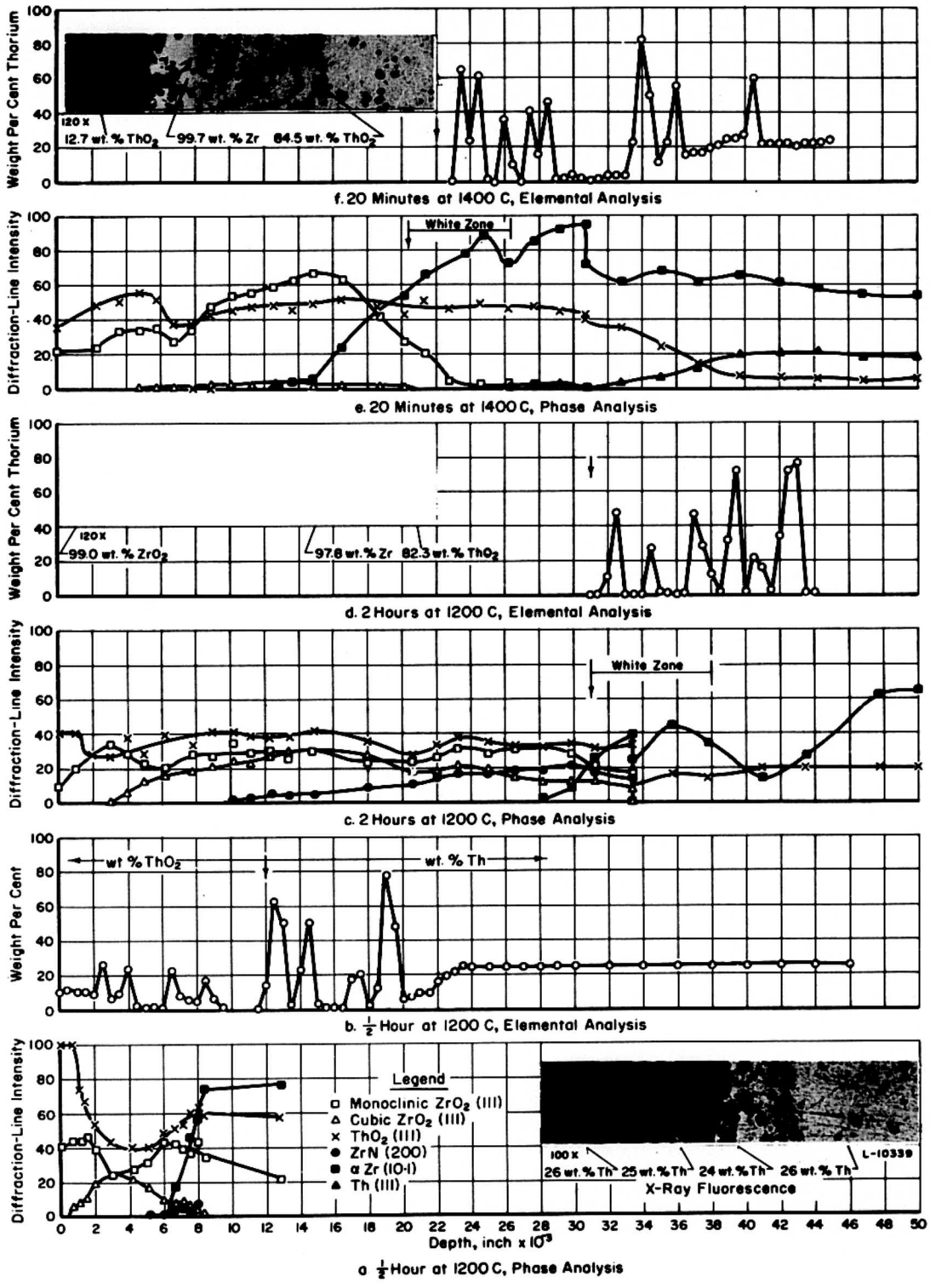

Fig. 1. Phase and elemental distribution for Zr-30Th alloys after oxidation.

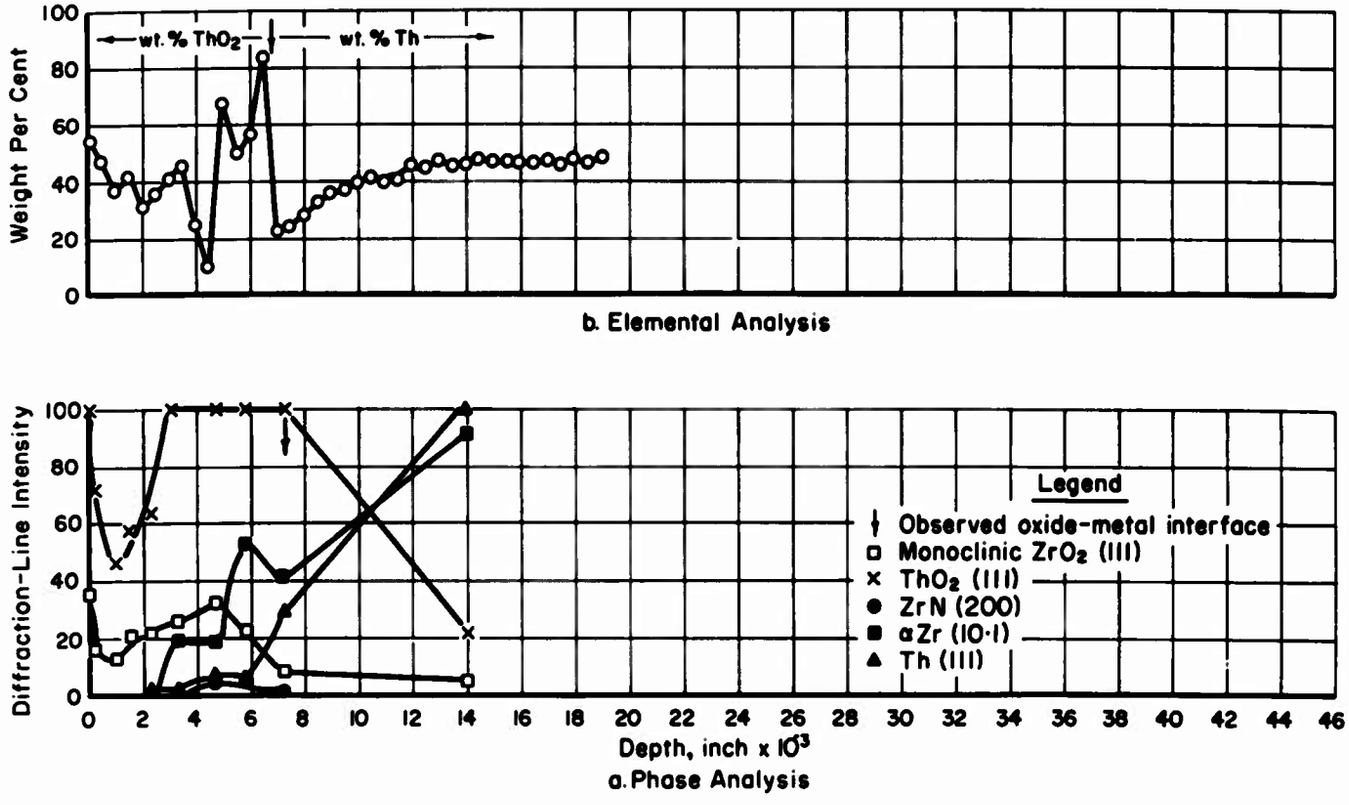

Fig. 2. Phase and elemental distribution for a Zr-55Th alloy oxidized one-half hour at 1200°C.

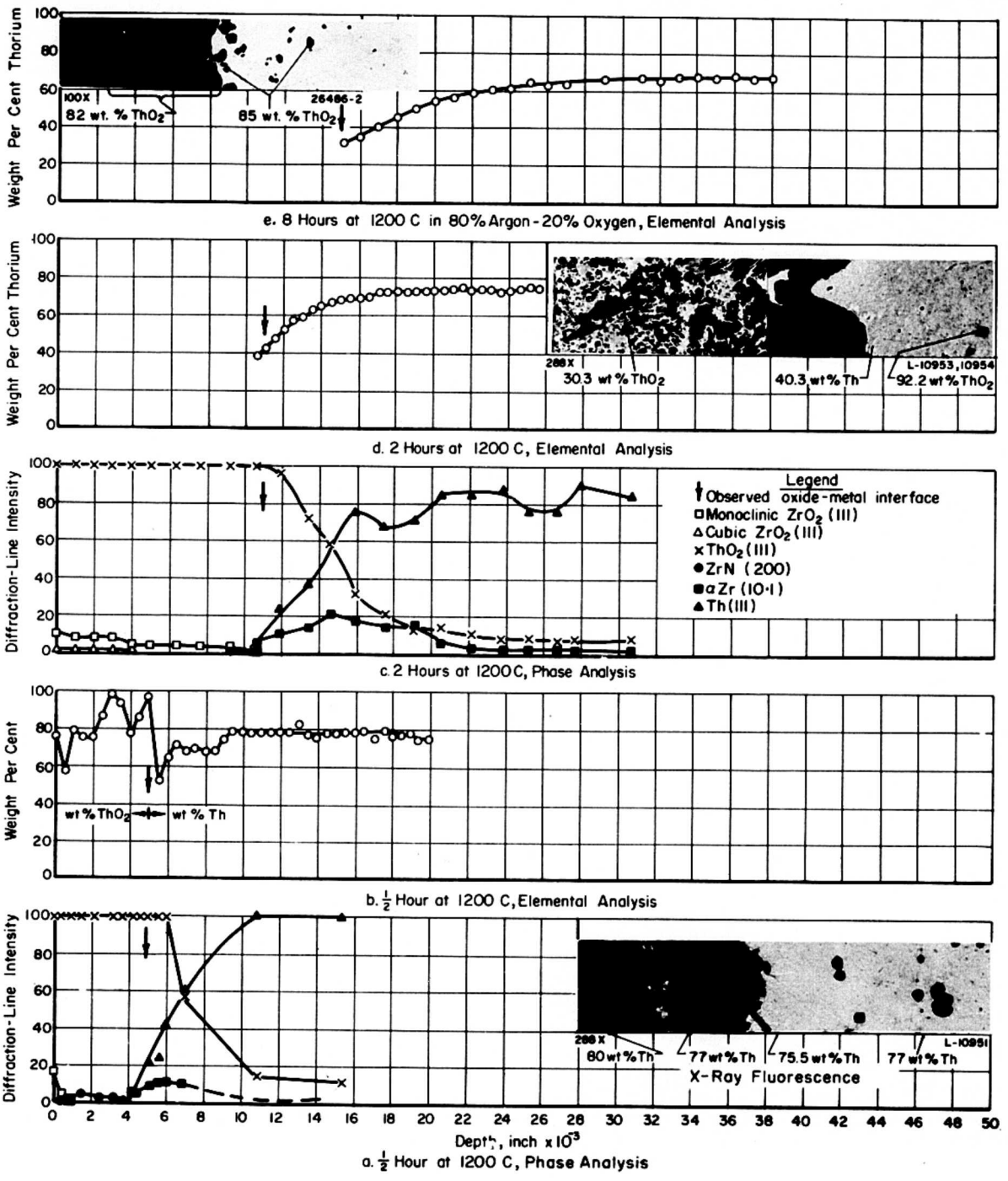

Fig. 3. Phase and elemental distribution for Zr-85Th alloys after oxidation.

The oxide scale on the Zr-30Th specimens was found to contain cubic ZrO_2 as well as monoclinic ZrO_2 and ThO_2. At the oxidizing temperature, cubic ZrO_2 was undoubtedly the product of oxidation, but this phase transforms to monoclinic upon cooling to temperatures below 500 C. However, the transformation is sluggish and some cubic structure was retained in this alloy. Thus, in evaluating the ZrO_2 to ThO_2 ratio, it is necessary to consider both forms of the ZrO_2. In the oxide layers the total diffraction intensity from ZrO_2 decreases and that of ThO_2 increases with increasing thorium content of the alloy. However, the intensities of the ZrO_2 diffraction lines drop sharply at or in the oxide layer ahead of the metal-oxide interface in all cases while the ThO_2 phase is seen to persist to a considerable depth into the substrate metal of the Zr-30Th alloy. The exact depth of the oxide-metal interface may vary by a few mils because of surface irregularities. Also, the apparent extension of ZrO_2 phases below the oxide-metal interface in Figures 1c and 1e results from non-uniform thickness of the oxide at the irregular metal-oxide interface, particularly near the edges of the specimens. In order to obtain better information about the metal immediately below the oxide-metal interface, the areas containing large amounts of oxide were coated with lead napthenate to prevent diffraction from these areas. Thus, two data points are given at the 0.0335-inch depth in Figure 1c and at the 0.0308-inch depth in Figure 1e. The visible oxide was coated for all measurements below the above mentioned depths. As a result of employing this technique, it was found that ThO_2 did form below the metal-oxide interface particularly in the Zr-30Th alloy but that ZrO_2 was not detectable below this point.

ZrN was observed in the oxide scale for several of the specimens. This phase was distributed within the oxide scale and was usually found adjacent to the oxide-metal interface, suggesting that air diffuses through the oxide layer and that nitrogen reacts with unoxidized particles of zirconium. The absence of ZrN on the surface would indicate that it will oxidize in air at atmospheric pressure, but within the oxide the partial pressure of oxygen is lower and the ZrN becomes stable.

Although X-ray fluorescence analyses show the Th-Zr ratio in the oxide and the base metal to be nearly identical, electron microprobe data on the oxide (Figures 1b, 2b, and 3b) show sharp fluctuations in traversing the scale. Only the thorium contents are plotted in these figures, but zirconium analyses were also made. Since the zirconium content varies inversely with the thorium content, the zirconium data are not presented. Immediately below the oxide-to-metal interface, the thorium content of the metallic phase is very low compared to that of the unaffected substrate metal forall alloys. Thus, short range diffusion of thorium toward the oxide layer is evident for all specimens examined. However, discrete particles contained in the metal of the Zr-30Th specimens have been identified as ThO_2 and show high thorium content by electron microprobe analysis. The ThO_2 present in the metal just below the metal oxide interface of this specimen is undoubtedly due to the diffusion of oxygen through the metal. The depth of diffusion varies inversely with thorium content of the alloy. If the thorium content is depleted by the formation of ThO_2, oxygen reacts with the remaining zirconium resulting in the formation of the white zone at the metal-oxide interface. This white zone is alpha zirconium, which has an expanded lattice parameter and has been stabilized at the oxidation temperature by oxygen and/or nitrogen in solid solution. This zone becomes very narrow for the 55 and 85Th specimens due to the fact that the thorium depletion is not sufficient to permit oxygen retention by the zirconium.

Although the microprobe analyses on individual particles show some residual zirconium in the particles believed to be ThO_2, and thorium in particles believed to be ZrO_2, the presence of a second phase in the particles cannot be ignored. Thus, the solubility of zirconium in ThO_2 or of thorium in ZrO_2 when formed by oxidation of the alloy could not be confirmed by these analyses. Since moderate solubility of ZrO_2 ($a = 5.10$ A) in ThO_2 ($a = 5.60$ A) or vice versa, would be expected to change significantly the lattice parameter of the respective phases, the X-ray diffraction data were examined for shifts in diffraction line position. The maximum shift observed throughout this study would indicate a change in lattice parameter by 0.4 per cent. If this shift were converted into solid solubility, assuming Vegard's law to apply, it would correspond to a 4 per cent solubility of ZrO_2 in ThO_2 or of ThO_2 in ZrO_2. No attempt was made to investigate the solubility by precision lattice parameter measurements.

Summary

The products of the oxidation of Zr-Th alloys oxidized at 1200 and 1400 C are monoclinic ZrO_2, cubic ZrO_2, ZrN, and ThO_2. Only ThO_2 was detected by X-ray diffraction examination of the Zr-85Th alloy oxidized in 80 per cent argon - 20 per cent oxygen. The relative intensities for the ThO_2 and ZrO_2 phases coincide quite well with the thorium and zirconium contents of the alloy being oxidized. ZrN was observed in the oxide layer for all specimens after air oxidation. However, its position varied, being near the oxide-metal interface on the Zr-30Th alloy, but extending toward the air-oxide interface for alloys of higher thorium content.

The white zone immediately below the oxide scale is alpha-zirconium stabilized by either oxygen or nitrogen. Its width decreases with increasing thorium content and increases with time at temperature for a constant thorium content. X-ray fluorescence and electron microprobe analysis have shown that there is but limited bulk diffusion of the metallic elements during the oxidation of Zr-Th alloys at 1200 and 1400 C, but that localized diffusion, initiated by the formation of ThO_2 particles, takes place at the metal-metal + oxide boundary.

The mechanism of oxidation of Zr-Th alloys at 1200 and 1400 C is thus one of diffusion of the oxidizing medium through the oxide and the substrate metal with only a short range diffusion of thorium at the metal-metal + oxide boundary. This does not eliminate the possibility of nonselective cation diffusion into the oxide.

4.2 The Zr-Th-N System

One specimen of a Zr-30 weight per cent Th alloy nitrided 6 hours at 1300 C and oxidized 10 minutes at 1200 C has been studied for oxidation behavior.

The phase distribution and composition variations throughout the oxide and base metal are shown in Figure 4. It is of interest to note that only monoclinic ZrO_2 was observed to a depth of 0.003 inch below the air-oxide interface even though thorium was observed at this depth by electron microprobe analysis. Below a depth of 0.003 inch and above the oxide-metal interface

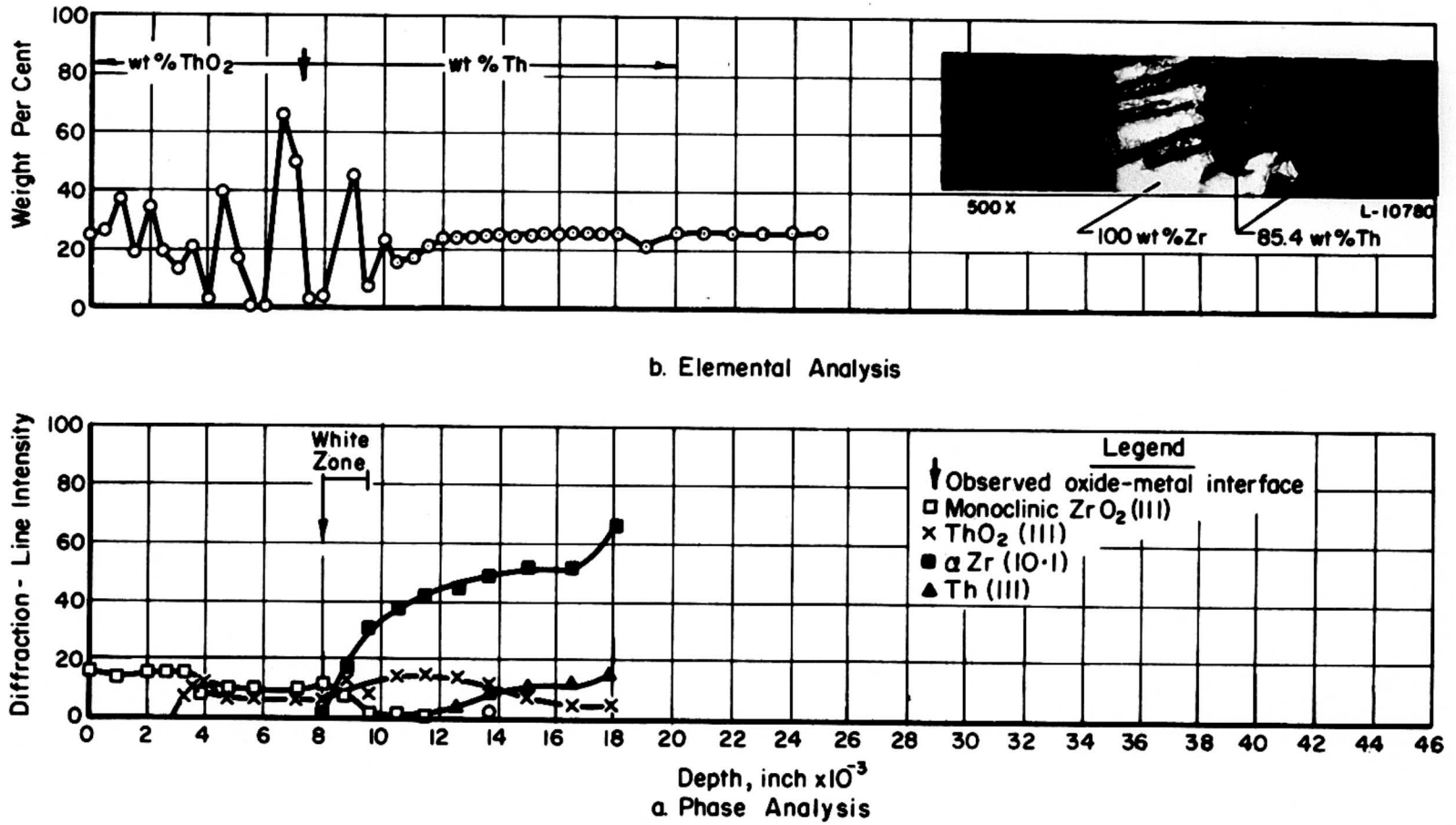

Fig. 4. Phase and elemental distribution for a Zr-30Th alloy nitrided 6 hours at 1300°C, oxidized 10 minutes at 1200°C.

monoclinic ZrO_2 plus ThO_2 occur in a constant ratio while the thorium and zirconium contents exhibit sharp peaks and valleys. The amount of the ZrO_2 increases slightly at this depth before decreasing. Some preferred orientation of the oxide phases was observed and might alter the phase distribution somewhat but the relative intensities shown in Figure 4 are believed to represent relative changes in the concentration of phases. ZrN was observed at three widely separated points and was therefore no included in Figure 4. A white zone, as seen in the photomicrograph, formed at the oxide-metal interface and was identified as alpha zirconium with an expanded lattice parameter. The gray phase extending across and immediately below the white zone was found to be ThO_2.

The variations in elemental composition throughout the oxide and base metal are presented in Figure 4b. The gradient of increasing thorium content observed in the outer .003 inch of the oxide scale where only monoclinic ZrO_2 was observed by X-ray diffraction may indicate a solid solubility of ThO_2 in monoclinic ZrO_2 when formed from the alloy nitride by oxidation at 1200 C. However, the oxide phases beneath this layer are typical of oxidized Zr-30Th alloy. A very narrow thorium-rich oxide layer was observed at the oxide-white zone interface and extending into, across, and immediately below the white zone. This oxide analyzed 85.4 weight per cent Th, but contained a second phase, probably ZrO_2. The white zone itself analyzed 100 weight per cent Zr. Below the white zone, a short gradient of increasing thorium was observed in the substrate metal. This gradient coincides with the decrease in the number of ThO_2 particles.

Summary

The compositional and structural studies of a nitrided Zr-30Th alloy after oxidation at 1200 C have shown monoclinic ZrO_2, ThO_2, and possibly ZrN to be the products of oxidation. No cubic ZrO_2 was observed, indicating a complete transformation to the monoclinic variety upon cooling. Of interest is the apparent solubility of ThO_2 in monoclinic ZrO_2 near the air-oxide interface. However, more work would be needed to establish this point conclusively. Beneath a thin outer layer of oxide, which undoubtedly was originally nitride, the oxidation behavior is very similar to that of the Zr-30Th alloy before nitriding.

The thorium-rich oxide structures close to the white (alpha zirconium) zone and the thorium gradient extending from the white zone to the unaffected substrate are a result of localized diffusion to form the particles of ThO_2.

The mechanism of oxidation of this nitrided Zr-30Th alloy is similar to that of the previously discussed Zr-30Th alloys except at the nitrided surface.

4.3 The Zr-Y System

The structural and compositional properties of the reaction products on zirconium alloys containing 5, 10, 25, 35, and 50 weight per cent Y oxidized at 1200 C for 1/2 hour, and 1600 C for 1/4 hour, have been studied. The phase distribution and average metal composition were studied, as a function of depth below the air-oxide interface on the Zr-5, 10, 25, 35 and 50 Y alloys oxidized at 1200 C, plus the Zr-5 and 10 Y alloys oxidized at 1600 C. As a result of the irregularities in the surface of the Zr-25, 35, and 50 Y alloys oxidized at 1600 C, it was not possible to perform the analysis as a function of depth. However, certain areas of interest could be analyzed. The compositions of specific areas in the Zr-5 and 35 Y specimens oxidized at 1200 C and in the Zr-10, 35 and 50 Y specimens oxidized at 1600 C were obtained by electron microprobe techniques. The results of these analyses are presented in Figures 5 and 6, in which the products of air oxidation of the Zr-Y alloys are shown to be monoclinic ZrO_2, cubic ZrO_2, Y_2O_3, and ZrN.

Oxidized at 1200 C

Results on 1200 C oxidation are presented in Figure 5. The relative amounts of zirconium and yttrium oxides are proportional to the amounts of those elements present in the alloy. X-ray fluorescence analysis of large areas show that the Y/Zr ratio is constant throughout the oxide and base metal even though local variations in composition are detected by the electron microprobe. The X-ray diffraction studies show that the cubic ZrO_2 to monoclinic

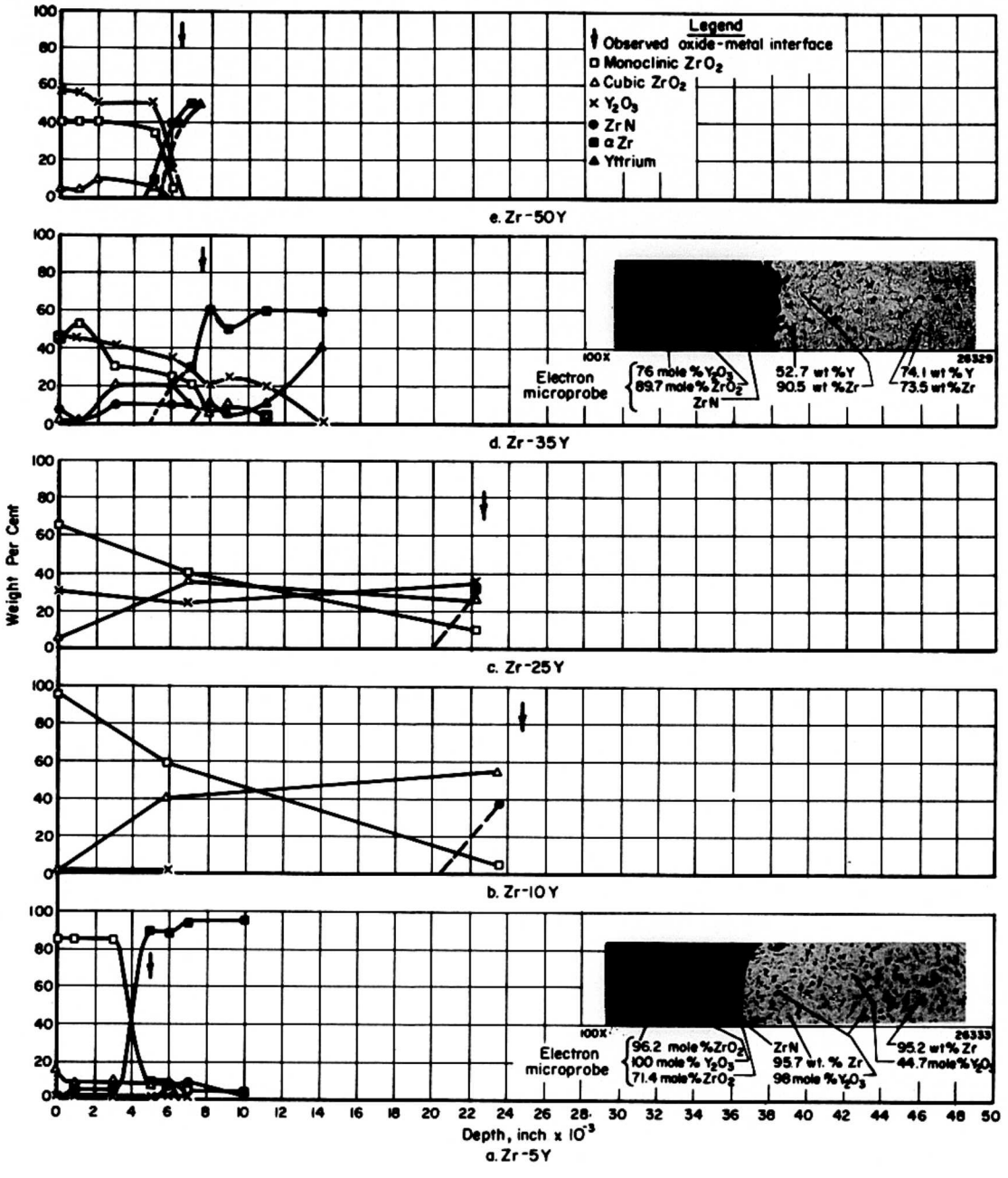

Fig. 5. Phase and elemental distribution for Zr-Y alloys after oxidation for one-half hour at 1200°C.

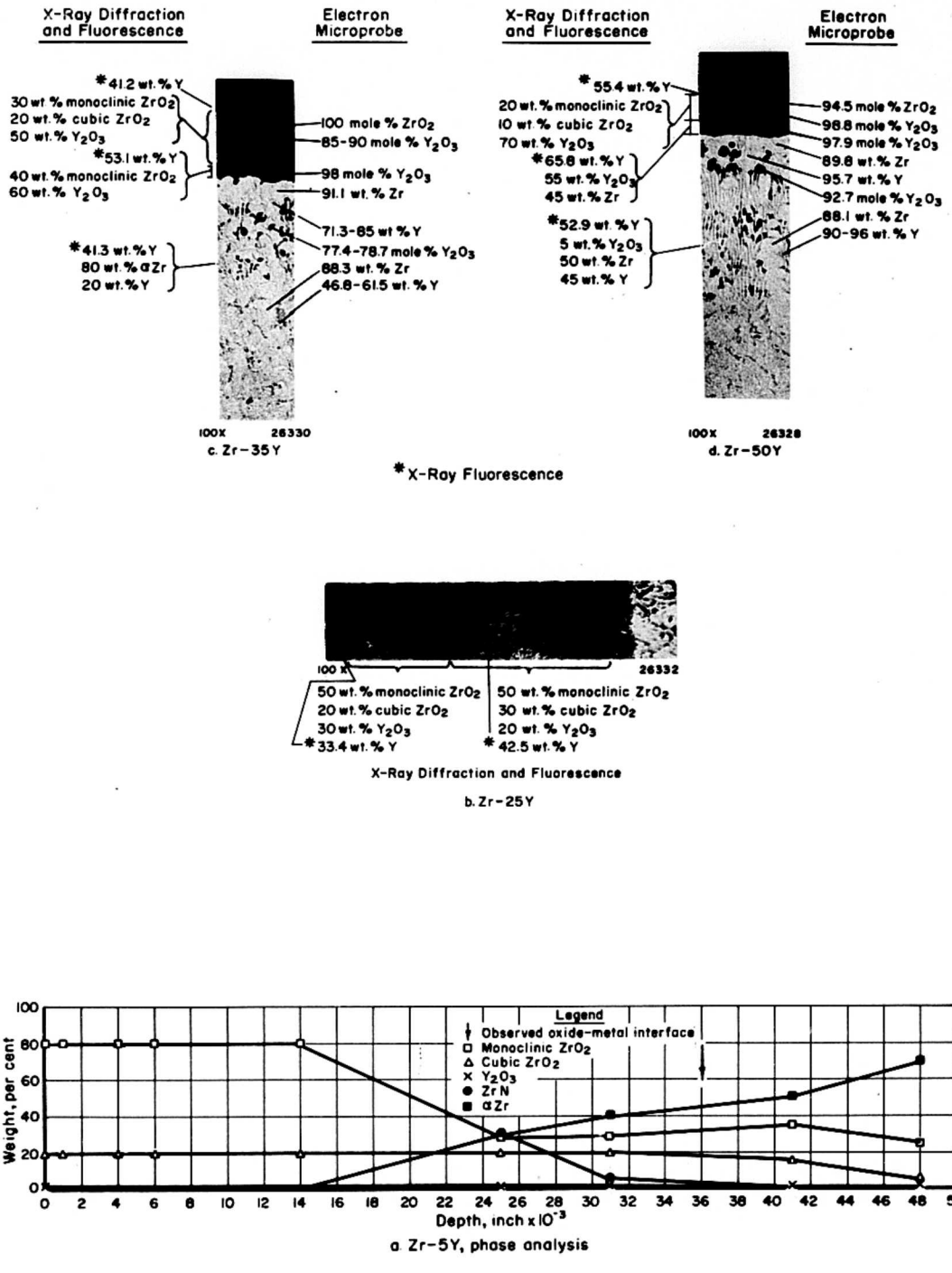

Fig. 6. Phase and elemental distribution for Zr-Y alloys after oxidation for one-quarter hour at 1600°C.

ZrO_2 ratio varies significantly among the alloys oxidized at 1200 C. This ratio is essentially constant with depth below the air-oxide interface for the specimens containing 5 and 50 weight per cent Y, but increases with depth for the 10, 25, and 35 weight per cent Y specimens. The last three specimens have thicker oxide layers and the thickness of the oxide increases with the above ratio. This relationship is particularly evident for the oxide layers on the Zr-10 and 25 Y specimens. The Y_2O_3 content remains essentially constant throughout the oxide scale while the cubic ZrO_2 content increases, and the lattice parameter of the cubic ZrO_2 is not expanded. Thus, it is doubtful that the cubic high temperature modification of ZrO_2 is stabilized by solid solution of Y_2O_3 in it when formed by 1200 C exposure to air. However, solid solubility of ZrO_2 in Y_2O_3 is indicated by a shift in the diffraction lines for Y_2O_3.

Electron microprobe analyses were made on the Zr-5 and 35 Y specimens oxidized at 1200 C in an attempt to determine compositional variations of the different structures observed metallographically. High zirconium and yttrium bearing structures are indicated by the analyses presented adjacent to the photomicrographs in Figures 5a and 5d. Unfortunately, these analyses are influenced by the small size and low density of the areas examined and cannot be employed to ascertain the extent of solid solubility between the zirconium and the yttrium oxides. Large variations in composition between particles confirm the existence of Zr-rich and Y-rich oxide phases. A metallic appearing structure near the oxide-metal interface was found by electron microprobe analysis to be a Zr-rich phase which coincides in position with the ZrN phase observed by X-ray diffraction.

Oxidized at 1600 C

Results on the 1600 C oxidation products are presented in Figure 6. The surfaces of the Zr-Y alloys after oxidation at 1600 C were irregular due to melting of the substrate metal. Hence, phase distribution analyses with depth below the air-oxide interface were made on only one specimen, the Zr-5Y alloy. The bulk composition of the oxide and the metal was determined by X-ray fluorescence to be constant throughout. Specific areas in the oxide layers on Zr-25, 35, and 50 Y alloys oxidized at 1600 C were analyzed and the results are given adjacent to the respective photomicrographs of Figure 6b, 6c, and 6d.

It can be seen from a bulk analysis of the white oxide, by X-ray diffraction, that it contained monoclinic ZrO_2, cubic ZrO_2, and Y_2O_3 with the amount of monoclinic ZrO_2 decreasing and the amount of Y_2O_3 increasing with increasing yttrium content. The oxide adjacent to the metal in the Zr-25 weight per cent Y alloy oxidized at 1600 C contained both monoclinic and cubic ZrO_2 plus Y_2O_3, while the dark oxide adjacent to the metal in the Zr-35 and 50 weight per cent Y alloys oxidized at 1600 C was Y_2O_3. The monoclinic ZrO_2 reported in the dark oxide of the Zr-35Y alloy is believed to be the result of poor separation of that oxide from the outer white oxide. The alpha zirconium observed in the Zr-50 weight per cent Y alloy came from the metal immediately below the dark oxide.

The results of the electron microprobe analyses of the Zr-35 and 50 weight per cent Y alloys oxidized at 1600 C are presented in Figure 6c and 6d adjacent to their respective photomicrographs. The data show Zr-rich and Y-rich phases in the outer oxide layer, a Y-rich oxide layer next to the metal-oxide interface and a metallic layer of nearly pure zirconium adjacent to the oxide. The substrate metal is a mixture of Y-rich and Zr-rich phases with Y_2O_3 extending to a depth of 0.02 inch below the metal-oxide interface.

As in the case of the 1200 C oxidation products, the lattice parameters of the oxide phases produced at 1600 C indicated no solid solubility of Y_2O_3 in ZrO_2 except for the oxide on the Zr-25 weight per cent Y specimen. The Y_2O_3 diffraction lines from the outer oxide scale were shifted slightly toward a lower lattice parameter while at the oxide-metal interface, the diffraction lines positions corresponded those of pure Y_2O_3. The lattice parameter of the alpha Zr, adjacent to the oxide, on the Zr-5, 35, and 50 weight per cent Y specimens was expanded suggesting that oxygen and/or nitrogen had dissolved in the zirconium during the oxidation treatment.

SUMMARY

The oxidation products of Zr-Y alloys at 1200 and 1600 C were found to be ZrO_2, Y_2O_3, and ZrN. Both monoclinic and cubic ZrO_2 were observed. The monoclinic variety is believed to be a transformation product, formed on cooling, while the cubic high temperature form of ZrO_2 was stabilized to room temperature.

The oxidation of Zr-Y alloys, up to 50 Y at 1200 C, and Zr-5 and 10 Y at 1600 C has been shown to take place with very little or no bulk diffusion. Electron microprobe analysis of the Zr-5Y alloy, oxidized at 1200 C, has shown ZrO_2 to contain 3.8 mole per cent Y_2O_3 and zirconium to contain 4.5 weight per cent Y in solid solution. These values closely agree with the published data for the ZrO_2-Y_2O_3[1] and Zr-Y[2] systems. However, some of the electron probe data for the Zr-35Y alloy oxidized at 1200 C were not in agreement with the literature. The zirconium-rich oxide phase on the Zr-35Y alloy was shown to contain 10.3 mole per cent Y_2O_3 and the yttrium-rich oxide to contain 24.0 mole per cent ZrO_2. The solubility of 24.0 mole per cent ZrO_2 in Y_2O_3 is not too different from that proposed by Duwez, et al,[1] but the ZrO_2-rich boundary of the two-phase region was placed at about 50 mole per cent Y_2O_3 by Duwez. This difference is probably the result of a nonequilibrium structure formed during oxidation in which there was insufficient time for diffusion to give the expected compositions. The variations in the base metal composition with the Zr-rich phase changing from 90.5 weight per cent zirconium at the oxide-metal interface to 73.5 weight per cent zirconium at the center and the Y-rich phase changing from 52.7 weight per cent yttrium at the oxide-metal interface to 74.1 weight per cent yttrium at the center of the specimen may be due to localized diffusion near the oxide-metal interface. However, the compositions of the two phases indicate much higher solubilities in the Zr-Y system than previously observed. Again this may be the result of a nonequilibrium alloy due to insufficient homogenization during preparation.

The oxidation of those alloys containing large amounts of a liquid phase at 1600 C (Zr-25, 35, and 50 Y) follows a somewhat different mechanism. The outer mixed oxide scale is believed to have formed on the solid alloy during heating to the test temperature. If one assumes that only the Y_2O_3 in the dark oxide of the Zr-25 Y alloy forms from the liquid phase and the ZrO_2 forms from the solid phase, then since the Zr-35 and 50 Y alloys are entirely liquid at 1600 C, the only product of oxidation of liquid Zr-Y alloys is Y_2O_3. In those alloys that are entirely liquid, yttrium has a greater mobility and diffuses to the air or oxide-liquid interface to form the Y_2O_3 layer. This, of course, leaves the zirconium-rich layer of metal which appears to be oxygen stabilized alpha

The oxidation of Zr-Y alloys, up to 50 Y at 1200 C, and Zr-5 and 10 Y at 1600 C has been shown to take place with very little or no bulk diffusion. Electron microprobe analysis of the Zr-5Y alloy, oxidized at 1200 C, has shown ZrO_2 to contain 3.8 mole per cent Y_2O_3 and zirconium to contain 4.5 weight per cent Y in solid solution. These values closely agree with the published data for the ZrO_2-Y_2O_3 [1] and Zr-Y [2] systems. However, some of the electron probe data for the Zr-35Y alloy oxidized at 1200 C were not in agreement with the literature. The zirconium-rich oxide phase on the Zr-35Y alloy was shown to contain 10.3 mole per cent Y_2O_3 and the yttrium-rich oxide to contain 24.0 mole per cent ZrO_2. The solubility of 24.0 mole per cent ZrO_2 in Y_2O_3 is not too different from that proposed by Duwez, et al, [1] but the ZrO_2-rich boundary of the two-phase region was placed at about 50 mole per cent Y_2O_3 by Duwez. This difference is probably the result of a nonequilibrium structure formed during oxidation in which there was insufficient time for diffusion to give the expected compositions. The variations in the base metal composition with the Zr-rich phase changing from 90.5 weight per cent zirconium at the oxide-metal interface to 73.5 weight per cent zirconium at the center and the Y-rich phase changing from 52.7 weight per cent yttrium at the oxide-metal interface to 74.1 weight per cent yttrium at the center of the specimen may be due to localized diffusion near the oxide-metal interface. However, the compositions of the two phases indicate much higher solubilities in the Zr-Y system than previously observed. Again this may be the result of a nonequilibrium alloy due to insufficient homogenization during preparation.

The oxidation of those alloys containing large amounts of a liquid phase at 1600 C (Zr-25, 35, and 50 Y) follows a somewhat different mechanism. The outer mixed oxide scale is believed to have formed on the solid alloy during heating to the test temperature. If one assumes that only the Y_2O_3 in the dark oxide of the Zr-25 Y alloy forms from the liquid phase and the ZrO_2 forms from the solid phase, then since the Zr-35 and 50 Y alloys are entirely liquid at 1600 C, the only product of oxidation of liquid Zr-Y alloys is Y_2O_3. In those alloys that are entirely liquid, yttrium has a greater mobility and diffuses to the air or oxide-liquid interface to form the Y_2O_3 layer. This, of course, leaves the zirconium-rich layer of metal which appears to be oxygen stabilized alpha

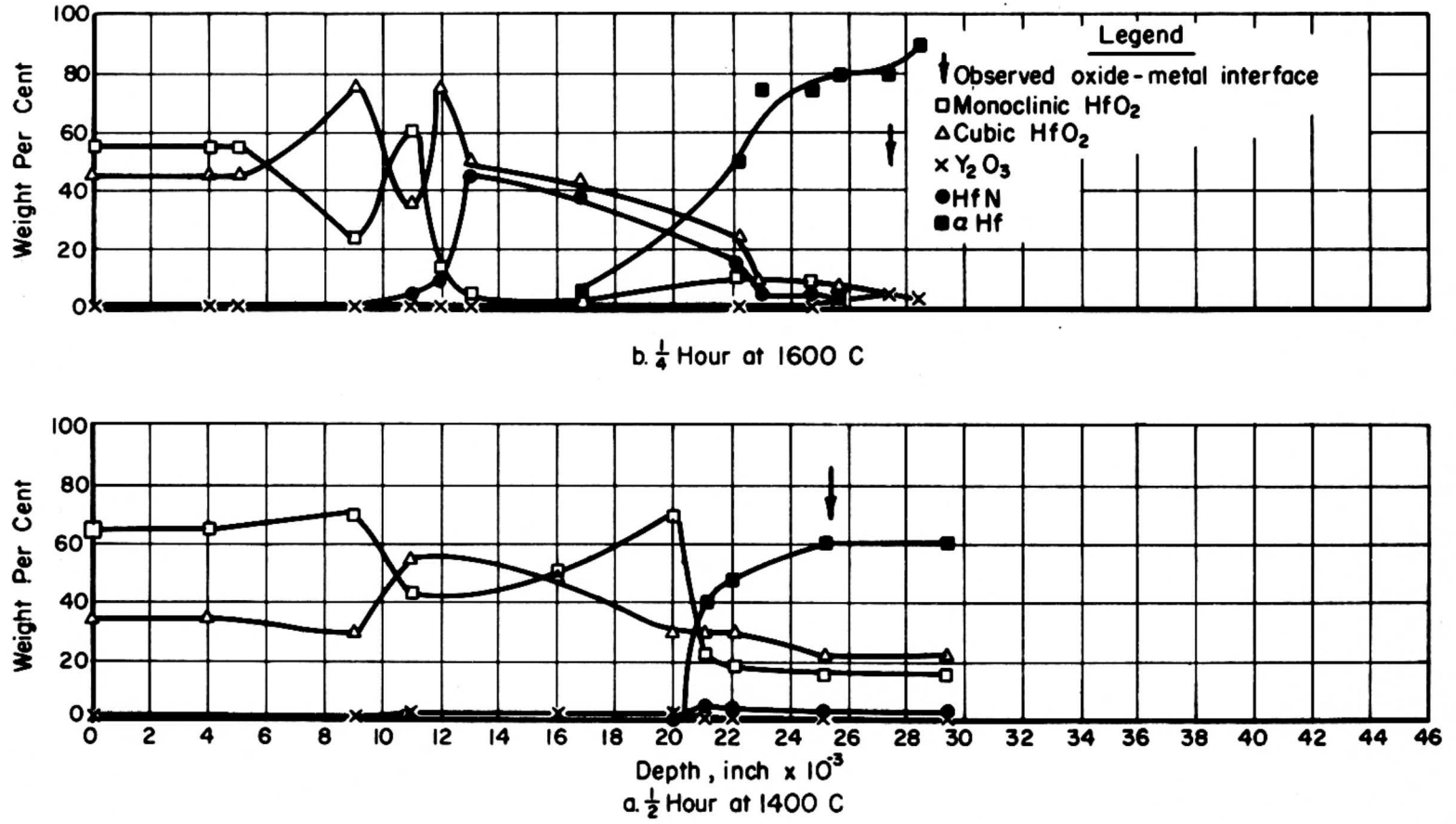

Fig. 7. Phase distribution for Hf-18 at % (10 wt. %) Y alloy after oxidation.

The results of X-ray fluorescence analysis show but little change in composition throughout the major portion of the oxide. However, the alloy oxidized at 1600 C appears to be enriched in hafnium near the air-oxide interface while both specimens show an increase in yttrium in the interior of the oxide. The increase in yttrium content near the oxide-metal interface of the specimen oxidized at 1600 C corresponds closely to the increase in Y_2O_3 observed by X-ray diffraction.

Summary

The products of oxidation of Hf-18 Y alloys at 1400 and 1600 C have been found to be monoclinic HfO_2, cubic HfO_2, and Y_2O_3. The monoclinic HfO_2 is believed to be a transformation product while the cubic HfO_2 was stabilized to room temperature. A change in the monoclinic to cubic HfO_2 ratio occurs in the black oxide layer where the yttrium content is a maximum. Presumably, the cubic HfO_2 is stabilized by Y_2O_3. The increased amount of HfN after the 1600 C oxidation may be a result of depletion of available oxygen from the air by the liquid phase or due to a more rapid diffusion of nitrogen through the oxide.

The expansion of the Hf lattice immediately below the oxide probably results from oxygen diffusion into the metal while the increased yttrium content in the center of the 1400 C oxide and near the oxide-metal interface of the 1600 C oxide may be a result of long-range diffusion of yttrium into the oxide.

4.5 The W-Hf System

A survey of the structural and compositional characteristics of two oxidized W-Hf alloys has been made, (1) W-19 weight per cent Hf oxidized 2-1/4 hours at 1300 C, and (2) W-69 weight per cent Hf oxidized 1/2 hour at 1300 C.

The substrate of the W-19Hf alloy was found to consist of W-Hf solid solution, W_2Hf and Hf, indicating a nonequilibrium condition. The size and distribution of a dendritic phase, presumably W_2Hf, varied throughout the substrate as would be expected in the case of the arc cast button used for this specimen. The metallic particles at the metal-oxide interface were found to consist of W_2Hf and two W-Hf solid-solution phases evidenced by diffraction line doubling. This doubling may be interpreted as caused by the presence of the original solid solution and a phase with expanded lattice parameter which may be due to solid

solution of oxygen or to depletion of tungsten in the body centered cubic structure of the W-Hf solid solution. The oxide layer adjacent to the metal was found to be single phase and has been identified only by structure type (cubic a_o = 3.75 Å). The oxide at the air-oxide interface consisted of three phases, HfO_2, $W_{18}O_{49}$ and an unidentified phase.

As would be expected, the phase distribution of the W-69Hf alloy was somewhat different. A large amount of the oxide scale had flaked off before the specimen was received for analyses. However, it was possible to investigate certain remaining areas. The oxide adjacent to the substrate contained HfO_2 and metallic tungsten which was not observed in the base metal. This tungsten phase had an expanded lattice parameter. The outer layer of oxide on the W-69Hf alloy specimen contained at least four oxide phases, HfO_2, $W_{18}O_{49}$, the previously mentioned cubic (a_o = 3.75 Å) phase, and the unidentified compound observed on the W-19Hf alloy.

The results of electron microprobe analyses of specific areas on the W-19Hf alloy are given in Figure 8a, adjacent to the areas analyzed.

Since the oxide phases are mixed and in some cases unidentified, it was not possible to convert the elemental analyses to weight per cent of a given oxide phase. Also, since the electron beam was not able to resolve the substrate into separate phases, the composition given in Figure 8a represents an average of both phases and, of course, may change radically from area to area. The bright particles in the substrate of the W-69Hf alloy, Figure 8b, analyzed 67 weight per cent tungsten, corresponding to W_2Hf, while the matrix analyzed between 21 and 33 weight per cent tungsten. Unfortunately the oxide layer could not be resolved in the microprobe specimen.

Summary

The presence of hafnium in the W-19Hf alloy was probably the result of an incomplete peretectic reaction upon cooling. Also, the range in composition of the substrate in the W-69Hf alloy (21-33 weight per cent W) is probably the result of an incomplete eutectic reaction on cooling of the arc cast button. These results indicate that the alloys analyzed were not in an equilibrium condition. Therefore, the oxidation characteristics of these alloys may differ to some extent from those which would be observed for the equilibrium structure.

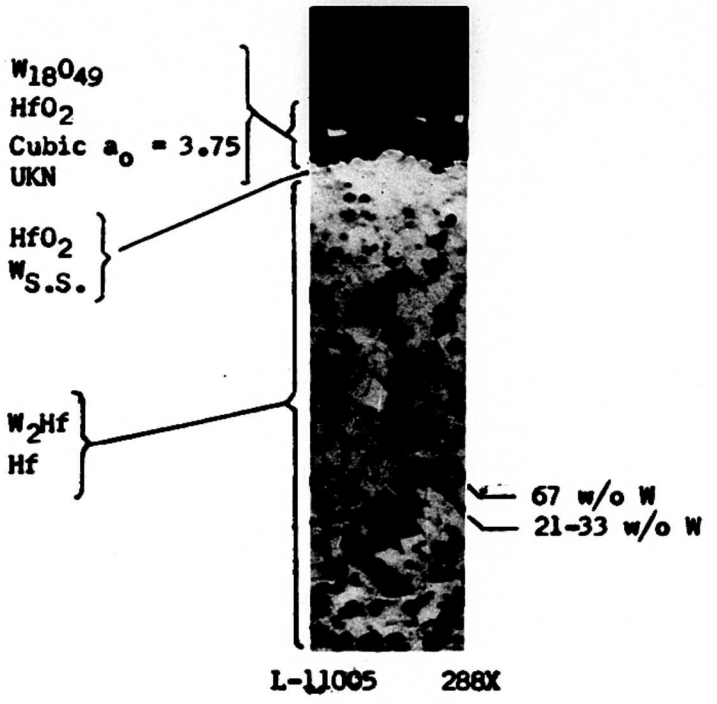

(b) W-69Hf Oxidized 1/2 hour

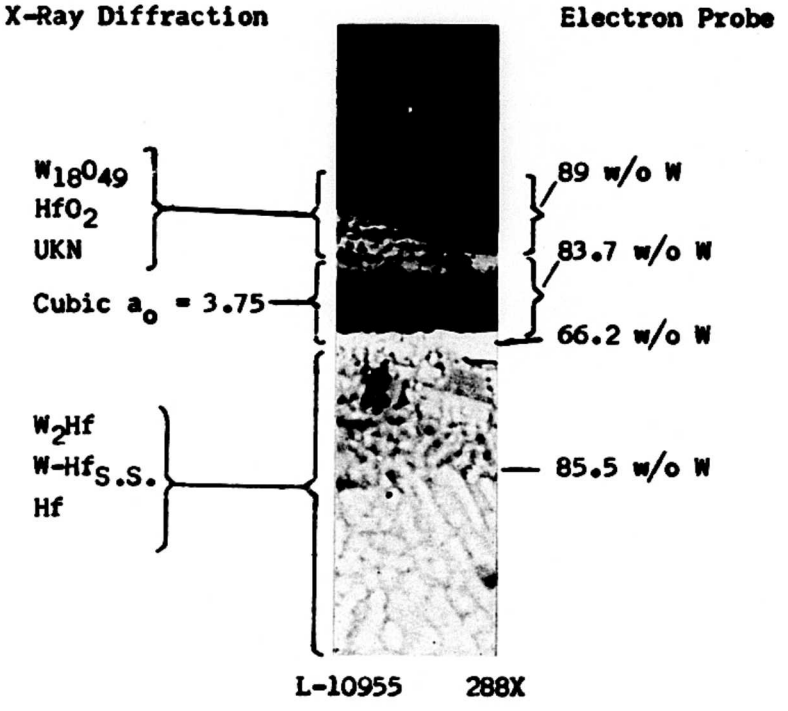

(a) W-19Hf Oxidized 2-1/4 hours

Fig. 8. Phase and elemental distribution for W-Hf alloys after oxidation at 1300°C.

Although only a limited investigation of the W-Hf system was intended, some observations on the oxidation characteristics of W-19 and 69Hf alloys can be made. The products of oxidation are complex consisting of $W_{18}O_{49}$, HfO_2, a cubic ($a_o = 3.75$ Å) phase plus another unidentified phase. They form in distinct layers which may be created by the diffusion of oxygen and/or extended diffusion of the metallic constituents, particularly tungsten. Of particular interest was the formation of the cubic oxide phase adjacent to the metal substrate. This phase appears to be an adherent, uniform layer and may provide oxidation protection of the substrate.

4.6 The Hf-W-Re System

Alloys with the nominal compositions 38 weight per cent Hf-37 weight per cent W-25 weight per cent Re and 32.6 weight per cent Hf-16.7 weight per cent W-50.7 weight per cent Re oxidized at 1000 C for one hour and 1600 C for five minutes have been examined. In addition, an alloy containing 28.8 weight per cent Hf-0.4 weight per cent W-70.8 Re was examined by electron microprobe after oxidation for one hour at 1000 C. Unfortunately, these specimens were received too late in the current contract period to allow time for a complete study. Therefore, the results presented below should be considered somewhat tentative.

X-ray diffraction of fluorescence analyses were performed on the above-mentioned alloys at depths determined from the micrographs supplied by General Telephone and Electronics Laboratories. These analyses were intended to provide information about specific areas. Structural variations shown in the micrographs of Figures 9 and 10 were analyzed. The 37 W alloy oxidized one hour at 1000 C contained two layers, (a) a gray-green outer oxide, and (b) a black inner oxide, as shown in Figure 9a. Both of these layers occurred within 0.013" of the air-oxide interface. The micrograph of the 16.7 W alloy oxidized at 1000 C (Figure 10a) indicated an oxide 0.0136" thick. However, the oxide on our specimen was very irregular with metal first being observed, in the center of the specimen, at a depth of 0.009". Because of the large irregularities, no attempt was made to locate the white zone immediately below the oxide.

Line drawings of the diffraction patterns of the oxides from the areas indicated in Figures 9 and 10 are shown in Figures 11 and 12, where it can be seen that the oxidation products give very complex X-ray diffraction patterns.

The presence of HfO_2 and rhenium metal has been established and indicated on Figure 12L. As yet, the analysis of the X-ray diffraction data is incomplete, but there are indications of tungsten oxides although complete patterns for these phases were not observed. The patterns, Figure 11C and 12K, observed in the yellow-green nodules taken from the surface of oxidized specimens were quite different from those obtained for the bulk oxide in that HfO_2 or Re were not present. Almost every pattern contained weak diffraction lines which could not be identified. A complete analysis of the oxide phases on these specimens could not be made under the present program.

Compositional analyses were made of the layers in the oxide scale and of the substrate metal by electron microprobe methods. In addition, X-ray fluorescence intensities were determined for the Hf and Re to obtain data on bulk composition variations. These results are presented in Figures 9 and 10, adjacent to the photomicrographs of polished cross sections.

The oxide formed at 1600 C, adjacent to the substrate metal, was found to have the same composition as the substrate for both the 16.7 W and the 37 W alloys. However, the central oxide layer on the 37 W alloy, was slightly higher in tungsten and rhenium content (36 to 44 and 27 to 30 respectively) than the base metal. Through the external oxide on this specimen, the tungsten and rhenium contents decrease rapidly to a minimum at the air-oxide interface. The compositions of the central and external oxide layers on the 16.7 W alloy remain nearly constant or slightly increasing in rhenium content. However, the tungsten content decreases in the external oxide layer. X-ray fluorescence intensity data show a corresponding concentration of the Hf content in the external oxide layer.

The oxide scale on the 16.7 W alloy after oxidation at 1000 C was found to contain little or no Re while the tungsten and hafnium contents increased from 19 weight per cent to 32 weight per cent and 30 weight per cent to 62.5 weight per cent, respectively. The other specimen, which contained 28.8 weight per cent Hf-0.4 weight per cent W-70.8 Re when oxidized at 1000 C was found to contain a much lower Re content in the oxide than in the substrate metal. At the oxide-metal interface, the microstructures show a narrow white zone in both specimens oxidized at 1000 C. This zone has the same metal compositions as the unaffected substrate but may contain oxygen in solid solution, as a result of oxygen diffusion through the oxide layer.

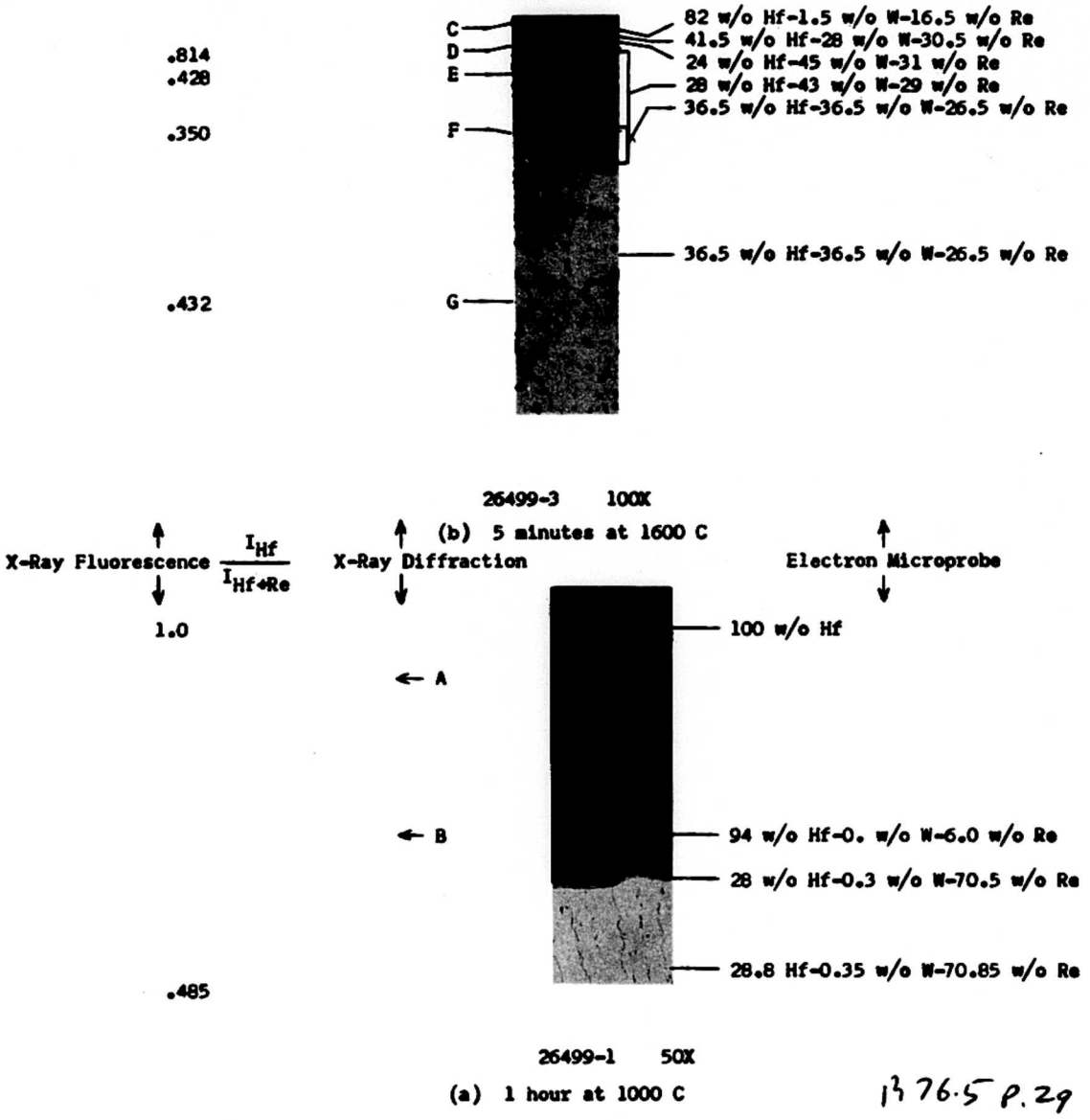

Fig. 9. Phase and elemental distribution for 38Hf-37W-25Re alloys after oxidation.

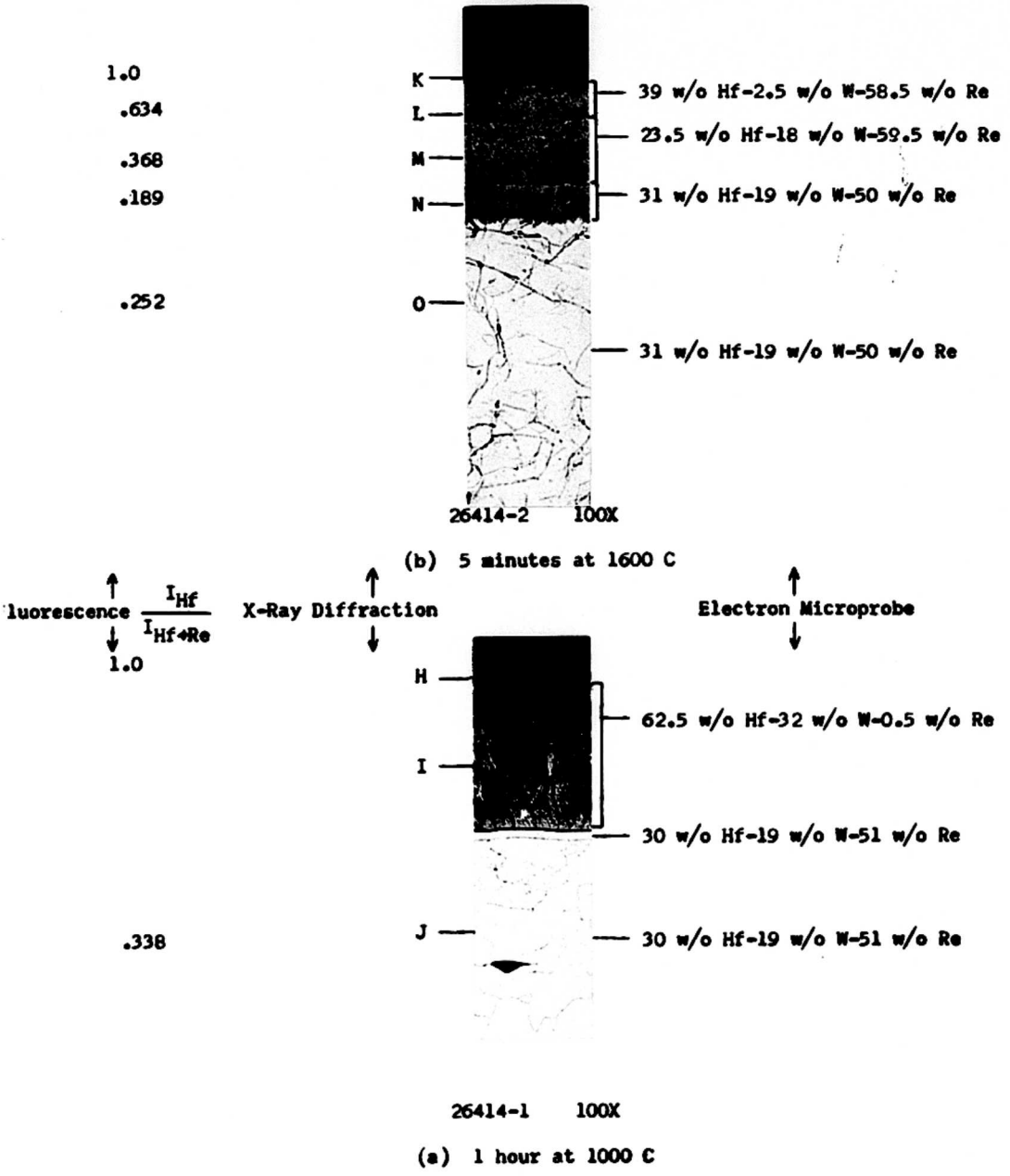

Fig. 10. Phase and elemental distribution for 32.6 Hf-16.7W-50.7Re alloys after oxidation.

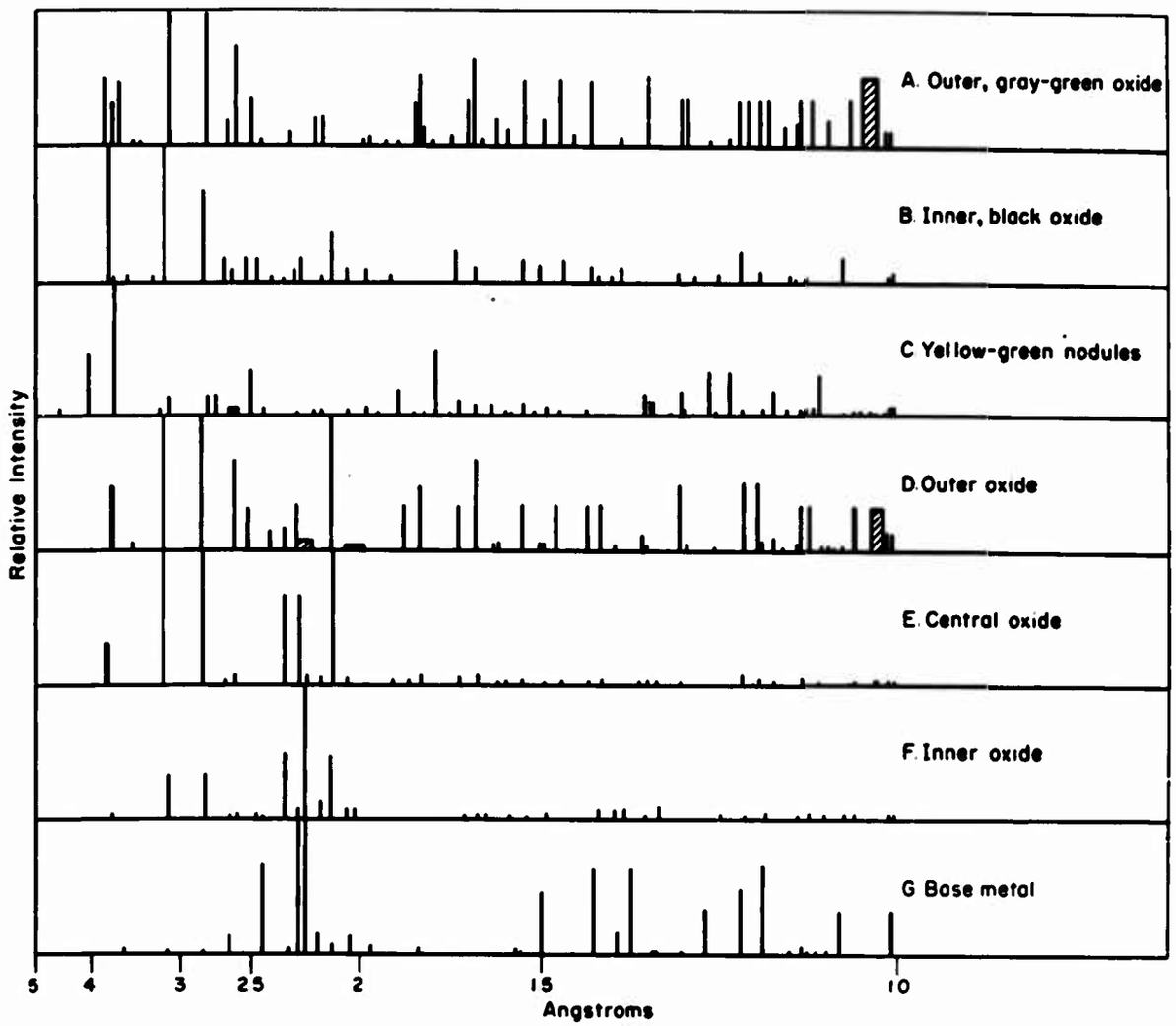

Fig. 11. Observed X-ray diffraction patterns for the indicated areas of 38 wt. % Hf-37 wt. % W-25 wt% Re alloys after oxidation.

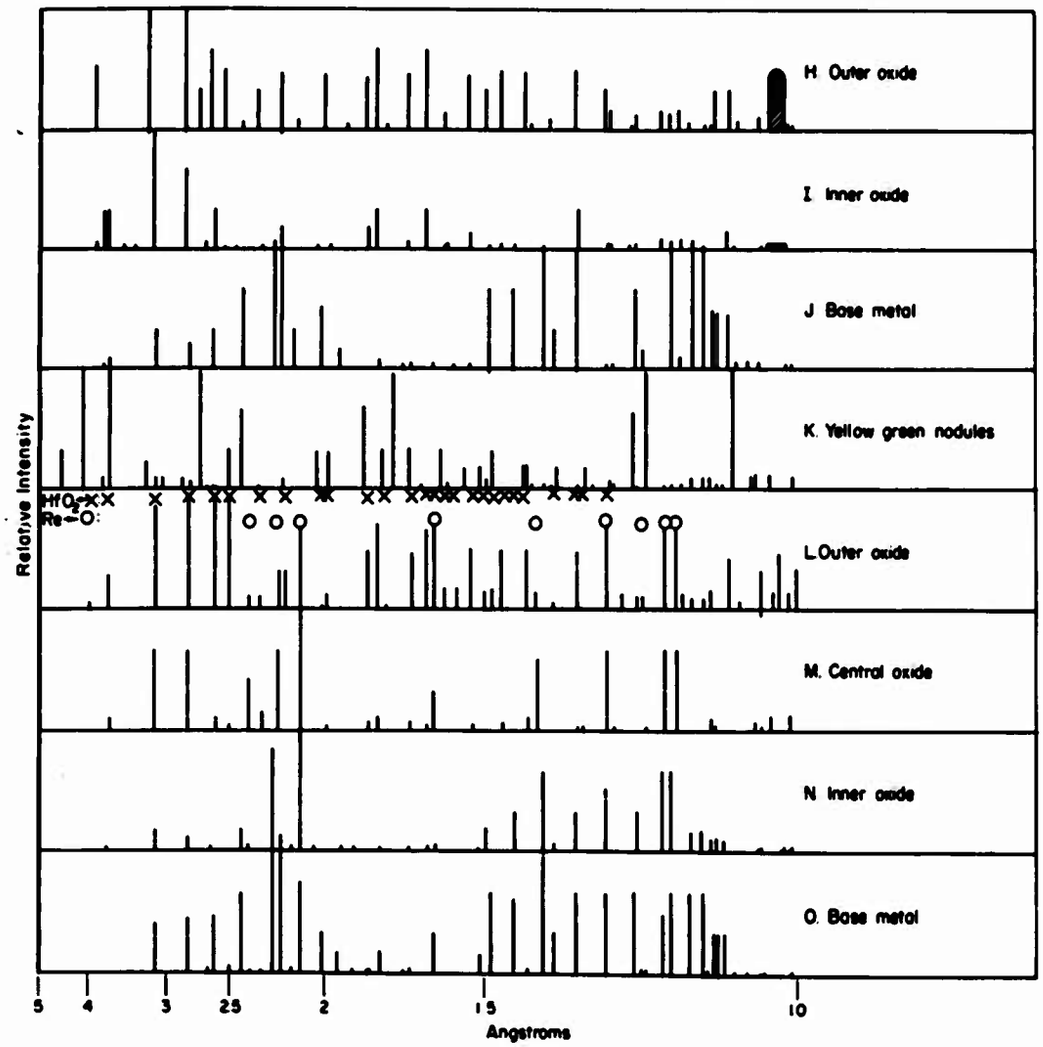

Fig. 12. Observed X-ray diffraction patterns for the indicated areas of 32.6 wt.%Hf-16.7 wt.% W-50.7 wt.% Re alloys after oxidation.

Summary

As a result of the limited studies on the Hf-W-Re alloys, some observations on their oxidation can be made. The hafnium and rhenium variations between the alloys and the oxide after oxidation at 1000 C are similar in that they contain higher hafnium and lower rhenium in the oxide than does the base metal. Presumably the rhenium is lost from the oxide by vaporation during the oxidation treatment.

After oxidation at 1600 C three oxide layers are formed which give different but unidentifiable diffraction patterns with different ratios of hafnium, tungsten, and rhenium. While tungsten and rhenium were lost by vaporation from the outer oxide layer, there is an increase in tungsten and rhenium content in the central oxide layer. The inner oxide layer has essentially the same metal content as the substrate metal. This relationship between oxide composition and position in the scale suggests that the alloy oxidizes mainly by anion diffusion, but that compositional changes occur by cation diffusion and vaporization in the outer layers of the scale.

5. DISCUSSION OF RESULTS

The oxidation processes for six alloy systems have been investigated at two temperatures, except in the case of W-Hf. In all but two systems, the Hf-Y and the Zr-Th-N, the effect of changing the ratio of alloying elements was studied. The other systems investigated were Zr-Th, Zr-Y, and Hf-W-Re.

Internal oxidation of the metal substrate is found to occur in Zr-Th and Zr-Y at 1600 C and possibly in Hf-Y (however, metallographic examination was not made on the last system). The other systems show a uniform oxide-metal interface. However, in nearly every case oxygen penetrates the oxide layer and forms a solid solution with the base metal adjacent to the oxide layer. Short-range diffusion of one element is observed for several systems, but the bulk oxide is found to be essentially the same as the base metal except for the Hf-W-Re alloys where concentration changes occur in the outer layers of the oxide. In this case, vaporization of W and/or Re is indicated.

The structure and composition of the oxide phases are identified except in the case of the Hf-W-Re and one of the oxide phases for the W-Hf alloy. In most cases there is but limited solid solubility between the oxide phase when formed by oxidation of the alloys. However, solid solution of ZrO_2 in Y_2O_3 is indicated by the shift in the diffraction pattern of the latter phase. In several of the alloys containing zirconium, the high-temperature cubic modification of ZrO_2 is observed. Although the transformation of cubic ZrO_2 to the low temperature monoclinic ZrO_2 is sluggish, thus explaining the presence of the cubic form, it is also possible that a small amount of solid solution of the alloying elements (yttrium or thorium) contributes toward stabilizing the cubic ZrO_2. A similar result is indicated for the Hf-Y alloy. ZrN and HfN are formed in several systems containing zirconium and hafnium and the location of these phases within the oxide suggests the existence of a lower oxygen partial pressure within the oxide layer than at the air-oxide interface. Thus, the oxide scales provide some reduction in the oxidizing potential of the atmosphere. Because of this change in oxidizing potential, the oxide at the air-oxide interface differs from that at the metal-oxide interface. Thus, the present studies are directed primarily at the advancing interfaces and the mechanism of reaction therein.

In the Zr-Th systems, the metal side of this interface is first depleted of Th by the formation of ThO_2 particles, then oxygen dissolves in the remaining Zr until it becomes saturated, after which ZrO_2 forms. The same behavior occurs for the Zr-Th-N specimen, after the nitrided surface is removed by oxidation, and for the Zr-Y specimen in which Y_2O_3 particles are formed. The Zr-Y specimens when oxidized at 1600 C are liquid and a continuous layer of Y_2O_3 forms which appears to protect zirconium from oxidation. The Hf-Y alloy oxidation is very similar to that of the Zr-Y alloys. Oxidation of tungsten alloys W-Hf and W-Hf-Re, produces an adherent oxide at the metal-oxide interface with little or no change in metal composition from that of the substrate metal. However, the W-Hf alloy compositions are quite variable because of the multiphase base metal structure. The oxide phases in these systems are much more complex than in the other systems investigated. In one case (the W-Hf alloy) a cubic oxide phase is formed adjacent to the oxide-metal interface while in the W-Hf-Re alloy all of the unidentified oxide phases are of low symmetry. In the latter

case, HfO_2 and metallic rhenium were also observed except in the extreme outer layer of oxide. The diffraction patterns of the several oxide layers on these alloys have not been completely identified. The cubic (a_o = 3.75 Å) oxide phase observed in the W-Hf oxides has been compared with the several reported phases of tungsten and hafnium. There are similarities between the cubic pattern and some of the stronger lines of the pattern for the high temperature modification of WO_3, but many of the lines do not match. It is possible, however, that the presence of hafnium in the oxide does alter its structure sufficiently to produce the observed cubic phase. Further work is needed to define the structural properties of this cubic oxide phase.

REFERENCES

1. Duwez, P., et al, "The Zirconia-Yttria System", Journal of the Electrochemical Society, 98, No. 9, 356 (1951).

2. Gschneidner, K. A., Jr., Rare Earth Alloys, D. Van Nostrand Co., Inc., Princeton, New Jersey (1961).

Data in this report are recorded in Battelle Laboratory Record Books No. 19406, pp 1-100; 20107, pp 1-89; 16744, pp 40-100; and 19605, pp 1-80.

The period of work covered is from July 1, 1962 to April 30, 1963.

APPENDIX II

METAL OXIDE AND OXIDE-OXIDE PHASE DIAGRAMS

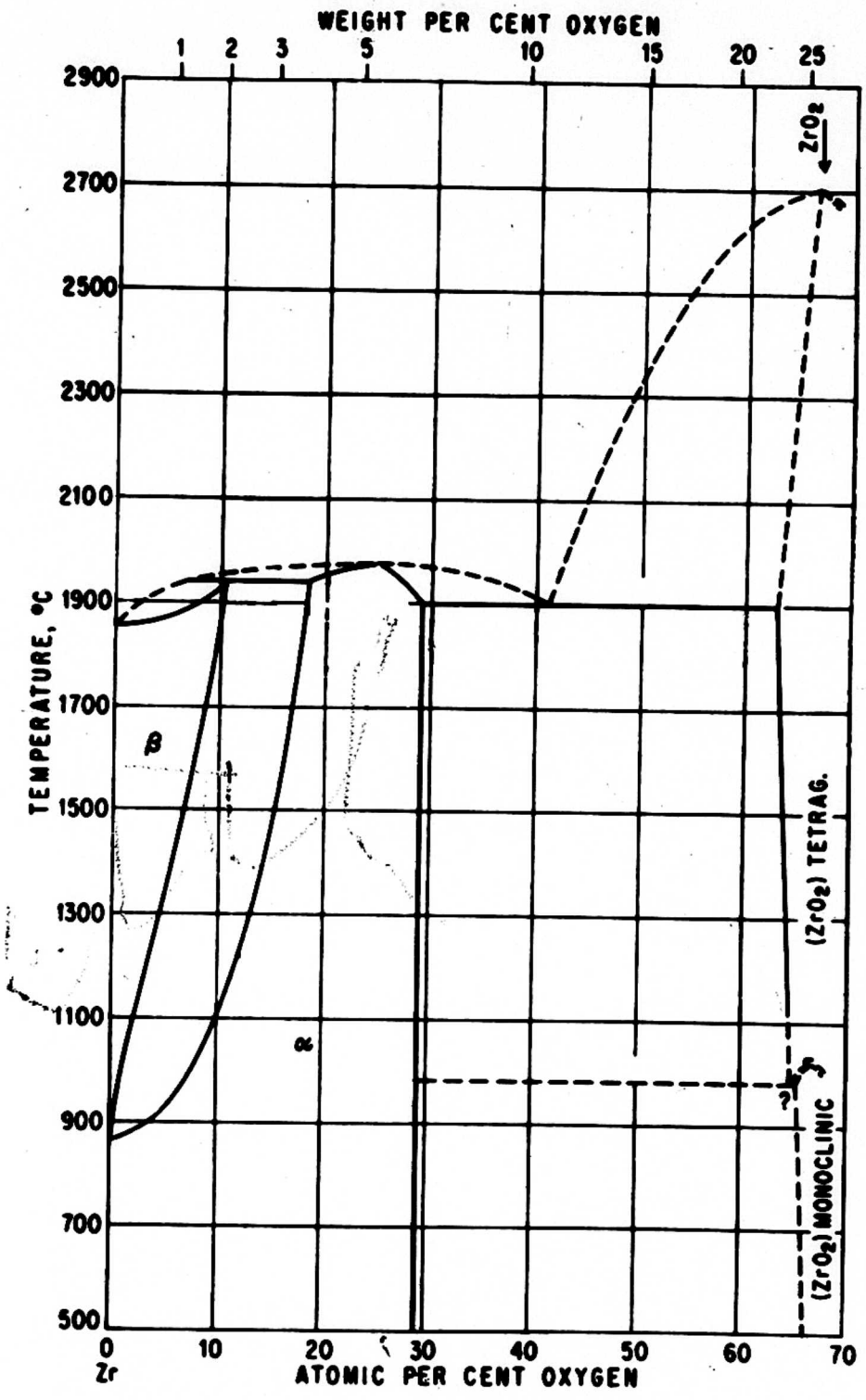

Fig. II -1. The zirconium-oxygen system.[7]

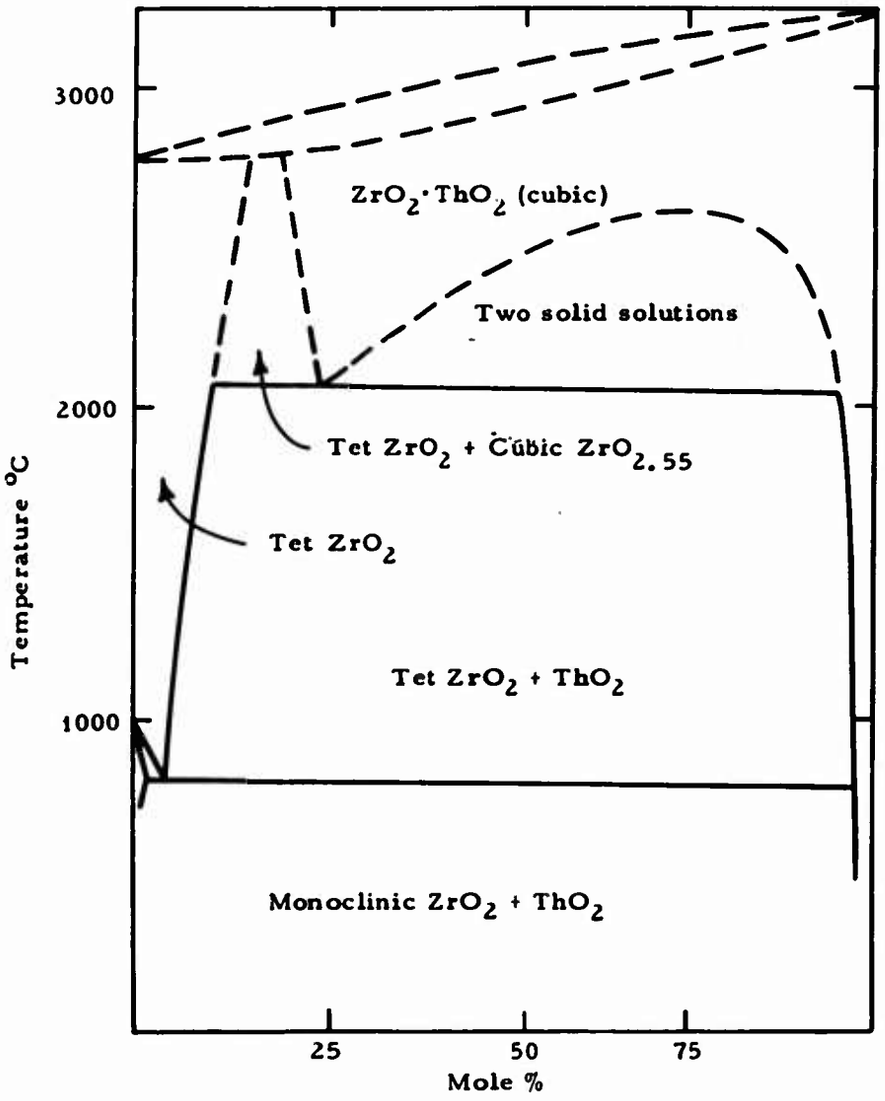

Fig. II-2. The ThO_2-ZrO_2 phase diagram.[6]

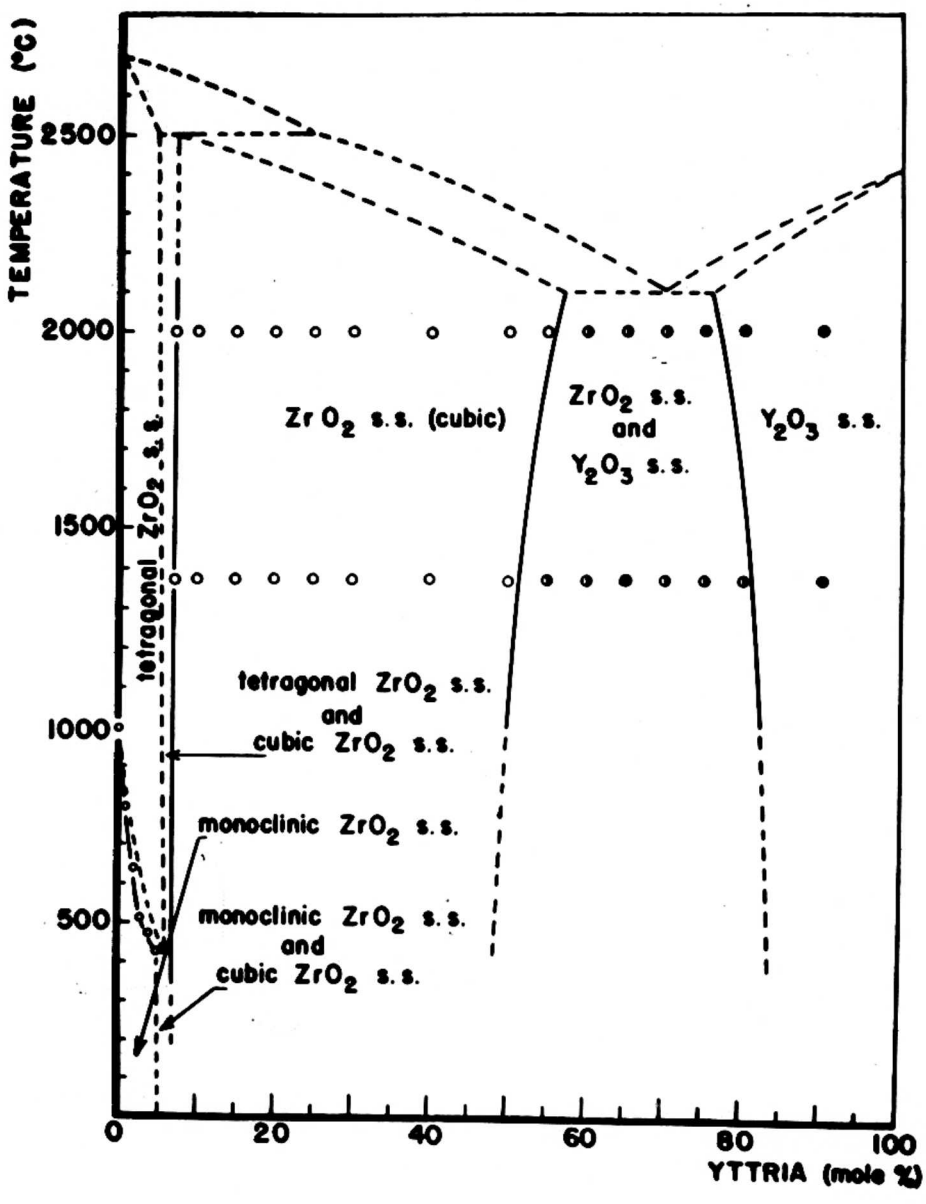

Fig. II-3. Tentative phase diagram of the zirconia-yttria system.[12]

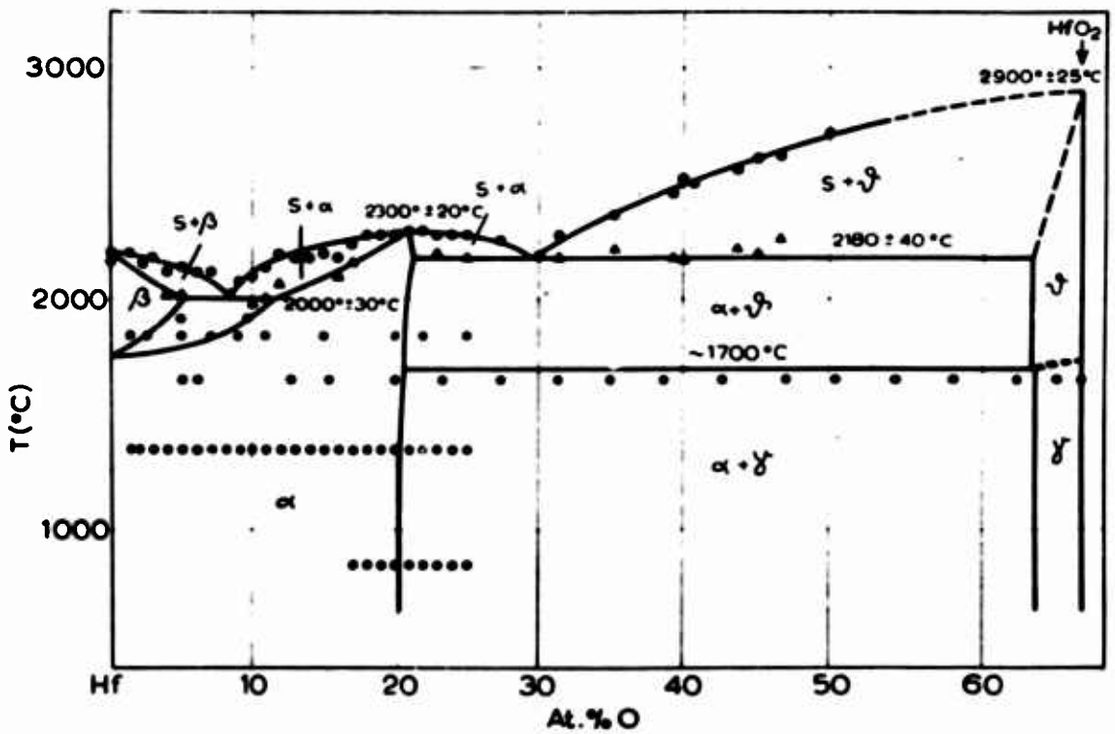

Fig. II-4. The hafnium-oxygen system.[18]

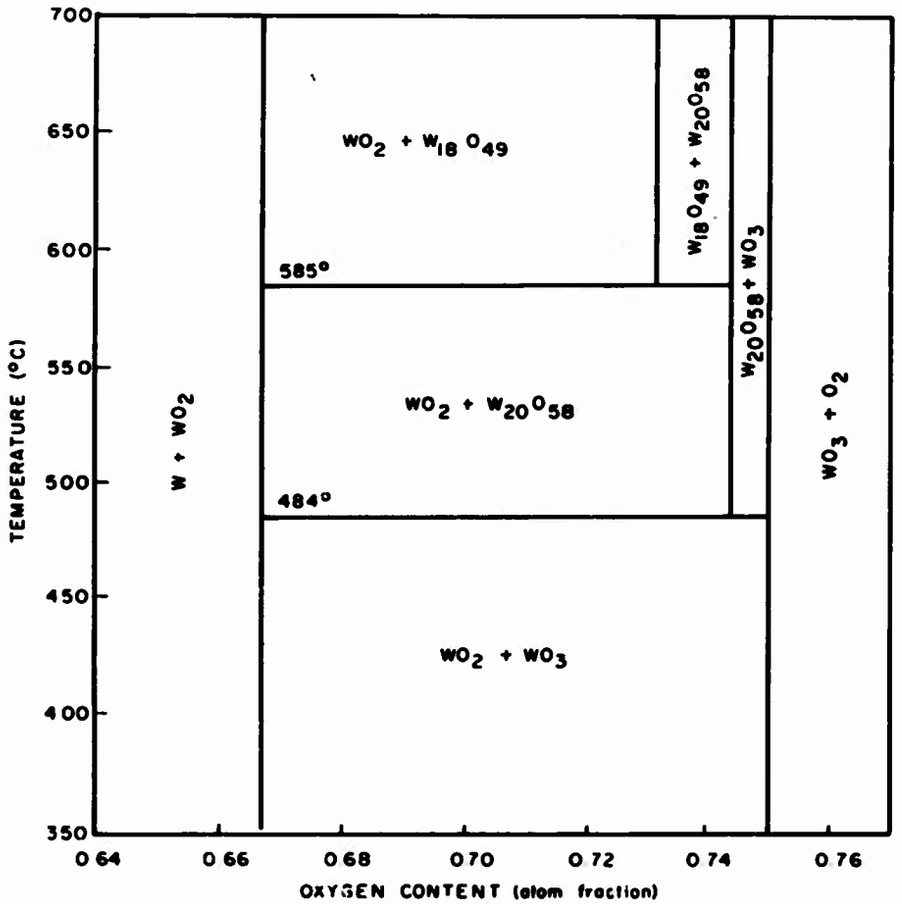

Fig. II-5. Phase diagram of the tungsten-oxygen system.[19]

UNCLASSIFIED